

Stich

QC
189
S6

TRANSACTIONS of the SOCIETY OF RHEOLOGY

VOLUME V • 1961

V. 5 - 8
1961 - 64

INTERSCIENCE PUBLISHERS • NEW YORK • LONDON

TRANSACTIONS of the SOCIETY OF RHEOLOGY

Editor: E. H. LEE
Brown University

Preface.....	1
Presentation of the Bingham Medal to Bruno H. Zimm:	
Introduction: F. D. DEXTER.....	3
Biographical Comments: HERMAN F. MARK.....	5

SYMPOSIUM ON MECHANICS OF CONTINUA

HERSHEL MARKOVITZ: Introduction to the Symposium on Mechanics of Continua.....	7
M. W. JOHNSON, JR.: On Variational Principles for Non-Newtonian Fluids.....	9
J. L. ERICKSEN: Conservation Laws for Liquid Crystals.....	23
B. BERNSTEIN: Remarks on Materials of the Rate Type and the Principle of Determinism.....	35
BERNARD D. COLEMAN and WALTER NOLL: Normal Stresses in Second-Order Viscoelasticity.....	41
A. J. ZIEGENHAGEN, R. B. BIRD and M. W. JOHNSON, JR.: Non-Newtonian Flow Around a Sphere (Abstract).....	47

SYMPOSIUM ON THE RHEOLOGY OF SUSPENSIONS

FREDERICK H. GASKINS: Introduction to the Symposium on the Rheology of Suspensions.....	51
W. F. AMES and V. C. BEHN: Application of the Method of Composition and Linear Regression Analysis to a Problem Involving a Pseudoplastic Suspension.....	53
A. F. GABRYSH, TAIKYUE REE, H. EYRING, NOLA MCKEE, and I. CUTLER: Flow Properties of Attapulgitic Suspension in Water.....	67
ROBERT H. HAYNES: The Rheology of Blood.....	85
D. W. CRIDDLE and JAY CORTES, JR.: Shear Viscosities and Stress-Relaxation Viscosity Parameters of Gelled Oils.....	103
J. G. SAVINS, G. C. WALLICK, and W. R. FOSTER: The Differentiation Method in Rheology (Abstract).....	113

HARRY H. HULL: The Normal Forces and their Thermodynamic Significance.....	115
A. B. METZNER, W. T. HOUGHTON, R. A. SAILOR, and J. L. WHITE: A Method for the Measurement of Normal Stresses in Simple Shearing Flow.....	133

(continued)

INTERSCIENCE PUBLISHERS NEW YORK • LONDON

M3540
44
2 new

WLADIMIR PHILIPPOFF: Experimental Tests of Symmetry Conditions in Laminar Flow.....	149
WLADIMIR PHILIPPOFF: Elastic Stresses and Birefringence in Flow.....	163
F. D. DEXTER, J. C. MILLER, and W. PHILIPPOFF: Flow Birefringence of Molten Polyethylene.....	193
JOHN G. BRODNYAN and E. LLOYD KELLEY: The Rheology of Polyelectrolytes. I. Flow Curves of Concentrated Poly(acrylic Acid) Solutions.....	205
WILLIAM H. FISCHER, WALTER H. BAUER, and STEPHEN E. WIBERLEY: Yield Stresses and Flow Properties of Carboxypolymethylene-Water Systems.....	221
E. W. MERRILL, H. S. MICKLEY, A. RAM, and G. PERKINSON: Upper Newtonian Regime in Polymer Solutions. I. Polystyrenes in Toluene....	237
RALPH SHANGRAW, WAYNE GRIM, and ALBERT M. MATTOCKS: An Equation for Non-Newtonian Flow.....	247
H. NAKAYASU, H. MARKOVITZ, and D. J. PLAZEK: The Frequency and Temperature Dependence of the Dynamic Mechanical Properties of a High Density Polyethylene.....	261
A. J. KOVACS: Bulk Creep and Recovery in Systems with Viscosity Dependent upon Free Volume.....	285
S. R. BODNER: A Theory for the Occurrence of Intrinsic Resonances in Stressed Solid Materials.....	297
RAYMOND R. MYERS and RAY D. HOFFMAN: The Distribution of Pressures in the Roll Application of Newtonian Fluids.....	317
C. C. McCABE and N. N. MUELLER: Capillary Rheometry as a Technique for Predicting Processing of Elastomers.....	329
E. B. BAGLEY and H. P. SCHREIBER: Effect of Die Entry Geometry on Polymer Melt Fracture and Extrudate Distortion.....	341
E. B. BAGLEY: The Separation of Elastic and Viscous Effects in Polymer Flow.....	355
A. FARAROUTI and R. C. KINTNER: Flow and Shape of Drops in Non-Newtonian Fluids.....	369
H. NAKAYASU and T. G. FOX: Molecular Weight-Temperature-Concentration Relationships for the Viscosity of Polyvinyl Acetate and Its Solutions in Diethyl Phthalate and in Cetyl Alcohol (Abstract).....	381
THEODORE P. YIN and JOHN D. FERRY: Dynamic Mechanical Properties and Creep of Poly-2-ethyl Butyl Methacrylate (Abstract).....	381

Copyright © 1961 by
INTERSCIENCE PUBLISHERS, INC.

Library of Congress Catalog
Card Number 57-11926

INTERSCIENCE PUBLISHERS, INC.
250 Fifth Avenue, New York 1, N. Y.

For Great Britain and Northern Ireland:
INTERSCIENCE PUBLISHERS LTD.
88/90 Chancery Lane, London, W. C. 2

Preface

Volume V of the *Transactions of the Society of Rheology* (1961) comprises the majority of the papers presented at the Thirty-first Annual Meeting of the Society held at the Mellon Institute, Pittsburgh, Pennsylvania, October 31–November 2, 1960. Abstracts are included of those papers not printed in full, with the reference to the complete paper where this is available at this time. Two Symposia were arranged for this Meeting, and the papers so invited are printed together ahead of the contributed papers, with an introductory statement by the member arranging them. The first symposium on the Mechanics of Continua was organized by Dr. Herschel Markovitz, and the second on the Rheology of Suspensions by Mr. Frederick H. Gaskins. Mr. J. T. Bergen as Program Chairman for the Meeting was, with his Committee: E. A. Collins, F. H. Gaskins, H. Markovitz, and M. C. Williams, responsible for arranging the full, varied, and interesting program.

At the Smoker during the Meeting, the Bingham Medal was presented to Dr. Bruno H. Zimm, of the School of Science and Engineering, University of California at La Jolla. Frank D. Dexter's introductory comments and bibliographical notes by Herman F. Mark follow this Preface.

Congenial facilities for the Meeting were provided by Mellon Institute through the able organization of Herschel Markovitz and his Local Arrangements Committee: R. M. Arnold, D. J. Plazek, H. L. Toor, and N. Weber.

In accordance with our Constitution, the Officers of the Society elected last year, continue their terms through the Annual Meeting 1961:

President

J. H. Elliott
Research Center
Hercules Powder Co.
Wilmington 99, Delaware

Vice-President

J. D. Ferry
Department of Chemistry
University of Wisconsin
Madison, Wisconsin

Secretary-Treasurer

W. R. Willets
Titanium Pigment Corp.
99 Hudson Street
New York 13, New York

Editor

E. H. Lee
Division of Applied Mathematics
Brown University
Providence 12, Rhode Island

The Executive Committee includes the Officers, J. H. Dillon, Past President, and R. S. Marvin and J. P. Tordella as elected members.

I would like to take this opportunity to thank the referees and authors, and especially Mrs. Ezoura Fonseca, for the diligent and expert assistance which made it possible to get all papers to Inter-science by this date.

Particular thanks are also due John G. Brodnyan who was extremely helpful in assisting Frederick H. Gaskins with the processing of Transactions papers for the Symposium on Suspensions, while Frederick Gaskins was recuperating from his unfortunate accident.

E. H. Lee

Providence, Rhode Island
March, 1961

Presentation of the Bingham Medal to Bruno H. Zimm

Introduction

F. D. DEXTER, *Union Carbide Plastics Co., Bound Brook, New Jersey*

Mr. President, ladies and gentlemen. I am most honored to have this opportunity to introduce our 1960 Bingham medalist. This man is Dr. Bruno H. Zimm. I know I may surprise you by naming our honored medalist so early in the show. It seems rather traditional to follow the "I give you the man who" technique wherein, like a German verb, the recipient's name is the last thing to pop out of the introduction. This has always puzzled me, for it is quite the reverse of the manner in which we all present our scientific findings. Possibly this may arise because the introducer feels the occasional



need to fortify the audience (or the recipient) before baring the facts. Happily there is no need tonight for such fortification since the medalist is well known, his accomplishments well recognized, and his qualifications undisputed.

The Bingham Medal, which honors the founder of our society, the late Prof. E. C. Bingham, was made possible through the efforts of Mrs. Bingham and some industrial concerns. Past medalists represent a nucleus of rheological science and I feel it appropriate to list their names.

Melvin Mooney
Henry Eyring

1948
1949

W. F. Fair, Jr.	1950
Percy W. Bridgeman	1951
A. Nadii	1952
John D. Ferry	1953
Turner Alfrey	1954
Herbert Leaderman	1955
Arthur V. Tobolsky	1956
Clarence M. Zener	1957
R. S. Rivlin	1958
Egon Orowan	1959

Dr. Bruno H. Zimm received his doctorate from Columbia University in 1944, where he studied the vapor pressure of alkali halides under Dr. Joseph E. Mayer. After graduation, our medalist made contributions in such numbers that it is beyond the scope of this talk to discuss all or even a large portion of them. Rather, I would like to trace some of his key developments to show the manner in which he lays the ground work for understanding complex phenomena.

In 1944, Dr. Zimm went to the Polytechnic Institute of Brooklyn, where, working under Dr. Herman Mark, he developed an osmometer capable of measuring the molecular weight of very small samples at temperatures up to 150°C. He followed this up at the University of California, where he went in 1946, by developing a unique method of making and interpreting light-scattering measurements. Here he developed what essentially amounted to a double extrapolation method for determining molecular weight and indicating molecular shape factors for the polymer.

His interest was then directed toward the development of the hydrodynamic theory for viscoelastic properties of solutions of large molecules. This theory took into account the important parameter of hydrodynamic interaction and represented a major step forward in the theory of viscoelastic properties. Shortly following this, he developed a dynamic method for the measurement of the viscoelastic properties of solutions which used a unique longitudinally oscillating tube system.

I believe that these accomplishments, selected from many made by Dr. Zimm, illustrate well his type of valuable contributions; going from basic factors of work up through soundly founded theory to define complex phenomena in fundamental and understandable terms. This indeed represents the goal of our scientific endeavors in the field of rheology.

Biographical Comments

HERMAN F. MARK, *Polytechnic Institute of Brooklyn, Brooklyn, New York*

Bruno H. Zimm started his studies at Columbia University in 1938, and received his Ph.D. in 1944, with Professor Joseph E. Mayer on the vapor pressures of alkali halides. In 1943 he became interested in Polymer Chemistry and began to work at the Polymer Research Institute at the Polytechnic Institute of Brooklyn. His first activities were devoted to the characterization of large molecules in solution with the aid of statistical thermodynamics. A particularly important contribution of great practical value at this time was the construction of a new simple and inexpensive osmometer which is extremely popular and very widely used today. This instrument permits one to make reliable, quick osmotic measurements with very small quantities (a few milligrams) of polymeric substances in almost any kind of solvent and up to temperatures of about 140°C.

From the Polytechnic Institute of Brooklyn, Dr. Zimm went to the University of California in Berkeley as Assistant Professor, continued to work in the Polymer Field, and made an important contribution to the light-scattering method by conceiving a system which permits a simultaneous extrapolation to zero concentration and zero angle in the course of measurements of the scattered intensity of dilute polymer solutions over a wide angular range. The so-called "Zimm-Rack" is now almost exclusively used in the evaluation of molecular weight, of molecular weight distribution, and of the spatial extension of polymer molecules in solution.

After a year of teaching at Harvard University, Dr. Zimm in 1951 joined the Research Department of the General Electric Company in Schenectady where he became interested in a variety of subjects, all of which he pushed ahead very vigorously and successfully. Thus he succeeded, by an ingenious photochemical modification of emulsion polymerization, to produce polystyrenes with very narrow molecular weight distributions. Later he worked out a rigorous statistical theory of the transition of randomly coiled macromolecules into helices and also made an important contribution to the mechanical relaxation spectrum theory of polymeric materials in solution and in the solid state by applying the normal mode treatment to the problem.

Introduction to the Symposium on Mechanics of Continua

HERSHEL MARKOVITZ, *Mellon Institute, Pittsburgh, Pennsylvania*

This is the second symposium on this subject held at a meeting of the Society of Rheology in recent years. I would like to express the hope that this has become enough of a habit so that we could venture to call it the Second Annual Symposium on the Mechanics of Continua. Those experimental rheologists who are interested in the basic questions of the field certainly need to become more aware of the theoretical work being done. Furthermore, such an Annual Symposium would provide the opportunity for the practitioners of theoretical mechanics to meet together to discuss their own work among themselves and also to find out from the experimental papers how actual materials behave.

The boundary value problems which need to be solved to get an idea of stress and deformation behavior in experimental situations are difficult enough when dealing with linear materials. Only the simplest of these can be solved exactly. Here Prof. Johnson presents some variational principles which allow approximate solutions in the case of some Reiner-Rivlin fluids. Ziegenhagen, Bird, and Johnson (in a paper of which only an abstract appears here) have used such an approach to discuss flow around a sphere.

The status of some of the basic "laws" of mechanics of continua is discussed by Prof. Ericksen and Dr. Bernstein. The former finds that the basic conservation laws appear to be inappropriate when dealing with liquid crystals which have a built in, distinguishable direction. The latter wonders whether the principle of determinism might not be a constitutive relationship rather than a universal law.

Dr. Coleman and Prof. Noll, for simple shearing motion, have derived from their general formulation a second-order theory with equations of the linear theory of viscoelasticity being adequate for the shearing stresses but with the existence of time dependent differences in the normal stresses.

On Variational Principles For Non-Newtonian Fluids*

M. W. JOHNSON, JR., *Department of Engineering Mechanics,
University of Wisconsin, Madison, Wisconsin*

1. Introduction

We consider steady flow of a non-Newtonian fluid where the inertia terms identically vanish or may be neglected. The boundary value problem is discussed in Section 2. In Section 3 two alternative variational principles are stated which have as Euler equations and natural boundary conditions all of the differential equations and boundary conditions of the boundary value problem. These principles require no conditions of admissibility on trial functions other than those of differentiability and symmetry of stress and rate of deformation tensors. From these fundamental theorems principles for velocities and stresses are derived by adding natural conditions as admissibility conditions. This approach of first formulating principles from which other desired principles easily follow by adding natural conditions as constraints has been used previously by Reissner for elasticity.^{1,2}

The treatment in Section 3 is essentially the same as that given previously in ref. 3 except that the boundary conditions are here taken in less general form in order to simplify the treatment while a non-homogeneous fluid is here considered in order to allow the application in Section 7 to be made to the time-smoothed Navier-Stokes' equations. In Section 4 we give some new results concerning the functions Γ and $\hat{\Gamma}$ defined by eqs. (2.6) and (3.2). In Section 5 we obtain sufficient conditions for the velocity and stress principles to be minimum

* This research was done at the U. S. Army Mathematics Research Center, University of Wisconsin, Madison, Wisconsin, under U. S. Army Contract No. DA-11-022-ORD-2059.

and maximum principles. The results obtained are stronger than in ref. 3 in that here behavior with regard to large variations is established while in ref. 3 only local behavior of the functionals near an extremum was considered. In Section 6 we apply the results of Section 5 to the generalized Newtonian fluid.

2. The Boundary Value Problem

We use Cartesian tensors, the summation convention, and $(-),_i = \partial(-)/\partial x_i$. Let v_i be rectangular Cartesian components of the velocity vector, τ_{ij} be components of the stress deviation tensor, p the pressure, and ρ the density. For steady flow of the incompressible isotropic Reiner-Rivlin fluid the differential equations consist of six stress-rate of deformation relations (ref. 4, p. 228),

$$\tau_{ij} = G_1 d_{ij} + G_2 d_{ik} d_{kj} \quad (2.1)$$

three equations of motion,

$$\tau_{ij,j} - p_{,i} + \rho f_i = \rho v_{i,j} v_j \quad (2.2)$$

and the incompressibility condition,

$$v_{i,i} = 0 \quad (2.3)$$

The rate of deformation tensor, d_{ij} , is given by

$$d_{ij} = 1/2(v_{i,j} + v_{j,i}) \quad (2.4)$$

In eq. (2.1) G_1 and G_2 are arbitrary functions of the invariants,

$$\text{II} = d_{ij} d_{ij}, \quad \text{III} = d_{ij} d_{jk} d_{ki} \quad (2.5)$$

of the rate of deformation tensor.

We limit consideration to stress-rate of deformation relations (2.1) which can be written in the form

$$\tau_{ij} = \partial \Gamma(d_{pq}, x_r) / \partial d_{ij} \quad (2.6)$$

where Γ is a given function of the components d_{ij} and of the coordinates x_i . We note that allowing Γ to be an explicit function of the x_i does not add difficulties in the developments to follow. We, therefore, include the possibility of an inhomogeneous fluid which proves useful in the application discussed in Section 7. We assume that Γ is a symmetric function of components d_{ij} so that $\partial \Gamma / \partial d_{ij} = \partial \Gamma / \partial d_{ji}$ and hence $\tau_{ij} = \tau_{ji}$.

We also limit consideration to flows where the inertia terms in the equation of motion (2.2) identically vanish or may be neglected.

$$\tau_{ij,j} - p_{,i} + \rho f_i = 0 \quad (2.7)$$

Therefore, the system of equations under consideration, (2.3)–(2.7), may contain nonlinear terms only in the stress-rate of deformation relations (2.6).

We assume that the bounding surface is fixed and consists of non-overlapping regions S_v and S_t on which the following conditions are prescribed:

$$S_v: v_i = \bar{v}_i(x_r) \quad (2.8)$$

$$S_t: \tau_{ij}n_j - pn_i = \bar{l}_i(x_r) \quad (2.9)$$

where \bar{v}_i and \bar{l}_i are given functions and n_j are the direction cosines of the normal to the bounding surface. We note that more general boundary conditions as well as a more general form of the equation of motion are considered in ref. 3.

3. The Variational Principles

Consider the functional

$$J = \iiint_V \{ [1/2(v_{i,j} + v_{j,i}) - d_{ij}] \tau_{ij} - \rho f_i v_i + \Gamma - p v_{i,i} \} dV \\ - \iint_{S_v} (\tau_{ij} n_j - p n_i) (v_i - \bar{v}_i) dS - \iint_{S_t} \bar{l}_i v_i dS \quad (3.1)$$

where the volume integral is over the entire volume of fluid and the surface integrals over the regions S_v and S_t . The volume is assumed to be smooth enough to allow application of Gauss' theorem. The variational equation $\delta J = 0$ has as its Euler equations the differential eqs. (2.3), (2.4), (2.6), and (2.7), and as natural boundary conditions eqs. (2.8) and (2.9). The only conditions of admissibility are that all quantities be sufficiently differentiable and that τ_{ij} and d_{ij} be symmetric tensors. That is, all quantities in expression (3.1) are to be varied independently. The proof of this theorem is similar to that given in ref. 3 and will not be repeated here.

An alternate variational theorem with no constraints can be obtained if the stress-rate of deformation relations (2.6) are solvable for the d_{ij} in the form

$$d_{ij} = \partial \hat{\Gamma}(\tau_{pq}, x_r) / \partial \tau_{ij} \quad (3.2)$$

Then the Legendre transformation,

$$\Gamma(d_{pq}, x_r) - d_{ij}\tau_{ij} = -\hat{\Gamma}(\tau_{pq}, x_r) \quad (3.3)$$

exists and the functional (3.1) takes the form

$$H = \iiint_V \{ 1/2(v_{i,j} + v_{j,i})\tau_{ij} - \rho f_i v_i - \hat{\Gamma} - p v_{i,i} \} dV \\ - \iint_{s_B} (\tau_{ij} n_j - p n_i)(v_i - \bar{v}_i) dS - \iint_{s_t} \bar{l}_i v_i dS \quad (3.4)$$

The equation $\delta H = 0$, the variations of all quantities being arbitrary, has the following Euler equations:

$$\begin{aligned} \tau_{ij,j} + \rho f_i - p_{,i} &= 0 \\ 1/2(v_{i,j} + v_{j,i}) - (\partial \hat{\Gamma} / \partial \tau_{ij}) &= 0 \\ v_{i,i} &= 0 \end{aligned} \quad (3.5)$$

and eqs. (2.8) and (2.9) as natural boundary conditions.

With d_{ij} defined by expression (2.4), we see that the Euler equations and natural boundary conditions are the differential equations and boundary conditions of the boundary value problem given by eqs. (2.3), (2.7), (2.8), (2.9), and (3.2). Again there are no admissibility conditions other than differentiability conditions and the condition that τ_{ij} be symmetric.

From these two fundamental principles other principles can be easily derived by using the general principle (see ref. 8, p. 233) that the addition of natural conditions as constraints does not change the stationary character of the functional.

A variational principle for velocities can be obtained by taking as admissibility conditions eqs. (2.3), (2.4), and (2.6) and boundary condition (2.8). The functional (3.1) becomes under these restrictions as follows:

$$J_r = \iiint_V \{ -\rho f_i v_i + \Gamma(1/2(v_{p,q} + v_{q,p}), x_r) \} dV - \iint_{s_t} \bar{l}_i v_i dS \quad (3.6)$$

The variational equation $\delta J_r = 0$ with variations restricted by the above admissibility conditions has as Euler equations the differential eq. (2.7) and as natural boundary condition (2.9). The natural conditions take the form

$$\rho f_i + \left(\frac{\partial \Gamma}{\partial d_{ij}} \right)_{,j} - p_{,i} = 0$$

$$S_i: \frac{\partial \Gamma}{\partial d_{ij}} n_j - p n_i = \bar{t}_i \quad (3.7)$$

The variational problem consisting of the equation $\delta J_v = 0$ and admissibility conditions (2.3) and (2.8) involves only variations of the velocity components v_i . Expressions (2.4) and (2.6) serve now to define d_{ij} and τ_{ij} .

A variational principle for stresses is obtained by taking as admissibility conditions differential eq. (2.7) and boundary condition (2.9). Use of Gauss's theorem on the terms $1/2(v_{i,j} + v_{j,i})\tau_{ij} - p_{,i}$ in the volume integral and use of the admissibility conditions transforms expression (3.4) into

$$H_R = - \iiint_V \hat{\Gamma} dV + \iint_{s_v} (\tau_{ij} n_j - p n_i) \bar{v}_i dS \quad (3.8)$$

The variational equation $\delta H_R = 0$ has as its Euler equations eqs. (2.3) and (3.2) and as its natural boundary condition (2.8). One can prove this directly by calculating δH_R using Lagrange multipliers to account for the admissibility conditions. Note that the roles of admissibility conditions and Euler equations are interchanged for the variational principles corresponding to functionals J_v and H_R .*

4. The Functions Γ and $\hat{\Gamma}$

For the Newtonian fluid eq. (2.1) takes the form

$$\tau_{ij} = 2\mu d_{ij} \quad (4.1)$$

where μ is the viscosity coefficient. The functions Γ and $\hat{\Gamma}$ are hence given by

$$\Gamma = \mu d_{ij} d_{ij}, \quad \hat{\Gamma} = (1/4\mu) \tau_{ij} \tau_{ij} \quad (4.2)$$

We note that, if Γ given by (4.2)₁ is inserted in functional (3.6), we obtain a functional and corresponding variational principle for veloci-

* The variational principles for velocities and stresses have been given previously by Hill¹² in a paper entitled "New Horizons in the Mechanics of Solids." The writer thanks the referee for bringing this paper to his attention. The special cases of the Newtonian fluid are discussed by Hill¹³ and of Bingham plastic by Prager.¹⁴

ties which according to Lamb⁵ is due to von Helmholtz. The principle corresponding to functional (3.6) generalizes this classical principle to non-Newtonian fluids. In the case of the Newtonian fluid the functional given by von Helmholtz represents the excess of dissipation over twice the rate at which work is being done by the body force f_i and the surface traction \bar{l}_i . For non-Newtonian fluids the functional, in general, apparently has no such physical interpretation.

Stress-rate of deformation relations for many non-Newtonian fluids can be written in the form of eq. (2.6). For the generalized Newtonian fluid⁹ the stress-rate of deformation relation is of the form

$$\tau_{ij} = 2\eta(\text{II})d_{ij} \quad (4.3)$$

where the viscosity coefficient η is a function of the second invariant. The function Γ is given by

$$\Gamma = \int^{\text{II}} \eta(\text{II}) d\text{II} \quad (4.4)$$

In order to obtain $\hat{\Gamma}$ we form from (4.3) the expression

$$\text{II}_\tau \equiv \tau_{ij}\tau_{ij} = 4\eta^2(\text{II})\text{II} \quad (4.5)$$

If (4.5) is solved for II in terms of II_τ , in the form $\text{II} = g(\text{II}_\tau)$, then we obtain

$$d_{ij} = [1/2\eta(g)]\tau_{ij} \quad (4.6)$$

so that $\hat{\Gamma}$ is given by

$$\hat{\Gamma} = \int^{\text{II}_\tau} [d\text{II}/4\eta(g)(\text{II})] \quad (4.7)$$

The constants of integration in (4.4), and (4.7) must be chosen so that transformation (3.3) holds in order that functions J and H have the same extremal values.

For the power model,⁹

$$\eta = m\text{II}^{(n-1)/2} \quad (4.8)$$

where n and m are given constants, we obtain

$$\Gamma = \frac{2m}{n+1} \text{II}^{(n+1)/2}, \quad \hat{\Gamma} = \frac{n}{n+1} \left(\frac{1}{2m} \right)^{1/n} \text{II}_\tau^{(n+1)/2n} \quad (4.9)$$

When there are no body forces, no region S_t , and for the generalized Newtonian model (4.3), functional (3.6) reduces to that given by Bird⁶ and used⁷ for the analysis of non-Newtonian flow around a sphere. A variational principle for the special case of the power law model was given earlier by Tomita.¹⁰

Corresponding to the general Reiner-Rivlin model (2.1) Γ must be a function of the invariants II and III. Therefore,

$$\tau_{ij} = 2(\partial\Gamma/\partial\text{II})d_{ij} + 3(\partial\Gamma/\partial\text{III})d_{ik}d_{kj} \quad (4.10)$$

Comparing eq. (4.10) with eq. (2.1) we obtain

$$\partial\Gamma/\partial\text{II} = \frac{1}{2}G_1(\text{II}, \text{III}), \quad \partial\Gamma/\partial\text{III} = \frac{1}{3}G_2(\text{II}, \text{III}) \quad (4.11)$$

The differential eqs. (4.11) can be solved for Γ if G_1 and G_2 satisfy the restrictions

$$\frac{1}{2}\partial G_1/\partial\text{III} = \frac{1}{3}\partial G_2/\partial\text{II} \quad (4.12)$$

$d\Gamma$ is then an exact differential and Γ is given by the following line integral:

$$\Gamma = \int^{(\text{II}, \text{III})} [\frac{1}{2}G_1 d\text{II} + \frac{1}{3}G_2 d\text{III}] \quad (4.13)$$

This result is due to R. B. Bird (private communication). It is not known at present whether or not restriction (4.12) is realistic.

5. Maximum and Minimum Principles

Let v_i , τ_{ij} , d_{ij} , and p now be solutions of the boundary value problem. The introduction of $v_i + \delta v_i$, $\tau_{ij} + \delta\tau_{ij}$, etc., into expressions (3.1) and (3.4) in place of v_i , τ_{ij} , etc., and expansion by Taylor's formula of Γ and $\hat{\Gamma}$ gives

$$J = J_0 + \delta J + J_2, \quad H = H_0 + \delta H + H_2 \quad (5.1)$$

where J_0 and H_0 are given by expressions (3.1) and (3.4). $\delta J = 0$ and $\delta H = 0$ since v_i , τ_{ij} , etc., are now solutions of the boundary value problem. Thus,

$$J = J_0 + J_2, \quad H = H_0 + H_2 \quad (5.2)$$

where the remainder terms are given by

$$\begin{aligned}
J_2 = \iiint_V \left\{ \frac{1}{2} (\delta v_{i,j} + \delta v_{j,i}) - \delta d_{ij} \right\} \delta \tau_{ij} \\
+ \frac{1}{2} \frac{\partial^2 \Gamma(\bar{d}_{pq}, x_r)}{\partial d_{ij} \partial d_{kl}} \delta d_{ij} \delta d_{kl} - \delta p \delta v_{i,i} \Big\} dV \\
- \iint_{S_v} \delta(\tau_{ij} n_j - p n_i) \delta v_i n_j dS \quad (5.3)
\end{aligned}$$

and

$$\begin{aligned}
H_2 = \iiint_V \left\{ \frac{1}{2} \delta(v_{i,j} + v_{j,i}) \delta \tau_{ij} \right. \\
\left. - \frac{1}{2} \frac{\partial^2 \hat{\Gamma}(\bar{\tau}_{pq}, x_r)}{\partial \tau_{ij} \partial \tau_{kl}} \delta \tau_{ij} \delta \tau_{kl} - \delta p \delta v_{i,i} \right\} dV \\
- \iint_{S_v} \delta(\tau_{ij} n_j - p n_i) \delta v_i n_j dS \quad (5.4)
\end{aligned}$$

where \bar{d}_{ij} and $\bar{\tau}_{ij}$ indicate replacement of d_{ij} and τ_{ij} by appropriate "intermediate" functions.

We are interested primarily in finding sufficient conditions such that $\delta J = 0$ and $\delta H = 0$ are either maximum or minimum problems; that is, so that under all admissible variations J_2 and H_2 should be either positive or negative. If admissibility conditions are those of the velocity principle, then the variations must satisfy the following conditions:

$$\begin{aligned}
\delta v_{i,i} &= 0 \\
\delta d_{ij} &= \frac{1}{2} (\delta v_{i,j} + \delta v_{j,i}) \\
S_r: \delta v_i &= 0
\end{aligned} \quad (5.5)$$

Introduction of conditions (5.5) into expression (5.3) reduces it to the form

$$J_2 = \iiint_V \frac{1}{2} \frac{\partial^2 \Gamma(\bar{d}_{pq}, x_r)}{\partial d_{ij} \partial d_{kl}} \delta d_{ij} \delta d_{kl} dV \quad (5.6)$$

From expression (5.6) we see that J_r attains a minimum (or maximum) at its extremum if the quadratic form $(\partial^2 \Gamma / \partial d_{ij} \partial d_{kl}) \delta d_{ij} \delta d_{kl}$ is positive (negative) definite for all \bar{d}_{pq} in the given domain of definition and for all variations.

For example, for the Newtonian fluid with Γ given by (2.9)₁ we obtain

$$\partial^2 \Gamma / \partial d_{ij} \partial d_{kl} = 2\mu \delta_{ik} \delta_{jl} \quad (5.7)$$

so that

$$J_2 = \iiint_V \mu \delta d_{ij} \delta d_{ij} dV \geq 0 \quad (5.8)$$

Thus, J_p attains an absolute minimum at its extremal value relative to arbitrarily large variations. This result establishes the uniqueness of slow flow of a Newtonian fluid.

On the other hand, if admissibility conditions are those of the stress variational principle, the variations must satisfy

$$\begin{aligned} \delta \tau_{ij,j} - \delta p_{,i} &= 0 \\ S_i: \delta(\tau_{ij} n_j - p n_i) &= 0 \end{aligned} \quad (5.9)$$

Use of Gauss' theorem in (5.4) gives

$$\begin{aligned} H_2 = \iiint_V \left\{ -\delta v_i \delta \tau_{ij,j} - \frac{1}{2} \frac{\partial^2 \hat{\Gamma}(\bar{\tau}_{pq}, x_\tau)}{\partial \tau_{ij} \partial \tau_{kl}} \delta \tau_{ij} \delta \tau_{kl} + \delta p_{,i} \delta v_i \right\} dV \\ + \iint_{S_i} \delta(\tau_{ij} n_j - p n_i) \delta v_i dS \end{aligned} \quad (5.10)$$

Use of expressions (5.9) reduces expression (5.10) to the following:

$$H_2 = \iiint_V \left\{ -\frac{1}{2} \frac{\partial^2 \hat{\Gamma}(\bar{\tau}_{pq}, x_\tau)}{\partial \tau_{ij} \partial \tau_{kl}} \delta \tau_{ij} \delta \tau_{kl} \right\} dV \quad (5.11)$$

We see that H_R takes on a minimum (maximum) at its extremal value if the quadratic form $-(\partial^2 \hat{\Gamma} / \partial \tau_{ij} \partial \tau_{kl}) \delta \tau_{ij} \delta \tau_{kl}$ is positive (negative) definite for all $\bar{\tau}_{pq}$ and for all variations.

For example, for slow flow of a Newtonian fluid,

$$\hat{\Gamma} = (1/4\mu) \tau_{ij} \tau_{ij} \quad (5.12)$$

and, hence,

$$H_2 = - \iiint_V (1/4\mu) \delta \tau_{ij} \delta \tau_{ij} dV \leq 0 \quad (5.13)$$

We conclude that H_R assumes an absolute maximum at its extremum value.

Under conditions given above where the minimal (or maximal) nature of either variational principle can be established, we are insured of the uniqueness of the solution. It is possible to show that the reciprocal principle is a maximum (minimum) principle under the same conditions that the velocity principle is a minimum (maximum) principle. To do this define the second variations $\delta^2 J$ and $\delta^2 H$ by replacing \bar{d}_{ij} and $\bar{\tau}_{ij}$ by the extremal values, d_{ij} and τ_{ij} , in expressions (5.3) and (5.4). Then, when admissibility conditions of the reciprocal principle are satisfied, we have from (5.11)

$$\delta^2 H_R = - \iiint_V \frac{1}{2} \frac{\partial^2 \hat{\Gamma}(\tau_{pq}, x_r)}{\partial \tau_{ij} \partial \tau_{kl}} \delta \tau_{ij} \delta \tau_{kl} dV \quad (5.14)$$

On the other hand, if the admissibility conditions (5.5) of the velocity principle are applied to expression (5.4), we obtain

$$\delta^2 H_V = \iiint_V \left\{ \delta d_{ij} \delta \tau_{ij} - \frac{1}{2} \frac{\partial^2 \hat{\Gamma}(\tau_{pq}, x_r)}{\partial \tau_{ij} \partial \tau_{kl}} \delta \tau_{ij} \delta \tau_{kl} \right\} dV \quad (5.15)$$

But, from eq. (3.2), for small variations,

$$\delta d_{ij} = \frac{\partial^2 \hat{\Gamma}(\tau_{pq}, x_r)}{\partial \tau_{ij} \partial \tau_{kl}} \delta \tau_{kl} \quad (5.16)$$

Comparing (5.14) and (5.15), we obtain

$$\delta^2 H_V = -\delta^2 H_R \quad (5.17)$$

which yields the desired conclusion. The second variations give only the behavior near the extremum but this is enough to establish the above result. Of course, the velocity principle yields a minimum at an extremum and the stress principle a maximum only if $\delta^2 J_v \geq 0$ or $\delta^2 H_R \leq 0$ for all variations.

Under conditions sufficient to insure that the velocity principle is a minimum principle and the reciprocal principle is a maximum principle, we conclude that the extremum value of J has the following upper and lower bounds:

$$H_R \leq J_0 \leq J_V \quad (5.18)$$

where H_R and J_v are functionals of any admissible trial functions for the respective variational principles. This result should prove useful in estimating the accuracy of approximate solutions made by use of the

Ritz-method. Result (5.18) has been established for Newtonian fluids by expressions (5.8) and (5.13).

6. Minimum and Maximum Principles for the Generalized Newtonian Fluid

With Γ given by (4.4), we have

$$\frac{\partial^2 \Gamma}{\partial d_{ij} \partial d_{kl}} = 2\eta \delta_{ik} \delta_{jl} + 4(\partial\eta/\partial\Pi) d_{ij} d_{kl} \quad (6.1)$$

Hence,

$$J_2 = \iiint_V \left\{ \eta(\bar{\Pi}) \delta d_{ij} \delta d_{ij} + 2[\partial\eta(\bar{\Pi})/\partial\Pi] (\bar{d}_{ij} \delta d_{ij})^2 \right\} dV \quad (6.2)$$

Expression (6.2) yields the following conclusions:

(1) The slow flow of a dilatant fluid ($\eta > 0$, $(\partial\eta/\partial\Pi) > 0$) is unique. The velocity variational principle is a minimum principle and the reciprocal principle is a maximum principle.

(2) The slow flow of a pseudoplastic fluid ($\eta > 0$, $(\partial\eta/\partial\Pi) < 0$) is unique, the velocity principle is a minimum principle, and the stress principle a maximum principle if throughout the region of flow the following condition holds:

$$\eta + 2(\partial\eta/\partial\Pi)\Pi > 0 \quad (6.3)$$

Result (1) is evident. Theorem (2) follows upon application of Schwartz's inequality to the second term of expression (6.2) to obtain

$$\eta \delta d_{ij} \delta d_{ij} - 2 \left(-\frac{\partial\eta}{\partial\Pi} \right) (\bar{d}_{ij} \delta d_{ij})^2 \geq \left[\eta - 2 \left(-\frac{\partial\eta}{\partial\Pi} \right) \bar{d}_{kl} \bar{d}_{kl} \right] \delta d_{ij} \delta d_{ij} \quad (6.4)$$

We note that it may be possible to obtain conditions weaker than (6.3) by methods more refined than those used in this paper.

Let us apply these theorems to the power law model which is given by expression (4.8). Values of n greater than unity correspond to dilatant behavior while values of n less than unity to pseudoplastic. Condition (6.3) becomes simply $n > 0$, which is apparently obeyed by most real fluids (see ref. 9, p. 13).

7. Application to the Time-Smoothed Navier-Stokes' Equations

An interesting application of the above results can be made to the time-smoothed equations for the Newtonian fluid. The time-smoothed equations for steady mean flow can be taken in the form

$$\begin{aligned}\bar{v}_{i,i} &= 0 \\ \bar{\tau}_{ij} &= 2\mu\bar{d}_{ij}, \quad \bar{d}_{ij} = \frac{1}{2}(\bar{v}_{i,j} + \bar{v}_{j,i}) \\ \rho\bar{v}_{i,j}\bar{v}_j &= \bar{\tau}_{ij,j} - \bar{p}_{,i} + \rho\bar{f}_i - R_{ij,j}\end{aligned}\quad (7.1)$$

where bars here indicate time-smoothed quantities and R_{ij} are the components of Reynolds' stress. It has been noted by Rivlin¹¹ that the turbulent Newtonian fluid may, for certain purposes, be regarded as a non-Newtonian fluid. Insofar as the time-smoothed equations are concerned this can be shown by the following simple transformation. Setting $\bar{P}_{ij} = \bar{\tau}_{ij} - R_{ij}$, we can write system (7.1) as follows:

$$\bar{v}_{i,i} = 0, \quad \bar{d}_{ij} = \frac{1}{2}(\bar{v}_{i,j} + \bar{v}_{j,i}) \quad (7.2)$$

$$\rho\bar{v}_{i,j}\bar{v}_j = -\bar{p}_{,i} + \bar{P}_{ij,j} + \rho\bar{f}_i \quad (7.3)$$

$$\bar{P}_{ij} = 2\mu\bar{d}_{ij} - R_{ij} \quad (7.4)$$

In order to complete the system of equations, some expression for R_{ij} must be added. If this is done, if the term $\rho\bar{v}_{i,j}\bar{v}_j$ in (7.3) identically vanishes for the flow considered or may be neglected, and if eq. (7.4) can be put in the form (2.6), then the equations are of the same form as for the non-Newtonian fluid considered in Section 2 and the variational principles discussed here may be applied.

For example, for Prandtl's mixing length theory we set

$$R_{ij} = \rho l^2 (2\bar{d}_{ki}\bar{d}_{kl})^{1/2} \bar{d}_{ij} \quad (7.5)$$

We note that the mixing length l is a function of position and hence the non-Newtonian fluid corresponding to the turbulent Newtonian fluid is not homogeneous. In this case eq. (7.4) can be written as

$$\bar{P}_{ij} = \frac{\partial \Gamma(\bar{d}_{pq}, x_r)}{\partial \bar{d}_{ij}} \quad (7.6)$$

where

$$\Gamma = \mu\bar{d}_{ij}\bar{d}_{ij} - (\sqrt{2}/3)\rho l^2 (\bar{d}_{ij}\bar{d}_{ij})^{3/2} \quad (7.7)$$

Note Added in Proof: Equation (2.6) and condition (4.12) for the existence of the potential Γ were given by Reiner [*Am. J. Math.*, **67**, 350 (1945)]. The writer thanks Professor Reiner for bringing this to his attention.

References

1. Reissner, E., *J. Math. Phys.*, **32**, 129 (1953).
2. Reissner, E., *Proc. Symp. Appl. Math.*, **8**, 1 (1958).
3. Johnson, M. W., Jr., *Phys. Fluids*, **3**, 871 (1960).
4. Truesdell, C., *J. Rational Mech. Anal.*, **1**, 125 (1952).
5. Lamb, H., *Hydrodynamics*, 6th ed., Dover, N. Y., 1932, pp. 617-619.
6. Bird, R. B., *Phys. Fluids*, **3**, 539 (1960).
7. Ziegenhagen, A. J., R. B. Bird, and M. W. Johnson, Jr., *Trans. Soc. Rheology*, **5**, 47 (1961).
8. Courant, R., and D. Hilbert, *Methods of Mathematical Physics*, Vol. 1, Interscience, N. Y., 1953.
9. Bird, R. B., W. E. Stewart, and E. N. Lightfoot, *Transport Phenomena*, Wiley, N. Y., 1960.
10. Tomita, Y., *Bull. Japan Soc. Mech. Engrs.*, **2**, 469 (1959).
11. Rivlin, R. S., *Quart. Appl. Math.*, **15**, 212 (1957); **17**, 447 (1960).
12. Hill, R., *J. Mech. and Phys. Solids*, **5**, 66 (1956).
13. Hill, R., *Quart. J. Mech. Appl. Math.*, **9**, 313 (1956).
14. Prager, W., *R. von Mises Presentation Volume*, Academic Press, New York, 1954, pp. 208-216.

Synopsis

Two fundamental variational principles, related by a Legendre transformation, are given which have as their Euler-Lagrange equations and natural boundary conditions *all* of the differential equations and boundary conditions of the problem of the steady flow of an incompressible non-Newtonian fluid where the inertia terms identically vanish or may be neglected. By restricting the class of admissible functions a principle for velocities and a principle for stresses is obtained from the fundamental principles. The treatment is essentially the same as that given previously by the writer except that here an inhomogeneous fluid is considered while simpler boundary conditions are considered in order to simplify the analysis. New results on conditions for minimum and maximum principles are given and the results applied to the generalized Newtonian fluid. It is also shown that the time-smoothed Navier-Stokes' equations can be transformed to the form of the Euler-Lagrange equations of the variational principles given.

Conservation Laws for Liquid Crystals*

J. L. ERICKSEN, *The Johns Hopkins University, Baltimore, Maryland*

I. Introduction

That liquid crystals exist has been known since about 1888, when Reinitzer¹ discussed some of their properties. However, continuum theories of their mechanical behavior are still in a rather unsettled state. The firmest part seems to be a partial theory, the hydrostatic theory summarized by Frank.² For purposes of formulating and assessing dynamical theories, it would be desirable to have available appropriate forms of the laws of conservation or balance of mass, linear momentum, energy, and moment of momentum. We present reasoning and analyses leading to unconventional forms of these which seem to us appropriate, assuming that the aforementioned hydrostatic theory, or a natural generalization thereof, adequately describes static behavior.

II. General Conservation Laws

We begin with rather general forms of conservation laws discussed by Grad:³

$$\frac{d}{dt} \int_V \rho dV = 0 \quad (1)$$

$$\frac{d}{dt} \int_V p_i dV = \oint_S t_{ij} ds_j + \int_V f_i dV \quad (2)$$

$$\frac{d}{dt} \int_V e dV = \oint_S u_i ds_i + \int_V g dV \quad (3)$$

$$\frac{d}{dt} \int_V m_{ij} dV = \oint_S v_{ijk} ds_k + \int_V h_{ij} dV \quad (4)$$

* This work was supported by a grant from the National Science Foundation.

Here V denotes any material volume with boundary s , ds_i being the vector element of area, directed outward relative to V ; ρ , p_i , e , and $m_{ij} = -m_{ji}$ are, respectively, the densities of mass, linear momentum, and bivector moment of momentum. The surface integrands can be thought of as fluxes of these quantities, the volume integrands as volume source densities. As is customary, we call t_{ij} the stress tensor and f_i the body force. As will be discussed, eq. (2) only partially describes conservation of linear momentum. Equation (16) given below supplements it.

III. Packet Dynamics

Molecular constitution of liquid crystals is discussed, e.g., by Chatelain.⁴ The name is applied to a variety of high polymers having rather diverse properties. For our purposes, an oversimplified description will suffice. Such a liquid consists of tiny, cylindrically symmetric packets of rodlike molecules. Within a packet, the molecules are parallel to each other. They are fairly free to move parallel to themselves so the length of a packet is somewhat variable. The orientation of the molecules can change in a rather systematic manner as we move from packet to packet.

We idealize a moving packet as a line segment of variable direction and length, having mass M . The mass per unit length need not be uniform. We may then represent the packet by equations of the form

$$y_i = y_i(\lambda, t) = x_i(t) + \lambda n_i(t) \quad (5)$$

Here y_i represents any point on the segment at time t , x_i is a particular point, n_i is a variable vector indicating the direction of the segment, and λ is a parameter taking on values in some fixed interval I . In terms of a mass density $\mu(\lambda)$

$$M = \int_I \mu(\lambda) d\lambda$$

There is no loss in generality in taking

$$\int_I \lambda \mu(\lambda) d\lambda = 0 \quad (6)$$

$$\int_I \lambda^2 \mu(\lambda) d\lambda = M \quad (7)$$

That is, if these are not satisfied for one choice of λ , they are for $\lambda' = a\lambda + b$, where a and b are constants. These transformations preserve the form of eq. (5). When eq. (6) holds

$$\int_I \mu(\lambda) y_i(\lambda, t) d\lambda = M x_i(t) \quad (8)$$

so $x_i(t)$ represents the center of mass. We also have

$$\int_I \lambda \mu(\lambda) y_i(\lambda, t) d\lambda = M n_i(t) \quad (9)$$

By straightforward calculations, we obtain for the total linear momentum, kinetic energy, and moment of momentum of the packet, respectively,

$$\int_I \mu \frac{\partial y_i}{\partial t} d\lambda = M \dot{x}_i \quad (19)$$

$$\frac{1}{2} \int_I \mu \frac{\partial y_i}{\partial t} \frac{\partial y_i}{\partial t} d\lambda = \frac{1}{2} M (\dot{x}_i \dot{x}_i + \dot{n}_i \dot{n}_i) \quad (11)$$

$$\int \mu y_{[i} \frac{\partial y_{j]}{\partial t} d\lambda = M (x_{[i} \dot{x}_{j]} + n_{[i} \dot{n}_{j]}) \quad (12)$$

where the dots denote time derivatives and the square bracket denotes the antisymmetric part. For example,

$$x_{[i} \dot{x}_{j]} = \frac{1}{2} (x_i \dot{x}_j - x_j \dot{x}_i)$$

It seems natural to identify \dot{x}_i with the macroscopically observed velocity of the fluid and to introduce a vector field $n_i(x_j, t)$ identifiable with the n_i used above. Comparing eqs. (2)–(4) with eqs. (10)–(12) leads us to write

$$p_i = \rho \dot{x}_i \quad (13)$$

$$e = \frac{1}{2} \rho (\dot{x}_i \dot{x}_i + \dot{n}_i \dot{n}_i) + \rho \epsilon \quad (14)$$

$$m_{ij} = \rho (x_{[i} \dot{x}_{j]} + n_{[i} \dot{n}_{j]}) \quad (15)$$

where ϵ denotes the internal energy per unit mass, internal energy being interpreted as usual as total energyless kinetic energy. Ericksen⁵ uses precisely these equations in developing a theory of anisotropic fluids which is too oversimplified to describe liquid crystals.

He uses a dumbbell molecule model to motivate them. He also employs equations of the form

$$\frac{d}{dt} \int_V \rho \dot{n}_i dV = \int_V k_i dV$$

to supplement eqs. (1)–(4). We adopt a generalization.

$$\frac{d}{dt} \int_V \rho \dot{n}_i dV = \oint_S w_{ij} ds_j + \int_V k_i dV \quad (16)$$

Oseen⁶ employs a similar equation in his theory of liquid crystals. In terms of our model, eq. (16) describes motion of the segment about its center of mass. In continuum equations, the dot indicates the material derivative.

The segment model is useful in making a first estimate of effects of external fields. Suppose, for example, that we are interested in the influence of the earth's gravitational field on the fluid. If we make the customary approximation that the gravitational force per unit mass is a constant, say θ_i and ignore all other forces, we would have

$$\mu \frac{\partial^2 y_i}{\partial t^2} = \mu \theta_i$$

Hence, using eqs. (6), (7), (8), and (9)

$$M \ddot{x}_i = \int_I \mu \frac{\partial^2 y_i}{\partial t^2} d\lambda = \theta_i \int_I \mu d\lambda = M \theta_i$$

$$M \ddot{n}_i = \int_I \lambda \mu \frac{\partial^2 y_i}{\partial t^2} d\lambda = \theta_i \int_I \lambda \mu d\lambda = 0$$

suggesting that this force contributes the usual term $\rho \theta_i$ to f_i but contributes nothing to the vector k_i in eq. (16).

IV. Hydrostatics

The hydrostatic theory of liquid crystals is based on the assumption that the free energy per unit volume ψ is a function of unit vector m_i and its gradients, being a quadratic function of the gradients. Equilibrium equations are obtained from the variational equation

$$\delta \int_V \psi dV = 0 \quad (17)$$

where m_i is varied subject to the conditions that m_i remain a unit vector and $\delta m_i = 0$ on the boundary. Nothing other than m_i is varied. In terms of our model, m_i is proportional to n_i , and changes

in length of n_i are assumed to be insignificant. Principles of virtual work somewhat similar to that discussed below are sometimes used.

For our purposes, it is desirable to generalize this theory. We assume that

$$\varphi = \psi/\rho = \varphi(\rho; n_i; n_{j,k}, T) \quad (18)$$

where T denotes temperature. When n_i and $n_{j,k}$ are missing, this reduces to the type of equation generally assumed for ordinary fluids. Simplifications such as the assumptions of incompressibility or of the constancy of the magnitude of n_i are frequently reasonable and useful. However, we exclude them since they would only complicate our development. We generalize eq. (17) by varying n_i , ρ , and x_i independently subject to the condition

$$\delta\rho + (\rho\delta x_j)_{;j} = 0 \quad (19)$$

which states that the quantity of matter is not varied. The temperature is considered to be a fixed constant. By calculations given in the Appendix, we find that we can write

$$\delta \int_V \rho \varphi dV = \oint_S (\alpha_{ij} \delta x_i + \beta_{ij} \Delta n_i) ds_j - \int_V [\alpha_{ij,j} \delta x_i + (\beta_{ij,j} + \gamma_i) \Delta n_i] dV \quad (20)$$

where

$$\alpha_{ij} \equiv -\rho^2 \frac{\partial \varphi}{\partial \rho} \delta_{ij} - \rho \frac{\partial \varphi}{\partial n_{k,j}} n_{k,i} \quad (21)$$

$$\beta_{ij} \equiv \rho \frac{\partial \varphi}{\partial n_{i,j}} \quad (22)$$

$$\gamma_i = -\rho \frac{\partial \varphi}{\partial n_i} \quad (23)$$

and Δn_i is the variational equivalent of \dot{n}_i ,

$$\Delta n_i \equiv \delta n_i + n_{i,j} \delta x_j \quad (24)$$

Considering the form of eq. (20), it is natural to assume a principle of virtual work of the form

$$\delta \int_V \rho \varphi dV = \oint_S (a_i \delta x_i + b_i \Delta n_i) ds + \int_V (c_i \delta x_i + d_i \Delta n_i) dV \quad (25)$$

where a_j , b_j , c_j , and d_j represent generalized surface and body forces applied to the fluid. This is tantamount to assuming the differential equations of equilibrium

$$\alpha_{ij,j} + c_i = 0 \quad (26)$$

$$\beta_{ij,j} + \gamma_i + d_i = 0 \quad (27)$$

together with the equations

$$\alpha_{ij} ds_j = a_i ds \quad (28)$$

$$\beta_{ij} d\delta_j = b_i ds \quad (29)$$

on the boundary.

For an ordinary fluid in equilibrium, α_{ij} reduces to the usual stress tensor, coinciding with the t_{ij} occurring in eq. (2). Out of equilibrium, the two differ, $t_{ij} - \alpha_{ij}$ being the viscous stress. This, and eqs. (2), (16), (26), and (27) suggest that we should set

$$t_{ij} = \alpha_{ij}, \quad f_i = c_i \quad (30)$$

$$w_{ij} = \beta_{ij}, \quad k_i = \gamma_i + d_i \quad (31)$$

for liquid crystals in equilibrium. Out of equilibrium, it might be expected that the occurrence of forces of a viscous nature will arise so that some or all of these equations may become inappropriate.

For eq. (25) to be consistent with eq. (17) we must have $d_i = 0$. From eq. (31) and the remarks at the end of Section III, this condition should hold as a good approximation if the applied body forces result purely from the gravitational field of the earth.

V. Linear Momentum

Conservation of linear momentum is partially described by eq. (2), with p_i given by eq. (13), viz.

$$\frac{d}{dt} \int_V \rho \dot{x}_i dV = \oint_S t_{ij} ds_j + \int_V f_i dV \quad (32)$$

which is a conventional form. An unusual feature is that the stress tensor t_{ij} will generally not be symmetric, as is fairly obvious from eqs. (21) and (30). The customary differential equations

$$\rho \ddot{x}_i = t_{ij,j} + f_i \quad (33)$$

follow from eqs. (1) and (32).

Along with eq. (32), we have the rather similar equation involving n_i , given as eq. (16). An equivalent differential form is

$$\rho \dot{n}_i = w_{ij,j} + k_i \quad (34)$$

The hydrostatic analysis suggests that it may be useful to write

$$k_i = r_i + d_i \quad (35)$$

where r_i represents an intrinsic part, given by

$$r_i = \gamma_i \quad (36)$$

in equilibrium, and d_i represents an extrinsic part.

VI. Energy

Clues as to an appropriate form of the law of conservation of energy are contained in the principle of virtual work, eq. (25). First, the internal energy per unit mass ϵ should be given in terms of φ by the usual thermodynamic equation

$$\epsilon = \varphi + T\eta = \varphi - T\partial\varphi/\partial T$$

where η denotes entropy per unit mass. Statically, the kinetic energy vanishes, so that $\rho\epsilon = e = \text{total energy}$. We thus have

$$\begin{aligned} \delta \int_V e dV &= \rho \int_V \rho(\varphi + T\eta) dV \\ &= \delta \int_V \rho \varphi dV + T \delta \int_V \rho \eta dV \\ &= \delta \int_V \rho \varphi dV + \delta Q \end{aligned}$$

where δQ is interpretable as heat added to the fluid in the virtual displacement, assumed to take place reversibly.

Second, using eqs. (28)–(31), we have

$$\oint_S (a_i \delta x_i + b_i \Delta n_i) ds = \oint_S (t_{ij} \delta x_i + w_{ij} \Delta n_i) ds_j$$

Third, the rate at which heat is added to a material is commonly written as

$$- \oint_S q_i ds_i + \int_V q dv$$

where q_i is the heat flux vector, the volume integral representing any volume source of heat. A natural extrapolation of these eqs. (14) and (30) gives the dynamical energy equation

$$\begin{aligned}
\frac{d}{dt} \int_V \epsilon dV &= \frac{d}{dt} \int_V [\rho \epsilon + {}^{1/2} \rho (\dot{x}_i \dot{x}_i + \dot{n}_i \dot{n}_i)] dV \\
&= \oint_V (t_{ij} \dot{x}_i + w_{ij} \dot{n}_i - q_j) ds_j + \int_V (f_i \dot{x}_i + d_i \dot{n}_i + q) dV
\end{aligned} \quad (37)$$

which would be obtained from eq. (3) by setting

$$\begin{aligned}
u_j &= t_{ij} \dot{x}_i + w_{ij} \dot{n}_i - q_j \\
g &= f_i \dot{x}_i + d_i \dot{n}_i + q
\end{aligned}$$

From eq. (37) one can deduce an equivalent differential form. Using eqs. (1) (33) and (34), one can simplify this to obtain

$$\rho \dot{\epsilon} = t_{ij} \dot{n}_{i,j} + w_{ij} \dot{n}_{i,j} - q_{j,j} - r_i \dot{n}_i - q \quad (38)$$

The conventional form is obtained by setting $w_{ij} = r_i = 0$. Ericksen⁵ uses eq. (38) with $w_{ij} = 0$, $r_i \neq 0$ for a simple theory of anisotropic fluids.

VII. Moment of Momentum

Ordinarily, the law of conservation of moment of momentum is equivalent to the statement that the stress tensor is symmetric. For liquid crystals, we have noted that the stress is generally not symmetric.

Statically, this law should reflect the fact that all torques are in balance. Again statically, this statement seems to be equivalent to the statement that the free energy is unaffected by rigid motions. At least this is true in nonlinear elasticity theory, as is discussed by Murnaghan⁷ and Noll (§16),⁸ and in Toupin's⁹ theory of elastic dielectrics (§10). We thus explore what ensues from the statement that φ is unaffected by rigid motions. Formally we should have

$$D\varphi \equiv \varphi(\rho; n'_i; n'_{j,k}; T) - \varphi(\rho; n_i; n_{j,k}; T) = 0 \quad (39)$$

whenever the primed and unprimed variables are so related that

$$\begin{aligned}
n'_i &= R_{ij} n_j \\
n'_{i,j} &= R_{ik} R_{jp} n_{k,p}
\end{aligned} \quad (40)$$

where R_{ij} represents any rigid rotation,

$$R_{ij} R_{ik} = \delta_{jk}, \quad \det. R_{ij} = 1,$$

Simple forms of φ used in studying hydrostatic behavior of liquid crystals satisfy eq. (39).

Fix n_i and consider eq. (39) for arbitrary infinitesimal rotations

$$R_{ij} = \delta_{ij} + \Omega_{ij}, \quad \Omega_{ij} = -\Omega_{ji}, \quad \Omega_{ij}\Omega_{kl} \approx 0$$

From eq. (40), we have approximately

$$\begin{aligned} n'_i - n_i &= \Omega_{ij}n_j \\ n'_{i,j} - n_{i,j} &= \Omega_{ik}n_{k,j} + \Omega_{jk}n_{i,k} \end{aligned} \quad (41)$$

From eqs. (39) and (41)

$$\begin{aligned} D\varphi &\approx \frac{\partial\varphi}{\partial n_i} (n'_i - n_i) + \frac{\partial\varphi}{\partial n_{i,j}} (n'_{i,j} - n_{i,j}) \\ &= \left[\frac{\partial\varphi}{\partial n_i} n_j + \frac{\partial\varphi}{\partial n_{i,k}} n_{j,k} + \frac{\partial\varphi}{\partial n_{k,j}} n_{i,k} \right] \Omega_{ij} \\ &= 0 \end{aligned}$$

for arbitrary antisymmetric Ω 's. In other words, the tensor within the square bracket must be symmetric. Using eqs. (21)–(23), this condition can be written

$$\gamma_j n_i - \gamma_i n_j + \alpha_{ij} - \alpha_{ji} + \beta_{ik} n_{j,k} - \beta_{jk} n_{i,k} = 0$$

Since eqs. (30), (31), and (36) also hold in equilibrium, we could also write this as

$$r_j n_i - r_i n_j + t_{ij} - t_{ji} + w_{ik} n_{j,k} - w_{jk} n_{i,k} = 0 \quad (42)$$

when $w_{ij} = r_j = 0$, this reduces to the conventional statement that the stress is symmetric, which is customarily assumed to hold in or out of equilibrium. It thus seems reasonable to assume that eq. (42) holds in dynamical situations.

From eqs. (4) and (15), one can deduce the differential equations

$$\rho(x_{[i}\ddot{x}_{j]} + n_{[i}\ddot{n}_{j]}) = n_{ijk,k} + h_{ij}$$

Using eqs. (33) and (34) to eliminate \ddot{x}_i and \ddot{n}_j , we get

$$x_{[i}f_{j]} + x_{[i}t_{j]k,k} + n_{[i}k_{j]} + n_{[i}w_{k,k]} = v_{ijk,k} + h_{ij} \quad (43)$$

Now

$$\begin{aligned} x_{[i]t_{jk},k} &= {}^{1/2}(x_{it_{jk},k} - x_{jt_{ik},k}) \\ &= {}^{1/2}(x_{it_{jk}} - x_{jt_{ik}})_{,k} + {}^{1/2}(t_{ij} - t_{ji}) \end{aligned}$$

Similarly,

$$n_{[i]w_{jk},k} = {}^{1/2}(n_{iw_{jk}} - n_{jw_{ik}})_{,k} + {}^{1/2}(n_{jkw_{ik}} - n_{ikw_{jk}}).$$

Making these substitutions in eq. (43) and using eqs. (35) and (42), we obtain

$$(x_{[i]t_{jk}} + r_{[i]w_{jk}})_{,k} + x_{[i]f_{jk}} + n_{[i]d_{jk}} = v_{ijk} + h_{ij}$$

suggesting that

$$v_{ijk} = x_{[i]t_{jk}} + n_{[i]w_{jk}}$$

$$h_{ij} = x_{[i]f_{jk}} + n_{[i]d_{jk}}$$

We might have started with these relations, arguing that v_{ijk} should represent the torque associated with surface forces and h_{ij} the torque associated with extrinsic body forces, which is one way to interpret these equations. We could then deduce eq. (42).

The integral equivalent of eq. (42) is then

$$\begin{aligned} \frac{d}{dt} \int_V \rho(x_{[i]\dot{x}_{jk}} + n_{[i]\dot{n}_{jk}})dV &= \oint_S (x_{[i]t_{jk}} + n_{[i]w_{jk}})ds_k \\ &+ \int_V (x_{[i]f_{jk}} + n_{[i]d_{jk}})dV \end{aligned} \quad (44)$$

VIII. Appendix

To verify eq. (20), we recall eq. (19),

$$\delta\rho + (\rho\delta x_{j,j}) = \delta\rho + \rho_{,j}\delta x_j + \rho\delta x_{j,j} = 0 \quad (45)$$

and note that

$$\begin{aligned} \delta n_{j,k} + n_{j,k,i}\delta x_i &= (\delta n_j + n_{j,i}\delta x_i)_{,k} - n_{j,i}\delta x_{i,k} \\ &= \Delta n_{j,k} - n_{j,i}\delta x_{i,k} \end{aligned} \quad (46)$$

where Δn_i is given in the parentheses or by eq. (24). Now, using the divergence theorem and eq. (45),

$$\begin{aligned} \delta \int_V \rho\varphi dV &= \oint_S \rho\varphi\delta x_i ds_i + \int_V \delta(\rho\varphi)dV \\ &= \int_V \rho(\delta\varphi + \varphi_{,i}\delta x_i)dV \end{aligned}$$

Using eqs. (45), (46), and (21)–(23),

$$\begin{aligned}
 \rho(\delta\varphi + \varphi_{,i}\delta x_i) &= \rho \left[\frac{\partial\varphi}{\partial\rho} (\delta\rho + \rho_{,i}\delta x_i) + \frac{\partial\varphi}{\partial n_j} (\delta n_j + n_{j,i}\delta x_i) \right. \\
 &\quad \left. + \frac{\partial\varphi}{\partial n_{j,k}} (\delta n_{j,k} + n_{j,k,i}\delta x_i) \right] \\
 &= \rho \left[-\rho \frac{\partial\varphi}{\partial\rho} \delta x_{j,j} - \frac{1}{\rho} \gamma_j \Delta n_j \right. \\
 &\quad \left. + \frac{\partial\varphi}{\partial n_{j,k}} (\Delta n_{j,k} - n_{j,i}\delta x_{i,k}) \right] \\
 &= \alpha_{ik}\delta x_{i,k} - \gamma_j \Delta n_j + \beta_{jk}\Delta n_{j,k} \\
 &= (\alpha_{ik}\delta x_i + \beta_{jk}\Delta n_j)_{,k} - \alpha_{ik,k}\delta x_i - (\beta_{jk,k} + \gamma_j)\Delta n_j
 \end{aligned}$$

Integrating both sides over V and using the divergence theorem, we obtain eq. (20).

IX. Conclusions

We have presented reasoning and analyses leading to unconventional forms of the laws of conservation which seem to us appropriate for liquid crystals. Integral versions of those proposed are given as eqs. (1), (16), (32), (37), and (44). They are consistent with and extrapolated from a generalization of the existing hydrostatic theory.

Oseen's⁶ rather inexplicit dynamical theory does not fit very neatly into this framework. Reduced to the static case, his theory is more complex than the static theory here considered. Virtually nothing is known about its predictions. The earlier theory of Anzelius,¹⁰ which is better developed, employs conservation laws somewhat similar to those discussed above. We have attempted to improve upon his versions. His theory is criticized by Oseen.⁶ We feel that these investigations, combined with the ideas contained here, should be helpful as guides in formulating new dynamical theories.

By introducing suitable assumptions as to how ϵ , t_{ij} , etc., are affected by superimposing rigid motions, one can deduce from our version of the law of conservation of energy all other conservation laws here discussed. It would make this paper unduly long to discuss this fact in detail.

References

1. Reinitzer, F., *Wien. Monatssh. Chem.*, **9**, 421 (1888).
2. Frank, F. C., *Discussions Faraday Soc.*, **25**, 19 (1958).
3. Grad, H., *Comm. Pure Appl. Math.*, **5**, 455 (1952).
4. Chatelain, P., *Bull. soc. Franç. minéral. et crist.*, **77**, 323 (1954).
5. Ericksen, J. L., *Arch. Rational Mech. Anal.*, **4**, 231 (1960).
6. Oseen, C. W., *Trans. Faraday Soc.*, **29**, 883 (1933).
7. Murnaghan, F. D., *Am. J. Math.*, **59**, 235 (1937).
8. Noll, W., *J. Rational Mech. Anal.*, **4**, 3 (1955).
9. Toupin, R. A., *J. Rational Mech. Anal.*, **5**, 849 (1956).
10. Anzelius, A., *Uppsala Univ. Årsskr., Mat. och Naturvet*, **1931**, 1.

Synopsis

Commonly used forms of the laws of conservation of linear momentum, moment of momentum, and energy seem inadequate for describing liquid crystals. We present reasoning which leads to forms which seem more appropriate.

Remarks on Materials of the Rate Type and the Principle of Determinism

B. BERNSTEIN, *U. S. Naval Research Laboratory, Washington, D.C.*

In the more classical phenomenological theories of matter,¹ parameters which describe the behavior of a material react instantaneously to changes in other parameters. In formulating the constitutive relations for such materials, one writes a set of functions relating these parameters, so that when the additional physical principles, such as conservation of mass, momentum, moment of momentum, energy, and charge, are adjoined one obtains a determinate mathematical system and is able to formulate and solve problems. In the theory of elasticity, for example, stress is expressed as a function of strain or of displacement gradients and perhaps of entropy. However, such theories, though they have found wide and successful application, are not general enough to describe many observed phenomena such as relaxation and creep. A wider class of constitutive relations is required for the phenomenological description of many materials, such as plastics, now not only observed in the laboratory but used in extensive commercial application. With these considerations in mind there have arisen theories of materials with memory.

Restricting ourselves to mechanical theories, we say that a material with memory is one for which the stress at a given time at a given point of a given material body depends upon the history of the motion of the body. Theories of this type were presented by Volterra,² by Green and Rivlin,³⁻⁵ and by Noll.⁶ The equations of linear viscoelasticity in integral form⁷ constitute a theory of this sort. On the other hand, there exist theories of materials of the rate type such as linear viscoelasticity in the differential equation form,⁷ hypoelasticity, and others such as given by Noll.⁸ Theories of the rate type are known to have been formulated as early as 1867.⁹

The purpose of our discussion is to examine some gaps in the formulation of theories of the rate type. We wish in particular to ask if it

is desirable in general to apply to these theories the principle of determinism as formulated by Noll in 1958.⁶ To this end, we cite some of the content of Noll's work in the next four paragraphs.

If we wish to let the present stress at a given point of a given body depend on the history of the entire motion of that body up to the present time, we say that stress is a functional of the motion. However, arbitrary functionals are not allowed for this purpose, and so it is necessary to stipulate restrictions on the class of functionals that are admissible. These restrictions are based on general physical principles and should apply to *all* materials. Other restrictions may be imposed, and in general *are* imposed, but these define or help to define a given theoretical material and are thus called constitutive equations.

Let the material points of a body be labeled by X , say, with coordinates X^A . Let s_{ij} denote the stress tensor and t the time. Then the principle of determinism as formulated by Noll⁶ reads:

The stress $s_{ij}(t)$ at a particular particle X at time t is determined by the past history of the motion of an arbitrarily small neighborhood of X .

This principle is not presented as a constitutive assumption, but rather as a general principle.

Our question is whether or not it should be considered constitutive. To this end let us examine the definition of a hypoelastic material as given by us in 1960.^{10,11}

The equations of hypoelasticity may be written⁸

$$\dot{s}_{ij} = s_{ik}\omega_{jk} + s_{jk}\omega_{ik} + A_{ijk}d_{kl} \quad (1)$$

using cartesian tensor notation, where v_i is the velocity, $v_{i,j}$ the velocity gradients, $\omega_{ij} = \frac{1}{2}(v_{i,j} - v_{j,i})$, $d_{ij} = \frac{1}{2}(v_{i,j} + v_{j,i})$, A_{ijk} is an invariant or isotropic tensor function of the stress, and \dot{s}_{ij} the material derivative of s_{ij} . Now, as we have pointed out, the eqs. (1) do not suffice in general to define a hypoelastic material, any more than a set of first-order differential equations suffices to define a solution. In the latter case, one must specify initial conditions. Similarly, in the former case, one must specify the possible initial conditions in order to define a material.

To resolve the difficulty, we let an assignment over the body of stress and displacement gradients, denoted by $\{s_{ij}, x_A^i\}$ (where the spatial coordinates x^i are assigned as functions of the material coordinates X^A and $x_A^i = \partial x^i / \partial X^A$), be called a stress-configuration pair.

Two stress-configuration pairs are called equivalent if one may be reached from the other along a solution to eqs. (1), and thus they are resolved into equivalence classes called stress-configuration classes. Then we say that a set of eqs. (1) together with a stress-configuration class defines a representation of a hypoelastic material. Two representations are equivalent if they differ by a change of material coordinates. An equivalence class of stress-configuration classes is called a hypoelastic material.

We found this definition of a hypoelastic material to be consistent with that of an elastic material in case the two coincided. Indeed, this definition of a hypoelastic material seemed to be just what was needed to complete the specification of a hypoelastic material. But this definition is not consistent with the principle of determinism.

Indeed, let ${}^0x_A{}^k$ be a specification of displacement gradients such that $\{\overset{1}{s}_{ij}, {}^0x_A{}^k\}$ and $\{\overset{2}{s}_{ij}, {}^0x_A{}^k\}$ are equivalent where $\overset{1}{s}_{ij} \neq \overset{2}{s}_{ij}$. Then these two stress-configuration pairs are admissible for the same hypoelastic material. Consider the motion for which the body has always been at rest with displacement gradients ${}^0x_A{}^k$. In this case the present stress could be $\overset{1}{s}_{ij}$ or $\overset{2}{s}_{ij}$. But by the principle of determinism the present stress should be known *uniquely* and hence this principle is not consistent with our definition.

In order to apply the principle of determinism to hypoelasticity, one must give the stress at $t = -\infty$, or at some finite time, in order to specify a material. Our work on hypoelasticity^{10,11} and elasticity raises the question whether this is always desirable.

Now, hypoelastic materials comprise but few of the materials of the rate type. The question remains then to supply the possible initial conditions in addition to the constitutive equations. Before this can be done it is necessary to decide whether the principle of determinism must hold.

Tied closely to these questions is the matter of material symmetry. According to Noll's definition,⁶ the symmetry (isotropy) group of a material is the group of local isochoric mappings of the body into itself which do not change the stress history in a given motion. But since the stress history of a hypoelastic material depends on the knowledge of the stress at some time as well as on the motion, there remains a question of what to do about this stress when applying this definition. Let us say, then, that in applying it we leave the stress at $-\infty$ fixed in the material.

We wish, then, to propose another definition of material symmetry for hypoelastic materials which, perhaps, can be carried over in principle to more general materials of the rate type. In particular, we shall give a definition of isotropy, but the reader can readily extend this definition to other types of material symmetry.

Let a representation of a hypoelastic material be given. Then we have an assignment of an equivalence class of stress-configuration pairs over the set of \mathfrak{M} material points. Of course a representation over \mathfrak{M} yields a representation for any (permissible) subset of \mathfrak{M} . Now an orthogonal transformation of the form

$$'X^A = 0_B{}^A X^B + 0^A, \quad 0^A, 0_B{}^A = \text{const.}, \quad 0_B{}^A 0_C{}^B = \delta_C{}^A \quad (2)$$

in general does not transform \mathfrak{M} into itself unless the body is infinite in extent in all directions. We shall therefore define isotropy under the assumption that \mathfrak{M} is infinite in extent and say that a general hypoelastic body is isotropic if it may be imbedded in an isotropic one which is infinite in extent.

Then we say that a hypo-elastic material (infinite in extent) is isotropic with respect to a given representation if any transformation of \mathfrak{M} into itself, which is orthogonal with respect to the coordinates corresponding to the representation, leaves the representation, i.e., the stress-configuration class, unchanged.

Under the transformation (2), the stress-configuration pair

$$\{s_{ij}, x_A{}^k\} \quad (3)$$

goes into

$$\{s_{ij}', x_B{}^k 0_A{}^B\} \quad (4)$$

where s_{ij}' is the stress at X' in the stress-configuration pair (3).

Suppose, now, that we are dealing with a material which is both hypoelastic and elastic. Then at each X , there is exactly one value of s_{ij} for each $x_A{}^k$. Suppose that the material is isotropic with respect to the given representation in the sense of our above definition. Consider, then, a configuration for which $x_A{}^k = \delta_A{}^k$. Let us consider translations

$$'X^A = X^A + 0^A$$

which are special cases of (2). Then (3) and (4) become

$$\begin{aligned} & \{s_{ij}, \delta_A{}^k\} \\ \text{and} \quad & \{s_{ij}', \delta_A{}^k\} \end{aligned} \quad (5)$$

respectively, and hence $s_{ij} = s_{ij}'$. Thus s_{ij} is uniform. Now apply a general transformation of the form (2). Then we see that (5) is equivalent to

$$\{s_{ij}, \delta_B^k 0_A^B\} \quad (6)$$

Consider any rotation of the material

$$\begin{aligned} {}'x^i &= 0_j^i x^j + 0^i, \quad 0_j^i, 0^i = \text{const.} \\ \delta_{ik} 0_j^i 0_l^k &= \delta_{jl} \end{aligned} \quad (7)$$

By performing this rotation we see that (5) is equivalent to

$$\{0_i^p 0_j^q s_{pq}, 0_l^k \delta_A^l\} \quad (8)$$

Given any rotation (7), 0_B^A in (2) may be chosen so that

$$\delta_B^k 0_A^B = 0_l^k \delta_A^l$$

from which we have that (8) may be written

$$\{0_i^p 0_j^q s_{pq}, \delta_B^k 0_A^B\} \quad (9)$$

Now (6) and (9) are possible stress-configuration pairs for the same elastic material corresponding to the same configurations and hence the stresses must be equal. Since 0_i^p uses an arbitrary rotation, the stress in (9), and hence (5), must have the form

$$s_{ij} = -p \delta_{ij}$$

where p is a constant. It then follows from Theorem V of ref. 11 that the material is isotropic in the sense of elasticity theory, i.e., stress is invariant under orthogonal transformations of the material into itself.

Now consider a hypoelastic elastic material which is also elastic and is isotropic in the sense of elasticity theory. Then the stress corresponding to a configuration such that $x_A^i = \delta_A^i$ is a uniform hydrostatic pressure,^{1,12} i.e., the stress-configuration class contains

$$\{-p \delta_{ij}, \delta_A^k\} \quad (10)$$

where p is a constant. From (1) it is immediately apparent that

$$\{-p \delta_{ij}, 0_A^k\} \quad (11)$$

where 0_A^k is any orthogonal matrix, is in the same stress-configuration class as (10) since we may get from (10) to (11) by a rotational motion. But (11) may be arrived at from (10) also by the transformation (2).

Thus (2) transforms one member of the given stress-configuration class into a member of the *same* class. We will immediately see that this implies that (2) preserves the stress-configuration class, and hence the representation, if we note, using eqs. (1), that if (3) goes into (4), under (2), then every stress-configuration pair equivalent to (3) goes into one equivalent to (4) under (2). Thus we have a definition of isotropy for hypoelastic materials which is consistent with that for elastic materials. But this definition does not involve the principle of determinism.

References

1. Truesdell, C. A., *J. Rational Mech. Anal.*, **1**, 125 (1952).
2. Volterra, V., *Theory of Functionals*, Blackie and Son, London and Glasgow, 1930.
3. Green, A. E., and R. S. Rivlin, *Arch. Rational Mech. Anal.*, **1**, 1 (1957).
4. Green, A. E., and R. S. Rivlin, *Arch. Rational Mech. Anal.*, **3**, 82 (1959).
5. Green, A. E., and R. S. Rivlin, *Arch. Rational Mech. Anal.*, **4**, 387 (1960).
6. Noll, W., *Arch. Rational Mech. Anal.*, **2**, 197 (1958).
7. Alfrey, T., and E. F. Gurnee, *Rheology*, **1**, 387 (1956).
8. Noll, W., *J. Rational Mech. Anal.*, **4**, 3 (1955).
9. Maxwell, J. C., *Phil. Trans. Roy. Soc. London*, **A157**, 49 (1867); *Papers*, **2**, 26.
10. Bernstein, B., *Trans. Soc. Rheology*, **4**, 23 (1960).
11. Bernstein, B., *Arch. Rational Mech. Anal.*, **6**, 89 (1960).
12. Rivlin, R. S., and J. L. Ericksen, *J. Rational Mech. Anal.*, **4**, 323 (1955).

Synopsis

The principle of determinism is discussed with respect to materials of the rate type. It is pointed out that this principle is consistent with one definition of such a material, but not with a second definition. Since the second definition seems convenient in the case of hypoelastic material in relation to elastic materials, it is suggested that the principle of determinism might be a constitutive assumption. A definition of material symmetry for hypoelastic materials, using the second definition of such materials, is given. It is shown for elastic hypoelastic materials that this definition of symmetry is consistent with the usual definition of isotropy for elastic materials.

Normal Stresses in Second-Order Viscoelasticity*

BERNARD D. COLEMAN, *Mellon Institute, Pittsburgh, Pennsylvania*, and WALTER NOLL, *Department of Mathematics, Carnegie Institute of Technology, Pittsburgh, Pennsylvania*

I. Introduction

The classical linear theory of viscoelasticity should perhaps be called *infinitesimal viscoelasticity* because it is a theory which can be applicable only to those physical situations in which the deformation computed relative to a fixed configuration has been infinitesimal at all times in the past. Simple materials are defined by the property that the stress is given by a functional of the history of the deformation gradient. In ref. 1 we formulated a differentiability assumption in function space and used this assumption to prove that infinitesimal viscoelasticity is valid for simple materials when the deformation has been infinitesimal for all times in the past. By strengthening our differentiability assumptions for the functionals used to define simple materials we have been able also to derive second- and higher-order theories of viscoelasticity. In the present note we indicate some predictions concerning the normal stresses derived from the second-order theory of incompressible viscoelastic fluids.

II. Theory

We first consider a class of motions called simple shearing motions. These motions are defined by the property that in some Cartesian coordinate system x^1, x^2, x^3 , the velocity field $v = \{v^1, v^2, v^3\}$ has the form

$$v^1 = 0, \quad v^2 = v(x^1, t), \quad v^3 = 0 \quad (1)$$

* This work was supported by the Air Force Office of Scientific Research under Contract No. AF49(638)541 and by the National Science Foundation under Grant NSF-G5250.

where t is the present time. Let us now put

$$\lambda_t(s) = \int_0^s \frac{d}{dx^1} v(x^1, t - \sigma) d\sigma \quad (2)$$

and let us assume that

$$\epsilon = \sup_{s>0} |\lambda_t(s)| \quad (3)$$

is small, i.e., that

$$\epsilon \ll 1 \quad (4)$$

Physically, this assumption means that we are limiting our attention to simple shearing motions with the property that the configuration of the fluid at all past times differs from the present configuration by only a small deformation. (Shearing vibrations with small amplitude have this property. In the case of sinusoidal vibrations ϵ measures the amplitude of the strain.)

Now, in the general theory of simple materials, it is easily shown* that the principle of material objectivity, the isotropy of our fluid, and the eqs. (1) imply that in our present Cartesian coordinate system certain components of the stress tensor $\mathbf{T} = \mathbf{T}(x^1, t)$ vanish:

$$T_{23} = T_{32} = T_{31} = T_{13} = 0 \quad (5)$$

Furthermore, it follows from our assumption of incompressibility that the trace of \mathbf{T} , i.e., $T_{11} + T_{22} + T_{33}$, is indeterminate in the sense that it is not determined by the history of the motion but depends on the present values of surface and body forces acting on the entire fluid mass. Thus, for simple shearing motions in incompressible fluids we seek relations which give us the *shearing stress* $T_{12} = T_{21}$ and the *normal stress differences* $T_{11} - T_{22}$, $T_{22} - T_{33}$ in terms of the function $\lambda_t(s)$.

Our general differentiability assumptions for simple fluids permit us to derive the following expression for T_{12} , $T_{11} - T_{22}$ and $T_{22} - T_{33}$:

$$T_{12} = T_{21} = \int_0^\infty \mu(s) \lambda_t(s) ds + o(\epsilon) \quad (6a)$$

$$T_{11} - T_{22} = o(\epsilon) \quad (6b)$$

$$T_{22} - T_{33} = o(\epsilon) \quad (6c)$$

* The proof of (5), given for steady flows in §3 of ref. 2 and for periodic flows in §5 of ref. 3, is clearly valid for an arbitrary dependence of $\lambda_{(t)}(s)$ on s .

where the order symbol $o(\epsilon)$ has the meaning

$$\lim_{\epsilon \rightarrow 0} \epsilon^{-1} \sigma(\epsilon) = 0 \quad (7)$$

In other words, to within terms of order one in ϵ we have the familiar result of infinitesimal viscoelasticity theory that the shearing stress is given by an integral involving the shearing strain and that the normal stress differences vanish. The function $\mu(s)$ is related as follows to the stress relaxation function $\phi(s)$ (determined from measurements of the decay of shearing traction following the application of a sudden infinitesimal simple shearing strain):

$$\mu(s) = 1/2(d/ds)\phi(s), \quad \phi(s) = -2 \int_0^\infty \mu(s) ds \quad (8)$$

If we take into account not only terms of order one but also terms of order *two* in ϵ , we obtain the following expressions for the shearing stress and the normal stress differences: *

$$T_{12} = T_{21} = \int_0^\infty \mu(s) \lambda_t(s) ds + o(\epsilon^2) \quad (9a)$$

$$T_{11} - T_{22} = \int_0^\infty \mu(s) \lambda_t^2(s) ds + o(\epsilon^2) \quad (9b)$$

$$T_{22} - T_{33} = \int_0^\infty \int_0^\infty \alpha(s_1, s_2) \lambda_t(s_1) \lambda_t(s_2) ds_1 ds_2 + o(\epsilon^2) \quad (9c)$$

where

$$\lim_{\epsilon \rightarrow 0} o(\epsilon^2)/\epsilon^2 = 0 \quad (10)$$

and where the function α depends on the material under consideration and is symmetric in the sense that

$$\alpha(s_1, s_2) = \alpha(s_2, s_1) \quad (11)$$

It is worth noting that, as we go from the first-order approximation (6) to the second-order approximation (9), the linear dependence of the shearing stress on the history of the motion is not yet altered. However, we do pick up a new nonlinear effect—the normal stress differences.

* See §6 of ref. 1.

Of particular interest is the normal stress difference $T_{11} - T_{22}$; apparently, to within terms of order two in ϵ , this difference is completely determined by the material function $\mu(s)$ or, equivalently, by the stress relaxation function $\phi(s)$. It seems remarkable that this definite prediction about $T_{11} - T_{22}$ follows from no more than general hypotheses about invariance and smoothness and we hope that some experimenter will check our conclusion for real materials. One way to test the relation implied by (9a) and (9b) is to measure T_{12} and $T_{11} - T_{22}$ in some motion equivalent to sinusoidal simple shearing flow. Since the measurement of $T_{11} - T_{22}$ in simple shearing flow itself appears difficult we sketch below the extension of eqs. (9) to a larger class of flows.

We consider the class of flows for which the contravariant components of the velocity field have the form (1) in some appropriate curvilinear orthogonal coordinate system x^1, x^2, x^3 . We assume that this orthogonal coordinate system is such that the matrix (g_{ij}) of the covariant components of the unit tensor \mathbf{I} has the form

$$(g_{ij}) = \begin{pmatrix} (g_1)^2 & 0 & 0 \\ 0 & (g_2)^2 & 0 \\ 0 & 0 & (g_3)^2 \end{pmatrix} \quad (12)$$

where g_1, g_2 , and g_3 are three positive functions of x^1 and x^3 . If we now put

$$\lambda_t(s) = \frac{g_2(x^1, x^3)}{g_1(x^1, x^3)} \int_0^s \frac{d}{dx^1} v(x^1, t - \sigma) d\sigma \quad (13)$$

then it is easily shown that eqs. (5)–(9) still hold for the *physical components* T_{ij} of the stress tensor in the extended class of flows. We illustrate this remark by considering a nonsteady Couette-type flow for which the contravariant components of the velocity field have the form

$$v^r = 0, \quad v^\theta = \omega(r, t), \quad v^z = 0 \quad (14)$$

in a cylindrical coordinate system,

$$x^1 = r, \quad x^2 = \theta, \quad x^3 = z \quad (15)$$

In this case we have

$$g_1 = g_3 = 1 \quad \text{and} \quad g_2 = r \quad (16)$$

so that (13) becomes

$$\lambda_t(s) = r \int_0^s \frac{d}{dr} \omega(r, t - \sigma) d\sigma \quad (17)$$

and for eqs. (5) and (9) we have

$$T_{\theta z} = T_{z\theta} = T_{zr} = T_{rz} = 0 \quad (18)$$

$$T_{r\theta} = T_{\theta r} = \int_0^\infty \mu(s) \lambda_t(s) ds + o(\epsilon^2) \quad (19a)$$

$$T_{rr} - T_{\theta\theta} = \int_0^\infty \mu(s) \lambda_t^2(s) ds + o(\epsilon^2) \quad (19b)$$

$$T_{\theta\theta} - T_{zz} = \int_0^\infty \int_0^\infty \alpha(s_1, s_2) \lambda_t(s_1) \lambda_t(s_2) ds_1 ds_2 + o(\epsilon^2) \quad (19c)$$

Let us consider that the Couette motion takes place between two long coaxial cylinders, with radii R_1 and R_2 , $R_1 < R_2$. We assume that the cylinders rotate about the common axis with different angular velocities and that the fluid adheres to the cylinders. Let $\Upsilon_t(s)$ be that function which gives the angular displacement at time $t - s$, $s \geq 0$, of a point P on the outer cylinder with respect to a point Q on the inner cylinder where Q is such that the angular displacement of P and Q at time t is zero; i.e.,

$$\Upsilon_t(s) = \int_0^s [\omega(R_2, t - \sigma) - \omega(R_1, t - \sigma)] d\sigma \quad (20)$$

We shall assume that the gap between the cylinders is small

$$(R_2 - R_1)/R_1 \ll 1 \quad (21)$$

and that the relative angular displacement of the cylinders has always been small:

$$\sup_{s>0} |\Upsilon_t(s)| \ll 1 \quad (22)$$

If we can assume that we have approximately homogeneous strain throughout,* then $\lambda_t(s)$ is approximately independent of r and is given by

$$\lambda_t(s) \approx [R_1/(R_2 - R_1)] \Upsilon_t(s) \quad (23)$$

* This must be justified by a theoretical consideration of the equations of motion; we omit such a discussion.

Under these conditions it is easily shown that eqs. (19a) imply that the moment $M(t)$ per unit height on the cylinders is approximately given by

$$M(t) \approx [2\pi R_1 R_2 (R_2 - R_1)] \int_0^\infty \mu(s) \gamma_t(s) ds \quad (24)$$

while for the difference in the normal stresses at the inner and outer cylinders we get, using eqs. (19),

$$T_{rr}(R_2) - T_{rr}(R_1) \approx [(R_2 - R_1) R_1] \int_0^\infty \mu(s) \gamma_t^2(s) ds \quad (25)$$

The symbol \approx in eqs. (23)–(25) is meant to indicate that the error in these approximate formulas is of the order of $[(R_2 - R_1)/R_1]^2$.*

The approximate formulas (24) and (25) suggest the feasibility of testing in practice our theoretical prediction about the normal stress difference $T_{11} - T_{22}$ by measuring the phase difference of the torque and angular displacement (as a function of frequency) and then testing whether such information can successfully predict the phase of the difference in radial thrusts at the inner and outer cylinders in the range in which the amplitude of the radial thrust difference is proportional to the square of the amplitude of the motion.

References

1. Coleman, B. D., and W. Noll, to appear in *Revs. Modern Phys.*, April 1961.
2. Coleman, B. D., and W. Noll, *Arch. Rational Mech. Anal.*, **3**, 289 (1959).
3. Coleman, B. D., and W. Noll, *Ann. N. Y. Acad. Sci.*, **89**, 672 (1961).

Synopsis

On the basis of the recently proposed second-order theory of incompressible viscoelastic fluids, certain predictions concerning the normal stresses are made. In particular, a formula is given for the normal stress difference at the inner and outer cylinder in a nonsteady Couette-type motion. This formula involves no material functions other than the stress relaxation function for shear.

* The error analysis needed to show this is similar to the one given in §8 of ref. 2.

Abstract

Non-Newtonian Flow Around A Sphere

A. J. ZIEGENHAGEN and R. B. BIRD, *Department of Chemical Engineering*, and M. W. JOHNSON, JR., *Department of Engineering Mechanics, University of Wisconsin, Madison, Wisconsin*

This development concerns incompressible fluids whose rheological behavior is described by:

$$\tau = -\eta \Delta \quad (1)$$

Here τ is the viscous part of the momentum-flux tensor, Δ is the rate-of-deformation tensor (with cartesian components $\Delta_{ij} = \partial v_i / \partial x_j + \partial v_j / \partial x_i$), and η is the viscosity. The latter is assumed to depend only on II , the second invariant of Δ :

$$II = \sum_i \sum_j \Delta_{ij} \Delta_{ji} \quad (2)$$

That is, viscoelastic effects and cross-viscosity effects are ignored.

For such fluids it has been shown¹ that for steady, creeping flow the equations of motion are the Euler-Lagrange equations which correspond to the extremalization of the integral:

$$J = \iiint_V \left[\frac{1}{2} \int_0^{II} \eta dII \right] dx dy dz \quad (3)$$

where V is the volume of the flow system, on the surface of which the velocity is specified. Constraining conditions are that the velocity satisfy the equation of continuity and the boundary conditions. This variational principle has been extended to include more general boundary conditions and more general non-Newtonian materials.^{2,3}

The above principle can be used to get approximate velocity profiles for non-Newtonian flow around a sphere. Once the velocity distribution has been found, then the drag force is obtained from integrating

the total rate of energy dissipation in the region outside the sphere.⁴ The result may be written:

$$F_{drag} = 6\pi\eta_0 v_\infty R \Xi \quad (4)$$

where η_0 is the limiting value of η as Π approaches zero, v_∞ is the approach velocity of the fluid along the z -axis, R is the radius of the sphere, and Ξ is the dimensionless correction factor:

$$\Xi = \frac{1}{6} \int_1^\infty \int_0^\pi \frac{\eta}{\eta_0} \frac{\Pi}{(v_\infty/R)^2} \sin \theta \, d\theta \, \xi^2 d\xi \quad (5)$$

Here $\xi = r/R$ is the dimensionless radial coordinate, and θ is the angle measured downwards from the z -axis.

In order to illustrate the use of the variational method, we considered the two-constant model:

$$\eta = \eta_0 - \eta_1 \Pi \quad (6)$$

in which η_1 was taken to be positive (pseudoplastic fluid). A trial stream function (defined in the usual way⁴) of the form

$$\psi(r, \theta) = v_\infty R^2 \sin \theta \cdot \sum_{i=0}^{\infty} c_i g_i(\xi) \quad (7)$$

was used.

Zeroth Approximation: Use one term in the sum in eq. (7) with $c_0 = 1$ and the Newtonian function $g_0 = -1/4\xi^{-1} + 3/4\xi - 1/2\xi^2$. Then substitution of (7) into (5) gives:

$$\Xi = 1 - 0.4140H \quad (8)$$

where $H = (\eta_1/\eta_0)(v_\infty/R)^2$.

First Approximation: Use two terms in the sum, with c_0 and g_0 as above. Take $g_1 = -1/2\xi^{-1} + 1 - 1/2\xi$, and extremalize J to get c_1 as a function of H . Then one gets

$$\Xi = 1 - 0.3759H - 1.508H^2 \quad (9)$$

The only previous calculations for non-Newtonian flow around a sphere was a zeroth approximation variational calculation by Tomita⁵ for a power-law fluid. It is the authors' intention to extend the above calculations and then compare with the experimental measurements of Slattery.⁶

A. J. Ziegenhagen wishes to thank the Ethyl Corporation for a graduate research fellowship; R. B. Bird wishes to acknowledge the support provided by the National Science Foundation Grant G11996; and M. W. Johnson, Jr., was supported in part by the Mathematics Research Center, U. S. Army, Contract No. DA-11-022-ORD-2059.

References

1. Bird, R. B., *Phys. Fluids*, **3**, 539 (1960).
2. Johnson, M. W., Jr., *Phys. Fluids*, **3**, 871 (1960).
3. Johnson, M. W., Jr., to be published.
4. Bird, R. B., W. E. Stewart, and E. N. Lightfoot, *Transport Phenomena*, Wiley, New York, 1960.
5. Tomita, Y., *Bull. Japan Soc. Mech. Engrs.*, **2**, 469 (1959).
6. Slattery, J. C., Doctoral Dissertation, Department of Chemical Engineering, University of Wisconsin, 1959.

Introduction to the Symposium on Rheology of Suspensions

FREDERICK H. GASKINS, *Aeroprojects Inc., West Chester,
Pennsylvania*

The rheology of suspensions has received attention ever since someone first pumped mixtures such as sand and water. Recent attempts to characterize the flow of solid-liquid dispersions are illustrated by the work with reactor fuel slurries. Current interest is devoted to a wide variety of disperse systems—organic and inorganic, synthetic, biological, and natural.

The subjects included in this symposium indicate the breadth of these variegated interests.

The first presentation treats a natural suspension: sewage sludge. Next is a discussion of the flow characteristics of a typical clay dispersion. Consideration of the components which may contribute to the peculiar flow of blood centers attention on this most important biological suspension. Thereafter, experimental results are presented for the practically important dispersion, grease.

These papers should make it evident that a number of scientific disciplines and technological approaches are interrelated in the study of the rheology of suspensions. We hope that these presentations will not only demonstrate the scope of the scientific problem, but will also lead to the realization that the term "suspension" encompasses many material systems of practical importance as well as interest to the Rheologist.

Application of the Method of Composition and Linear Regression Analysis to a Problem Involving a Pseudoplastic Suspension

W. F. AMES and V. C. BEHN,* *University of Delaware, Newark, Delaware*

Introduction

In a recent paper the first author illustrated a method of obtaining a mathematical model, describing physical phenomena, which depends upon more than one independent variable.¹ The purpose of this paper is to demonstrate the method of composition of a model in combination with linear regression analysis, utilized to fit and test the model.

The variables to be assembled in the model include shear stress, shear rate, and concentration by weight of a particular pseudoplastic suspension, digested sewage sludge. Experimental evidence is then used to provide the hypotheses on which the model is constructed, and this same data is used to calculate and test the coefficients in the theoretical model. For completeness, a brief review of the regression analysis techniques utilized is given.

The general approach used in this paper is applicable to problems involving only empirical knowledge of the general relations, to theoretical problems, and to situations involving a combination of theory and empiricism. Presentation of the data in the form suggested in this paper is more satisfying technically than, say, a series of two dimensional graphs and may well give additional insight into physical mechanism. Consequently the technique should be of use to engineers and scientists in a wide variety of problems.

* Present address: School of Civil Engineering, Cornell University, Ithaca, New York.

I. Flow Behavior of Pseudoplastic Suspensions

A. General Considerations

A number of fluids, such as suspensions and solutions of high molecular weight, exhibit a power law behavior in laminar flow. That is, paired values of shear stress and shear rate have a straight line relationship on double logarithm paper. It is then convenient to express the relationship between, τ , the shear stress, and du/dr , the shear rate as

$$\tau = K(du/dr)^n \quad (1)$$

In eq. (1), K is referred to as the coefficient of consistency, and n is the coefficient of flow behavior.² Actually n is a measure of the degree of non-Newtonian behavior. When n is exactly equal to one, the material is Newtonian, and eq. (1) reduces to Newton's equation of viscosity. When n is less than one the fluid is termed pseudoplastic, and when n is greater than one the material is classified as a dilatant.

Knowledge of these flow parameters may be quite useful when a fluid is transported many miles by pipe line, and this is not infrequently true of digested sewage sludge suspensions. While this suspension is frequently classified as a Bingham Plastic following the work of Babbitt and Caldwell,³ Behn has suggested that the pseudoplastic power law model may also be applicable.⁴

B. Experimental Considerations

Experimental evidence collected in our laboratories does indicate that digested sewage sludge suspensions can be analyzed by the power law model, at least for a given range of concentration by weight of solids. This evidence is presented in Figure 1 as a plot of shear stress versus shear rate at variable concentration.

These results were obtained at 20°C. utilizing a MacMichael viscometer with torsion wires certified by the manufacturer, and bob length calibrated by Bureau of Standards oils. Basic data taken include cup speed, angular deflection of the torsion wire, calibrated bob length, and cup and bob radii. These quantities were then used to calculate paired values of shear stress and shear rate at the bob by means of the equations of Krieger and Elrod⁵ and Krieger and Maron⁶ as suggested by Metzner.²

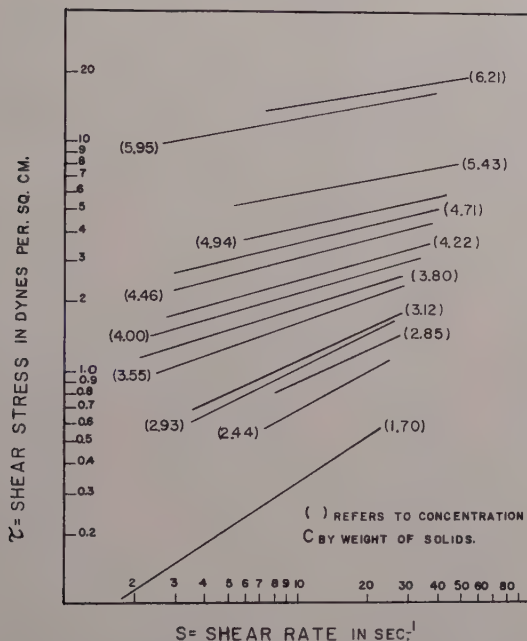


Fig. 1. Shear stress vs. shear rate at variable concentration by weight of solids. All data at 20°C.

These experimental results may now be used as the basis for deriving a more generalized form of eq. (1) by means of the method of composition.

II. The Method of Composition

The purpose of the method of composition is to bring the three variables involved in the experimental analysis into one equation. In particular, it is desirable to express the shear stress as a function of concentration by weight of solids, C and shear rate, S , as follows

$$\tau = f(C, S) \quad (2)$$

where S has been substituted for du/dr as a convenience.

In order to develop a specific functional relationship between τ , C , and S , two basic relationships are required. The first of these is

$$\partial(\ln \tau) / \partial(\ln S) = g_1(C) \quad (3)$$

and it is merely a mathematical restatement of the previous observation that the slope of $\ln \tau$ versus $\ln S$ is a constant for any fixed concentration, but varies with the concentration. To obtain a second relationship, $\ln \tau$ is plotted against $\ln C$ for various values of S in Figure 2. The data shows some evidence of linearity for each

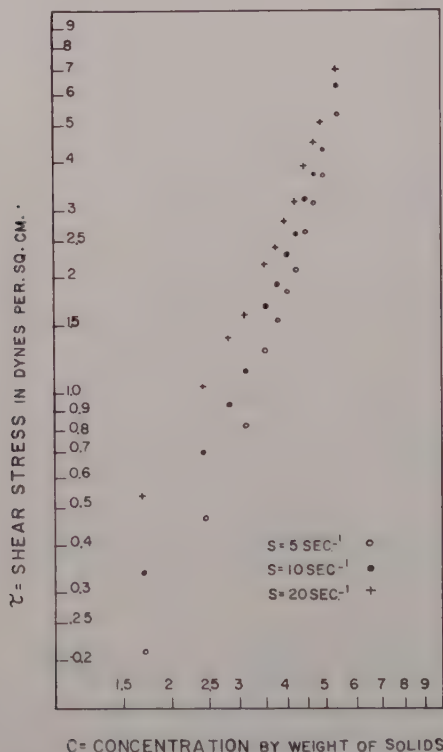


Fig. 2. Shear stress vs. concentration at variable shear rate (log-log plot).

value of S but is definitely concave upward. If the data points at the low concentrations are discarded, linearity of the data is not an unreasonable hypothesis and the relationship

$$\partial(\ln \tau) / \partial(\ln C) = h_1(S) \quad (4a)$$

results.

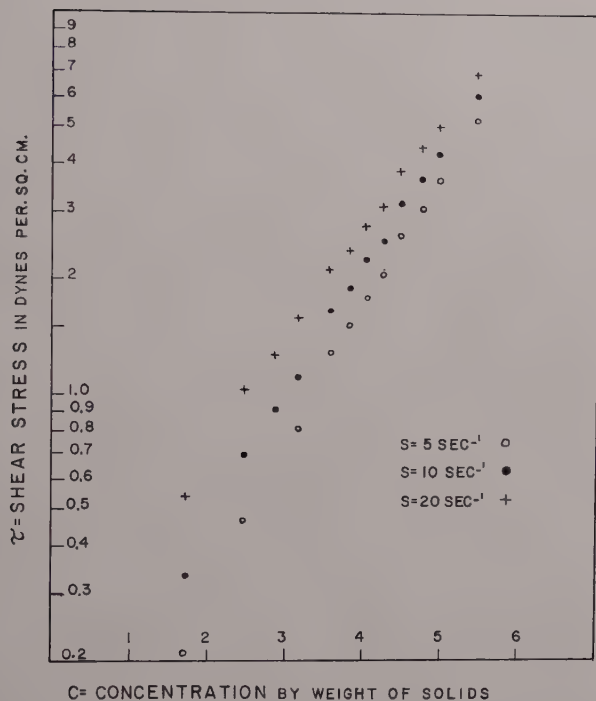


Fig. 3. Shear stress vs. concentration at variable shear rate (semi-log plot).

On the other hand, if $\ln \tau$ is plotted against C for various values of S as is shown in Figure 3, the linearity assumption is also not unreasonable. The relationship analogous to eq. (4a) in this case is

$$\partial(\ln \tau) / \partial C = H_1(S) \quad (4b)$$

Without further information it is difficult to choose between hypothesis (4a) and (4b). Both models will be analyzed in Section IV by statistical regression analysis, and the choice of the best model will then be based on those results.

The method of composition consists of obtaining an equation of the form (2) from eqs. (3) and (4a) [or (4b)]. Only that resulting from eqs. (3) and (4a) is demonstrated. Integration of eq. (3) with respect to $\ln S$ yields

$$\ln \tau = g_1(C) \ln S + g_2(C) \quad (5)$$

and integration of eq. (4a) with respect to $\ln C$ yields

$$\ln \tau = h_1(S) \ln C + h_2(S) \quad (6)$$

Here $g_2(C)$ and $h_2(S)$ are "constants" of partial integration.

Since eqs. (5) and (6) represent the same equation, they may be equated as follows:

$$g_1(C) \ln S + g_2(C) = h_1(S) \ln C + h_2(S) \quad (7)$$

Upon differentiation of eq. (7) with respect to S there results

$$g_1(C)/S = (dh_1/dS) \ln C + (dh_2/dS) \quad (8)$$

which may be rewritten in the form

$$g_1(C) = S(dh_1/dS) \ln C + S(dh_2/dS) \quad (9)$$

The left-hand side of eq. (9) is a function only of C and therefore the right-hand side must also be a function of C . Hence

$$S(dh_1/dS) = a_3 \text{ (} a_3 \text{ an absolute constant)} \quad (10a)$$

$$S(dh_2/dS) = a_2 \text{ (} a_2 \text{ an absolute constant)} \quad (10b)$$

Upon integration of eqs. (10a) and (10b) there results

$$h_1(S) = a_3 \ln S + a_1 \quad (11a)$$

$$h_2(S) = a_2 \ln S + a_0 \quad (11b)$$

Substitution of eqs. (11a) and (11b) into eq. (6) yields

$$\ln \tau = a_0 + a_1 \ln C + a_2 \ln S + a_3 \ln S \ln C \quad (12)$$

or upon exponentiating and setting $e^{a_0} = A$

$$\tau = AC^{a_1}S^{(a_2 + a_3 \ln C)} \quad (13)$$

If eqs. (3) and (4b) are the hypotheses used, there results by a similar procedure

$$\tau = Ae^{a_1 C}S^{(a_2 + a_3 C)} \quad (14)$$

For constant (nonzero) concentration, both expressions reduce to the power law [eq. (1)]. Equation (14) has the added advantage that at zero concentration τ has a nonzero value.

Regression analysis techniques may now be used to determine the coefficients in eqs. (13) and (14). In addition, regression tests will be

applied to choose between the two models and to establish the validity of the chosen equation which results when the numerical values of the constants are inserted.

III. Statistical Techniques

Considered broadly, regression analysis has two goals: First, to estimate or predict one variable from the values of one or more other variables, and second, to obtain a causal explanation of one variable as a function of one or more other variables. Since this technique is to be used in the problem at hand, and since the methods do not seem to have had as much application as one could rightfully expect, a brief review is given here. The techniques are not original with the authors, and are sketched in general form for more completeness. For further details and examples the reader is referred to the excellent literature, of which only a few references are cited.⁷⁻¹⁰

The basic steps of regression analysis are discussed below with the assumption that the observations (x_i, y_i) , $i = 1, 2, 3, \dots, n$, have been obtained experimentally, and that the true values are (X_i, Y_i) , $i = 1, 2, 3, \dots, n$.

Step 1: *Assume* that there are differences between (x_i, y_i) and (X_i, Y_i) which result from random fluctuations.

Step 2: *Assume* (from empirical and or theoretical information) that the relationship between X and Y takes the form $F(X, Y, B_0, B_1, \dots, B_k) = 0$, where k , the number of coefficients, is less than n , the number of observations.

Step 3: *Choose* an estimate of F , say $\hat{F} = F(X, Y, b_0, b_1, \dots, b_k)$ where the b 's are estimated values of the B 's such that \hat{F} is of the form F which best fits the data according to some criterion, usually least squares.

Step 4: *Test* the goodness of fit of F and decide whether a function of the form F adequately describes the observed data.

The actual procedural method is as follows: Let y be a quantity which is believed to be dependent upon the variables $x_1, x_2, x_3, \dots, x_p$. The general form of the linear regression model used here is

$$y = B_0 + \sum_{j=1}^k B_j f_j(x_1, x_2, \dots, x_p) + R \quad (15)$$

where the f_j are functions of the given variables and do not contain the coefficients B_j . (Linearity here means linearity only in the

coefficients B_j .) We have assumed that the rational portion of the function and the random portion, R , are additive. Further we have assumed that all the random effects may be lumped into one and be described by a single probability function.

Let the matrices β , U , and V be defined as follows:

$$\beta = \begin{bmatrix} b_0 \\ b_1 \\ b_2 \\ . \\ . \\ . \\ b_k \end{bmatrix}, U = \begin{bmatrix} 1 & f_{11} & f_{21} \dots f_{k1} \\ 1 & f_{12} & f_{22} \dots f_{k2} \\ . & . & . \\ . & . & . \\ . & . & . \\ 1 & f_{1n} & f_{2n} \dots f_{kn} \end{bmatrix}, V = \begin{bmatrix} y_1 \\ y_2 \\ . \\ . \\ . \\ y_n \end{bmatrix}$$

In these definitions the n observations are y_i , $i = 1, 2, 3, \dots, n$, the known values are x_{ji} and $f_{ji} = f_j(x_{1i}, x_{2i}, \dots, x_{ki})$. The b 's result from the following analysis.

The solution of the normal equations $U^T U \beta = U^T V$, which is obtained by applying least squares criterion, gives minimum variance, unbiased, linear estimates of the unknown parameters (B_k 's) and this estimate is denoted by the elements of the β matrix. The notation U^T means the transpose of the matrix U . The solution of the normal equations in matrix form is

$$\beta = (U^T U)^{-1} U^T V \quad (16)$$

where U is not square so that $U^T U$, which is square (and symmetric) must be inverted. The superscript, -1 , denotes an inverse matrix. This equation then yields as solution the b coefficients. (Due to the need for the inverse matrix $(U^T U)^{-1}$ in Step 4, it is desirable to solve the normal equations by matrix inversion instead of by elimination methods.)

The last step in the analysis is to test the significance of the proposed model, and this may be done by a number of statistical devices. Some of the useful information which would demonstrate goodness of fit might properly include the following:

(a) Simple correlation coefficients between each pair of variables. These measure how well the two variables correlate, ignoring variations in other variables.

(b) Multiple correlation coefficient. A measure of how much variation in each of the dependent variables can be explained by the independent variables considered.

(c) Standard error of estimate. A measure of the accuracy of prediction of the dependent variable from the independent variables considered.

(d) Standard deviation of each multiple regression coefficient. How accurately each multiple regression coefficient is known.

(e) " F "-test. How well do the data fit the equation chosen.

(f) " t "-test. How significant is each independent variable in explaining the dependent variable variation.

(g) Sum of squares of the residuals (calculated minus observed values).

The F test is sometimes called the variance ratio test. It is used to decide whether two independent estimates of variance can reasonably be accepted as being two estimates of the variance of a single normally distributed universe. The F test provides a bench mark to ascertain whether a chosen model is warranted. Student's " t " test makes it possible to determine whether a regression coefficient is consistent with some assigned value. Multiple correlation coefficients are useful in that they define quantitatively the degree of relationship between the variables in the chosen model. The sum of the squares of the residuals offers additional information on the overall goodness of fit between observed and calculated values.

The student of statistical methods will observe that other useful results may be obtained within this same framework of basic data. For example, confidence limits for the b coefficients may be obtained with the use of the above-mentioned inverse matrix. For this and further details on the statistical tests described, the reader is referred to the literature.

The application of this type of analysis to the data demonstrated in Figure 1 may now be considered.

IV. Analysis of Experimental Data

The purpose of the application of the linear regression analysis is threefold:

(a) To determine the numerical magnitude of the coefficients for eqs. (13) and (14) from the experimental data.

(b) To test the adequacy of the equations for predicting the shear as a function of shear rate and concentration.

(c) As a result of the tests in (b), to choose between eqs. (13) and (14) as predictors of shear.

For convenience the eq. (13) so derived will now be converted to a basis of common logarithms.

$$\tau = 10^{b_0} C^{b_1} S^{(b_2 + b_3 \log C)} \quad (17)$$

In eq. (17), τ has units of dynes/cm.² and the data ranges from 0.09 to 37.75. The concentration is in per cent by weight dry solids and takes values from 1.7 to 6.21. S , the shear rate, is in units of sec.⁻¹ and experimental data varies from 1.62 to 53.0. Altogether 115 data points are available, but because of computer limitations only 99 are used.

In order to develop the coefficients by this analysis, eq. (17) must be linearized by taking logarithms. The result becomes

$$\log \tau = b_0 + b_1 \log C + b_2 \log S + b_3 \log S \log C \quad (18)$$

Letting $\log \tau = Y$, $\log C = X_1$, and $\log S = X_2$, we have the linear model

$$Y = b_0 + b_1 X_1 + b_2 X_2 + b_3 X_1 X_2 \quad (19)$$

In a similar fashion eq. (14) becomes

$$\log \tau = b_0 + b_1 C + b_2 \log S + b_3 C \log S \quad (20)$$

which is again in linear form.

The results of the regression analysis are given in Table I where eq. (13) is described as model A and eq. (14) as model B. There are altogether 99 data points and 95 degrees of freedom for regression.

The multiple correlation coefficient is not significantly better for model B than for model A. In addition, the coefficients in model B appear to be estimated with less precision (on a percentage basis), based on the computed standard deviation, than those for model A. The " F " and " t " tests, although highly significant at the 1% level (see the Biometrika Statistical Tables) for both models, are greater in each case for model A.

Model B, on the other hand, has the advantage that at $C = 0$ the result is immediately

$$\tau = 10^{b_0} (du/dr)^{b_1} \quad (21)$$

TABLE I

Result		Model A	Model B
(a) Multiple regression coefficients:			
	b_0	-1.9616	-1.8672
	b_1	3.3594	0.4660
	b_2	0.8169	0.8206
	b_3	-0.8426	-0.1161
(b) Multiple correlation coefficient:			
		0.9919	0.9945
(c) Standard error of estimate:			
		0.0482	0.0493
(d) Standard deviation of each multiple regression coefficient:			
	b_1	0.1039	0.0193
	b_2	0.0593	0.0725
	b_3	0.0998	0.0163
(e) "F" test:			
		1890.13	1375.18
(f) "t" test for each multiple regression coefficient:			
	b_1	32.33	24.20
	b_2	13.79	11.32
	b_3	8.44	7.11

or direct reduction to the power law. A limiting process applied to model A (as $C \rightarrow 0$) may or may not yield a limiting value.

It would appear from the above analysis that model A is the best predictor for the data considered and is therefore adopted here as the "generalized power law." However, model B is not a poor model and it may happen that in certain circumstances it will be the proper choice. In any event, they should be compared by the above procedure before one is chosen over the other.

The sum of the squares of the residuals for the 99 data points (based on model A) is concentrated substantially in the data points where $C = 1.7\%$ and where $C = 6.21\%$ (see Fig. 1).

These discrepancies at the two extremities of the data may be explained on the basis of either large experimental error or failure of the postulates used in the method of composition. At the low concentration the material approaches Newtonian behavior. For example, Sirman has shown with capillary viscometer tests that a particular suspension of this type was Newtonian at a concentration of 2.8%.¹¹ At the higher concentrations the material is still essentially pseudoplastic, but in the range of shear rates which are applicable,

the power law as represented by eq. (1) does not strictly hold. Experimentally, the possibility of settling of the suspension exists at the lower concentration, while at the higher concentration the bob has a tendency to oscillate due to the structure of the suspension. While experimental error is quite possible, especially at the higher concentration, it is thought that the deviations represented by the analysis of the residuals is more closely related to failure of the model.

In any case, the overall correlation is believed quite satisfactory, at least from an engineering viewpoint.

V. Summary and Conclusions

Tests upon a digested sewage sludge at 20°C. with a MacMichael viscometer have provided experimental data relating shear stress to shear rate at varying concentration by weight of solids. Preliminary examination of this data revealed that for the range of data covered (1) the rate of change of the logarithm of the shear stress with respect to the logarithm of the shear rate apparently is a constant for a given concentration of solids, and (2) the rate of change of the logarithm of the shear rate with respect to the concentration (logarithm of the concentration) is apparently a constant for a given shear rate.

On the basis of these hypotheses the method of composition was used to derive two possible extensions of the well-known power law, namely

$$\tau = 10^{b_2} C^{b_1} S^{(b_2 + b_3 \log C)} \quad (\text{Model A})$$

and

$$\tau = 10^{b_0} e^{b_1 C} S^{(b_2 + b_3 C)} \quad (\text{Model B})$$

These equations may be recognized as more generalized forms of the well-known power law for pseudoplastics, reducing to that law at constant concentration.

With the aid of the techniques of regression analysis, data was analyzed involving a range of (1) shear stress, τ , of 0.09 to 37.75 dynes/cm.², (2) shear rate, S , of 1.62 to 53.0 sec.⁻¹, and (3) concentration, C , of 1.7 to 6.21 wt.-% of solids. As a result of this analysis, the minimum variance best estimates of the b coefficients were found for both models.

Statistical tests revealed that model A was the best predictor of the shear stress as a function of concentration and shear rate for the range

of data considered. However, the second equation may prove useful over wider ranges of concentration and in other problems. In addition, these tests led to the conclusion that model A was eminently satisfactory from an engineering standpoint. But further examination of the residuals of calculated versus observed values suggested that an even higher correlation could be obtained by eliminating data at both extremes of concentration. While experimental error at both higher and lower concentrations, particularly the former, is a distinct possibility, a possible deviation from the model is considered more likely. This arises at the low concentration from the almost Newtonian behavior, while at the higher concentrations the fluids, although pseudoplastic, begin to deviate from the power law model in the shear rate range encountered.

For the range of data considered, the coefficients of consistency and flow behavior are respectively

$$K(C) = 0.0113C^{3.3954}$$

and

$$n(C) = 0.8169 - 0.8426 \log C$$

While the generalized power relation may have sound theoretical foundation, such proof has not been developed here. Hence, extrapolation of this model using the above coefficients, outside the range of data considered, should not be attempted.

The combined utilization of the method of composition and regression analysis has yielded predictive and analytical information in a concise and useful form.

The data used in this paper were taken by Mr. D. R. Tatman, Graduate Student in Civil Engineering at the University of Delaware.

Grateful acknowledgment is given that this study was supported substantially by a grant of the National Institute of Health, United States Public Health Service.

References

1. Eckstein, B. H., E. H. Olson, and W. F. Ames, *Textile Research J.*, **28**, 701 (1958).
2. Metzner, A. B., "Non-Newtonian Technology," in *Advances in Chemical Engineering*, T. B. Drew and J. W. Hoopes, Eds., Academic Press, New York, 1956.
3. Babbitt, H. E., and D. H. Caldwell, *Ing. Eng. Chem.*, **33**, 249 (1941).

4. Behn, V. C., "Flow Equations For Sewage Sludges," *Journal Water Pollution Control Federation*, in press.
5. Krieger, I. M., and H. Elrod, *J. Appl. Phys.*, **24**, 134 (1953).
6. Krieger, I. M., and H. S. Maron, *J. Appl. Phys.*, **25**, 72 (1954).
7. Bennett, C. A., and N. L. Franklin, *Statistical Analysis in Chemistry and the Chemical Industry*, Wiley, New York, 1954.
8. Owens, O. L., *The Design and Analysis of Industrial Experiments*, Hafner, New York, 1956.
9. Mood, A. F., *Introduction to the Theory of Statistics*, McGraw-Hill, New York, 1950.
10. Hald, A., *Statistical Theory with Engineering Applications*, Wiley, New York, 1952.
11. Sirman, J. M., "Determination of the Flow Parameters of Waste Sludges by Means of a Capillary Viscometer," Thesis, University of Delaware, Newark, Delaware, June, 1960.

Synopsis

Experimental data obtained for a digested sewage sludge has been obtained relating shear stress to shear rate at varying concentrations by weight of solids. Examination of the data leads to two hypotheses which are used in a "method of composition" to obtain a "generalized power relation"

$$\tau = b_0 C^{b_1} (du/dr)^{(b_2 + b_3 \log C)}$$

where τ = shear stress, C = concentration by weight of solids in the pseudoplastic suspension, and du/dr is shear rate. Statistical regression analysis is used to obtain the coefficients from the data and to test the adequacy of the model. The results are highly satisfactory, yielding predictive and analytical information in a concise and useful form.

Flow Properties of Attapulgate Suspension in Water

A. F. GABRYSH, TAIKYUE REE, H. EYRING, NOLA McKEE,
and I. CUTLER, *Department of Chemistry, University of Utah,
Salt Lake City, Utah*

Introduction

The introduction of colloidal material into a solvent causes an increase in viscosity which varies with such properties as structure, size, and shape of the particles. Suspension frequently display either thixotropy, dilatancy, or both. To gain a satisfactory way of recording the rheological factors, much interesting work on thixotropy and dilatancy has been reported in books¹⁻⁴ and recorded in the literature.⁵⁻¹⁰ The flow mechanisms have been frequently discussed by various rheologists.^{8,11-13} Experimentally these investigators have derived empirical equations expressing viscosity-concentration and other relationships, but no satisfactory theory has been proposed which explains thixotropy and dilatancy quantitatively.

The flow behavior of attapulgate (Attagel #30) colloidal suspension in water is here studied and considered in terms of the relevant stresses and strains, since as far as we know, the rheological study of the system has not yet been done. The stress-strain-time relations with respect to the variables of temperature, concentration, and pH are given here and discussed in terms of thixotropy and dilatancy defined as having the following characteristics:

- (1) An *isothermal* structural change is brought about by applying mechanical disturbance to a system.
- (2) When the mechanical disturbance is removed, the system recovers its original structure only after a sufficiently long time.
- (3) The flow curve (shear rate versus shear stress) of the system has a hysteresis loop.

This definition is accepted currently by some authors^{1,2,4} and was recently used successfully,^{11,15} although some investigators still include in thixotropy and dilatancy other phenomena.

Experimental Details

1. Apparatus

The viscometer used for the flow studies reported in this paper was of the concentric-cylinder type (Couette type). The latter type of viscometers is widely used for the measurement of flow curves of non-Newtonian materials.¹⁶⁻¹⁹ The automatic concentric-cylinder rotational viscometer built²⁰ at this Laboratory provides means of increasing and decreasing the applied rates of shear and control of the time such that each shear rate is applied to the sample for a desired duration at any given moment. Since flow properties may change rapidly with time and shear rate, the automatic control is important

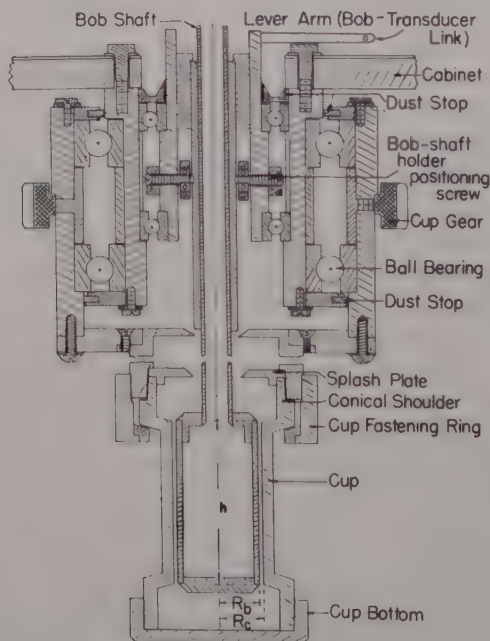


Fig. 1. Schematic representation of the cylinder assembly of the viscometer.

for materials which are time-dependent. Because of these automatic controls, the viscometer can record a continuous flow curve in a minimum time of 11 sec. up to a rate of shear of about 4500 sec.^{-1} for a proper selection of gear and cylinder sets.

Figure 1 shows the essential details of the viscometer which, with minor modifications, is similar to the Green-Weltmann type.^{11, 16, 18} The sample is sheared between the two co-axial cylindrical surfaces of the cup and bob shown schematically in Figure 1. The present study was made using a cylinder set which had a ratio (R_b/R_c) of 0.885, where R_b and R_c are the radii of the bob and cup, respectively. With the aid of the automatic controls, the viscometer recorded a continuous flow curve in 30 sec. with a peak rate of shear of about 700 sec.^{-1}

2. Recording

A Leeds-Northrup Speedomax type G X-Y recorder plotted the flow curves by recording the instantaneous torque values obtained from a Statham Model G1 transducer and the instantaneous values of rotational speed obtained from a tachometer.

3. Temperature

A constant-temperature water bath is mounted such that it glides vertically over the cup. The motion of the bath is aided by a spring load so that it can be readily moved for changing of samples. Stops provide correct positioning.

The bath water is supplied from an insulated tank fitted with electric heaters and a thermo-regulator. Temperature is controlled at the cup surface within 0.2°C. over a temperature range of 1 to 92°C. Measurements indicate that the sample in the cup gained temperature equilibrium with the water in approximately 20 min. while standing still. The thermal equilibrium was achieved before measurements were begun.

The heat generated in the sample because of the shearing action was not measurable and is considered minimized in this experiment because the continuous flow curve was taken in a relatively short time of 30 sec. to a rate of shear of only about 700 sec.^{-1} . In some cases, the inside of the hollow bob was flushed with the bath water to minimize the heat effect.

4. Structural Properties

The structure of attapulgite was worked out by Bradley,²¹ electron micrographed by Bates,²² and it is completely described by Grim.²³ The composition has been known to be $(\text{OH}_2)_4(\text{OH})_2\text{Mg}_5\text{Si}_8\text{O}_{20}\cdot 4\text{H}_2\text{O}$;

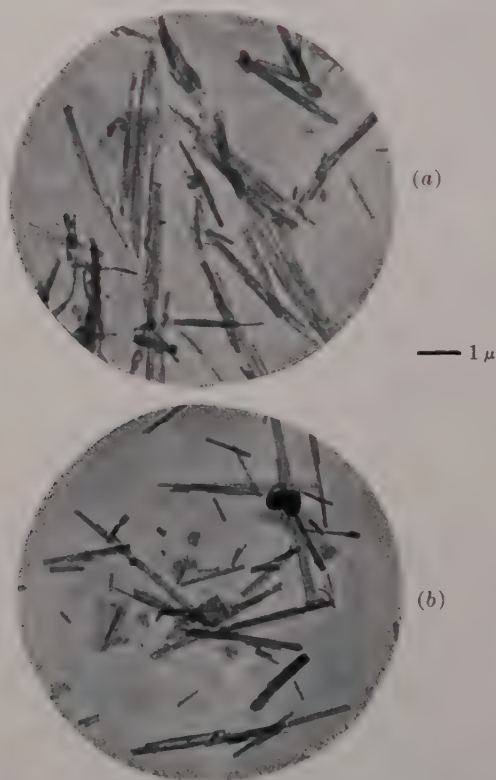


Fig. 2. Electron micrographs of (a) the sample taken from the nonsheared region, and (b) specimen taken from the sheared region.

here the substitution of Al^{+3} for some of the Si^{+4} is probable, and it is considered that substitution of Al^{+3} for either Mg^{+2} or Si^{+4} or both should weaken the structure.

The specimens used in this study were taken from material (known as Attagel #30) which was obtained from the Minerals and Chemical

Corporation of America, Menlo Park, New Jersey. According to this company's specification, the chemical analysis (volatile-free basis) of this clay (specific gravity 2.36) is: silicon (SiO_2), 67.0%; aluminum (Al_2O_3), 12.5%; magnesium (MgO), 11.0%; iron (Fe_2O_3), 4.0%; calcium (CaO), 2.5%; other, 3.0%. The specimens had needle-like particle shape, typical of this material. The bulk density (tamped volume weight) was approximately 5.6 g./cc. and the surface area approximately 210 m.²/g. on a moisture-free basis.

5. *Electron Micrographs*

Photomicrographs were made with a Phillips EM 100B electron microscope. The tube voltage and beam current were 80 kv. and 40 ma., respectively. The exposure time at minimum intensity was 10 sec. Magnification was established on the basis of a grid of 28,880 lines per inch.

Two micrograms are shown in Figure 2, where a collodion membrane was used as the sample-supporting film, and the metallic shadow method was not employed. Figure 2a is for the sample taken from the bottom of the cup of the viscometer after a series of experiments was performed, and Figure 2b is for the sample from the annular space. Since the shearing action does not occur at the bottom, the microgram, Figure 2a, is exactly the same as that taken for the commercial sample. Here the needle-like crystals make bundles. Figure 2b shows clearly that because of the shearing action the bundle was separated into needle-like pieces, which broke down further to shorter pieces.

6. *Mixing*

Various methods of mixing attapulgite with water were tried. Preliminary results show that the viscosity of attapulgite suspension changes as a function of stirring speed and time.

The results given here are for a sample prepared as follows: The desired quantities of attapulgite and distilled water (pH = 5.7) were weighed out; the initial blending of sample in water was made by hand stirring with a glass rod for 5 min.; the mixture was then further stirred by a mechanical mixer for an additional 15 min. at a constant speed of 60 rpm.

Results

1. Calibration

Experimental procedure is presented in the photograph of a strip of recorder chart, Figure 3. First a "response histogram" is made of deflections under increment loading, Figure 3a. The response of the transducer is noted for loading and unloading. The results signify the

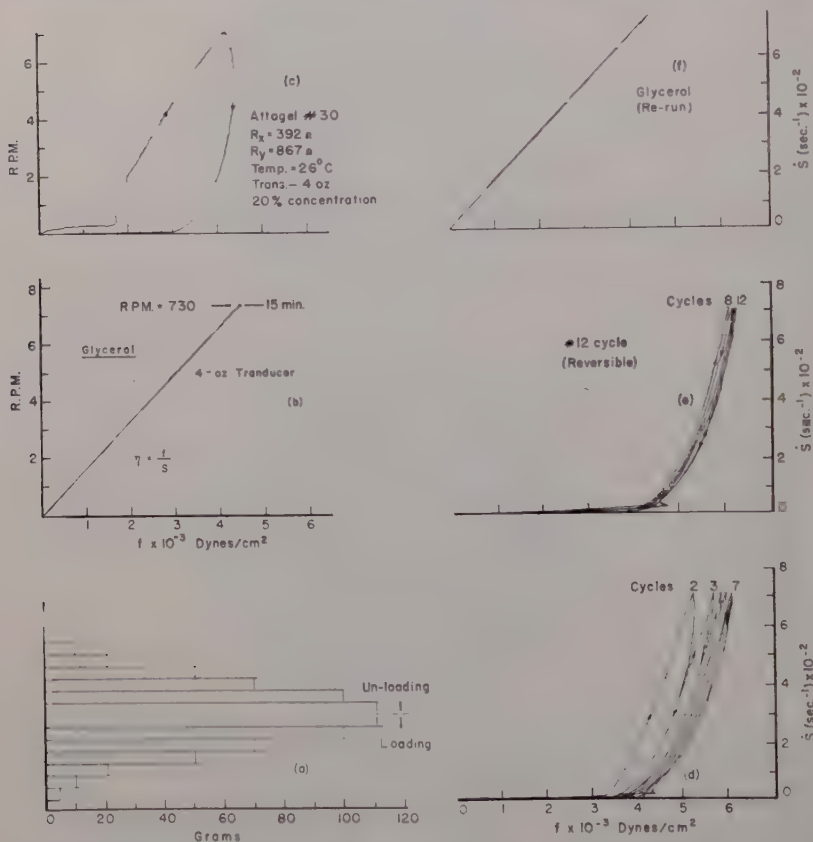


Fig. 3. Sequence of the experimental procedure. (a) Transducer-response calibration. (b) Calibration against a glycerol standard. (c) First flow curve of attapulgite suspension in water. (d) Decreasing hysteresis loops for successive cycles. (e) Continued successive cycling to the reversibility. (f) Re-run of the glycerol standard for a recheck on the machine operation.

accuracy of the response of the transducer to changing load during changing shear rates.

A calibrated standard is then run in the viscometer. Figure 3*b* shows the flow curve for a glycerol "standard." The ordinate and abscissa are drawn in to show the actual values for shear rate, $\dot{\gamma}$, and shear stress, f , respectively. In Figure 3*b*, one sees that the up and down curves, both straight lines passing through the origin, coincide; here the upcurve and downcurve are the flow curves which are obtained while the shear rate is uniformly increased or decreased, respectively, and are shown by upward and downward arrows in Figure 3. From the slope of the straight line in Figure 3*b*, the viscosity is given as $\eta = 6.38$ poises at 26°C., in agreement with the literature value 6.29 poises of 98% glycerol.

Following the "calibration," a flow curve, Figure 3*c*, was obtained on the attapulgite suspension in water. The flow curve recorded here is rheopectic (dilatant), i.e., the flow becomes more difficult with shear (compare the viscosities for the up and down curves). A family of successive 60-sec. cycles is shown in Figure 3*d*, where on cycle 6 the flow curve is nearly reversible (complete reversibility was obtained on cycle 10, Figure 3*e*), indicating a near complete buildup of structure (see below). Figure 3*f* shows the final recheck of the viscometer using the glycerol standard after the experiment shown in Figure 3*e*; the recheck confirms that there is no machine error during the experiments given in Figures 3*c* to 3*e*.

2. Temperature Dependence

The recorded temperature-dependent flow curves of attapulgite suspension in water are presented in Figures 4 to 7. The concentration is 20% by weight in distilled H₂O (pH = 5.7) with a pH range of 8.1 to 8.3 for the mixtures. All the cycles reported here are 60 sec. cycles; i.e., the time required for obtaining an up-down curve is 60 sec.

Figure 4 shows the first cycle flow curve obtained at the five temperatures using a new sample for each experiment. Figure 5 shows the family of curves resulting from successive cycling of the same sample; the final reversible curve (cycle 10) was followed by a 12-hr. rest period before the next cycle (dotted curve) was taken. Here, it is clear that the viscosity of the system increases with successive cycling, finally reaching a reversible flow curve, i.e., curve 10 shows

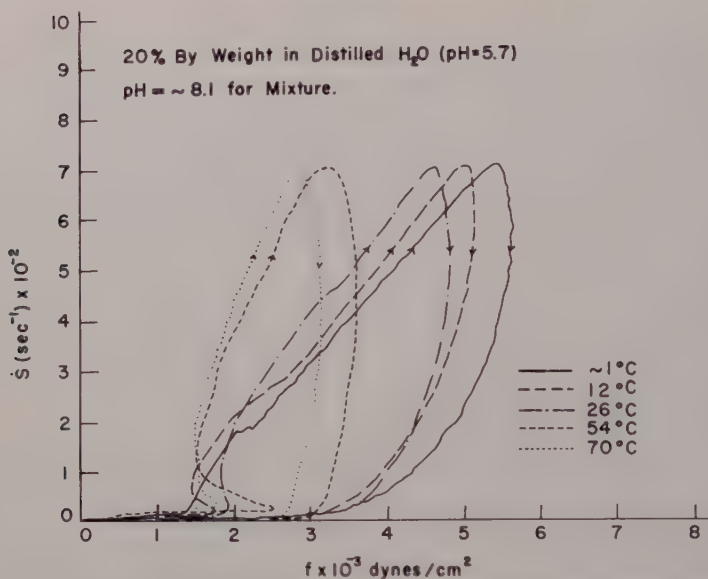


Fig. 4. First cycles for five temperatures; 20% suspension; pH ~ 8.2 .

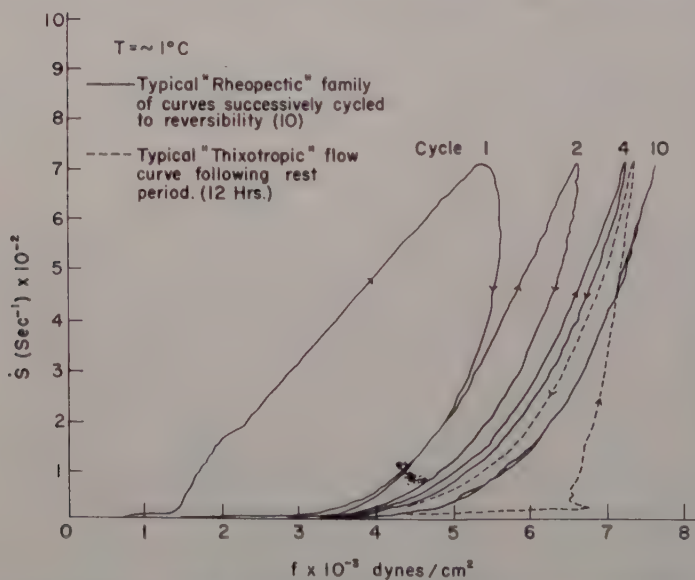


Fig. 5 Family of curves obtained by successive cyclings to reversibility; 20% suspension; pH ~ 8.2 .

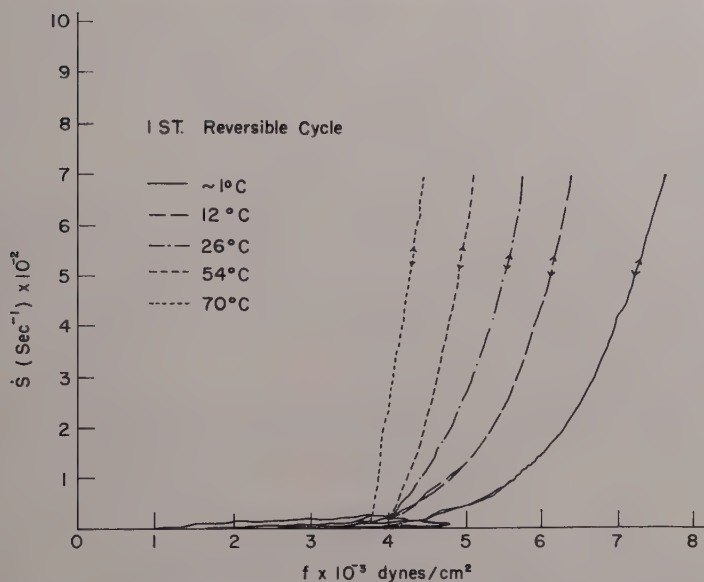


Fig. 6. Reversible flow curves after repeated cycling. The samples are those used in the experiments shown in Fig. 5; 20% suspension; pH \approx 8.2.

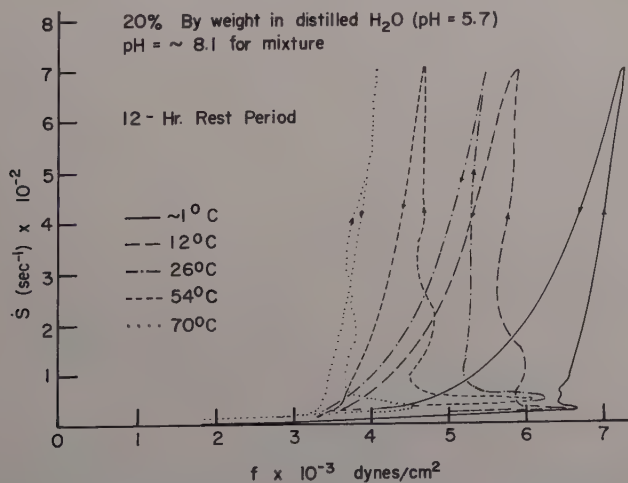


Fig. 7. First cycle following 12 hr. rest period after the first reversible curve was obtained; 20% suspension; pH \approx 8.2.

a complete structure build-up of the rheopectic material. The reason for appearance of the thixotropic curve (dotted) is considered in the Discussion. By successively cycling the system with the thixotropic curve, one again obtains a reversible curve like curve 10 (the details will be reported in a later communication).

It will be interesting to compare the present case with the case of grease. In grease we¹⁵ found that the hysteresis loop disappears with successive cycling, finally reaching a reversible curve without hysteresis loop, but the reversible curve appeared at the lower stress region, in contrast with the present case, i.e., in the case of grease, the structure breaks with shear, eventually attaining a completely broken down structure.

Figure 6 shows reversibility curves resulting from repeated cycling of samples whose first cycle curves are given in Figure 4. In Figure 7 are shown the resulting thixotropic curves following a 12-hr. rest period.

3. Viscosity versus pH

Measurements of pH changes with time, after adding a given quantity of HCl solution to the 20% sample, are shown in Figure 8, where

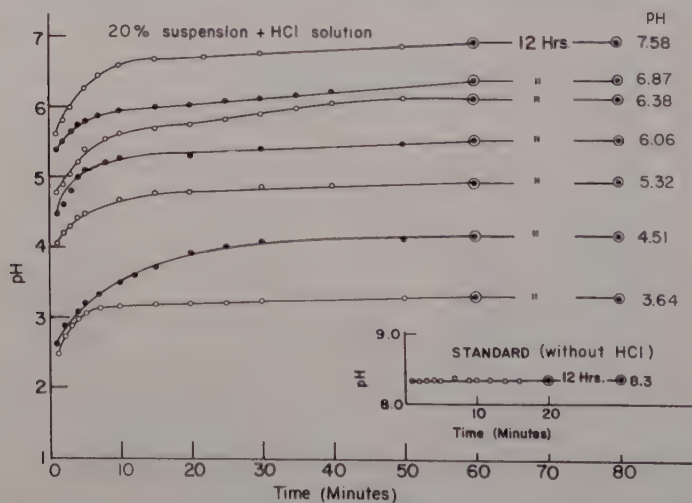


Fig. 8. pH change with time. Each curve was obtained for a sample of 20% suspension with a given amount of HCl solution. The pH value after 12 hr. is shown on each curve. $T = 26^{\circ}\text{C}$.

the inset shows the sample without HCl. One sees that the pH first increases with time, attaining near equilibrium value within 50 min.

Flow curves were taken on each sample after equal mixing (20

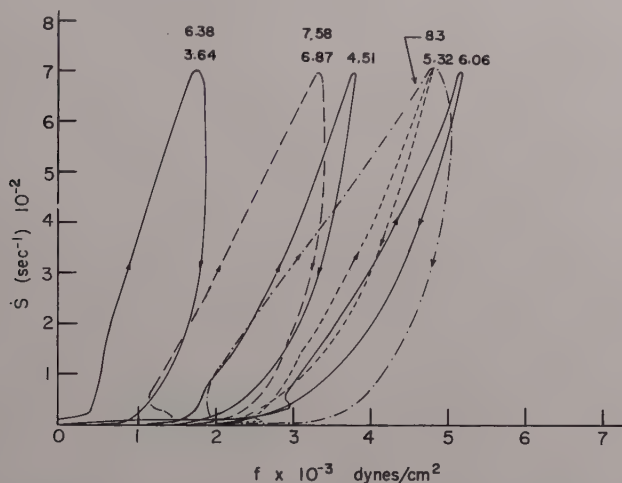


Fig. 9. First cycles for the samples with various pH. 20% suspension; $T = 26^\circ\text{C}$.

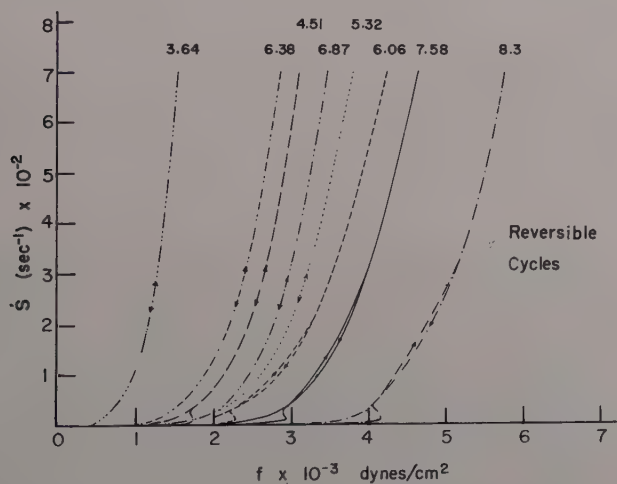


Fig. 10. First reversible cycles for the samples with various pH. The first cycles for these curves have been shown in Fig. 9. 20% suspension; $T = 26^\circ\text{C}$.

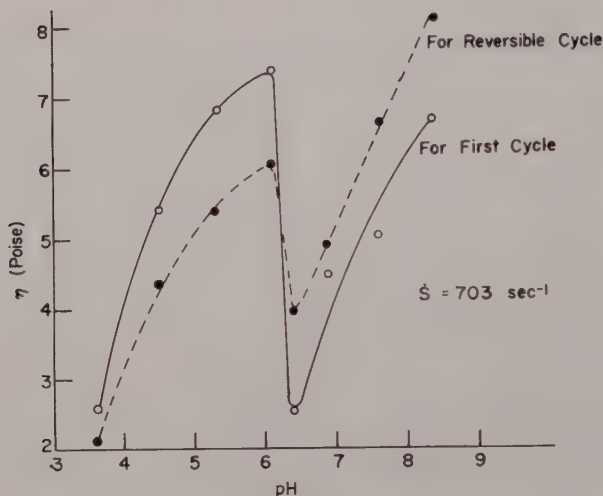


Fig. 11. Viscosity versus pH at $\dot{\gamma} = 703 \text{ sec}^{-1}$. The data are obtained from Figs. 9 and 10. 20% suspension; $T = 26^\circ\text{C}$.

min.) and rest times (13 hr.). First-cycle flow curves are shown in Figure 9. Flow curves for pH of 6.38 and 3.64 and those for pH of 7.58 and 6.87 were similar. The reversible cycles are shown in Figure 10. A plot of viscosity versus pH at the maximum shear rate (703 sec^{-1}) for the first cycle and the reversible flow curves is shown in Figure 11. It is well represented in the figures, especially in Figure 11, that the viscosity reaches a minimum value at $\text{pH} \approx 6.3$. That is, an inversion occurs at this pH value.

4. Soaking Time

From the many curves taken, we report here only a few of the flow curves for various soaking times after which the first cycle was taken. Figure 12 shows the flow curves on a 20% by weight sample (without addition of HCl) for various soaking periods. Here different samples were used for each soaking period. One may see that a longer soaking makes the flow easier for the first cycle, while the reverse is true for the reversible curves. Figure 13 shows the first-cycle flow curves for 16, 18, and 20 wt.-% samples for a soaking period of 1.5 hr. The change of the flow curves with concentration is as one expects.

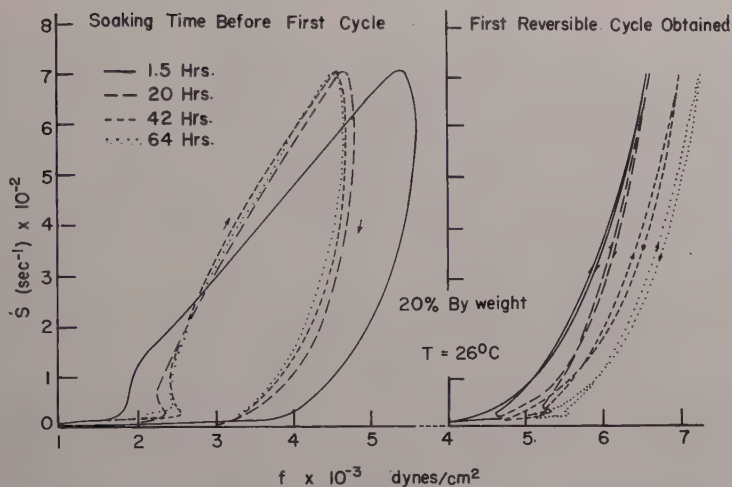


Fig. 12. First (the left-half) and reversible (the right-half) flow curves for a 20% suspension for four soaking periods. Without addition of HCl solution; $T = 26^\circ\text{C}$.

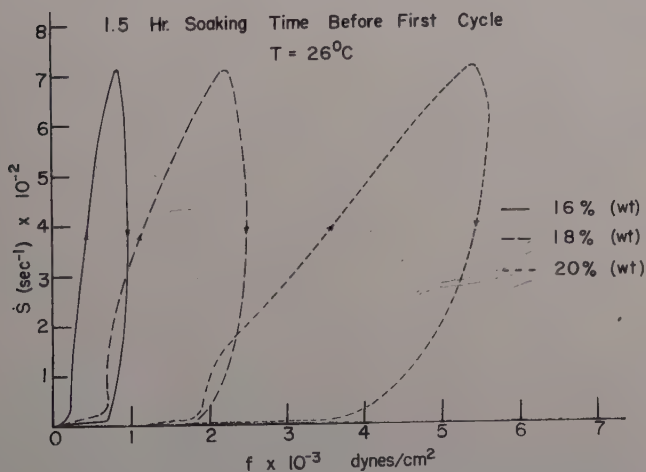


Fig. 13. First flow curves for three different weight-per cent suspensions following a 1.5-hr. soaking time after mixing. Without addition of HCl solution; $T = 26^\circ\text{C}$.

5. Relaxation Experiment

When the upcurve of Figure 14 for a new sample reached the preset maximum of the upcurve, the shear rate was kept constant and the change of the stress with time was observed. The stress grew first, then decayed as shown in the right-half part of Figure 14. After the newly attained peak stress decayed to its original peak stress of the upcurve, the shear rate was allowed to decrease, resulting in the down curve.

In Figure 15, a 60-sec. up-down curve was run on a new sample. The upcurve of the second cycle immediately followed the downcurve of the first cycle. At the peak of the second cycle, the shear rate was made constant. The growth-decay curve was again obtained as in the previous manner. When the built-up stress decayed to the original peak stress, the shear rate was then decreased to zero, resulting in the downcurve for the second cycle. The total time for the growth-decay curve in Figure 14 was approximately 40 min., while the time for the growth-decay curve in Figure 15 was about 85 min. The temperature measurements of water in the bob indicated no appreciable increase during the shearing process. It is interesting to compare the hysteresis loop in Figure 14 with that made up of the upcurve of the first cycle and the downcurve of the second cycle in Figure 15; the two loops are almost identical.

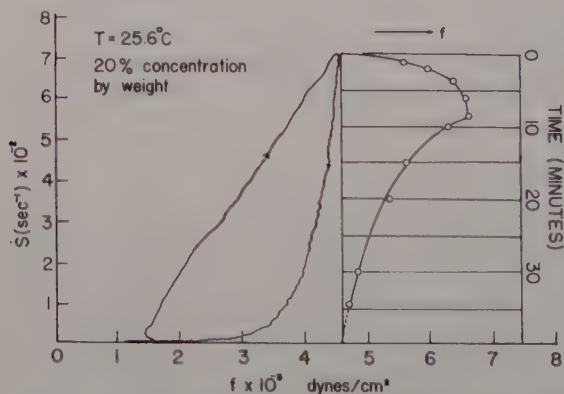


Fig. 14. Stress relaxation experiment. After the up-curve reached the peak strain rate, the latter was kept constant; the growth and decay of stress are shown in the right half. 20% suspension without adding HCl solution; $T = 25.6^\circ\text{C}$.

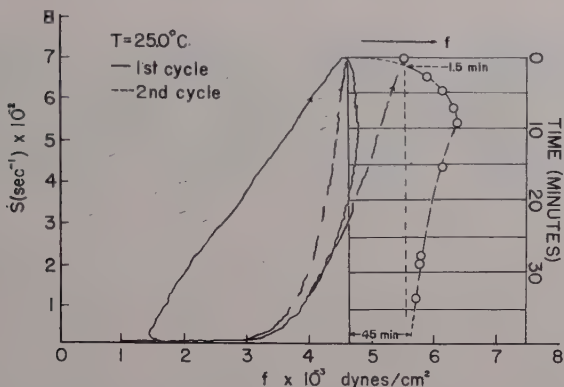


Fig. 15. Stress relaxation experiment. Refer to the text for the detailed explanation. 20% suspension without adding HCl solution; $T = 25^\circ\text{C}$. Note that the downcurve for the first cycle coincides with the upcurve for the second cycle below $\dot{\gamma} = 200 \text{ sec.}^{-1}$.

From the above stress-relaxation experiments, it is concluded that shearing brings two effects: structural build-up and break-down. The latter exceeds the former only when the system is sheared at a high shear rate ($\dot{\gamma} = 703 \text{ sec.}^{-1}$) for a long time (longer than 10 min.). Since our up-down curves are taken in 60 sec., the hysteresis loops must be due mainly to structural build-up. This conclusion can also be drawn from other experimental results, which are not reported here. It is also concluded that neither effect appears below 200 sec.^{-1} of $\dot{\gamma}$. The second conclusion comes from the fact that in Figure 15 the downcurve for the first cycle and the upcurve for the second cycle coincide in the low shear rate region, and also from the relaxation experiment conducted at low shear rates (not given here), which showed no change in stress.

Discussion

The experimental results are explained from the following model.

(1) As shown in the electron micrograph (Figure 2a), the un-sheared suspension includes multi-bundles of single crystalline needles, which separate from the bundle by shearing (Figure 2b).

(2) The single crystalline needles entangle with each other, making a network structure which increases viscosity.

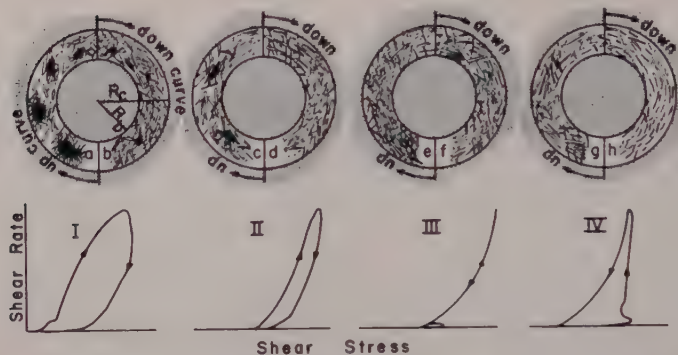


Fig. 16. Schematic representation of the model. (I) Multi-bundles of crystals (a) broken up into bundles plus single "needles" (b). Density of bundles decreases resulting in increased crossing of single crystalline needles, thus increasing viscosity. (II) Continued breakage of bundles (c) and (d) with increasing viscosity but decreasing "rheoplectic" loop. (III) No more bundle breaking into single needles (e) and (f). Reversibility shows complete build-up of the network structure. (IV) Thixotropy following rest period after reversibility (III) is reached. The network (g) breaks (h), thus decreasing viscosity.

(3) Shearing also brings about the breaking of single needles into shorter pieces (Figure 2b). As a result, the network becomes weak, resulting in a decrease of viscosity.

The proposed model is schematically represented in Figure 16. The two concentric circles indicate the cross sections of the bob and cup of the viscometer. The left-half and right-half of the annular space schematically express the states of suspension in the up-curve and down-curve stages, respectively. Thus, there are more multi-bundles in the up-curve stage than in the down-curve stage, whereas for the network of needles the reverse is true (Fig. 16I). As a consequence, the viscosity increases in the down-curve (see the rheoplectic loop in Fig. 16I). With repeated cycling, the density of the bundles decreases, resulting in a decreased rheoplectic loop (Fig. 16II). Finally, the rheoplectic loop disappears when *breakable* bundles under the experimental conditions (shear rate and shear stress) are completely broken (Fig. 16III). The system with reversibility followed by a 12-hr. rest period shows thixotropy (Fig. 16IV). This is due to the fact that during the rest period the network develops. The latter, however, breaks down by shear producing shorter pieces of needles.

Thus the viscosity in the down-curve stage is smaller than that in the up-curve stage (see the thixotropic loop in Fig. 16IV).

The relaxation experiments (Figs. 14 and 15) show that further shearing at the peak shear rate brings about more breaking of the bundles into single needles, thus resulting in the stress-growth. The stress decay following the latter is brought about by the breaking of single needles into shorter pieces because of the continued shearing.

Now we shall consider the effect of soaking times on flow curves. Longer soaking makes the density of the bundles smaller, as one would expect. Thus shorter soaking yields a larger rheopectic loop (see the left-half of Fig. 12). Also, longer soaking makes the separation of single needles from the bundle easier. As a result, more needles are produced, resulting in increased viscosity. Thus, the reversible curve for longer soaking periods appears at a higher shear-stress region (see the right-half of Fig. 12).

The effect of pH on the viscosity of the system is very striking. In our model the inversion at $\text{pH} = 6.3$ (see Fig. 11) is related to the iso-electric point of the system. It is assumed that dispersion of bundles into single needles reaches a minimum at $\text{pH} \simeq 6.3$. Thus the viscosity changes abruptly here. The effects of repeated shearing (reversible cycle determinations) on flow above and below $\text{pH} \simeq 6.3$ are quite opposite (see Fig. 11). When $\text{pH} > 6.3$, repeated shearing helps the dispersion, while the contrary is true if $\text{pH} < 6.3$. This may be due to the fact that the nature (e.g., charge) of colloidal needle-like particles changes completely at $\text{pH} < 6.3$. A definite conclusion will be drawn from further studies on the electrophoresis, osmotic pressure, zeta potential, etc., of the suspension.

As mentioned above, our model explains well, qualitatively, the observed facts. The Ree-Eyring generalized theory of viscous flow²⁴ will be applied in connection with the model in order to explain the results quantitatively. Further, experimental and theoretical studies is being carried out in this Laboratory. The results will be reported in a later communication.

The authors wish to express appreciation to the American Chemical Society for financial assistance given under grant no. PRF 211-A; to the National Science Foundation for its financial assistance; to Miss Belda Barlow for assistance in the preparation of the drawings and manuscript; and to the Minerals and Chemical Corporation of America for supplying the sample. One of us (A.F.G.) is indebted to Dr. Sherman D. Brown for discussions of data concerning pH changes.

References

1. Green, H., *Industrial Rheology and Rheological Structures*, Wiley, New York, 1949.
2. Fischer, E. K., *Colloidal Dispersions*, Wiley, New York, 1949.
3. Freundlich, H., *Thixotropy*, Herman, Paris, 1935.
4. Scott-Blair, G. W., *A Survey of General and Applied Rheology*, Pitman & Sons, London, 1949.
5. Engelhardt, W. V., *Kolloid-Z.*, **102**, 217 (1943).
6. Green, H., and R. N. Weltmann, *Ind. Eng. Chem. Anal. Ed.*, **15**, 201 (1943).
7. Green, H., and R. N. Weltman, *Ind. Eng. Chem. Anal. Ed.*, **18**, 167 (1946).
8. Jones, S. P., and J. K. Tyson, *J. Colloid Sci.*, **7**, 272 (1952).
9. Weltmann, R. N., *J. Appl. Phys.*, **14**, 343 (1943).
10. Weltmann, R. N., *Ind. Eng. Chem.*, **40**, 272 (1948).
11. Weltmann, R. N., *NLGI Spokesman*, **20**, No. 3, 34 (1956).
12. Wilson, J. W., and G. H. Smith, *Ind. Eng. Chem.*, **41**, 770 (1949).
13. Winkler, H. G. F., *Kolloid-Z.*, **105**, 29 (1943).
14. Hahn, S. J., T. Ree, and H. Eyring, *NLGI Spokesman*, **20**, No. 3, 12 (1957); **23**, 129 (1959); *Ind. Eng. Chem.*, **51**, 856 (1959).
15. Gabrysh, et al., to be published.
16. Green, H., *Ind. Eng. Chem. Anal. Ed.*, **14**, 576 (1942).
17. Buchdahl, R., J. G. Curado, and R. Braddicks, Jr., *Rev. Sci. Instr.*, **18**, 168 (1947).
18. Weltmann, R. N., and P. W. Kuhns, NACA TN3510, August 1955.
19. Smith, J. W., and P. D. Applegate, *Trade J.*, **126**, No. 23, 60 (1948).
20. Gabrysh, A. F., R. H. Woolley, T. Ree, H. Eyring, and C. J. Christensen, *Utah Engineering Experiment Station Bulletin*, **106**, Univ. of Utah, 1960.
21. Bradley, W. F., *Am. Mineral.*, **25**, 405 (1940).
22. Bates, T. F., *Circular No. 51*, College of Mineral Industries, Pennsylvania State University, 1958.
23. Grim, R. E., *Clay Mineralogy*, McGraw-Hill, New York, 1953, pp. 78-79.
24. Ree, T., and H. Eyring, *J. Appl. Phys.*, **26**, 793, 800 (1955); *Rheology*, Vol. II, F. R. Eirich, ed., Academic Press, New York, 1958, pp. 83-144.

Synopsis

The results reported here were obtained using a rotational viscometer constructed at this Laboratory, and concern the study of the flow properties of a attapulgite suspension in water. More particularly, the stress-strain-time relations with respect to variables of temperature, concentration, and pH are given in terms of rheopexy (dilataney) and thixotropy. The flow curve (shear rate, 0 to 700/sec. versus shear stress) exhibits first a rheoplectic hysteresis loop which is destroyed by repeated shearing, finally reaching a reversible and reproducible non-Newtonian flow curve. When the system with the reversible flow curve is rested for a long time (12 hr.), it presents a thixotropic loop. From stress relaxation experiments it is concluded that shearing introduces two effects, structural build-up and break-down, and that the rheoplectic hysteresis loop is brought about by the structural buildup. A model for explaining the observed fact is proposed.

The Rheology of Blood

ROBERT H. HAYNES, *Committee on Biophysics, University of Chicago, Chicago, Illinois*

Although the study of blood flow is a classic problem in both physiology and physics—many of Poiseuille's early experiments were on blood—unfortunately, this uniquely important suspension has received but little attention from modern rheologists. This is rather surprising, since it is required to flow under a wide range of interesting physical conditions in the normal circulatory system, and a change in blood flow is a common response to changes in the organism's environment. Furthermore, in several common diseases, both the blood and the blood vessels are altered in a rheologically interesting way.

For the purposes of this discussion, blood can be considered to be essentially a suspension of particles (red blood cells), about $8\ \mu$ in diameter, in a Newtonian solution. Apart from its ability to clot under certain conditions, blood has no peculiar rheological properties that are not shared by other physically similar suspensions. However, before embarking on a description of these properties, it is advantageous to outline briefly the physical conditions present in the circulation and the composition of blood.

In the circulatory system, blood is driven by an oscillatory pump through a very irregular and complex network of distensible vessels, whose radii and elastic properties vary widely in different parts of the system. In the large arteries, the flow is oscillatory, but the pulsations are dampened in the small vessels, and in the capillaries and veins the flow is effectively steady. Vessel diameters vary from about 2.5 cm. for the largest arteries and veins, down to about $8\ \mu$ for the capillaries; thus, the diameters of the red cells and the smallest vessels are about the same. Most of the pressure drop in the circulatory system occurs across the small arteries and the arterioles. These vessels, which are largely responsible for the peripheral control of the

circulation, have diameters on the range 20–200 μ , and the mean blood pressure drops from about 100 to 35 mm. Hg across them; the ultimate pressure in the veins is about 5 mm. Hg. Under normal circumstances, the shear rate at the vessel walls varies from a minimum of about 40 sec.^{-1} in the large veins, to a maximum of about 1300 sec.^{-1} in the arterioles; nominal values in the large arteries and capillaries would be about 400 and 800 sec.^{-1} , respectively.

Constitution of Vertebrate Blood

Vertebrate blood is a suspension of cells in a rather complex solution called plasma. The precise composition, and the dimensions of the cells, varies somewhat among different individuals, and more markedly from species to species; however, in this paper we will consider primarily human blood.

The specific gravity of human blood is about 1.06 and its viscosity, at high shear rates in a wide bore cylindrical tube, is roughly 3 times that of water at body temperature (37°C.). The volume fraction of the cells is called the "hematocrit," and it varies from 41 to 45% in normal adults. It should be noted that the specific gravity of the cells (1.09) is slightly greater than that of plasma (1.03), and the cells will settle out under gravity if the suspension is left to stand without stirring.

The plasma is a slightly alkaline (pH 7.4) solution, with a relative viscosity about 1.7 at body temperature. The dry matter content is about 70 g./l.: 100 cc. of plasma contain 91 cc. of water, 6.5 g. of protein, 0.6 g. of inorganic salts (mostly NaCl), and 1.4 g. of substances, such as glucose, and urea, which are transported by the blood stream. The plasma proteins are ellipsoidal in shape, except for β -lipoprotein, which is spherical (200 A. in diameter). The ellipsoidal proteins have a minor axis of about 40 A., and a major axis that varies from 150 A. for albumin, to 300 A. for α -lipoprotein, and 900 A. for fibrinogen. Although plasma contains these proteins, Bingham and Roepke,¹ and other workers, have found no detectable non-Newtonian properties under ordinary conditions. However, plasma does have one very remarkable rheological property, and that is its ability to clot under certain circumstances.

When blood vessels are broken and blood escapes over the injured tissues, a complex series of reactions takes place which leads to the formation of a plasma clot, in which the blood cells become enmeshed,

and which usually seals off the hemorrhage. Coagulation arises from the interaction of two proteins, thrombin and fibrinogen, which form the fibrous clot protein, fibrin. Fibrinogen is carried in the plasma, but, in order to avoid intravascular clotting, thrombin is not, but rather is activated from a plasma precursor (prothrombin) by calcium ions and the so-called thromboplastic substances derived from the platelets and the injured tissue. If a beaker of blood is allowed to clot, and then left to stand, the clot gradually retracts and squeezes out a clear fluid called serum. Thus, blood serum is merely blood plasma minus the proteins involved in clotting. Clotting can be suppressed by the addition of citrate, oxalate, or specific anticoagulants, such as heparin. It is clear that if one wishes to study *in vitro* the rheological properties of the suspension as it exists in the intact circulation, then the clotting mechanism must be removed. This is done most simply by adding an anticoagulant to the fresh sample; however, in order to get more uniform samples it is advantageous to resuspend the blood cells in serum or a special cell preservative solution, acid-citrate-dextrose (ACD). It should be noted that unless one works under sterile conditions, blood samples become quickly infected by airborne bacteria, and so it is often necessary to add some bacteriostatic agent unless the measurements can be made within a few hours.

The blood cells can be divided into two broad categories: the red cells, or erythrocytes, and the white cells, or leukocytes. An average leukocyte count is about 6000/mm.³, whereas there are about 5×10^6 red cells per mm.³ Since all types of leukocytes make up only 0.9% of the total cell volume, it is reasonable to assume that the non-Newtonian properties, as observed *in vitro*, arise primarily from the presence of the red cells in suspension.

The shape of the red cell is of interest since it is a biconcave disc, and is thought to be reasonably well adapted for a rapid and even diffusion of gas from its periphery towards its interior, since it constitutes a sort of compromise between a sphere and a thin disc. The essential dimensions of a normal, wet human red cell are shown in Figure 1. It is a solid of revolution about the vertical axis in the diagram; standard deviations of the various dimensions are also indicated in the diagram. It should be emphasized that the dimensions quoted here are for wet cells, whereas most measurements are made in dried smears or films where shrinkage reduces the mean diameter by about 1 μ . The mean diameter of human red cells in dried films is

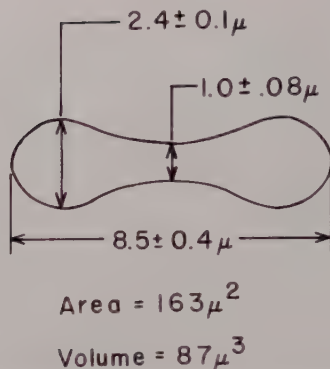


Fig. 1. Dimensions (with standard deviations) of a normal wet human erythrocyte. (Drawn on basis of data given by Ponder.²)

about 7.5μ ; Ponder² has tabulated this dimension for 117 different vertebrate species and found that it ranges from 2.1 to 9.2μ . The diameter distribution of human red cells is symmetrical about the mean, with a standard deviation of about 0.4μ ; thus, blood is reasonably monodisperse. This diameter distribution is used in clinical medicine, since it is of diagnostic significance in certain diseases; for example, the mean dried cell diameter increases to about 8.5μ and the standard deviation to almost 1μ in pernicious anaemia.

Important changes can be induced in the form of the red cells by various treatments. For example, in hypotonic saline, the cells take on fluid, swell, become spherical, and ultimately lose their hemoglobin. Similarly, certain chemical agents, such as rose bengal, are capable of changing the normal biconcave discs to spheres at constant volume. This disc-sphere transformation might provide an interesting system for studies on the rheological effects of the shapes of the suspended particles. However, it would appear that no such work has been done to date.

Finally, it should be noted that different red cell shapes are characteristic of certain pathological states. For example, in hypochromic anaemia the cells tend to be flatter, with a greatly increased axial ratio, whereas in congenital hemolytic icterus the cells have a lower axial ratio; one of the most marked changes is in a hereditary disease known as "sickle-cell anaemia" in which the cells are neither discs nor spheres, but "sickle" shaped.

Rheological Properties of Red Cell Suspensions in Vitro

As one would expect, the apparent viscosity of blood depends on the shear rate and the tube diameter as well as the volume fraction of cells. A slight thixotropy has also been reported.³ Most, if not all, of the *in vitro* viscosity measurements have been carried out on resuspended cells rather than fresh, whole blood. Although it would appear that the properties of such modified suspensions do not differ significantly from those of whole blood, nevertheless, one must be cautious in extrapolating the results of the *in vitro* studies to the intact circulation. For example, Copley and Scott Blair⁴ have recently

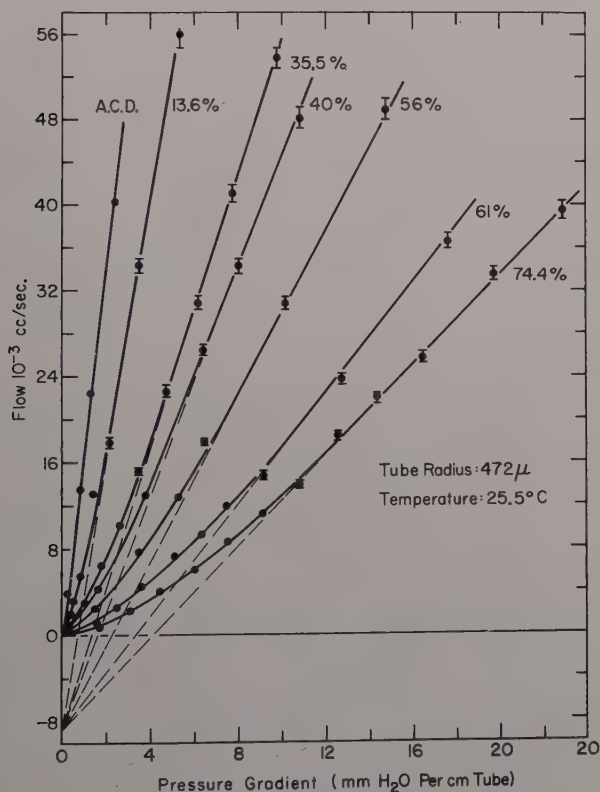


Fig. 2. Pressure-flow curves for suspensions of human erythrocytes (hematocrit in volume-%) in acid-citrate-dextrose solution. (Redrawn after Haynes and Burton.⁵)

shown that the apparent viscosity depends on the nature of any surface film (for example, fibrin) that may be present on the tube wall; similarly, the nature of the lining surface of intact blood vessels would be expected to vary from one part of the circulatory system to another, and to depend on the physiological state of the animal. However, bearing such difficulties in mind, it is usually assumed that the *in vitro* behavior of red cell suspensions reflects, at least in broad outline, corresponding properties of blood *in vivo*.

A typical set of pressure-flow curves for red cells resuspended in acid-citrate-dextrose (ACD) is shown in Figure 2. The measurements were made at 25.5°C. in a glass tube of radius 472 μ for a variety of cell volume fractions as indicated on the graph. Similar curves have been obtained in other tubes and at different temperatures. (For further experimental details, see Haynes and Burton.⁵) The curves pass through the origin,⁶ are nonlinear at low flow rates, but gradually become linear as the flow increases. The back extrapolations of the linear segments of these curves appear to converge, within the error of the measurement, to a common "nodal" point on the negative flow axis. Although all of our measurements have indicated that this point is independent of cell volume fraction from about 10 to 75%, Dr. Charles Wunder at the State University of Iowa has found that the back extrapolation appears to move toward the origin below about 20% (personal communication). However, the strong convergence that does seem to exist at this point is still somewhat remarkable. It is clear, from the curves of Figure 2, that the apparent viscosity of such suspensions depends on the volume fraction of cells and the rate of shear. However, the viscosity also depends on the tube diameter if this is reduced below about 400 μ . This latter effect is well illustrated in a plot of the consistency variables (wall shear rate versus wall stress) for tubes in this range. K  min⁷ made a very accurate series of measurements of the apparent viscosity of defibrinated ox blood (40% hematocrit), and the curves of Figure 3 have been calculated from his data. These curves indicate the same general behavior as the pressure-flow data of Figure 2, but in addition reveal a fall in viscosity as the tube radius is reduced. This is known as the Fahraeus-Lindqvist effect among physiologists,⁸ although among rheologists it would be just another example of the sigma phenomenon.⁹

Before discussing the dependence of viscosity on tube diameter and

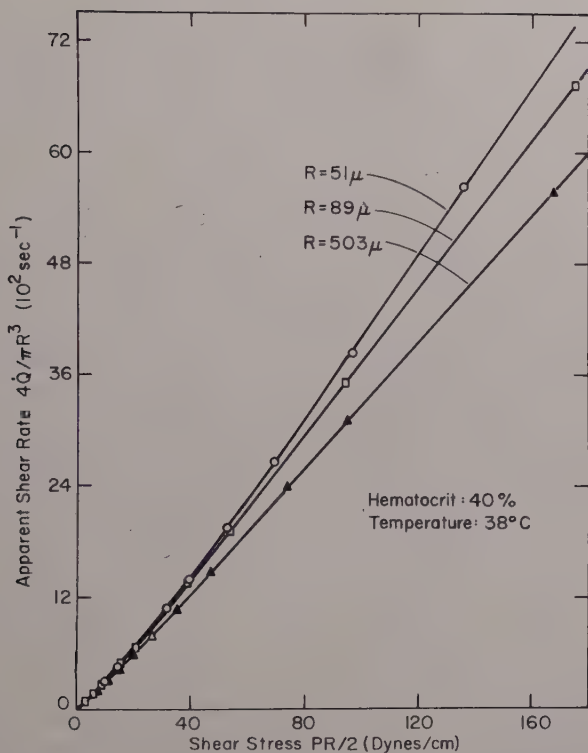


Fig. 3. Consistency curves for a 40% suspension of ox erythrocytes measured in tubes of three radii. (Points calculated⁶ from data of Kümin.⁷)

hematocrit in more detail, it should be noted that the range of shear rates over which these measurements have been made, while adequate for physiological purposes, is none too large from the rheological standpoint. In particular, one would like to be assured that the curves of Figures 2 and 3 have indeed become linear and reached their final slope. It would appear that the highest wall shear rate so far reported is about $13,500 \text{ sec.}^{-1}$ (in Kümin's tube, 89μ radius), and a log-log plot of the data shows a unit slope over the range $2,000$ – $13,500 \text{ sec.}^{-1}$ in this case. In larger tubes (cf. Fig. 3) the curves appear to reach linearity at somewhat lower shear rates. The higher hematocrit curves of Figure 2 have only just achieved linearity, and so the numerical value of the nodal point could be in error to the extent that the

straight lines do not truly reflect the limiting slopes of the curves. Since there are also reasons for desiring more accurate data at very low shear rates, there is clearly a need to extend these measurements over a much wider range of shear rates.

Effect of Cell Volume Fraction on Viscosity

The hematocrit dependence of the apparent viscosity at high shear (obtained from the asymptotic slope of the pressure-flow curves) is shown in Figure 4 for various tube radii. These curves are approximately exponential, except at very low hematocrits.^{5,11} The effect of increasing tube radius has almost reached its plateau at 747 μ . The curve for a tube of radius 5.5 μ is especially interesting. This corresponds in size to the capillaries in the circulatory system, and is only slightly larger than the red cells themselves; however, the viscosity at high shear shows little or no dependence on hematocrit over a surprisingly wide range (0–40%). These very difficult measurements in such small tubes were recently carried out for the first

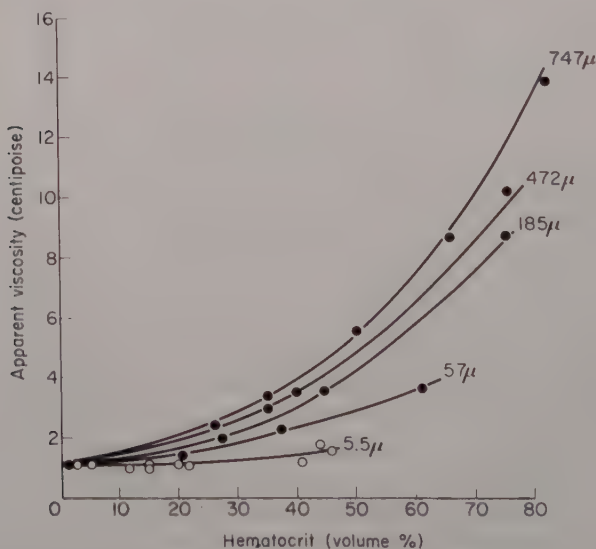


Fig. 4. Apparent viscosity at high shear of human erythrocytes as a function of hematocrit in tubes of different radii. (The lower curve for a tube of radius 5.5 μ was kindly provided by Dr. John Prothero of the University of Western Ontario. The upper curves are redrawn after Haynes and Burton.⁵)

time by Dr. John Prothero in Prof. A. C. Burton's laboratory, at the University of Western Ontario. Although such a result might have been anticipated from the gradual flattening of the other curves with decreasing radius, nevertheless it is of physiological interest, since great local fluctuations in hematocrit occur in the capillary network; thus, such a relatively constant viscosity should help to maintain a smooth movement of blood through these vessels.

Effect of Shear Rate on Viscosity

It is clear from the curves of Figures 2 and 3 that the viscosity decreases as the flow or shear rate is increased. However, in many physiological problems, one is more interested in the dynamic behavior of blood as the flow rate or applied pressure changes, and in such instances the apparent viscosity η , calculated by a direct application of Poiseuille's law, is not the most informative coefficient to use in studying this effect. For example, curves of apparent viscosity versus shear rate give no immediate indication that the pressure-flow curves become effectively linear at moderate flow rates. This shortcoming is not present in plots of the differential viscosity (η'), which is proportional to the slope of the pressure-flow curves. Another coefficient of interest is the "generalized viscosity" (η^*), which is proportional to the ratio of the applied stress to the rate of shear at the tube wall. These three coefficients are plotted in Figure 5 as a function of the rate of shear at the tube wall. In each case, the lower curve, which remains flat down to rather low shear rates, is the differential viscosity. The upper curve is the apparent viscosity, and the middle curve is the generalized viscosity. These three coefficients are related, but two are required to specify the behavior of the suspension at any given shear rate (see mathematical appendix).

Although the shape of the pressure-flow and viscosity curves suggests that the shear dependence can be interpreted phenomenologically as a "structural viscosity," it is not completely clear what the structural change might be. The mechanism usually suggested is the axial accumulation of the red cells.^{3,10,12} According to this theory, the red cells would tend to rotate in the variable shear field present in a cylindrical tube, and therefore should be subject to a transverse Magnus force which would make them drift toward the tube axis. This axial drift would be opposed by mutual collisions among the cells, so that as the flow rate is increased an equilibrium situation

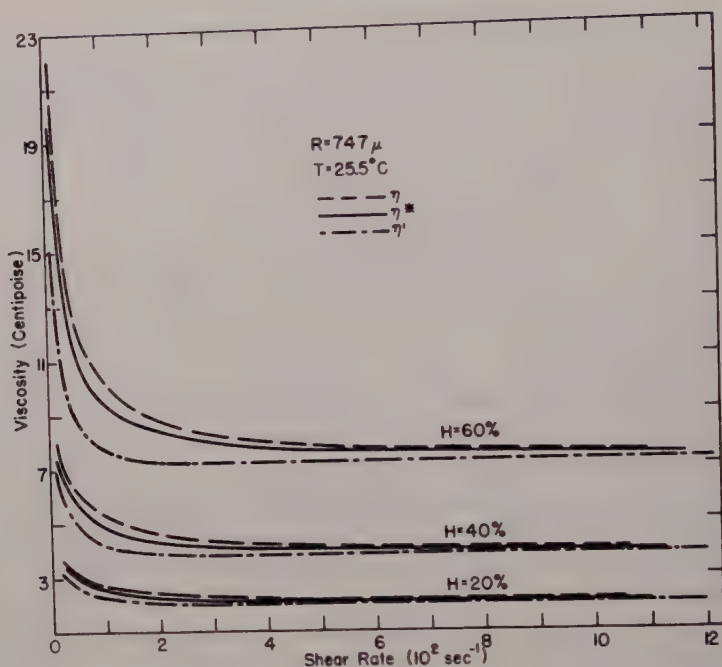


Fig. 5. Apparent, generalized, and differential viscosity coefficients of suspensions of human erythrocytes (three hematocrits) as a function of the shear rate at the tube wall.

would finally be reached in which fluid near the tube wall is deficient in red cells as opposed to the axial core. There can be little doubt but that, qualitatively, such an effect would explain the gross behavior of blood. However, despite numerous reports by physiologists of an effectively cell-free marginal zone in blood flowing both *in vivo* and *in vitro*,^{13,14} there have been few quantitative studies of the effect. Taylor¹⁵ has measured a rather large and reproducible decrease in cell concentration near the tube wall as the flow rate increases, but the experiments of Bayliss¹⁶ suggest that axial accumulation is a somewhat elusive phenomenon, and if present, would play only a minor role in reducing the viscosity with increasing shear. On the other hand, Müller¹⁷ studied the flow of a suspension of small rubber discs in a glycerol solution of equal density through a horizontal tube whose diameter was twice that of the discs. He reported that as the sus-

pension emerged from the tube, the particles were centered about the tube axis and were surrounded by a marginal zone of clear solvent.

Although the existence of axial accumulation is supported by some direct experimental evidence, the theoretical situation is not clear; however, two approaches to this problem should be noted. The first is based on the hypothesis of Jeffery¹⁸ that a particle in suspension will move in such a way that the energy dissipation is a minimum. Saffman¹⁹ has investigated the effect of the inertia of the liquid on such a particle, which is of course neglected in the linearized Navier-Stokes equation, and he found that this would tend to slowly orient prolate and oblate spheroids in accordance with Jeffery's hypothesis; in addition, the inertial terms give rise to a transverse force on the particle making it move toward the tube axis, which Jeffery also predicted, since the extra energy dissipation due to the suspended particle is least in the region of minimum shear. Unfortunately, these inertial effects are much too small to account for either the orientation or the axial drift, and in the latter case the transverse velocity is ten times less than that required to account for the observations of Taylor.¹⁵ The second theoretical approach, based on the assumption that the rotation of the cells in the shear gradient would give rise to a transverse Magnus force, has not been worked out in detail for blood, although such a mechanism has been postulated for similar problems by Starkey²⁰ and Tollert.²¹

It should be emphasized that axial accumulation, whatever its basic cause, can occur only for hematocrits below about 50%, and although the general character of the shear dependence is the same at higher hematocrits, some other mechanism must be sought to account for it.

Effect of Tube Radius on Viscosity

The dependence of the viscosity at high shear on the radius of the tube in which the measurements are made is shown in Figure 6 for various hematocrits.⁸ Two theories have been proposed which might account for this effect. One, due to Dix and Scott Blair,²² suggests that the presence of particles of finite size in suspension means that there must exist unsheared laminae of finite thickness in the fluid, so that the total flow through the tube should be calculated by a summation rather than an integration. The characteristic parameter of this theory is the thickness of the unsheared laminae δ . Another theory attributes the effect to the formation of an essentially cell-free mar-

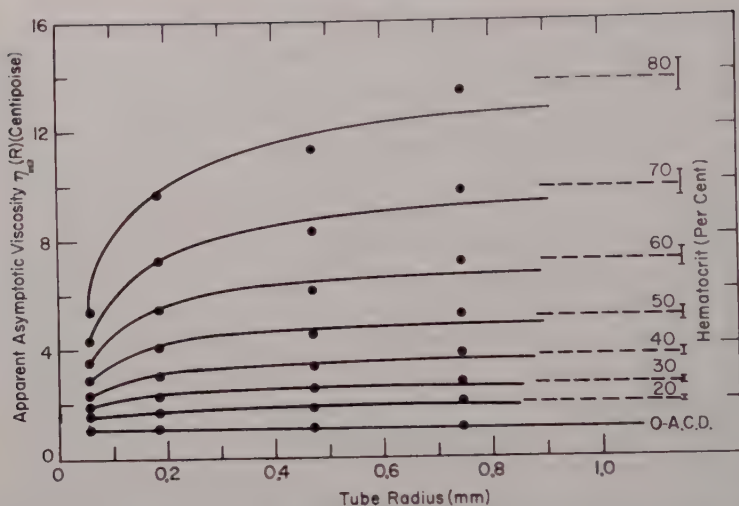


Fig. 6. Fahraeus-Lindqvist effect (sigma phenomenon) in suspensions of human erythrocytes. (Haynes.⁸)

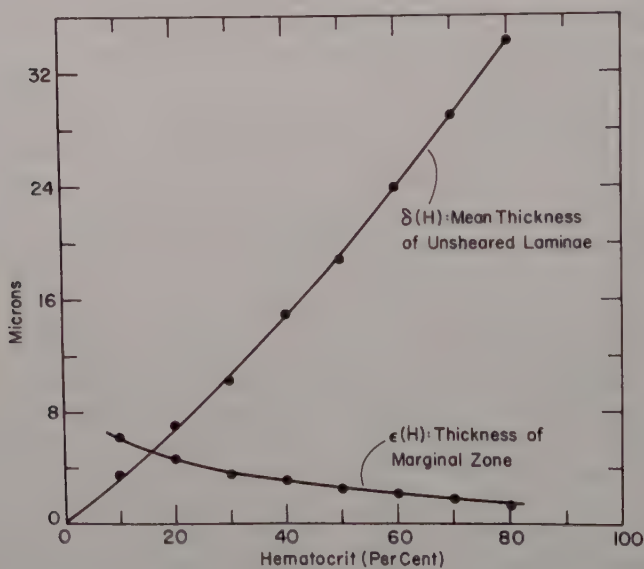


Fig. 7. Parameters in finite laminae (δ) and marginal zone (ϵ) theories of Fahraeus Lindqvist effect as a function of hematocrit. (Haynes.⁸)

ginal zone whose thickness is independent of the tube radius, and which would, therefore, have a greater influence on the flow in small tubes than in large tubes. In this latter theory, the characteristic parameter is the thickness of the marginal zone, ϵ . The equations of each theory are of the same form to the first order in $1/R$, and each fits the data equally well; however, the dependence of the two characteristic parameters on hematocrit is quite different, as shown in Figure 7. Although one would expect δ to increase with hematocrit due to the formation of clusters as the cells become more closely packed, nevertheless, the actual size required at high hematocrits seems rather large indeed. On the other hand, only a very thin marginal zone is required to account for the effect, and at high hematocrits, it may represent nothing more than a kind of "slippage" zone due to a deficiency of cell centers at the tube wall.²³ In view of the relative change in δ and ϵ with hematocrit, the marginal zone provides the more attractive interpretation of this effect.

It would be inappropriate to enter into a more lengthy discussion of the mechanism of the shear and tube radius dependence of blood viscosity, mainly because these problems have not as yet been completely solved; however, it does seem likely that both effects can be attributed to some sort of axial accumulation of the red cells with concomitant formation of a cell-free marginal zone.

Conclusions

The significance of these rheological properties of blood in the normal circulatory system can be conveniently summarized by classifying the vessels into four categories, depending on their diameters and the flow conditions usually present in them: first, the aorta and large arteries, in which the flow is pulsatile; second, the small arteries and arterioles where the pulsations are weak, but across which occurs the greatest drop in blood pressure; third, the capillaries, whose diameter is only slightly larger than the red cells themselves; and fourth, the venous system in which the pressure is low and the flow steady.

In the large arteries, Taylor²⁴ has found that only a 2% error is introduced into the calculation of the oscillatory flow by assuming that the viscosity of blood is independent of the shear and equal to its asymptotic value at high shear. Furthermore, these vessels have a

large diameter and so the effect of any marginal zone can also be neglected.

In the arterioles, the shear rate is generally high enough for asymptotic conditions to be reached, although the net flow is somewhat greater than would be otherwise anticipated on account of the existence of the Fahraeus-Lindqvist effect.

Capillary flow is still not well understood, although one significant point has emerged from the work of Prothero which indicates that local fluctuations in hematocrit would have little effect on the net flow through the network.

Conditions on the venous side resemble those in the arteries, except that since there are no pulsations, the small effect of the shear dependent viscosity on oscillatory flow is absent; the shear rate is low enough for the viscosity to be dependent upon it.

Thus, although blood has well-marked non-Newtonian properties, the conditions in the normal circulatory system are such that they can be neglected in many hemodynamic problems. Nevertheless, it is important to have a clear understanding of these effects because of their potential importance in the many circumstances when the flow rate in a given vascular bed is reduced below the normal values. Finally, for the pure rheologist, blood presents many interesting and challenging problems in the general study of the flow of disperse systems.

MATHEMATICAL APPENDIX

The pressure-flow curves of erythrocyte suspensions in glass tubes (Fig. 2) can be represented by an equation of the form⁵

$$\dot{Q} = M(R,H)P - B(R)[1 - e^{-k(R,H)P}] \quad (1)$$

where \dot{Q} is the volume flow rate, and P is the applied hydrostatic pressure per unit tube length; $M(R,H)$ is the final linear slope of the curves, which depends on the tube radius R and on the hematocrit H ; $B(R)$ is the back extrapolation, or nodal point, on the negative flow axis, which appears to depend only on the tube radius; $k(R,H)$ is the exponential constant that determines the shape of the nonlinear part of the curves. Although it is perhaps not customary to use the applied pressure gradient as an independent variable, it is convenient in the case of blood, since experimentally, the pressure is usually the independent variable.

The coefficients of apparent, differential, and generalized fluidity or viscosity (Fig. 5) are defined to be, respectively,

$$\phi = 1/\eta = (8/\pi R^4)(\dot{Q}/P) \quad (2)$$

$$\phi' = 1/\eta' = (8/\pi R^4)(d\dot{Q}/dP) \quad (3)$$

$$\phi^* = 1/\eta^* = 2F(PR/2)/PR \quad (4)$$

where $F(PR/2)$ is the shear rate at the tube wall. If the applied stress at a radial distance r from the tube axis is written as $\theta = Pr/2$, then it is easy to show that the flow can be written as the integral,

$$\dot{Q} = (8\pi/P^3) \int_0^{PR/2} \theta^2 F(\theta) d\theta \quad (5)$$

θ is a running variable and the integral is a function of its limits, so that by differentiating with respect to P and solving for F we get,

$$F(PR/2) = (1/\pi R^3)[3\dot{Q} + P(d\dot{Q}/dP)] \quad (6)$$

Thus, from eqs. (4) and (6), ϕ^* can be written as,

$$\phi^* = (6/\pi R^4)(\dot{Q}/P) + (2/\pi R^4)(d\dot{Q}/dP) \quad (7)$$

and using eqs. (2) and (3) we get the following relation connecting the three fluidity coefficients,

$$\phi^* = \frac{3}{4}\phi + \frac{1}{4}\phi' \quad (8)$$

or, in terms of viscosity,

$$(1/\eta') + (3/\eta) = (4/\eta^*) \quad (9)$$

If the pressure-flow relation (1) is used to write ϕ , ϕ' , and ϕ^* explicitly, then it is evident that all three are equal as zero and infinite shear stress is approached; let these limiting fluidities be ϕ_0 and ϕ_∞ , respectively. Equation (1) can now be rewritten in the form,

$$\phi' = \phi_\infty - (\phi_\infty - \phi_0)e^{-kP} \quad (10)$$

from which it is clear that the shear or stress dependent viscosity of blood can be interpreted in "structural" terms, if it is assumed that the "structural state" of the suspension is characterized by $(\phi_\infty - \phi')$ and that the fractional change in this quantity is directly proportional to the change in applied pressure.

The equations for the curves in Figure 6 are, first, on the basis of the Dix-Scott Blair finite laminae model,²²

$$[1/\eta_{\infty}(R)] = [1/\eta_{\infty}(\infty)](1 + \delta/R)^2 \quad (11)$$

where $\eta_{\infty}(R)$ is the viscosity at effectively infinite shear in a tube of radius R , and $\eta_{\infty}(\infty)$ is the asymptotic viscosity in a tube of effectively infinite radius; δ is the thickness of the unsheared laminae in steady flow. On the basis of the marginal zone hypothesis, where η_s is the viscosity of the suspending liquid in a marginal zone of thickness ϵ , and where the viscosity in the core is assumed to be equal to $\eta_{\infty}(\infty)$, we have, to the first order in $1/R$,

$$[1/\eta_{\infty}(R)] = [1/\eta_{\infty}(\infty)]\{1 + (4\epsilon/R)[(\eta_{\infty}(\infty)/\eta_s) - 1]\} \quad (12)$$

Equating the coefficients of $1/R$ in (11) and (12) gives the relation between ϵ and δ ,

$$\epsilon = \delta\eta_s/2[\eta_{\infty}(\infty) - \eta_s] \quad (13)$$

I wish to thank Dr. John Prothero, of the Biophysics Department, University of Western Ontario, for permission to use some of his unpublished data in this paper.

Note Added in Proof: R. E. Wells and E. W. Merrill [*Science*, **133**, 763 (1961)] have recently found that fresh plasma, to which no anticoagulant has been added, does indeed have a shear dependent viscosity as measured in a Couette viscometer, but that the shear dependence effectively vanishes upon the addition of oxalate or heparin, in agreement with the findings of Bingham and Roepke.¹

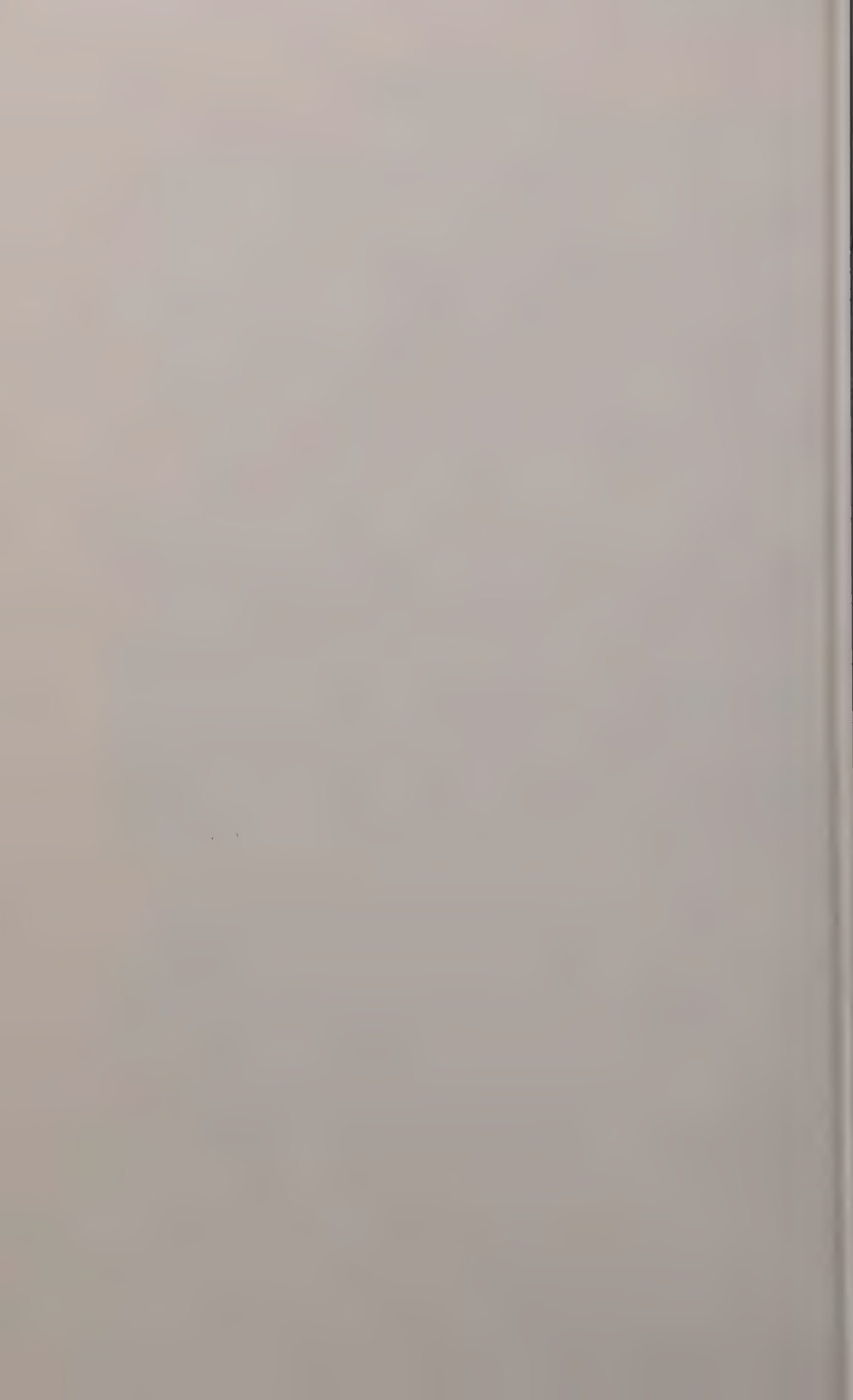
References

1. Bingham, E. C., and R. R. Roepke, *J. Gen. Physiol.*, **28**, 79 (1944).
2. Ponder, E., *Hemolysis and Related Phenomena*, Churchill, London, 1948.
3. Bayliss, L. E., in *Deformation and Flow in Biological Systems*, A. Frey-Wyssling, ed., North-Holland, Amsterdam, 1952, chapter 6.
4. Copley, A. L., and G. W. Scott Blair, *Rheol. Acta*, **1**, 170 (1958).
5. Haynes, R. H., and A. C. Burton, *Am. J. Physiol.*, **197**, 943 (1959).
6. Haynes, R. H., *Nature*, **185**, 679 (1960).
7. Kumin, K., Inaugural Dissertation, Bern, 1949.
8. Haynes, R. H., *Am. J. Physiol.*, **198**, 1193 (1960).
9. Scott Blair, G. W., *Rheol. Acta*, **1**, 123 (1958).
10. Haynes, R. H., and A. C. Burton, in *Proceedings of The First National Biophysics Conference*, H. Quastler and H. J. Morowitz, eds., Yale Univ. Press, 1959, p. 452.

11. Richardson, E. G., *Dynamics of Real Fluids*, Arnold, London, 1950.
12. Lewis, D. H., *J. Appl. Physiol.*, **6**, 716 (1954).
13. Schklarewsky, A., *Pflügers Arch. ges. Physiol.*, **1**, 603 (1868).
14. Thoma, R., in *Aberhalden's Handbuch der biologischen Arbeitsmethoden*, Abt. V, T. 4, H. 2, 1103 (1927).
15. Taylor, M. G., *Australian J. Exptl. Biol. Med. Sci.*, **33**, 1 (1955).
16. Bayliss, L. E., *J. Physiol.*, **149**, 593 (1959).
17. Müller, A., *Arch. Kreislaufforsch.*, **8**, 245 (1941).
18. Jeffery, G. B., *Proc. Roy. Soc.*, **A102**, 161 (1922).
19. Saffman, P. G., *J. Fluid Mech.*, **1**, 540 (1956).
20. Starkey, T. V., *Brit. J. Appl. Phys.*, **7**, 52 (1956).
21. Tollert, H., *Z. Elektrochem.*, **59**, 917 (1955).
22. Dix, F. J., and G. W. Scott Blair, *J. Appl. Phys.*, **11**, 574 (1940).
23. Vand, V., *J. Phys. & Colloid Chem.*, **52**, 314 (1948).
24. Taylor, M. G., *Phys. Med. Biol.*, **3**, 273 (1959).

Synopsis

Blood is a complex fluid of various cell types suspended in a solution (plasma) containing dissolved salts, carbohydrates, lipids, and proteins. It has several interesting rheological properties, the most important of which is its ability to form a dense clot under certain conditions, as in hemorrhage. However, from the standpoint of hemodynamics, certain other rheological properties, which arise primarily from the presence of the red cells in suspension, are also of considerable interest; these are the dependence of the apparent viscosity on the rate of shear and the tube size in which the blood is flowing. (In the circulatory system one finds a wide range of shear rates and vessel sizes.) The shear-dependent viscosity can be explained in terms of the axial accumulation of the red cells with concomitant formation of an effectively cell-free marginal zone at the tube or vessel wall. The dependence of viscosity on tube radius can also be explained in terms of such a cell-free marginal zone. In this paper, some of the experiments and theoretical approaches that have been used to elucidate these phenomena are discussed together with their physiological implications.



Shear Viscosities and Stress-Relaxation Viscosity Parameters of Gelled Oils

DEAN W. CRIDDLE and JAY CORTES, JR., *California Research Corporation, Richmond, California*

Introduction

Many studies have been made of the shear viscosity of greases,¹ and a few data are available for calculation of stress-relaxation viscosity parameters;² but these two viscosities have not been available on the same system for comparison. This experimental study provides these data on typical greases and shows the conditions under which they are equivalent for shear rates in the range of 10^{-5} to 10^{-2} sec.⁻¹.

Viscosity values of non-Newtonian materials can be specified in several ways. In this study we choose to discuss the viscosity and shear rate at a solid-grease interface in comparing values obtained from capillaries with those obtained from falling cylinders.

Stress-relaxation viscosity parameter (hereafter called internal viscosity) is used here as the product of the shear modulus and the stress-relaxation time at constant strain.³ A stressed body of high internal viscosity relaxes slowly at constant strain.

Experimental

Typical greases were selected with different compositions and properties, as listed in Table I.

For greases in capillaries we calculated the viscosity, shear stress, and shear rate at the wall, as discussed by Philippoff and Gaskins,⁴ from apparent viscosity data obtained by ASTM Method D 1092-55.⁵ The kinetic energy and the calculated end effect corrections were negligible; the elastic energy correction was assumed negligible for such capillaries (80:1 ratio of length to radius.) This assumption has been questioned by recent workers,⁴ but it enables us to compare

TABLE I
 Composition and Properties of Greases

Grease	Composition			Physical properties		
	Thickener Type	Wt.-%	Oil vis- cosity, poises at 25°C.	ASTM penetration ^b		Ultimate yield shear stress, ^o 10 ⁵ dynes/- cm. ²
				Un- worked	Worked	
A	Sodium GA-10 ^a	15	2.30	164	167	27.5
B	Sodium GA-10 ^a	13	2.30	174	189	16.0
C	Sodium GA-10 ^a	11	2.30	197	216	10.4
D	Sodium GA-10 ^a	7	2.30	265	305	2.7
E	Sodium GA-10 ^a	5	2.30	336	354	0.9
F	Lithium-calcium stearate	10	2.35	237	298	4.1
G	Sodium stearate	14	7.14	242	311	—
H	Lithium stearate	14	2.24	152	216	8.7
I	Polyethylene	9	10.1	258	—	2.1
J	Calcium soap and salt com- plex	29	4.10	301	313	2.1

^a Sodium salt of *N*-octadecylterephthalamate.

^b ASTM Test Method D 217-52T

^c Method of ref. 7, deformation rate = 2.0×10^{-2} sec.⁻¹.

"apparent viscosity" values with those in the literature for other greases.

From falling cylinder data we calculated the shear stress at the inner cylinder wall, where maximum shear occurs, and the viscosity at this wall; and from these results we calculated a shear rate at the cylinder wall. The assumption was made in calculating viscosity that the deformation is proportional to the stress across the narrow annulus. This leads to an error in the viscosity of less than 10%, which is within experimental error, and is negligible in terms of the overall 10⁶-fold change in viscosity as a function of shear rate.

Internal viscosities were calculated from shear moduli and from stress relaxation curves, as explained later. Shear moduli, *G*, were calculated from stress-strain data applied to an integrated equation for the geometry of the apparatus, i.e.,

$$G = (F/2\pi LY) \ln (b/a)$$

where F is the force and Y the displacement obtained from the initial slope of the stress-strain curve, and L is the length of concentric cylinders of outer and inner radii b and a .

For a falling cylinder viscometer⁶ we used two concentric cylinders 10.0 cm. long. The inner cylinder had an outside diameter of 1.66 cm., and the outer cylinder had an inner diameter of 2.70 cm. An Instron Tensile Tester was used to shear the sample and the stress-strain and stress-relaxation curves were recorded as described earlier.⁷ Shear rates below 2.0×10^{-3} sec.⁻¹ were obtained with a lever system coupled to the Instron Tester. All data were obtained at $25 \pm 2^\circ\text{C}$. Each experiment was done two or three times. The standard deviation for repeat determinations was 10% of the ultimate yield stress. Uniform specimens were prepared by homogenizing grease 60 strokes in an ASTM Grease Worker.⁸ The volume between the coaxial cylinders was filled with sample, and packed cylinders were aged for 10 to 15 days. Shear viscosity values (η) were calculated by the equation of Fox and Flory:⁶

$$\eta = (F/2\pi LV) \ln (b/a)$$

where F is the shear force when the coaxial cylinders of length L and radii a and b are displaced at a velocity V .

Results and Discussion

Typical shear viscosity data obtained in capillaries and in the falling coaxial viscometer are given in Figure 1. The two methods give consistent results, cover different shear rate ranges, and provide a wide range of values in bulk shear experiments for comparison with stress-relaxation internal viscosity.

Shear viscosities were calculated from ultimate yield shear stresses. Greases sheared continuously at $10,000$ sec.⁻¹ for over an hour are still decreasing in viscosity. Thus, the shear data were obtained under transient, nonequilibrium conditions rather than steady-state conditions.

Typical stress-strain curves are shown in Figure 2 for several different shear rates. These curves are essentially linear up to at least 25% of the ultimate yield stress, and these linear regions of the stress-strain curves were used to obtain shear moduli. The shear modulus of each grease tested was constant, within experimental error, for a wide range of strain rates, as shown in Figure 3.

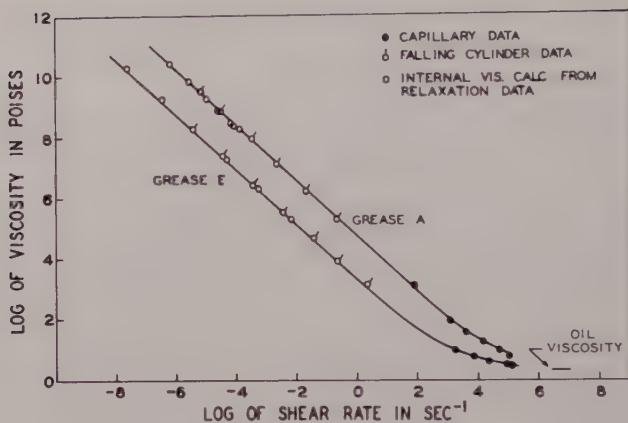


Fig. 1. Viscosity vs. shear rate for greases.

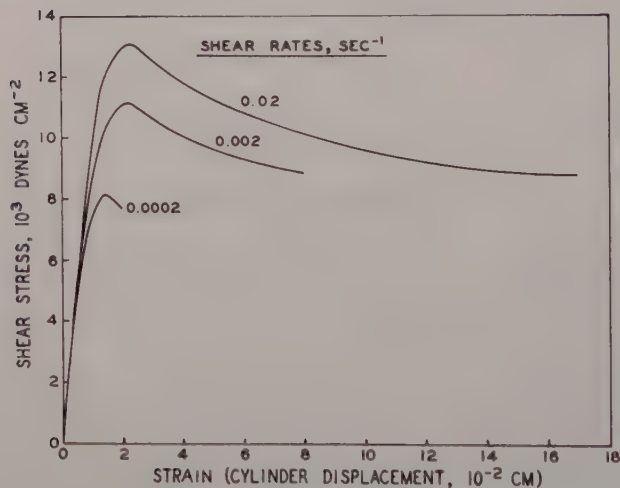


Fig. 2. Typical stress-strain curves for Grease C at three shear rates.

Typical stress-relaxation curves are shown in Figures 4A and 4B. The stress at the beginning of relaxation is called the starting stress. Stress relaxes more rapidly after rapid shearing of the grease and from higher starting stresses.

Relaxation experiments for 72 hr. (2.6×10^5 sec.) show that after

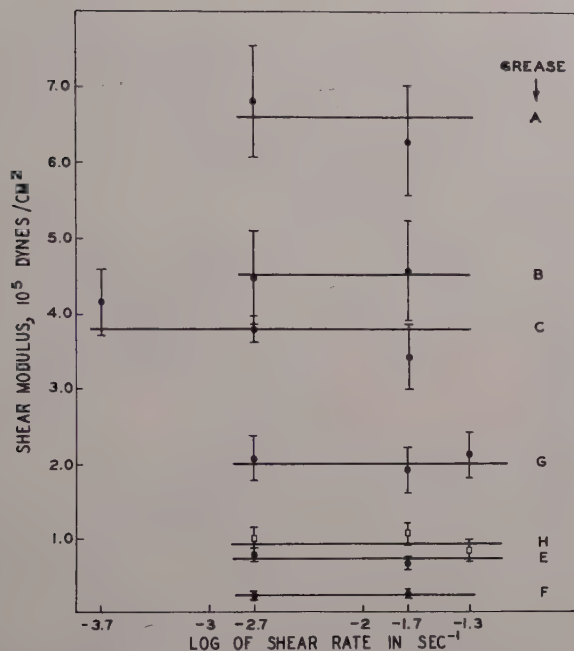


Fig. 3. Shear modulus vs. logarithm of shear rate for various greases.

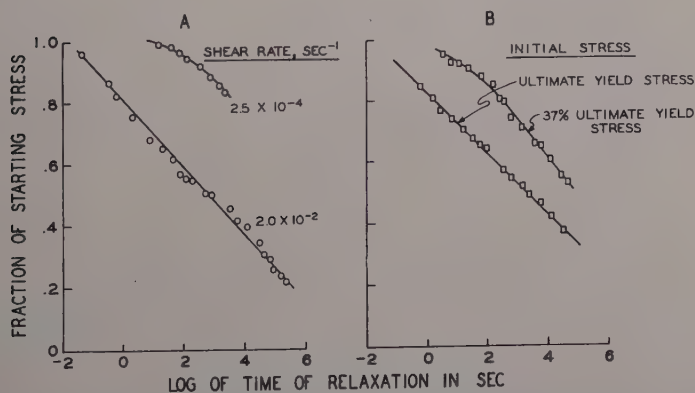


Fig. 4. Stress-relaxation curves. (A) Different deformation shear rates for Grease E. Relaxation from ultimate yield shear stress. (B) Different starting stresses, Grease A deformed at $2.0 \times 10^{-2} \text{ sec.}^{-1}$.

an initial period of a few seconds, greases relax linearly with logarithm of time. This was true for relaxation either from the ultimate yield stress or from initial stresses of only a fraction of the ultimate yield stress, as shown in Figure 4B. This relaxation law, and the conditions under which it holds, were predicted by Tobolsky and Eyring.⁹

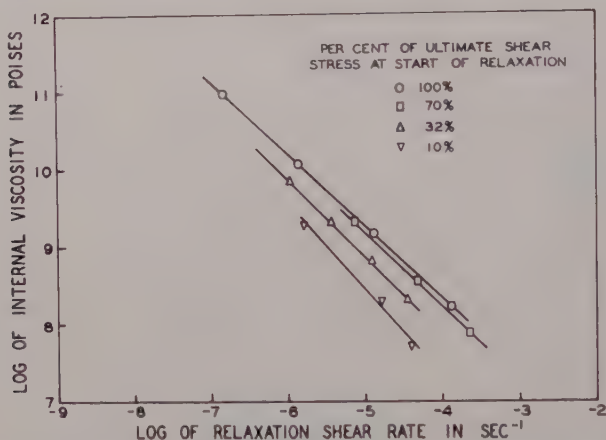


Fig. 5. Internal viscosity vs. relaxation shear rates for several starting shear stresses. Grease A deformed at $2.0 \times 10^{-2} \text{ sec.}^{-1}$.

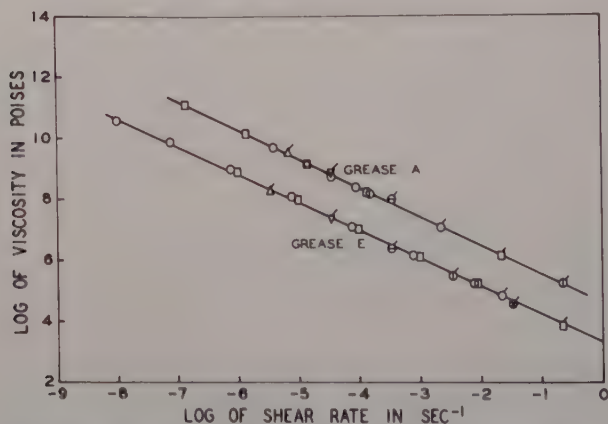


Fig. 6. Viscosity vs. shear rate curves. Shear viscosity data (tagged) and internal viscosity data (untagged) with the same symbol (O, \oplus , ∇ , or \square) were obtained in the same experiment. Relaxation followed the shear tests.

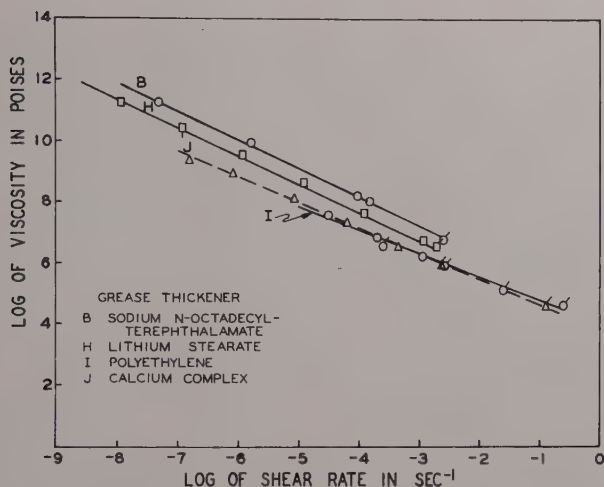


Fig. 7. Comparison of shear viscosities with internal viscosities. Tagged points are shear data, untagged points are internal viscosities using ultimate yield stress as initial stress.

Although we tried to interpret our data in terms of the Eyring models, our preliminary calculations failed to disclose the physical significance of the parameters involved. We then treated the data in terms of the stress-relaxation of elastic elements (Maxwell models) with a stress-relaxation internal viscosity. The latter treatment is preferred here because it discloses relationships between shear viscosity and stress-relaxation internal viscosity.

Internal viscosities, η_i , were calculated from the differential form of the equation for the decay of stress at constant extension:³

$$\eta_i = -G (dt/d \ln P)$$

where P is the stress at time t , and G is the shear modulus.

We define the *relaxation shear rate* as the ratio of shear stress at the inner cylinder wall to internal viscosity. At any time t , a relaxing system is experiencing a shear stress; and for that time an internal viscosity and a relaxation shear rate can be calculated. We note that the position of the curve of internal viscosities versus relaxation shear rates varies with the starting stress, as shown in Figure 5.

When greases relax from an initial stress equal to their ultimate yield point in shear, we find that the curve of internal viscosity versus relaxation shear rate is independent of deformation rate, and coincides with the falling cylinder data on viscosity versus shear rate (Figs. 6 and 7). This important finding is confirmed over a wide range of deformation rates, as shown by the data in Figure 6. The tagged points were obtained in shear and the untagged points were obtained from relaxation data. Hence, under these conditions the viscosity parameters characterizing the gel and the fluid states are identical.

The above relationships are valid for greases containing such widely differing thickeners as lithium stearate, polyethylene, sodium *N*-octadecylterephthalamate, and calcium soap and salt complex (Fig. 7).

An important practical application of this study is in measuring and specifying apparent viscosity at low shear rates for greases. The same relationships may apply to other plastic solids. This work indicates that a simple stress-strain curve plus a relaxation curve (where stress relaxes from the ultimate yield stress) may suffice to define apparent shear viscosities of non-Newtonian materials over several decades of shear rates.

We wish to thank Dr. O. L. Harle for his helpful discussions and suggestions in the preparation of this paper.

References

1. "Symposium on Flow Properties of Lubricating Greases," *NLGI Spokesman*, **20**, No. 3 (1956).
2. Hutton, J. F., and J. B. Matthews, *Proc. Second Intern. Congr. Rheology*, p. 408 (1953).
3. Eirich, F. R., *Rheology, Theory and Applications*, Vol. I, Academic Press, 1956, p. 700.
4. Philippoff, W., and H. F. Gaskins, *Trans. Soc. Rheology*, **2**, 263 (1958).
5. *ASTM Standards on Petroleum Products and Lubricants*, ASTM Committee D-2, Method D1092-55.
6. Fox, T. G., Jr., and P. Flory, *J. Am. Chem. Soc.*, **70**, 2384 (1948).
7. Criddle, D. W., and J. L. Dreher, *NLGI Spokesman*, **23**, 97 (1959).
8. *ASTM Standards on Petroleum Products and Lubricants*, ASTM Committee D-2, Method D217-52T.
9. Tobolsky, A. V., and H. J. Eyring, *J. Chem. Phys.*, **11**, 125 (1943).

Synopsis

The viscosities of gelled oils (lubricating greases) were measured in capillary viscometers and in a falling cylinder viscometer to cover a shear rate range of

10^{-5} to 10^{+5} sec. $^{-1}$. Stress-strain curves were obtained for the initial deformation in falling cylinder viscometers for shear rates of 10^{-6} to 2 sec. $^{-1}$. Shear stress-relaxation curves were obtained by observing elastic aftereffects following deformation at various strain rates and initial stresses. Elastic shear moduli were found to be independent of shear rate. Stress relaxation depends upon the deformation rate and the initial applied stress. Stress-relaxation viscosity parameters were calculated from elastic aftereffects of the gels for a variety of stress-relaxation conditions. Relaxation shear rates were defined and calculated for the stress-relaxation viscosity parameters. The viscosity-shear rate curves obtained from relaxation of greases from their ultimate yield shear points overlap and extend those curves obtained from shear experiments; hence, under some conditions the viscosity parameters characterizing the gel and the fluid states are identical.



Abstract

The Differentiation Method in Rheology

J. G. SAVINS, G. C. WALLICK, and W. R. FOSTER,
Socony Mobil Oil Co., Inc., Dallas, Texas

In most instances the approach to the problem of interpreting the non-Newtonian flow behavior of various systems has been in terms of what is referred to as the Integration Method. It consists of expressing flow properties in terms of an ideal model which is substituted into an integral equation relating observed kinematical and dynamical parameters. On integrating, the rheological parameters descriptive of the ideal model appear in an equation relating the pairs of observables.

A more general method of rheological analysis is to make no assumptions regarding the character of the function relating the observables to rheological parameters. This is the Differentiation Method. One differentiates the integral equation with respect to one of the observables, their derivatives, and the rheological function evaluated at that boundary. These derivatives can be obtained from the experimental data by graphical or computer techniques and then substituted into the differential equation to produce the unknown function in graphical form.

Since these methods basically represent different modes of analysis, considerably more insight into the probable response of real data obtained by the Differentiation Method can be obtained from a dual Differentiation Method-Integration Method analysis of the characteristics of ideal flow models. Such a procedure has been applied to suites of flow models representing a variety of Generalized Newtonian and Viscoplastic behavior using machine processing and computation methods for Poiseuille and Couette flows. We believe this study

represents one of the earliest reported instances of computer analysis in problems of this kind.

The salient features of this dual method of viscometric analysis are illustrated in the suites of predicted characteristic derivative functions which have been developed, and in the treatment of data on a variety of non-Newtonian suspensions and solutions.

END OF SYMPOSIUM

The Normal Forces and their Thermodynamic Significance

HARRY H. HULL, *R. R. Donnelley and Sons Co., Chicago, Illinois*

This paper is an extension and more rigorous presentation of two of the ideas presented in the paper "A Thermodynamic Approach to Rheology" which was read at the Society of Rheology meeting in 1959." These two ideas are: (1) The elastic energy of deformation of a fluid or solid at constant pressure and temperature is also the change in the Gibbs function (pressure and temperature constant). (2) This same elastic energy of deformation for a viscoelastic fluid in simple shear should be evident and measurable as a pressure normal to the shearing face.

Consider an elastic body in a constant temperature bath at atmospheric pressure. Now deform this body in shear slowly such that friction is negligible and the work is stored as an elastic energy of deformation. This is a thermodynamically reversible process. It is typical of the process which can be regarded as the limit of real processes with the approach of the frictional components of the process to zero.

The work done on this elastic body is energy, and this energy is divided into three portions, each reversible, as follows: (1) A portion is transferred into the surrounding constant temperature bath in an amount $-q$ or $-T\Delta S$. (2) A portion is transferred into the surrounding atmosphere because a change in volume did work on the atmosphere by the amount $P\Delta V$. (3) The remainder of the energy stays in the body in the form of internal energy ΔE .

The Gibbs function is $F = E - TS + PV$. An incremental change in the Gibbs function at constant temperature and constant pressure is $\Delta F^{PT} = \Delta E^{PT} - T\Delta S^{PT} + P\Delta V^{PT}$, which is identical to the sum of the three portions of the elastic energy of deformation. Hence, the strain energy at constant temperature and pressure is equal to the

change in the Gibbs function. Since the difference in the Gibbs function designated ΔF^{PT} is the maximum net work which can be obtained at constant temperature and pressure,¹⁷ this is the result which should be expected.*

This important relationship between strain energy and the Gibbs function seems to be little recognized in the literature on elastic deformation. Garner, Nissan and Wood recognize it as the Gibbs free energy.⁵⁻⁸ Flory⁴ refers to $\partial \Delta F / \partial T$, "where ΔF is the change in Gibbs free energy equal to $-W_{el}$ for a deformation (in elongation) at constant temperature and pressure." There are a number of references to the strain energy at constant volume as the Hemholtz free energy.^{3,28} This is correct if constant temperature is also stated. However, the more usual experimental situation is constant pressure and constant temperature, and if an exact equation is desired, the work done against the atmosphere must be included and the difference in the Gibbs function at constant pressure and temperature, ΔF^{PT} , is obtained.

Chemists are accustomed to think of the Gibbs function in terms of chemical change. Elastic deformation normally involves no chemical change and would be classed as a physical change. Actually the nature of the changes involved in differences of the Gibbs function is not specified and can include physical, chemical, and electrical changes or combinations of these. It is interesting to note that there are special systems where it has been shown that chemical energy can be reversibly transformed into mechanical energy through the generation of tensional forces. These systems have been discussed by Kuhn^{15,16} Hill,⁹ and Katchalsky,¹³ and it is proposed that muscular systems are of this type. This was one of the topics of discussion at the conference on contractability at Mellon Institute in January, 1960.²

The second major point of the first paper was that the strain energy of a viscoelastic fluid would be evident as a pressure normal to the shearing face and was reasoned as follows. If a solid is deformed elastically (with temperature and pressure constant), it can lose its elastic potential energy in two ways: (1) By allowing it to return to its original shape, and (2) by the process of molecular relaxation by which the random orientation of the molecules is restored without the body returning to its original shape.

* This development assumes that no electrostatic field is generated.

A viscoelastic fluid develops an energy of elastic deformation when undergoing shear. This elastic energy of deformation is implied in the name viscoelastic, but there is also adequate evidence that the elastic component of deformation of non-Newtonian fluids is real. Such a viscoelastic fluid has another method beside the above two by which it can lose its elastic energy of deformation. It can *flow* from the region undergoing shear to a region not undergoing shear. Since an unstressed field has a lower ΔF^{PT} (or what is equivalent, a lower elastic potential energy), there will be a pressure exerted against the shearing walls which constrains the fluid to the shear field.

This type of normal pressure has been stated to be the result of "cross elasticity" and is discussed by Reiner,²² Mooney,²⁰ Weissenberg and others. However, no attempt will be made here to determine whether the various descriptions of cross elasticity are consistent with the above explanation. Clegg¹ mentions large forces normal to the flow lines in a capillary and states that these are being studied further. His statement is part of the conclusions in a paper on the swelling of polyethylene immediately after extrusion. This swelling of extruded jets and threads has been described a number of times and is certainly consistent with the idea of the normal force being the result of elastic deformation. An hypothesis has been proposed by Spencer and Dillon²⁵ that this swelling is caused by the orientation of the molecules by the shearing action and their return to random orientation on exit from the nozzle. These two concepts are not contradictory to each other but are consistent and tend to confirm each other. The reason for this is that the presence of any orientation associated with a deformation means that there is an elastic energy of deformation. This will be discussed later in this paper.

There are various devices which measure pressures in stressed fluids, notably the Garner, Nissan, and Wood viscometer⁷ and the Weissenberg rheogoniometer.²⁴ These are useful devices, but the interpretation of their results is complicated by the curvature of the stress field they generate. The force they measure is not that which is at right angles to the shearing face if it were flat, but the pressure developed by a stretched curved envelope around the center of the instrument. It is as though a lot of rubber bands were stretched and wrapped around the center of the instrument.

Consider the Weissenberg rheogoniometer as shown in Figure 1. The shearing action generates an elastic energy of deformation which

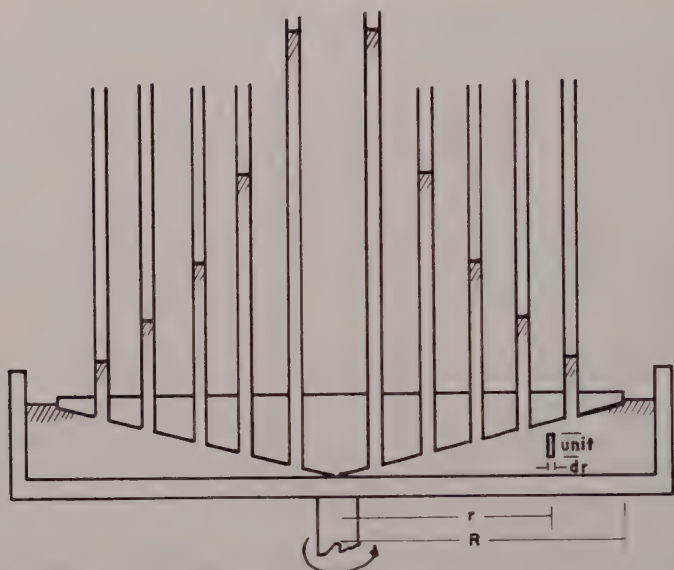


Fig. 1. Diagram of a Weissenberg rheogoniometer showing incremental unit used in the explanation of the distribution of pressure in the rheogoniometer.

exerts a tension which has a component X_{11} (units of force per unit of area) in the direction of shear. Since the material between the plate and cone is all deformed at the same rate of shear, X_{11} will be the same for all this material between the plate and cone. Take an element one unit high and dr in thickness, and with this element construct a complete band of radius r around the center of the rheogoniometer (refer to Fig. 1). This band will pull with a tension of $X_{11}dr$, and the total pull of both ends of the elemental band against a diameter of $2r$ will be $2X_{11}dr$ over an area of $2r$ along the diameter. Hence, the tension in the band will cause an increase in pressure within the band by the amount of $X_{11}dr \cdot r$, and the pressure increase at any point on the radius caused by tension X_{11} is the integral

$$\int_r^R X_{11}dr/r = X_{11} \ln(R/r)$$

where R is the outer radius. If a parallel plate is substituted for the cone, the rate of shear at any point is proportional to the distance from the center of rotation (r). If the tensional force X_{11} is proportional

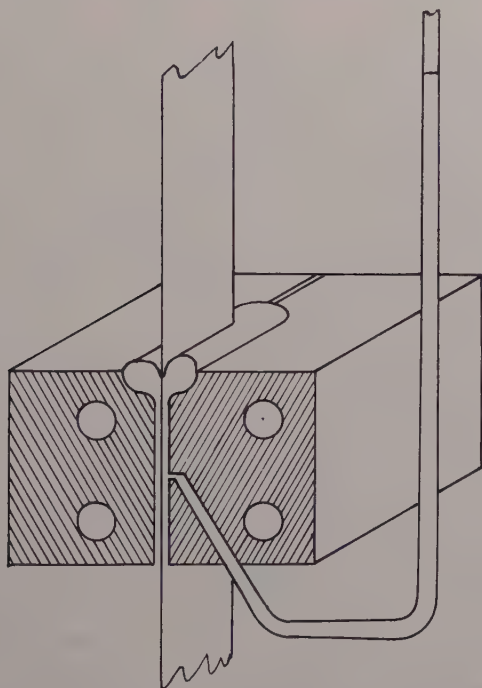


Fig. 2. Diagram of the cross section of the band viscometer used in this test. The openings within the blocks are for temperature control. The band is pulled down through the pool of fluid and draws the fluid with it.

to the rate of shear, then $X_{11} = k\dot{x} = k'\omega$ where \dot{x} is the rate of shear and ω is the rotational speed of the plate. Then pressure is

$$\int_r^R k'\omega r dr/r = k'\omega (R - r)$$

The data of Kotaka et al.¹⁴ have shown that the tensional force X_{11} is not a strictly linear function of the rate of shear and that the non-linearity varies with the material being stressed. The above is essentially a variation of the development given by Roberts²⁴ and Kotaka et al.

The curvature of the shear fields in the rotational-type viscoelastometers acts as a mechanical amplifier of the tensional X_{11} force without amplifying the other normal forces. This has resulted in some con-

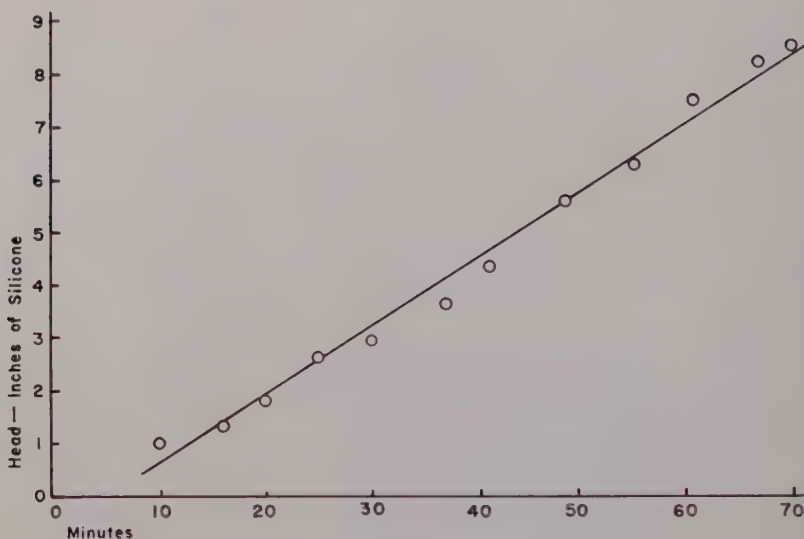


Fig. 3. Build up of head of silicone (12,500 cps.) by a manometer in the face of a band viscometer.

fusion in the interpretation of these forces. It was decided that a proper demonstration of the normal force perpendicular to the shearing face required plane shear fields and flat shearing surfaces. Accordingly, a band viscometer^{10,29} was modified by inserting a manometer in one face.

A band viscometer is shown in Figure 2. It consists of two blocks with flat surfaces held apart by shims. There is a small well in the top in which the fluid or paste to be tested is placed. A tape of cellulose acetate is pulled between the blocks and the tape pulls the fluid or paste with it between the parallel faces of the blocks. In normal use weights are hung on the end of the tape and allowed to pull the tape and the material to be tested between the blocks. After it has reached terminal velocity, the time for the tape to travel a known distance is recorded. By the use of various weights, data for a force-rate of shear graph can be obtained. The instrument used for this work was a slight modification of that previously described.¹⁰

In this test a $0.002'' \times 1.5''$ tape was pulled between the blocks with a motor and pulley at a rate of $4.25''/\text{sec.}$ with a clearance of $0.002''$ on each side of the tape. This gives a rate of shear of 2130

sec.⁻¹. This, however, can only be considered approximate, as the diameter of the pulley was increased by the build-up of tape and the tape was occasionally removed from the pulley during the runs. The face of one block contained a hole $1/16''$ in diameter which led to a manometer for the measurement of the normal pressure.

Although there were only four fluids tested, it was apparent that there were two distinct types. Two of the fluids showed a high-positive normal pressure when undergoing shear, and two showed small negative pressures which were negligible in comparison with the amount of the positive pressures generated by the other two.

Figure 3 shows the data on a silicone fluid, labeled 12,500 cps, which gave a high positive normal pressure. Although the tape was run for over 1 hr., a steady state was not reached, and it was concluded that the reason for this was that the back pressure of the manometer was built up from the material fed from between the blocks and this was available at a very slow rate. A system had to be used which did not depend upon the feeding of the fluid into the manometer if measurements of the normal pressure were to be made in a reasonable time. A back pressure was then introduced, and the rise or fall of the material in the manometer indicated which was greater, the normal pressure in the block or the back pressure. By this method it was determined that the normal pressure exerted by a sample of polybutene* (molecular weight reported to be 770) was over half an atmosphere. The actual pressure was not determined because the pressure was beyond the upper limit of the apparatus on hand.

The two fluids which gave the small negative pressures were polybutenes* with molecular weights which were stated to be 520 and 300. These are fluids which one would expect to be less viscoelastic or more Newtonian because of their lower molecular weight. The maximum suction was $3.25''$ of test fluid measured from the top of the block, and steady states were apparently reached with these fluids. It is presumed that this negative head was associated with some geometric factor of the assembly, since different readings were obtained with the same fluid and the only apparent difference was the assembly and disassembly of the apparatus. This negative pressure is not explained by the velocity head $V^2/2g$ since this is not sufficient to explain the readings by several magnitudes.

* The polybutenes used were the commercial grades known as Indapols L-10, L-100, and H-50 made by Amoco Chemical Corporation.

These experiments can be considered exploratory only. However, they do demonstrate the presence of large normal pressures in the presence of flat shear fields which were forecast by the theory in the first part of the paper. They also give information which will aid in the design of a more satisfactory instrument for the measurement of the normal pressures. Such an instrument would be useful for the characterization of many commercial materials as well as theoretical studies. The elasticity as a parameter of fluids which is not subject to simple measurement at present, and it is a parameter which is probably varying in an unknown manner with many commercial materials. Such an instrument is expected to be especially useful if it could be used to measure the elasticity of heavy pastes such as printing inks, paints, adhesives, molten plastics, and bread dough, for the elasticity is related to those various properties termed "length," "shortness," "spinnability," etc., which are usually judged by subjective methods at present.

The actual change ΔF^{PT} caused by a shear field is calculated by multiplying the pressure differential times the volume, just as it is for any gravitational or osmotic pressure head. If the volume is the molal volume, then ΔF^{PT} is obtained on a molal basis which is the customary terminology of the chemists.

Although the ΔF^{PT} calculation is obvious by analogy with that for gravitational field and osmotic pressure, it is interesting to confirm it by a method which can be generalized to include related effects. Consider a shear field with a height of H and a cross-sectional area of A opposed by a manometer with a height of h (referred to the same base as H) and a cross-sectional area of a . If ΔF^{PT} is the change per unit volume in Gibbs function caused by the shear field at constant P and T , and ρ is the density of the fluid, then the total potential energy of the system above the reference height is $AH\Delta F^{PT} + \frac{1}{2}\rho AH^2 + \frac{1}{2}\rho ah^2$. $\frac{1}{2}\rho ah^2$ is the work necessary to fill the manometer column from the reference height to h . The total volume of the system above the reference height is $V = AH + ah$, and h can be eliminated to obtain an equation for the total potential energy of the system in terms of H . The minimum total potential energy is found by taking the derivative with respect to H and equating to zero. This gives $\Delta F^{PT} = \rho(h - H)$, which is the pressure. This is interesting for it combines both the thermodynamic concept of a minimum

Gibbs function for equilibrium and minimum mechanical potential energy for equilibrium. This method can be extended to include the concentration differences caused by shear fields. The relation between osmotic pressure and the Gibbs function may also be developed in an analogous way.

In the above development we have applied the thermodynamics of equilibrium (referred to by some as thermostatics) to the steady state. This can be justified thermodynamically in this case, and this will be done in a separate paper which is being prepared. This has an interesting analogy with the assumption stated by Philippoff²¹ that "the deformational mechanics of *elastic solids* can be applied to flowing solutions." There is one exception to the above statement as has been pointed out, and that is that fluids can relax by flowing into fields of lower rates of shear, so the statement should be modified by stating that the mechanics are similar. If the mechanics are similar, we can also infer that the thermodynamics will also be similar.

The concept of the strain energy as a Gibbs function difference ΔF^{PT} and exerting a force normal to the shearing face is compatible with the information obtained from optical birefringence studies of fluids undergoing shear. Essentially these birefringence studies show that at low rates of shear a tension is present at 45° to the direction of shear, and as the rate of shear increases, the direction of the maximum tension moves asymptotically toward the direction of shear. According to Philippoff,²¹ the recoverable shear s is given by $2 \cot 2 \chi$ where χ is the angle of extinction. From this and the force of deformation it should be possible to calculate the elastic energy of deformation which should be equal to the ΔF^{PT} calculated from the pressure normal to the shearing face.

There is another means which should show the direction and relative value of the stresses in viscoelastic fluids that is not mentioned as such in the literature, and that is the shape of the suspended drops of low viscosity fluids in shear fields. These droplets are distorted by the normal forces just as a balloon would be pulled or pressed out of shape in one's hands. These droplets appear to be ellipsoids, and it is mathematically convenient to assume that they are. If they are not ellipsoids, the conclusions will be a reasonable approximation. The

direction of the tension of minimum pressure is, of course, given by the direction of the major axis of the ellipsoids. Mason^{19,23} and Taylor²⁶ both show that the major axis of the ellipsoids is at 45° at low rates of shear and that it approaches the direction of shear with increased rates of shear. (Some suspensions break up before they are near to the direction of shear, and some become asymptotic to it without breakup.) This is, of course, a similar type of behavior to that indicated by birefringence studies. The relative forces can be calculated from the various radii of curvature if we assume: (A) The surface tension is uniform on the surface of the drop. (B) That because of the low viscosity of the fluid, the internal pressure is the same in all directions. (C) The kinetic effects are negligible. (D) Since the shape of the drop conforms to the force field, it does not appreciably affect the distribution of forces in the fluid.

These are reasonable assumptions with low viscosity fluids suspended in high viscosity fluids which are subjected to low rates of shear. Just as the pressure exerted by surface tension in a spherical drop is $2\gamma/r$ and the pressure exerted by surface tension on a cylindrical shape is γ/r , the pressure exerted by any curved surface is $\gamma[(1/r_1) + (1/r_2)]$, where γ is the interfacial tension and r_1 and r_2 are the two radii of curvature. This formula is given by Rumscheidt and Mason.²³ If a is the major axis of an ellipsoid and b and c are the other two axes, the radius of curvature in the ab plane at the end of the axis is b^2/a , and the difference in pressure along the a and b axes is $\gamma[(a/b^2) + (a/c^2) - (b/a^2) - (b/c^2)]$.

There are no data published in the literature on the shape of low viscosity drops to confirm the above formulas. However, there are photographs of suspended drops of cyclohexanol phthalate (viscosity 155 poises) suspended in corn syrup of 71 poises in a paper by Mason and Bartok.¹⁹ This viscosity of the material in the drops is, of course, not negligible. Measurements on the photograph in this paper give $a = 4.60$ mm., $b = 2.09$ mm., $c = 2.45$ mm., and $\chi = 20^\circ$ at the maximum rate of shear of 3.93 sec.^{-1} . If it is assumed that the formula given by Lodge¹⁸ of $\Delta P = 2P_2 \text{ cosec } 2\chi$ applies, the pressure difference along the major axes can be calculated from the angle of inclination of the major axis, and from this the interfacial tension can be calculated. Its value was 63 dynes/cm. from the above data. This appears to be high, as would be expected from the appreciable viscosity of the material in the drops.

It is appropriate to call attention to certain thermodynamic properties of an ideal gas that are analogous to rubber-like deformation.^{4,27} The internal energy of an ideal gas depends on temperature only and is independent of pressure or volume. In other words, if an ideal gas is compressed and kept at constant temperature, the work done in compressing it is completely converted into heat and transferred to the surrounding heat sink. This means that work equals q which in turn equals $T\Delta S$.

There is a well-known relationship between probability and entropy which states that $\Delta S = R \ln \Omega$, where Ω is the probability that state (i.e., volume for an ideal gas) could be reached by chance alone. This is known as conformational entropy. This conformational entropy is, in this case, equal to the usual entropy, for there are no other changes or other energies involved. Note that though the ideal gas itself contains no additional energy, the compressed gas does exert an increased pressure. The energy for any isothermal work done by the perfect gas must come as thermal energy from its surroundings.

Treloar²³ and Flory⁴ show data on rubber for which the internal energy at constant temperature remains relatively constant for extension ratios up to three times (after which changes in internal energy are associated with the appearance of crystallization). This analogous behavior of an elastomer at moderate extension ratios to the ideal gas is mentioned by Flory. Like the ideal gas, the isothermal work done on rubber in deforming is converted to heat and transferred to the surrounding heat sink. (The small change in volume is negligible.) Here, as in the ideal gas, the conformational entropy at constant T is equal to that in the equation $q = T\Delta S$. The conformational entropy for elastic deformation of rubber in tension or shear is referred to the orientation rather than volume. It is R times the logarithm of the probability that the existing molecular orientation can be reached by chance alone.

This is very easy to picture. Consider a number of flexible long chain molecules such as could exist in a viscoelastic fluid. The conformation of each chain will be changing continually because of the thermal motion of the parts of the molecules. In a static fluid the mean position of one end of the molecular chain with respect to the other will be a zero vector. However, the mean distance between ends will have a mean value, and this mean will be equal in all directions. These relationships are described in detail by Flory.⁴ If these

molecules are placed in a shear field, they will be orientated.⁶ The mean position of one end with respect to the other will still be a zero vector, but the mean distance between the ends of the molecules will vary with direction. Mason's photographs* of fibers in a shear field suggest that such chain molecules first stretch out and then some may roll up in a ball. If the molecules stretch out, the thermal motion of the parts of the molecules will tend to restore them to the randomized state of the static condition, and this will cause a tension to be exerted, pulling the two ends of each molecule together. If the molecules are coiled, the thermal motion will tend to uncoil them. No matter what the orientation, it is obvious that the thermal motion will tend to remove that orientation. The thermal energy of the molecular parts is capable of doing work to restore the random orientation. Hence, any orientation indicates an elastic energy of deformation which is exerting a force equal to and opposing the force of deformation.

It has been shown that a rubber-like deformation is analogous to the compression of a perfect gas in both internal energy and entropy changes. It is also similar to a perfect gas in another respect; that is, the deformation force with deformation constant is directly proportional to the absolute temperature, just as for a perfect gas pressure is proportional to temperature with volume constant.

The deformation of solid rubber was shown to be similar to that of a perfect gas. It would be expected that there should be even better similarity for deformation of viscoelastic fluids, for a fluid can be considered halfway between a solid and a gas and the effect of molecular interactions should be less. Hence, the incremental difference of the Gibbs function $\Delta F^{p,T}$, as measured by the pressure normal to the shearing surface, provides a means of calculating the orientation by the following relationship: $\ln \Omega = (V\Delta P_{22} - P\Delta V)/RT$, where V is the molar volume, ΔP_{22} is the incremental pressure normal to a flat shearing surface, P is the atmospheric pressure, and ΔV is the change in molar volume on shearing.

In summary, an important relationship between rheology and thermodynamics has been presented in that the force normal to a flat shearing surface for a viscoelastic fluid is a measure of the energy of elastic deformation which is, in turn, the incremental difference of the Gibbs function at constant temperature and pressure.

An elementary prototype of a device for measuring this pressure has

* Shown as motion pictures at the 1959 Society of Rheology meeting.

been described, and some of the theoretical and practical uses of this instrument have been suggested.

This interpretation does not conflict with the other experimental evidence of the normal forces such as the rotational viscometers, the birefringence studies, and the shapes of drops suspended in shear fields.

APPENDIX I

A Note on the Justification of the Use of the Conventional Equilibrium Thermodynamics for the Steady State of a Viscoelastic Fluid Undergoing Shear

It is a fundamental assumption in classical thermodynamics that the properties of a body are determined by two variables plus composition. These two variables selected can be pressure and temperature in which case

$$B = f(P, T, c_1, \dots, c_{n-1})$$

where B can be volume, enthalpy, free energy as used by Lewis and Randall, etc. If B is an extensive property, it will be expressed as a molar quantity, if composition is constant, then:

$$B = f(P, T)_{\text{composition constant}}$$

This equation can also be stated as true of any physical property such as index of refraction, viscosity (if a fluid), and this also can be stated as the result of laboratory experience.

It is this equation, as well as the laws of thermodynamics, on which the theory of thermodynamics is based. This statement appears to be so elemental that it is overlooked in some textbooks. However, it is given in some; for example, Fermi (ref. 35, p. 2) in the form $f(P, T, V) = 0$, and Lewis and Randall state it in words (ref. 17, pp. 27, 242).

It is also known and mentioned in most thermodynamic textbooks that there are certain other variables which are commonly considered as held constant but which affect the properties (thermodynamic and physical) of a body. Some of these are surface area, electrical field, magnetic field, gravitational field, and the other stresses. (P is a stress and is always present.) It can be stated that if one of these variables besides P and T is varied, say X , then all* properties of that

body can be considered determined if P , T , and X are determined, i.e., $B = f(P, T, X)_{\text{composition constant}}$.

Other variables are treated in Lewis and Randall (ref. 17, p. 242). Young et al.^{*31} have treated the gravitational field as a third variable. Others have considered stress and strain as other variables.³²⁻³⁴

Consider now a body of one phase in simple shear held at constant temperature and pressure and subjected to a constant force of deformation in shear. If it is chemically stable under these conditions it will, in time, come to a steady state in which rate of shear is constant and all physical properties of that body are constant. This steady state can be approached from neighboring steady states which are different from the above in infinitely small steps of any one of the variables P , T , or X .

In other words, $B = f(P, T, X)_{\text{composition constant}}$ for the steady state. This is identical with the descriptions of a body in true thermodynamic equilibrium; for the thermodynamic functions such as the Gibbs function, the enthalpy, and the internal energy, are also defined just as they are in classical thermodynamics.

It should also be noted that molecules in a steady state in a shear field are orientated just as they are in rubber which has been deformed by shearing forces. This orientation is subject to the same statistical methods of study as has been used for rubber and should show entropy relationships similar to those for rubber.

These ideas, and others related to them, form the basis for a second paper I am preparing, "The Force of Deformation in Shear as a Variable of State."

APPENDIX II

Comment on a Criticism of This Paper

The ideas contained in this paper have been criticized on the grounds that a number of them have been expressed before and that they are not correct on the basis of certain data in Garner, Nissan, and Wood's last paper.⁷ These ideas are close to those expressed in their earliest paper and partially repudiated in later publications.^{7,8} Their repudiation was based on the application of the formula

* Certain thermodynamic functions are so defined so as to exclude the effects of certain other variables of state. This was noted to be true of chemical potential by Young et al.³¹

$$\partial \Delta F / \partial T = -\Delta S \quad (1)$$

to a series of pressure head readings at two rates of shear and three temperatures. From this they calculated very high values of internal energy (from 27 to 148 cm. of head).

The use of the above equation for this data is in error, and in its place the following is submitted.

The partial derivative with respect to temperature holding P and the rate of shear $\dot{\alpha}$ constant gives:

$$(\partial \Delta F^{PT} / \partial T)_{P\dot{\alpha}} = (\partial \Delta F^{PT} / \partial T)_{P\dot{\alpha}} - \Delta S^{PT} - T(\partial \Delta S^{PT} / \partial T)_{\dot{\alpha}P} + P(\partial \Delta V^{PT} / \partial T)_{\dot{\alpha}P} \quad (2)$$

This is a somewhat unusual partial derivative, but its meaning is very definite. ΔF^{PT} is the maximum isothermal work (or isothermal elastic energy of deformation) at temperature T and pressure P . At another temperature $T + \Delta T$, another value will be obtained for the maximum isothermal work (constant P). The meaning of the partial derivative of ΔF^{PT} is quite different than the partial derivative of F , $(\partial F / \partial T)_P = -S$.

Treloar states that ΔV^{PT} is very small for rubber, and it is reasonable to also assume $\partial(\Delta V^{PT} / \partial T)_{P\dot{\alpha}}$ is very small for a fluid undergoing shear. For iterative purposes we can assume that ΔE^{PT} is negligible just as it is in rubber (from Treloar). Then, $\Delta F^{PT} = -T\Delta S^{PT}$ and $\Delta S = -\Delta F^{PT} / T$ and by iterative methods ΔE^{PT} can be obtained.

In accordance with their use, the pressure head from the Garner, Nissan, and Wood viscometer may be presumed proportional to ΔF^{PT} . All energy quantities in the equation $\Delta F^{PT} = \Delta E^{PT} - T\Delta S^{PT} + P\Delta V^{PT}$ may be expressed as pressure heads. ΔF^{PT} and ΔS^{PT} can then be plotted against T and the slopes found, and then $(\partial \Delta E^{PT} / \partial T)_{P\dot{\alpha}}$ may be solved.

Garner, Nissan, and Wood's data and the results obtained with this revised method of calculation are shown in Table I. Since the plot of ΔF^{PT} against T indicates a value of zero for ΔF^{PT} at a temperature slightly above 30°F., ΔE^{PT} can also be estimated.

Since the calculation of these values involves the use of slopes which can only be crudely estimated, these values are believed to be perfectly consistent with the hypothesis that the free energy for rubber-like elastic deformation in this system is primarily due to the entropy term and that the change in internal energy ΔE^{PT} is small.

TABLE I
Garner, Nissan and Wood Data
 ΔF^{PT} cm. of head (corrected)

r.p.m.	8.0°C.	20.0°C.	30.0°C.
1000	6.1	4.9	2.8
1200	6.4	5.6	3.2
	$(\partial \Delta E^{PT} / \partial T)_{Pz}$ cm. of head/°C.		
1000	-0.011	-0.011	-0.016
1200	0.017	0.053	-0.18
Estimating ΔE^{PT} from these values, a second iteration can be calculated:			
1200	-0.013	-0.001	-0.019

It should be noted that the subscript of \dot{x} on eq. (2) is very important, and this can best be illustrated by the similar case of solid rubber under tension. There are two well-known conditions for the variation of temperature, one with extension (x) held constant $(\partial \Delta F^{PT} / \partial T)_{Px}$ and the other with force of deformation (X) held constant $(\partial \Delta F^{PT} / \partial T)_{PX}$. These are obviously different, for with the first ΔS^{PT} would normally remain approximately constant with change in temperature, while with the second ΔS^{PT} would decrease with increase in temperature.

References

1. Clegg, P. L., "Elastic Effects in the Extrusion of Polyethylene," in *The Rheology of Elastomers*, P. Mason and N. Wookey, eds., Pergamon Press, New York, London, 1958. Proceedings of Conference of British Society of Rheology, May 1957.
2. Carroll, W. R., *Science*, **132**, No. 3425, 475 (August 19, 1960).
3. Coleman, B. D., and W. Noll, *Arch. Rat. Mech. Anal.*, **4**, 97 (1959).
4. Flory, P. J., *Principles of Polymer Chemistry*, Cornell Univ. Press, Ithaca, New York, 1953.
5. Garner, F. H., and A. H., Nissan, *Nature*, **158**, 634 (1946).
6. Garner, F. H., G. F. Wood, and A. H. Nissan, *J. Inst. Petroleum*, **33**, 71 (1947).
7. Garner, F. H., A. H. Nissan, and G. F. Wood, *Roy. Soc. London. Phil. Trans.* **A243**, 36 (1950).
8. Garner, F. H., and A. H. Nissan, *Nature*, **164**, 541 (1949).
9. Hill, A. V., *Science*, **131**, No. 3404, 897 (March 25, 1960).
10. Hull, H. H., *J. Colloid. Sci.*, **7**, 316 (1952).
11. Hull, H. H., *Trans. Soc. Rheology*, **4**, 367 (1959) (abstract only).
12. Hull, H. H., *Proceedings of the Third Annual Meeting of the Technical Association of the Graphic Arts*, 83 (1951); *American Ink Maker*, **29**, No. 9, 33 (September, 1951).

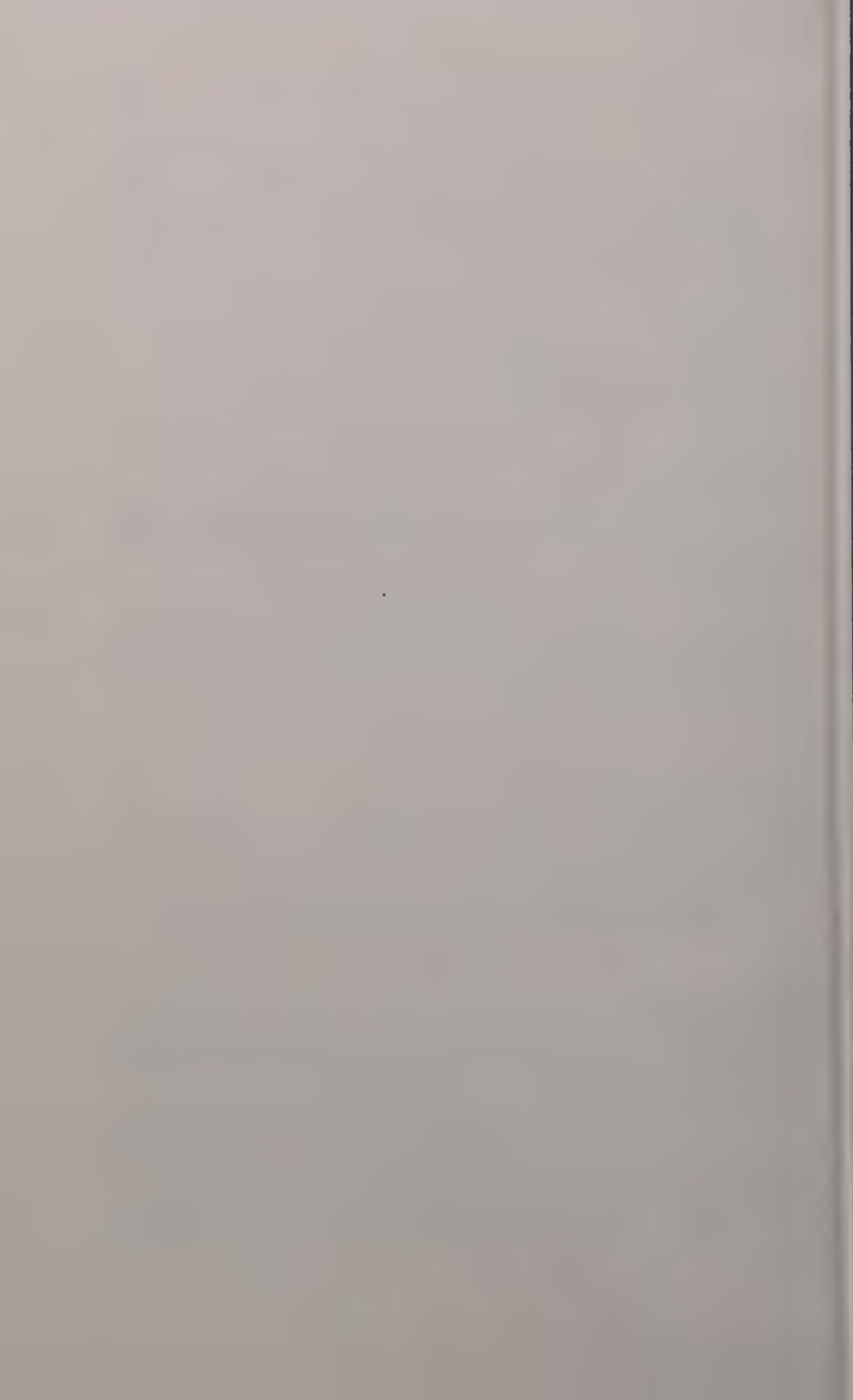
13. Katchalsky, A., S. Lifson, I. Michaeli, and M. Zwick, *Elementary Mechanochemical Processes*. To be published as part of a book on contractile polymers by Pergamon Press.
14. Kotaka, T., M. Kurata, and M. Tamara, *J. Appl. Phys.*, **30**, 1705 (1959).
15. Kuhn, W., *Makromol. Chemie*, **35**, 200 (1960).
16. Kuhn, W., A. Ramel, D. H. Walters, G. Ebner, and H. J. Kuhn, *Advances in High Polymer Physics*, **1**, 540 (1960).
17. Lewis, G. N., and M. Randall, *Thermodynamics*, McGraw-Hill, New York, 1923, p. 157.
18. Lodge, A. S., *Trans. Faraday Soc.*, **52**, 120 (1956).
19. Mason, S. G., and W. Bartok, *The Rheology of Disperse Systems*, C. C. Mill, ed., Pergamon Press, London, 1959.
20. Mooney, M., *J. Appl. Phys.*, **24**, 675 (1953).
21. Philippoff, W., *Trans. Soc. Rheology*, **1**, 95 (1957).
22. Reiner, M., *Deformation Strain and Flow*, Interscience, New York, 1960.
23. Rumscheidt, F. D., and S. G. Mason, *J. Colloid Sci.*, in press.
24. Roberts, J. E., "Pressure Distribution in Liquids in Laminar Shearing Motion and Comparison with Predictions from Various Theories," in *Proceedings Second International Congress of Rheology*, Harrison, ed., Academic Press, New York, 1954, pp. 91-8.
25. Spencer, R. S., and R. E. Dillon, *J. Colloid Sci.*, **3**, 163 (1948).
26. Taylor, G. I., *Proc. Roy. Soc.*, **A138**, 41 (1932); **A146**, 501 (1934).
27. Tobolsky, A. V., "Elastomer Thermodynamics," in William E. Ranz's *Thermodynamics and Engineering*, publication on a conference on thermodynamics held at Pennsylvania State University, June 27-29, 1955.
28. Treloar, L. R. G., *The Physics of Rubber Elasticity*, Oxford Univ. Press, 1958.
29. Wachholtz, F. V., and W. K. Asbeck, *Kolloid-Z.*, **93**, 280 (1940); **94**, 66 (1941).
30. Ziegler, H., *Ing. Arch.*, **25**, 58 (1957).
31. Young, T. F., K. A. Kraus, and J. S. Johnson, *J. Chem. Phys.*, **22**, 878 (1954).
32. Ting, T. W., and J. C. M. Li, *Phys. Rev.*, **106**, 1165 (1957).
33. Li, J. C. M., and T. W. Ting, *J. Chem. Phys.*, **27**, 693 (1957).
34. Crawford, F. H., *Proc. Am. Acad., Arts Science*, **78**, 165 (April, 1950).
35. Fermi, E., *Thermodynamics*, Dover, New York, 1956.

Synopsis

Thermodynamic methods are applied in the field of rheology to show that the elastic energy of deformation at constant temperature and pressure is an incremental difference in the Gibbs function at constant temperature and pressure. This is measurable in a viscoelastic fluid in a flat shear field as a pressure normal to the shearing face.

An elementary prototype of a device for measuring this normal pressure has been described, and some of the theoretical and practical uses of this instrument have been suggested.

This interpretation does not conflict with the other experimental evidence of the normal forces such as the rotational viscometers, the birefringence studies, and the shapes of drops suspended in shear fields.



A Method for the Measurement of Normal Stresses in Simple Shearing Flow

A. B. METZNER, W. T. HOUGHTON, R. A. SAILOR,* and J. L. WHITE, *University of Delaware, Newark, Delaware*

Introduction

The importance of normal stresses in all but the simplest fluids has been pointed out by many authors and observed in a variety of experiments.[†] However, quantitative experimental measurements to date have been comparatively limited and, with the exception of the birefringence studies of Philippoff and co-workers,^{3,4} are restricted to modest rates of shear. On the other hand, the processing applications in which such data are of primary interest frequently involve opaque fluids and very high shear rates. While the experimental studies reported to date do not meet a number of the desired requirements, they do serve to indicate that P_{11} is generally of a greater magnitude than either P_{22} or P_{33} .

Recently Gaskins and Philippoff⁹ suggested the measurement of the expansion of a jet of fluid issuing from a capillary (i.e., of the Barus¹ effect) as a means of measuring normal stresses. The purpose of this paper is to present an analysis of this problem which is free of errors or assumptions present in earlier analyses, and to confirm its utility by interpretation of some experimental data. The presentation will consist of three parts: (1) Analysis of laminar flow through round tubes to provide the necessary background for the subsequent analysis of the jet, (2) analysis of the fluid jet, and (3) experimental results.

* Present address: Research and Development Laboratories, Socony Mobil Oil Company, Paulsboro, New Jersey.

† In the present notation P_{11} , P_{22} , and P_{33} refer to the *deviatoric* components of the stress tensor. Markovitz,¹³ Philippoff,²⁰ and Roberts^{11,28,29} review most of the work in the areas of prediction and measurement of these stresses. Using the conventional system of Cartesian coordinates, the coordinate direction 1 is the direction of fluid motion.

Analysis of Laminar Flow Through Round Tubes

Reference to any fluid mechanics text (reference 30, for example) shows that the equations of motion may be written as follows:

$$\rho(D\bar{V}/Dt) = \text{div } \tau + \rho \bar{F} \quad (1)$$

τ denotes the total stress tensor and is related to the isotropic pressure and to the deviatoric stress tensor by the equation:

$$\tau = -pI + P \quad (1a)$$

where I is the unit tensor, P is the deviatoric tensor and

$$p = -1/3 \text{tr } \tau = -1/3(\tau_{11} + \tau_{22} + \tau_{33})$$

In well-developed, steady, ducted flow through round tubes:

$$u = u(r), \quad v = w = 0$$

and

$$\begin{bmatrix} \tau_{11} & \tau_{12} & \tau_{13} \\ \tau_{12} & \tau_{22} & \tau_{23} \\ \tau_{13} & \tau_{23} & \tau_{33} \end{bmatrix} = \begin{bmatrix} -p & 0 & 0 \\ 0 & -p & 0 \\ 0 & 0 & -p \end{bmatrix} + \begin{bmatrix} P_{11} & \tau_{12} & 0 \\ \tau_{12} & P_{22} & 0 \\ 0 & 0 & P_{33} \end{bmatrix}$$

The deviatoric stresses are related to the isotropic pressure and to each other through the equations of motion and the constitutive equation of the material. It should be noted that in many geometries the normal stresses are not compatible with the equations of motion and instabilities occur. Such behavior is discussed by Ericksen,⁷ for example, who has shown that such instabilities are not expected in the case of Poiseuille flow of interest here.

The equations of motion in the axial direction, denoted by 1, and the radial direction 2 become, respectively:

$$0 = -(\partial p / \partial x) + (1/r)(\partial / \partial r)(r\tau_{12})$$

$$0 = -(\partial p / \partial r) + (\partial P_{22} / \partial r) + [(P_{22} - P_{33})/r]$$

Integration of these equations from the centerline to any radius r yields:

$$\tau_{12} = (r/2)(+\partial p / \partial x) \quad (2a)$$

$$p(r, z) = p(0, z) + (P_{22})_r + \int_0^r (P_{22} - P_{33}) d \ln r \quad (2b)$$

where $(P_{22})_r$ denotes evaluation of $P_{22}(r)$ at the radius r .

Weissenberg³² proposed a general relationship between the stresses in a deformed material which was disproved for the case of vulcanized rubber²⁷ but was substantiated for viscoelastic liquids by Roberts²⁸ and Pilpel²¹ for the important special case of simple shearing flow, for which it predicts $P_{22} = P_{33}$. Recent qualitative results¹² support this conclusion also. While the reader may wish to recall the objections to such an equality given by Markovitz,¹³ at the present time the majority of the available experimental evidence supports this equality. Under these conditions eq. (2b) becomes:

$$p(r, z) = p(0, z) + (P_{22})_r \quad (3)$$

The total pressure in the tube thus consists of two parts: the hydrostatic pressure which decreases linearly in the direction of flow, and an "elastic" pressure equal to $(P_{22})_r$ which varies radially but is constant along the length of the tube. If one measures pressures above atmospheric, eq. (3) becomes, at the downstream end of the tube:

$$p(r, L) = (P_{22})_r \quad (3a)$$

Analysis of Jet Expansion

Consider the system sketched in Figure 1, which is a section of an actual fluid jet emerging from a tube as shown in Figure 2. The following assumptions will be made:

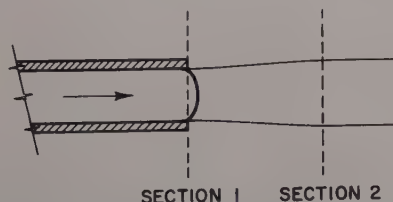


Fig. 1. Schematic of fluid jet showing positions of control surfaces for application of Newton's second law of motion.

1. The flow is steady, laminar, and isothermal, and the tube from which the fluid is issuing is of a sufficiently great L/D ratio to ensure that a well-developed velocity profile, characteristic of the steady state shear stress-shear rate behavior of the fluid, has been developed at the downstream end of the tube (Section 1). Under these assump-



Fig. 2. Photograph of jet of a polyisobutylene solution illustrating the Barus effect.

tions the flow conditions are those of steady, simple shear. This assumption, that the flow conditions are determined by the behavior of the fluid in the tube alone, presupposes that there is no "upstream propagation" of the normal stresses: i.e., that the flow at Section 1 is unaffected by conditions further downstream. This assumption is evidently valid in the special case of Newtonian fluids as no deviation from a constant pressure gradient (which would be created by such a propagation) has been measured. In the case of fluids showing strong normal stress effects the validity of this point is less obvious but can be checked by means of experimental data for different fluid velocities but at a given shear rate; i.e., with tubes of various diameters.

2. The assumptions leading to eq. (3a) are assumed applicable, i.e., it is assumed $P_{22} = P_{33}$.

3. The fluid is assumed to be incompressible.

4. Effects of interfacial and surface tension, at the end of the tube and in the jet, respectively, are negligible. This assumption is purely one of convenience as the surface forces may readily be added with no difficulty. However, under the experimental conditions of primary interest they are quite negligible.

5. Gravitational effects, and drag of the air on the jet* may be neglected.

Experimentally, the jet will be found to droop and its diameter will decrease when gravitational effects become important. This will generally not occur at jet velocities above the order of 100–200 cm./sec. except downstream from Section 2, the point of measurement.

In view of the last assumption, the velocity profile existing at

* Gavis and Gill¹⁰ have shown that under most conditions the drag of the air upon such a jet is quite negligible for the purposes in question, and, when this is not the case, may be rendered negligible by simply enclosing the jet in a partially-evacuated enclosure.

Section 1 will gradually decay and far enough downstream the fluid velocities in the jet will be equal at all radii. In this absence of shear no normal stresses will be generated and those which existed at Section 1 will also decay. Under these conditions the jet diameter d_j will approach a constant value: Section 2 is taken at any convenient position within this region. Experimentally, one may proceed to obtain d_j , the jet diameter at Section 2, in any convenient fashion, as for example, by photography or by use of a cathetometer.*

Applying Newton's second law to the portion of the fluid jet between Sections 1 and 2 of Figure 1, the *net* external force, in the flow direction, will be equal to the rate of change of fluid momentum. The only external forces, in view of the assumptions made, will consist of the total stress in the flow direction, τ_{11} , acting at Section 1, appropriately integrated over the entire cross section of the tube, and one obtains:

$$\int_0^R 2\pi r \rho u^2 dr - \pi R_j^2 \rho V_j^2 = \int_0^R 2\pi r \tau_{11} dr \quad (4)$$

where, from eqs. (1a) and (3a):

$$\tau_{11(r,L)} = -p_{(r,L)} + (P_{11})_r = [P_{11} - P_{22}]_r$$

Therefore,

$$\int_0^R 2\pi r \rho u^2 dr - \pi R_j^2 \rho V_j^2 = \int_0^R 2\pi r (P_{11} - P_{22})_r dr \quad (5)$$

The jet velocity V_j may be eliminated by means of the continuity equation:

$$\pi \rho R_j^2 V_j = \pi \rho R^2 V \quad (6)$$

From eq. (2a) one finds:

$$V = R(\tau_{12}/\tau_w) \quad (7)$$

* Gaskins and Philippoff⁹ have pointed out that one may relax the third assumption and carry out the experiment under conditions of a "drooping" jet, as the *horizontal* component of the velocity will nevertheless become constant and may be determined from a measurement of the jet's trajectory. By material balance one may then calculate d_j , uninfluenced by gravitational effects. In this way one may obtain data at somewhat lower shear rates, but the problem of erratic adhesion of the fluid to the end of the tube restricts the practical magnitude of any such velocity reductions.

just as in the case of simple fluids, where τ_w is defined in the notation section at the end of the paper.

Substituting eqs. (6) and (7) into eq. (5) and rearranging gives:

$$(\rho V^2/2)(D/d_j)^2 + 1/\tau_w^2 \int_0^{\tau_w} \tau_{12} [P_{11} - P_{22} - \rho u^2] d\tau_{12} = 0 \quad (8)$$

In simple shearing flow the deviatoric components of the stress tensor are functions of the local shear rate only, as is the shearing stress.^{5,8,19,25} If eq. (8) is multiplied by τ_w^2 and then differentiated with respect to τ_w , one may take $P_{11} - P_{22}$ as a function of τ_{12} only when evaluating the individual terms of the Leibnitz rule.³¹ Carrying out this operation,

$$\frac{1}{\tau_w^2} \frac{d}{d\tau_w} \left[\int_0^{\tau_w} \tau_{12} (P_{11} - P_{22}) d\tau_{12} \right] = \frac{(P_{11} - P_{22})_R}{\tau_w}$$

and solving for the normal stress difference one obtains, using the notation detailed at the end of the paper:

$$[P_{11} - P_{22}]_R = \frac{1}{\tau_w} \frac{d}{d\tau_w} \left[(\rho V^2 \tau_w^2) \int_0^1 \left(\frac{u}{V} \right)^2 \left(\frac{r}{R} \right) d \left(\frac{r}{R} \right) \right] \\ - \frac{\rho V^2}{n'} \left(\frac{D}{d_j} \right)^2 \left[n' + 1 + \frac{d \{ \ln(D/d_j) \}}{d \{ \ln(8V/D) \}} \right]$$

or

$$[P_{11} - P_{22}]_R = \frac{\rho V^2}{n'} \left\{ (n' + 1) \int_0^1 2 \left(\frac{u}{V} \right)^2 \left(\frac{r}{R} \right) d \left(\frac{r}{R} \right) \right. \\ \left. - \left(\frac{D}{d_j} \right)^2 \left[n' + 1 + \frac{d \{ \ln(D/d_j) \}}{d \{ \ln 8V/D \}} \right] \right\} \quad (9)$$

Note that in carrying out the differentiation, the integrand in eq. (9) is assumed independent of τ_w , since it is so in the case evaluated [see eq. (11)]. In order to evaluate $(P_{11} - P_{22})_R$ from experimental data the velocity distribution must be known in order to evaluate the one remaining integral. This may be obtained from shear stress-shear rate data since

$$u = \int_R^r \left(\frac{du}{dr} \right) dr = - \frac{2}{dp/dx} \int_{\tau_w}^{\tau_{12}} \left(\frac{du}{dr} \right) d\tau_{12}$$

Shear stress-shear rate data may be obtained from a variety of viscometric instruments, including capillary tube measurements interpreted by means of the Weissenberg-Rabinowitsch-Mooney equation,^{6,18,22} which may be written¹⁷:

$$(-du/dr)_R = [(3n' + 1)/4n'] (8V/D) \quad (10)$$

Rather than integrating the two above equations numerically or graphically to obtain the desired results, it is more convenient to fit an empirical equation to the shear stress-shear rate data and thereby obtain the integrals analytically. In this connection it is important to note that it is the product of the velocity (squared) and the radius which appears in eq. (9). The integral is thus influenced only to a negligible degree by velocities close to the center-line and is of maximum importance fairly close to the wall where r/R approaches unity. In the region between $r/R = 0.25$ and 1.0 the shear stress varies only 4-fold and yet this region contributes between 82 and 94% of the total value of the integral, depending on the degree to which the fluid is non-Newtonian. Obviously the choice of the empirical equation used is not a critical one and most of the empirical, 2- or 3-parameter equations will serve adequately, i.e., with negligible error. The present authors have chosen the "power-law":

$$\tau_{12} = K(-du/dr)^n$$

which yields, for the velocity profile¹⁷:

$$u/V = [(3n + 1)/(n + 1)] [1 - (r/R)^{(n+1)/n}] \quad (11)$$

but any other useful relation may be employed as desired.

The integral of eq. (9) is now evaluated as:

$$\int_0^1 2 \left(\frac{u}{V} \right)^2 \left(\frac{r}{R} \right) d(r/R) = \frac{3n + 1}{2n + 1}$$

and the normal stress difference as

$$(P_{11} - P_{22})_R = \frac{\rho D^2 (8V)^2}{64n'} \left(\frac{8V}{D} \right)^2 \left\{ (n' + 1) \frac{3n + 1}{2n + 1} - \left(\frac{D}{d_j} \right)^2 \left[n' + 1 + \frac{d(\log D/d_j)}{d(\log 8V/D)} \right] \right\} \quad (12)$$

For a power law fluid $n = n'$,¹⁷ but the distinction has been retained in eq. (12) in order to emphasize which terms in the equation depend upon the assumption of power law behavior and those which contain only n' and do not.

Equation (12) is the desired result: The difference of the deviatoric components of the two normal stresses, $P_{11} - P_{22}$, evaluated at a specified shear rate [given by eq. (10)] is directly obtainable from experimental measurements of the diameter ratio D/d_j and the steady-state shear stress-shear rate properties of the fluid (n', n). In earlier papers^{15, 16} a similar development was carried out, but only after a specific functional relationship between the normal stresses and shear rate had been assumed. The present development is entirely free of any such assumption.

Experimental Results

For fluids which exhibit no normal stress effects, $(P_{11} - P_{22})_R$ is equal to zero, d_j is constant, and eq. (12) gives:

$$d_j/D = \sqrt{(2n + 1)/3n + 1)} \quad (13)$$

For the special case of n equal to unity (Newtonian fluid), d_j/D is theoretically predicted to be equal to a value of 0.866.* A natural question which arises is whether any real liquid will exhibit a value of d_j/D this low, or whether some normal stresses will invariably be present at the shear rates employed. The data given in Table I show that in the case of water the predicted and experimental values are identical at the 95% confidence level; the alcohol results are similar within the accuracy of the measurements. The diameters of jets of concentrated syrups and glycerine solutions were greater than would be predicted for fluids exhibiting no normal stresses. This may constitute an interesting verification of the predicted possibility of normal stresses in fluids of constant viscosity.^{23, 24, 26}

Data on polymeric solutions expected to show larger normal stress effects are shown in Tables II and III and in Figures 3-6.

Figures 3-5 give complete data on a 0.7% carboxymethyl cellulose solution which, at the shear rates obtainable in a rheogoniometric device, is so slightly viscoelastic that no capillary rise whatever is observed in the usual type of apparatus described by Roberts.^{28, 29} The horizontal dashed line of Figure 4 locates the ratio d_j/D (0.89)

TABLE I
Contraction of Fluid Jets^a

Fluid	Run no.	d_j/D
Water	1	0.901
	2	0.815
	3	0.932
	4	0.877
	5	0.877
	6	0.866
	7	0.887
	True value: 0.879 ± 0.033^b	
	True value: 0.846 to 0.912 ^b	
Anhydrous ethanol	8	0.907
	9	0.897
	10	0.900

^a Shear rates employed varied between 20,000 and 30,000 sec.⁻¹.^b 95% confidence level.TABLE II
Normal Stresses, 0.7% CMC

$8V/D$, sec. ⁻¹	d_j/D	$(P_{11} - P_{22})_R$, psi	$(\tau_{12})_w$, psi	$(P_{11} - P_{22})/\tau_{12}$
0.79×10^4	0.992	0.279	0.0219	13
1.04×10^4	0.985	0.453	0.0253	18
1.67×10^4	0.963	0.893	0.0321	28
2.09×10^4	0.962	1.37	0.0353	39

TABLE III
Comparison of Normal and Shearing Stresses. 5% Solution of Polyisobutylene in Decalin^a

$8V/D$, sec. ⁻¹	d_j/D	$(P_{11} - P_{22})_R$, psi.	$(\tau_{12})_w$, psi.	$(P_{11} - P_{22})/\tau_{12}$
$D = 2.22$ mm.				
1.33×10^4	1.72	3.98	0.172	23
1.58×10^4	1.53	4.68	0.188	25
1.88×10^4	1.37	5.01	0.208	24
$D = 1.77$ mm.				
2.09×10^4	1.77	5.78	0.219	26
2.40×10^4	1.62	6.60	0.240	27
2.72×10^4	1.47	7.07	0.259	27

^a L/D of tubes used: 137-276.

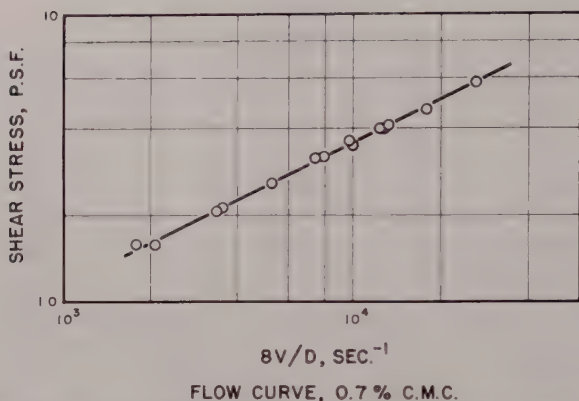


Fig. 3. Shear properties of a carboxymethylcellulose solution.

which would be expected of an inelastic fluid having the same power law exponent as this material. Not only is the ratio d_j/D considerably greater than 0.89, but the calculations summarized in Table II show that even for this dilute solution the normal stress difference $P_{11} - P_{22}$ may exceed τ_{12} appreciably at sufficiently high shear rates.*

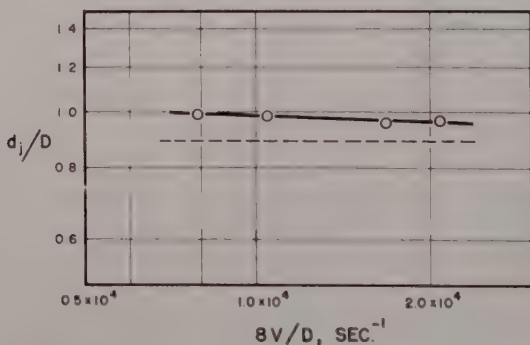


Fig. 4. Ratio of jet to tube diameters for the same CMC solution, as a function of $8V/D$. (To obtain the shear rates, $8V/D$ must be multiplied by approx. 1.25.) L/D of tubes used: 209.

* An earlier treatment of this problem,⁹ in which an energy balance approach was attempted, is incorrect in principle since there is energy dissipation between Sections 1 and 2 due to the viscous shear which accompanies the rearrangement of the velocity profiles, and this dissipation function was neglected. Due to accompanying algebraic errors in the development a result close to the correct value of 0.866 was predicted for these simple fluids, however.

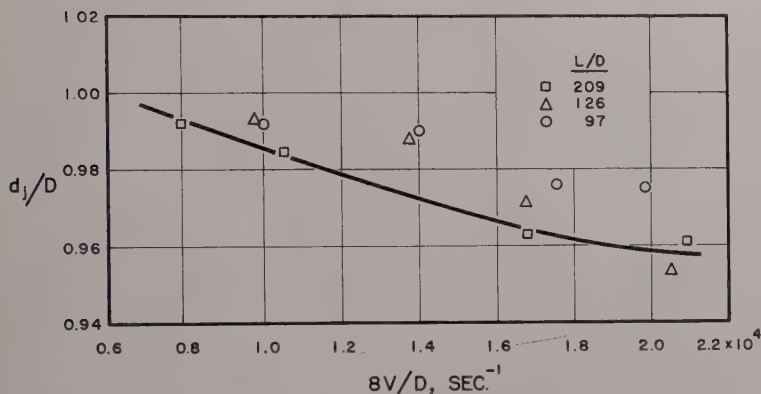


Fig. 5. Effect of L/D ratio of the tube used on d_j/D (CMC solution).

Figure 5 shows data on a greatly expanded scale, as compared to Figure 4 [the latter, however, gives the desired slope $d(\log D/d_j)/d(\log 8V/D)$ directly]. It is clear that long tubes must be used to obtain data which are not influenced by inlet effects. Since shearing stresses in an inlet region are obviously higher than those under well-developed flow conditions (at least in the region of interest near the tube wall, where the stresses are greatest^{2,30}), one would expect greater normal stresses, hence greater jet expansions, for jets issuing from the shortest tubes. Additionally, an incompletely developed velocity profile would tend to equalize the momentum terms of eq. (4), and cause d_j/D to approach a value of unity even in the absence

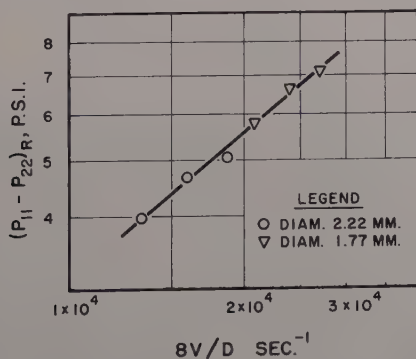


Fig. 6. Normal stress difference $(P_{11} - P_{22})_R$ of a 5% polyisobutylene solution as a function of shear rate [$u_R' \approx 1.25 (8V/D)$].

of normal stresses. These trends are clearly confirmed by Figure 5, and other data are available to show that for these materials L/D values of above about 200 have frequently been required under the conditions studied to date. The fact that inlet effects may persist so much longer in these materials than in simple fluids is not surprising and has actually been documented quite carefully in a much earlier study.¹⁴

In view of the problems of differentiating experimental data, it is interesting to note that the slope of Figure 4 is so low that the derivative term of eq. (12) contributes only about 10% to the calculated value of $P_{11} - P_{22}$. Furthermore, in no other case studied to date has the derivative accounted for more than 20%, so no difficulty is expected in its evaluation.

Table III and Figure 6 summarize results on a 5% solution of polyisobutylene in decalin. The ratios $(P_{11} - P_{22})/\tau_{12}$ given in Table III are for shear rates nearly an order of magnitude higher than any birefringence data reported before for so viscous a solution, and $1\frac{1}{2}$ orders of magnitude beyond any earlier direct force measurements. As nearly as can be determined by extrapolation, the data are in agreement with birefringence results on a similar solution,⁴ however. Of particular interest from an experimental viewpoint is the fact that two significantly different tube diameters were employed in obtaining these data. The obvious continuity of the measurements supports the correctness of eq. (12) and its freedom from incidental algebraic or arithmetic errors, as well as the applicability of the assumptions used in deriving this equation.*

Further Studies

Obviously further experimental data would be desirable to confirm and extend the utility of the equations developed herein and to supplement the measurements reported. Of especial value would be experimental measurements which would overlap data obtained in another, completely independent way, as, for example, by the rheo-
goniometric technique of Roberts.

*** Note Added in Proof:** It has recently been suggested that this experiment may be subject to spurious Reynolds number effects. At a given shear rate or $8V/D$, the non-Newtonian Reynolds number for the large tube exceeds that of the small one by 57%. Clearly the present data are free of any such difficulties.

R. B. Bird, D. C. Bogue, M. Mooney, and W. Philippoff are thanked for their constructive criticism and their willingness to discuss desirable or necessary revisions of the original manuscript.

This work has been supported by the Office of Ordnance Research, U.S. Army, whose aid is also gratefully acknowledged.

Notation

Any consistent set of units is permissible.

d_j = jet diameter (diameter of a jet in the absence of gravitational forces).

D = inside tube diameter.

F = body force.

L = tube length.

n' = flow behavior index defined by the logarithmic slope of the flow curve obtained from a capillary tube: $n' = d(\log \tau_w) / d(\log 8V/D)$.

r = radial position co-ordinate.

R = tube radius ($D/2$).

R_j = jet radius ($d_j/2$).

u = local velocity at position r ; u' : shear rate.

v = local velocity in radial direction.

\vec{V} = velocity vector.

V = mean or volumetric fluid velocity inside tube.

V_j = velocity of a jet uninfluenced by gravitational forces, or horizontal component of velocity of a jet issuing from a horizontal tube.

w = local velocity in tangential direction.

x = distance along axial coordinate.

π = 3.14

ρ = fluid density.

τ_{12} = shear stress; $(\tau_{12})_w$ or τ_w : point value of shear stress evaluated at tube wall.

References

1. Barus, C., *Am. J. Sci.*, **45**, No. 3, 87 (1893). See also R. Houwink, *Elasticity, Plasticity and the Structure of Matter*, Harren Press, Washington, 1953.
2. Bogue, D. C., *Ind. Eng. Chem.*, **51**, 874 (1959).
3. Brodnyan, J. G., F. H. Gaskins, W., Philippoff, and E. G. Lendrat, *Trans. Soc. Rheology*, **2**, 285 (1958).
4. Brodnyan, J. G., G. H. Gaskins, and W. Philippoff, *Trans. Soc. Rheology*, **1**, 109 (1957).

5. Coleman, B. D., and W. Noll, *Arch. Ratl. Mech. Anal.*, **3**, 289 (1959).
6. Eisenschitz, R., B. Rabinowitsch, and K. Weissenberg, *Mitt. deut. Materialprüfungsanstalt Sond.*, **9**, 91 (1929).
7. Ericksen, J. L., *Quart. Appl. Math.*, **14**, 319 (1956). W. O. Criminale, J. L. Ericksen, and G. L. Filbey, *Arch. Ratl. Mech. Anal.*, **1**, 410 (1958). J. L. Ericksen, in *Viscoelasticity: Phenomenological Aspects*, J. T. Bergen, ed., Academic Press, New York, 1960.
8. Ericksen, J. L., *Trans. Soc. Rheology*, **4**, 29 (1960).
9. Gaskins, F. H., and W. Philippoff, *Trans. Soc. Rheology*, **3**, 181 (1959).
10. Gavis, J., and S. J. Gill, *J. Polymer Sci.*, **21**, 353 (1956); **20**, 287 (1956).
11. Jobling, A., and J. E. Roberts, in *Rheology*, Vol. II, F. R. Eirich, ed., Academic Press, New York, 1958.
12. Kotaka, T., M. Kurata, and M. Tamara, *J. Appl. Phys.*, **30**, 1705 (1959).
13. Markovitz, H., *Trans. Soc. Rheology*, **1**, 37 (1957).
14. McMillen, E. L., *Chem. Eng. Prog.*, **44**, 537 (1948).
15. Metzner, A. B., in *Handbook of Fluid Dynamics*, V. L. Streeter, ed., McGraw-Hill, New York, 1961.
16. Metzner, A. B., E. L. Carley, and I. K. Park, *Modern Plastics* **37**, No. 11, 133 (1960).
17. Metzner, A. B., in *Advances in Chemical Engineering*, Vol. I, T. B. Drew, and J. W. Hoopes, Jr., eds., Academic Press, New York, 1956. Also in *Processing of Thermoplastic Materials*, E. C. Bernhardt, ed., Reinhold, New York, 1959.
18. Mooney, M., *J. Rheol.*, **3**, 210 (1931).
19. Oldroyd, J. G., *Proc. Royal Soc. (London)*, **A245**, 278 (1958).
20. Philippoff, W., *Trans. Soc. Rheology*, **1**, 95 (1957).
21. Pilpel, N., *Trans. Faraday Soc.*, **50**, 1369 (1954).
22. Rabinowitsch, B., *Z. physik. Chem.*, **A145**, 1 (1929).
23. Reiner, M., *Lectures on Theoretical Rheology*, Interscience, New York, 1960.
24. Reiner, M., *Am. J. Math.*, **67**, 350 (1945).
25. Rivlin, R. S., *J. Ratl. Mech. Anal.*, **5**, 179 (1956).
26. Rivlin, R. S., *Proc. Royal Soc.*, **A193**, 260 (1948).
27. Rivlin, R. S., and D. W. Saunders, *Phil. Trans. Royal Soc. (London)*, **A243**, 251 (1951).
28. Roberts, J. E., *Proceedings Second International Congress on Rheology*, V. G. W. Harrison, ed., 91 (1954). Academic Press, New York, Butterworth, London, 1954, p. 91; *Nature*, **179**, 487 (1957).
29. Roberts, J. E., Unpublished Report, No. ADE13/52, British Ministry of Supply.
30. Schlichting, H., *Boundary Layer Theory*, 4th ed. McGraw-Hill, New York, 1960.
31. Sokolnikoff, I. S., and E. S. Sokolnikoff, *Higher Mathematics for Engineers and Physicists*, McGraw-Hill, New York, 1941, p. 168.
32. Weissenberg, K., *Proceedings First International Congress on Rheology*, North-Holland, Amsterdam, 1949, p. 29.

Synopsis

A mathematical development is presented which enables the calculation of the normal stress difference $P_{11} - P_{22}$ in fluids undergoing steady simple shear, from experimental observations of the diameters of jets issuing from tubes of convenient size. This development is free of any assumed relationship between the normal stress and shear rate, and, as such, is applicable to all materials for which the experimental measurements are possible. This "capillary-jet" experimental technique enables measurements at much higher shear rates than obtained heretofore.

The applicability of this approach and the resultant equations are demonstrated by measurements on solutions of carboxymethylcellulose in water and of polyisobutylene in decalin.

Experimental Tests of Symmetry Conditions in Laminar Flow

WLADIMIR PHILIPPOFF, *Esso Research and Engineering
Company, Linden, New Jersey*

Introduction

In deformational mechanics as applied to the flow of polymer solutions, a statement of Weissenberg¹ requires the equality of stresses, P , in the plane normal to the direction of the flow for *any* material in laminar flow. This is described in the well-known equation $P_{22} = P_{33}$, where, 1 = direction of flow, 2 = direction normal to sheared plane, 3 = direction normal to the 1,2 plane. Recently Kotaka² introduced $m(P_{11} - P_{22}) = (P_{22} - P_{33})$. However, other theories of deformational mechanics summarized in Reiner's³ and Markovitz's⁴ papers do not require this identity. Therefore, the experimental check of this relation (or $m = 0$) gives the possibility of deciding on the validity of the different theories of deformational mechanics. Such checks have been reported by Roberts⁵ and Pilpel⁶ using the Weissenberg Rheogoniometer, which confirmed the statement for soap solutions. In recent investigations, we have used flow birefringence extensively. As applied to the problem under discussion, finding an optical anisotropy in the reference plane corresponds to finding a stress anisotropy. This general idea has been used by other investigators⁷⁻⁹ in shearing molten plastics, allowing them to cool under stress and determining the recoverable deformation, the birefringence of the cold specimen, or the deformation of a re-heated cube cut from the stressed sample. This procedure, that has also been checked, does not give conclusive evidence because the inevitable shrinking stresses cause too many errors such as a "spotty" birefringence. Therefore, in the following investigation, the mentioned equality of stresses has been made in a *flowing solution* without any thermal treatment.

Theoretical Expectations

Birefringences are expected to be observable in the three reference planes when the optical tensor is determined according to the stress-optical law. This law means that a proportionality exists between the birefringence Δn in a plane and the difference of the principal stresses ($\sigma_1 - \sigma_2$) in the same plane—the proportionality constant being the stress-optical coefficient C in Brewsters Br (10^{-13} cgs.):

$$\Delta n = C(\sigma_1 - \sigma_2)$$

For the 1,2 plane, usually observed in birefringence experiments:

$$\Delta n_{12} = \Delta n$$

inclined by χ_{12} to the X-axis. (Same as 1-axis above.)

For the 1,3 plane:

$$\chi_{13} = 0^\circ$$

$$\Delta n_{13} = \Delta n \cos 2\chi_{12} + \Delta n_{23}$$

And for the 2,3 plane:

$$\chi_{23} = 0^\circ$$

$$\Delta n_{23} = m_0 \Delta n \cos 2\chi_{12}$$

where m_0 corresponds to m in the mechanical equation ($P_{22} - P_{33}$) = $m(P_{11} - P_{22})$ and Δn may be positive or negative; $\chi < 45^\circ$.

Investigation of Flow Birefringence in the 2,3 Plane

From all the possibilities of measuring birefringence in the 2,3 plane, the one of directing a beam of polarized light along the axis of a capillary (see Fig. 1) has been used. A small stainless steel block with a capillary bore ($L/d = 10$, where L is the length and d the diameter of the capillary) and axial glass windows was connected to suction flasks with plastic tubing and placed on the stage of a polarizing microscope (Fig. 1). As the flow direction is axial, the observed plane is the 2,3 plane in which an optical anisotropy, should it exist, should be detectable as a "cross of isoclines." This experiment was first performed by Freundlich¹⁰ in 1915 with vanadium pentoxide (V_2O_5) solutions, and an anisotropy was found. The capillary in the instrument used here was calibrated in such a manner that both the

volume flow Q (in cc./sec.) and the applied pressure p can be re-calculated in terms of rate of shear, D , and shear stress, τ , respectively. The sensitivity was about six times less than in the usual instrument due to the shorter optical length used. The flow curves of the polymer solutions used have been measured previously; these measurements were adequate to determine the conditions of flow. The flow birefringence in this device was measured on the dozen or so solutions of polyisobutylene, rubber, polysiloxane, and nitrocellulose that were described by us in previous publications¹¹ including the two solutions

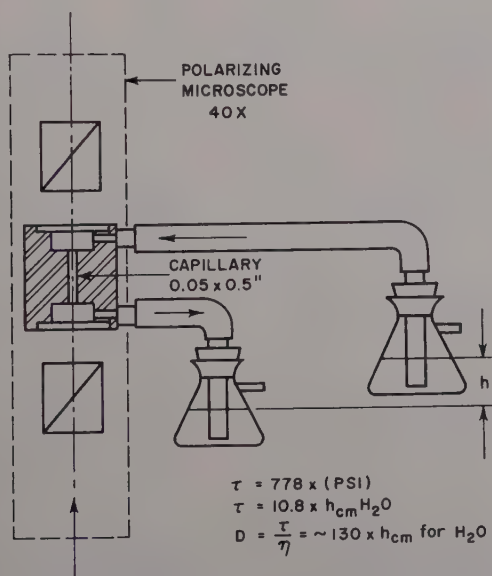


Fig. 1. Flow birefringence device for the 2,3 plane.

described in the results in the 1,3 plane. In all cases of polymer solutions there was no "cross of isoclines" even if the birefringence, Δn , in the 1,2 plane, which is usually observed in the flow birefringence instrument, was as much as 1000×10^{-8} units. One cannot state how small the detectable effects could be, but no change of the optical picture either with crossed Nicols or with a sensitive color plate was observed in flow (also using the regular optics from the birefringence instrument) even if the calculated rate of shear at suction of 10-20 cm. Hg ($\tau = 1500\text{--}3000$ dyne/cm.²) was higher than the one employed

in the flow birefringence (1,2 plane) measurements. These experiments therefore substantiate Weissenberg's assumption (or $m_0 = 0$) in the case of polymer solutions.

However, the positive result of Freundlich had to be reconciled. Six solutions which have *rigid particles* were investigated: a 0.016% and a 0.024% solution of vanadium pentoxide in water; a 0.128% suspension of cellulose crystallites in water; a solution of 0.03% tobacco mosaic virus (TMV) in a pH 7 buffer; a 0.206% of γ -polybenzyl-L-glutamate (PBLG) in dichlorethylene. The last solution, a synthetic, nearly monodisperse, polypeptide with a molecular weight of about 300,000, consists of tightly coiled helices, the equivalent of rigid rods, in this solvent with an intrinsic viscosity of $[\eta] = 7.6$ according to investigations of Doty and Blout.¹² Further, a dilute suspension of grease (soap crystals) in oil was tested.

The very dilute aqueous solutions were not investigated viscometrically. Their viscosity was assumed to be in first approximation equal to that of the solvent. Of course, this point can be investigated in more detail, but it is outside the scope of this paper. All these solutions did give, as Freundlich found, a *very distinct cross of isoclines* which is shown in Figure 2 for the 0.024% V_2O_5 solution. In the case of the PBLG, a higher rate of shear was necessary to observe the phenomenon. The cross was less clearly defined, due especially to the difficulties arising from the large volume flow and the limited amount of solution available.

The symmetry in all cases was that of a uniaxial crystal, the particles oriented radially. These symmetry conditions were described in a general fashion in a previous publication.¹³

Furthermore, an investigation of the "cross of isoclines" along the capillary axis was made by focusing the microscope objective to planes within 1 mm. of each other, starting from the influx end. The result was that the "cross of isoclines" increases the intensity and sharpness towards the outlet of the capillary, where Figure 2 was made.

This shows that the "cross of isoclines" is indeed a result of the Poiseuille flow in the capillary and not due to entrance-effects. The entrance-effects could possibly be responsible for Freundlich's results, as he had a L/d of 1 instead of 10 used in the present experiments.

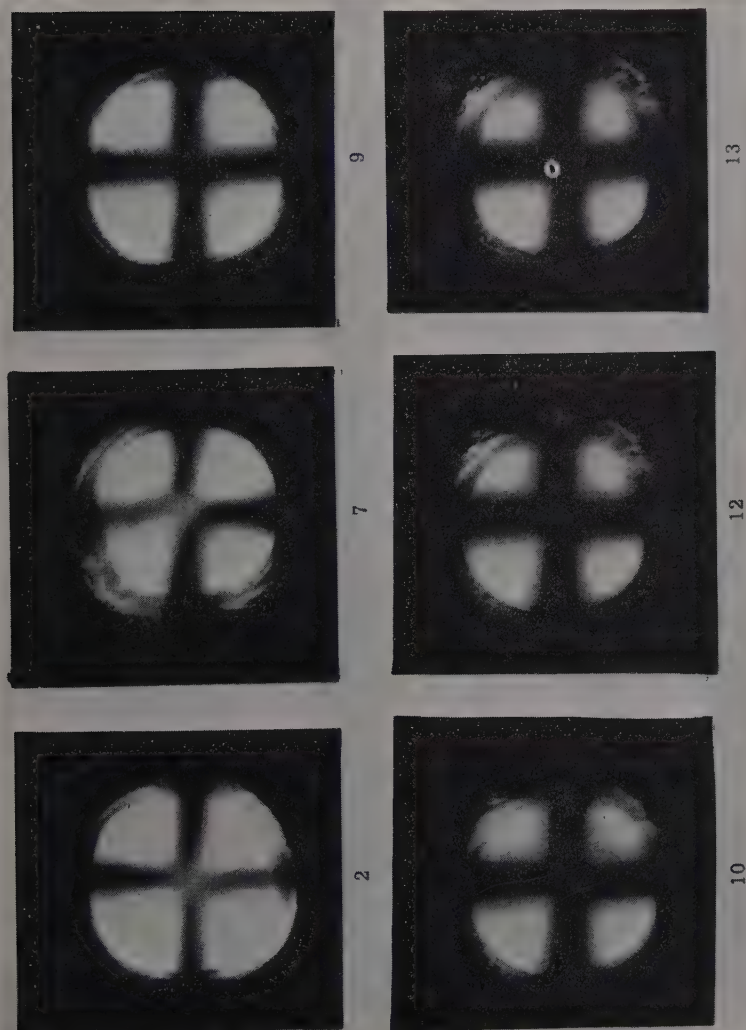


Fig. 2. Cross of isoclines for the 0.024% V_2O_5 solution. Numbers are millimeters from influx (top).

Flow Birefringence of Suspensions in the 1,3 Plane

Recently measurements of the flow birefringence in the 1,3 plane perpendicular to the planes of shear have been described by Foreman¹⁴ on V_2O_5 sols. The result was that flow birefringence is observable and it increases with the rate of shear similar to the effects observable in the 1,2 plane. However, comparative measurements on the same solution in the different planes have not been performed. Due to the courtesy of Dr. Foreman and the Baird Atomics Company in Boston, Dr. Foreman's instrument was made available to us. It was slightly modified to be used with a horizontal axis in our

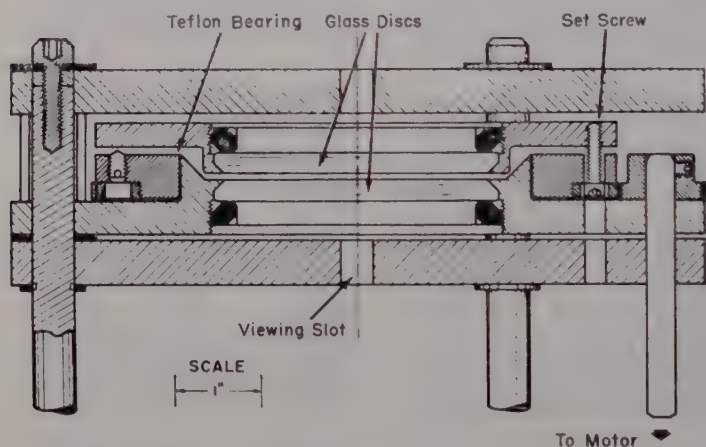


Fig. 3. Instrument of Foreman for the measurement of flow birefringence in the 1,3 plane.

flow birefringence instrument which allowed the determination of the extinction angle χ and a much more precise measurement of the birefringence Δn . It was driven by the same mechanical drive used in our flow birefringence instruments. However, the use of a "timing belt" was not possible. The belt used had a certain small slip when investigating viscous materials at high rates of shear. Therefore, a direct measurement of the rpm of the Foreman instrument had to be made. The original Foreman instrument is shown in Figure 3. Polarized light is transmitted through strain-free glass plates and a layer of 0.126 cm. of solution. The radius of observation can be

changed between 2 and 3 cm., giving us the possibility of checking results with different geometrical arrangements.

Due to the fact that only a thin layer of liquid was available, the measurements with the Foreman instrument are much less sensitive than those of regular flow birefringence instruments that have an optical path of about 70 mm. Therefore, only solutions with large birefringences could be investigated. Whereas in the regular instrument, the birefringence was $4 \times 10^{-8} \times (\text{degrees of compensator})$; for the Foreman instrument it was 240×10^{-8} , meaning a decrease in sensitivity of 60-fold.

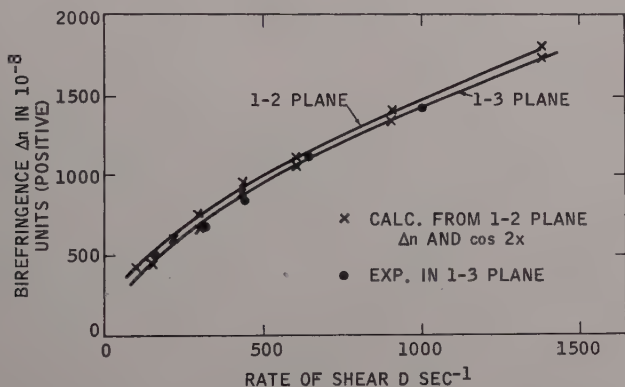


Fig. 4. Flow birefringence results in the 1,3 plane for 9% polyisobutylene (Vistanex) in decalin.

The rate of shear $D = 2\pi R(\text{rpm})/(60 \times 0.126) = 98.7$ (rps) for a radius of 2 cm. in sec^{-1} and 149.5 (rps) for one of 3 cm. in sec^{-1} .

Two solutions were investigated in more detail after ascertaining that the Foreman instrument gave results on polymer solutions. The first one was a 9% solution of polyisobutylene (Vistanex B-100, Enjay Co.) in decalin and the second was a 30% solution of commercial polystyrene PX 134 of Dow Chemical Co. in toluene. Whereas the polyisobutylene had a very small extinction angle χ for the rates of shear measurable in the Foreman instrument, the polystyrene solution had considerably larger ones amounting to about 30° . The results are shown in Figures 4 and 5. The birefringence in the 1,2 plane was measured separately (being positive for the polyisobutyl-

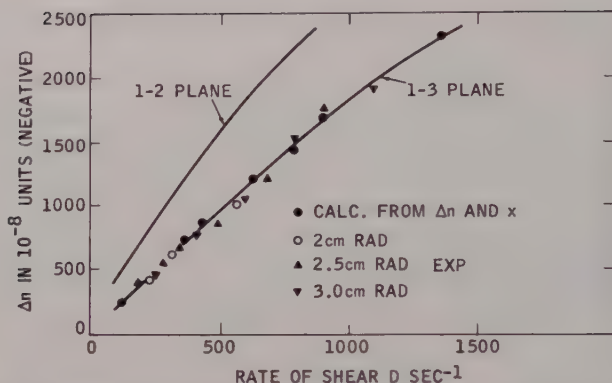


Fig. 5. Flow birefringence results in the 1,3 plane for 30% polystyrene in toluene.

ene, negative for the polystyrene) and the expected birefringence in the 1,3 plane calculated using the relation $\Delta n_{13} = \Delta n_{12} \times \cos 2\chi_{12}$. The measurements performed on the polyisobutylene solution are shown as circles and compare extremely well with the calculated data. However, in this case, due to the large value of $\cos 2\chi_{12}$, the values for the two planes differ very little. The experiments on the polystyrene solution in Figure 5 were performed with three different radii of observation: 2, 2.5, and 3 cm. In this case, $\cos 2\chi_{12}$ was considerably smaller than unity. The results scattered very little around the mean value for the three radii and compared well with the value calculated from the results determined for the same solution in the usual instrument in the same range of D . The experiments therefore show that the birefringence in the 1,3 plane for a polymer solution *can* be expressed according to the mentioned relationship within the limit of experimental error. The investigation of the 1,3 plane does not give us any more information than the one in the 1,2 plane, actually even less, as the extinction angle χ_{13} in the 1,3 plane is zero, i.e., the direction of the birefringence is tangential to the circular lines of flow. Foreman's mentioned experiments have proved that suspensions of rigid particles (V_2O_5 sol) equally have observable birefringence in the 1,3 plane.

Flow Birefringence of Suspensions in the 1,2 Plane

In order to have more conclusive results, the solutions with rigid particles were also investigated in the flow birefringence instrument,

where the birefringence in the 1,2 plane was measured as a function of D . The results are shown in Figure 6 where both the birefringence, Δn (positive in all cases), and the extinction angle, χ , are plotted against D . For the aqueous solutions, the hydrostatic height, h , was ~ 1 -2 cm. water; therefore, D was ~ 100 -200 sec^{-1} . However, for PBLG an $h \sim 20$ cm. H_2O with $D = 5,000$ -10,000 sec^{-1} was used.

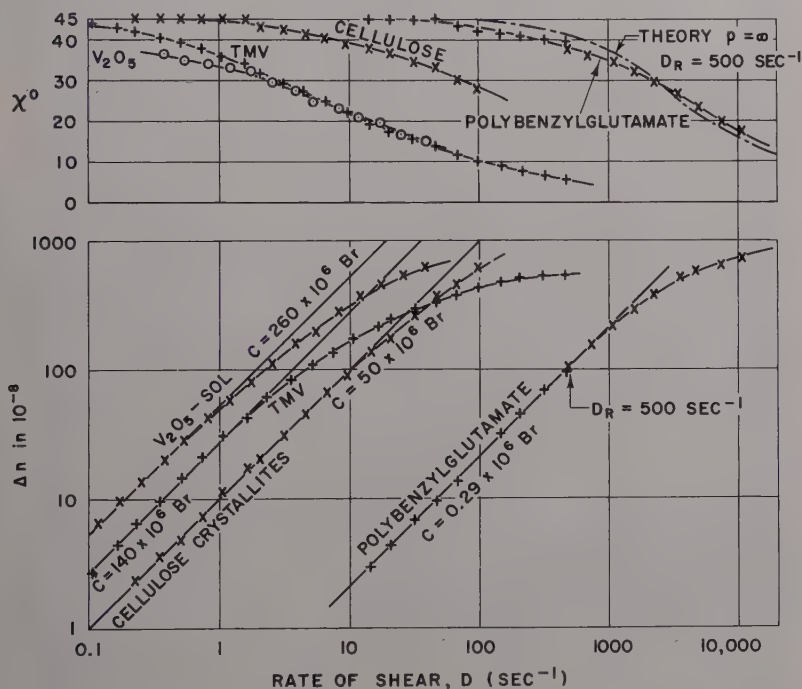


Fig. 6. Degree of birefringence, Δn , and extinction angle, τ , as function of the rate of shear, D , for the suspension of rigid particles. The PBLG was measured with a 1 mm. + and 0.4 mm. \times gap. Stress-optical coefficients, C , are listed in the figure.

All of the solutions at that rate of shear had a Δn of the order of 600×10^{-8} (1 wavelength phase retardation in the 7 cm. cylinder) and an extinction angle of about 10° for the V_2O_5 and the TMV, 25° for the cellulose crystallites and the PBLG. The solutions of rigid particles had, under the conditions of the experiments in the new capillary device, about the same Δn as the polymer solutions, notwithstanding

the large differences in τ and D . Such flow birefringence curves have probably never been measured before over as wide a range of D .

The PBLG solution had a relative viscosity at low rates of shear of 4.57 (or $\eta = 3.63$ cp.). It is known to be strongly dependent on the rate of shear, D ; at the D used it may only be a small fraction above the value for the solvent: 0.790 cp. Too little material was available to make a complete study of both the viscosity and birefringence behavior of this substance. Higher concentrations would have been easier to work with, but the amount of compound required was prohibitive.

Discussion

The described experiments seem to show that an optical anisotropy in the 2,3 plane, i.e., a "cross of isoclines," can *only* be observed in a suspension of *rigid* particles. The investigation of the flow birefringence in the 2,3 plane therefore gives the distinct possibility of deciding if particles are rigid or deformable. Apparently a triaxial optical asymmetry of the rigid particles is not necessary as the TMV and the PBLG have, so far as is known, a cylindrical symmetry. The further conclusion is that the occurrence of the "cross of isoclines" is not caused by a lack of validity of Weissenberg's statement but by the presence of *rigid* particles.

Further, to demonstrate the symmetry principle in the flow of deformable particles, we have resorted to a model experiment mentioned by Love¹⁵ in his book: a sphere, built up of cardboard discs with a hole along its axis, could be sheared in the plane of these discs. As is shown in Figure 7, under simple shear in the 1,2 plane the sphere is deformed to an elongated ellipsoid (or strain-ellipsoid). In the 1,3 plane at large deformations ($S > 1$) the projection is also an ellipse. However, in the 2,3 plane, independent of the amount of deformation, the projection remains circular. This model describes the behavior of the strain ellipsoid of an incompressible material in plane simple shear. The assumption, however, is that the same deformation occurs in deformable coiled molecules in laminar flow due to the forces exerted by the solvent. Similar deformations have been calculated in the well-known work of Kuhn and Kuhn¹⁶ and in a recent presentation of Pao.¹⁷

The discussion of the symmetry conditions of the model therefore make it plausible that in laminar flow no anisotropy in the 2,3 plane

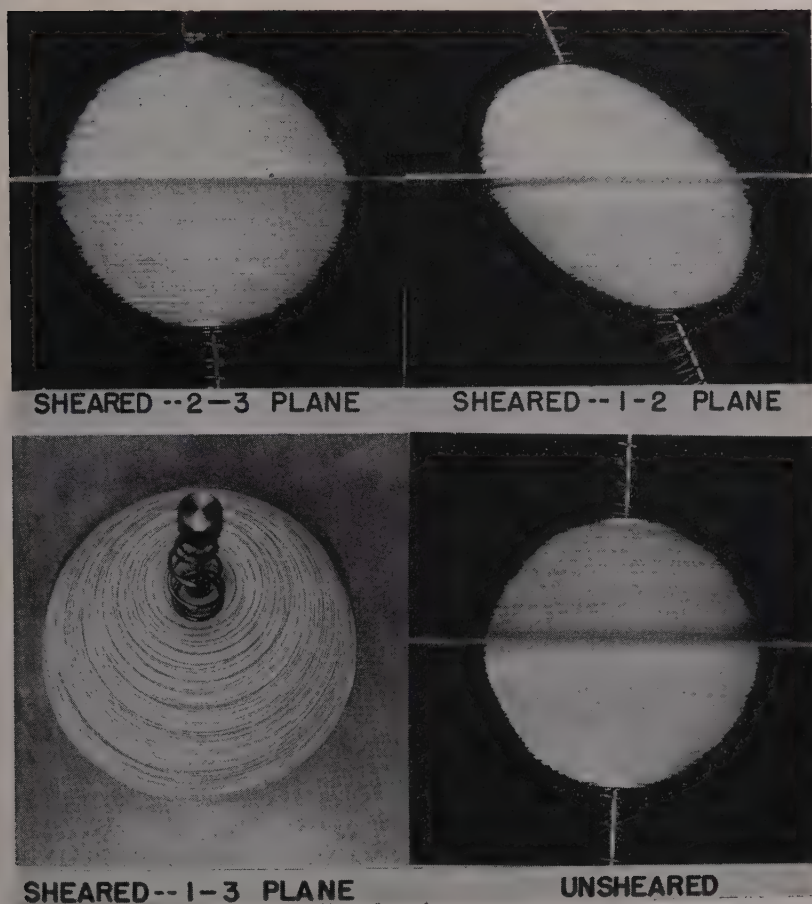


Fig. 7. Model of a sphere sheared in simple shear $s = 0.45$ in three dimensions.

can be detected in the case of deformable molecules whose shape is determined by the stress-tensor. Rigid particles, however, cause an effect as their shape is independent of the stress-tensor, only their orientation (extinction angle χ) varying with D . This determines a significantly different behavior of rigid and deformable particles in laminar flow. Effects in the 1,2 and 1,3 planes are observable with both kinds of particles; in the 2,3 plane only with rigid ones.

Very similar experiments on the shear deformation using drops have been made by Taylor¹⁸ and recently by Bartok and Mason.¹⁹ We

have also investigated the possibility of shearing drops or bubbles in plane shear in gels of aluminum soaps in a glass box, transparent in all 3 directions. The qualitative results are very similar to the model described; however, difficulties arise in the action of the interfacial tension and the formation of "sharp ends" at the apex of the ellipse. We did not consider it worthwhile to present these results; the cardboard model seems to describe the symmetry conditions more nearly similar to the mathematical requirements.

A large quantitative difference is further remarked in comparing the stress-optical coefficients, C , of polymer solutions and of suspensions of rigid particles. Polymers¹¹ have $C = 500$ –5000 Br. The suspensions investigated, as seen in Figure 6, have C calculated from the rate of shear and the viscosity of water at 25°C. nearly 100,000 times the value for the polymers. Knowing the concentration and estimating the saturation value of Δn , one can calculate the birefringence of the crystals that constitute the suspension, neglecting in first approximation the "Wiener-Effect." The values of $\Delta n = 0.1$ to 0.001 are similar to those measured for crystals as listed in mineralogical tables. The curves in Figure 6 do not comply to the one calculated by Scheraga,²⁰ probably because the particles were polydisperse, except for the more nearly monodisperse PBLG, where the Δn - D curve conformed well with the $p \rightarrow \infty$ curve of Scheraga; the χ - D curve, however, intersects the theoretical one, the deviation being $\sim \pm 2^\circ$. The rotary diffusion constant estimated graphically is 500 sec.⁻¹.

The sizes of the rigid particles were widely different: V_2O_5 has long filaments of unstated length, easily seen in the electron microscope. The cellulose crystallites were oblate ellipsoids of about the wavelength of light (5000 Å.) as the largest dimension. The TMV forms needles of 150 Å. breadth and 2000 Å. length. The sample used may have been somewhat aggregated, notwithstanding the precautions taken. The PBLG rods are considerably smaller than the other particles. This is especially well reflected in the much higher D required to cause the Δn —corresponding to a rotary diffusion constant of 500 sec.⁻¹ as compared to rough estimates of 1 sec.⁻¹ for the V_2O_5 , 2 sec.⁻¹ for the TMV, and 10 sec.⁻¹ for the cellulose crystallites. The particle size of the rigid suspensions was of the order of 10 – 100×10^6 in molecular weight, much larger than the one for the PBLG.

In this paper the conclusions of deformational mechanics have been combined with optics and, to some extent, with the physics of flow of

coiled molecules and rigid particles. The approach integrated all the information available to gain a deeper insight into the complicated conditions of deformation and flow. This combination seems to be a powerful tool for the purpose.

The help of the following persons is gratefully acknowledged: Professor P. Doty of Harvard University for the synthetic polypeptide; The American Viscose Corporation, Marcus Hook, Pa., Dr. J. T. Yang, for the cellulose crystallites; Dr. S. D. Rodenberg of the General Microbiology Department of the University of Pennsylvania for the sample of the tobacco mosaic virus and its assay; Dr. W. T. Foreman now of ITEK-Corp., Boston, Mass., and Dr. W. G. Driscoll of the Baird-Atomics Corp., Boston, Mass., for making the Foreman instrument available to us; and Dr. E. O. Forster of Esso Research and Engineering Company for the photographs shown in Figure 2.

The first experiments were performed at the Franklin Institute, Philadelphia, Pa., and presented in part on March 31, 1959 at the Meeting of the American Physical Society in Cambridge, Mass.

References

1. Weissenberg, K., Conf. British Rheologists' Club, 1948.
2. Kotaka, T., M. Kurata, and M. Tamura, *J. Appl. Phys.*, **30**, 1705 (1959).
3. Reiner, M., *Rheology*, Vol. I, F. Eirich, ed., Academic Press, New York, 1956, p. 9.
4. Markovitz, H., *Trans. Soc. Rheology*, **1**, 37 (1957).
5. Roberts, J. E., Ministry of Supply Report No. ADE 13/52, *Proc. 2nd Intern. Congr. Rheology*, 91 (1954).
6. Pilpel, N., *Trans. Faraday Soc.*, **50**, 1369 (1954); **51**, 1307 (1955).
7. Newbert, D., and D. W. Saunders, *Rheologica Acta*, **1**, 151 (1958).
8. Pollett, W. F. O., *Rheologica Acta*, **1**, 257 (1958).
9. Mooney, M., *J. Polymer Sci.*, **34**, 599 (1959).
10. Diesselhorst, H., and N. Freundlich, *Physik. Z.*, **16**, 419 (1915).
11. Philippoff, W., *Acta Rheologica*, **1** (1959) in press.
12. Doty, P., A. M. Holtzer, J. H. Bradbury, and E. R. Blout, *J. Am. Chem. Soc.*, **78**, 947 (1956).
13. Hess, K., H. Kiessig, and W. Philippoff, *Naturwiss.*, **26**, 184 (1938).
14. Foreman, W. T., *J. Chem. Phys.*, **32**, 277 (1960).
15. Love, A. E. H., *A Treatise on the Mathematical Theory of Elasticity*, 4th ed., Dover, New York, 1944, p. 71.
16. Kuhn, W., and H. Kuhn, *Helv. Chim. Acta*, **26**, 1394 (1943).
17. Pao, Y., Paper presented at the Physical Society Meeting at Philadelphia, Pa., March 1957.
18. Taylor, G. I., *Proc. Roy. Soc. London*, **A146**, 501 (1934).
19. Bartok, W., and S. G. Mason, *J. Colloid Sci.*, **14**, 13 (1959).
20. Scheraga, H. A., J. T. Edsall, and J. D. Gadd, *J. Chem. Phys.*, **19**, 1101 (1951).

Synopsis

By the use of new flow birefringence devices it is shown that flowing polymer solutions, probably consisting of deformable coiled molecules, are isotropic in the 2,3 plane but are anisotropic in the 1,3 plane. Weissenberg's statement of $P_{22} = P_{33}$ is therefore confirmed by optical measurements. Suspensions of rigid particles are anisotropic both in the 1,3 and in the 2,3 plane, and give a "cross of isoclines" in the 2,3 plane due to a radial (uniaxial) symmetry. Results of the measurements of the flow birefringence of the suspensions in the 1,3 plane are given together with a description of a model of the mechanism of deformation in plane simple shear. The combination of deformational mechanics, optics, and the analysis of the motion of individual particles forms a powerful tool for the description of the phenomenon of flow.

Elastic Stresses and Birefringence in Flow

WLADIMIR PHILIPPOFF, *Esso Research and Engineering Co.,
Linden, New Jersey*

I. Introduction

Viscoelastic effects in steady laminar flow of liquids can be assumed to be caused by elastic strains set up by the flow which have a distribution in space similar to the ones of an ideally elastic material stressed by the same forces. This is admittedly an assumption; however, it has already been useful in correlating the "recoil" with the "extinction angle" in flow birefringence or with the "normal stresses" on polymer solutions, and in correctly predicting the flow-birefringence in the "1-3" plane, see Figure 2, which had not been investigated before.

It therefore seemed timely to expand the previous treatment to make it more general, stressing the points of similarity between the distribution of stresses and the birefringence—phenomena that are amenable to an experimental investigation. Furthermore, this paper gives the theoretical background to two experimental papers also published in this volume, treating the flow-birefringence in different planes in space.

The idea presented here does not necessarily exclude other possibilities to explain the observed effects; also, it does not consider the influence of the rate of deformation beyond the existence of an elastic strain caused by it. Nor does it consider the possible influence of higher time derivatives of the strain on viscoelastic phenomena.

The treatment has been planned to be fairly complete and detailed, admittedly repeating some well-known facts and formulas, in order to give a systematic development of the relationships for readers not completely familiar with the type of mathematics used in the deformational mechanics of large deformations.

The so-called "normal stresses" or "Weissenberg effect" have been shown to be caused by an elastic deformation of the liquid in laminar flow. When the elastic deformation, s , reaches values larger than about one (nondimensional units), stresses occur in flow that do not exist either in liquids or in elastic bodies with small deformations. They are treated by a part of deformational mechanics of finite deformations. The particular aspects have been first treated by Mooney in 1940,¹ Weissenberg² about 1945, and Rivlin³ in 1948 and more recently in 1956.⁴

In a previous publication⁵ the summary of the theories has been given using, as Mooney did, Cartesian coordinates calculations.

It has been possible to recalculate the derivations of the previous publication using tensor calculus, make the mathematical treatment of the problem much more complete and general, and to distinguish between the geometrical effects and the effects caused by the materials themselves.

Why an elastic deformation—or synonymously why an elastic potential energy—exists in a flowing liquid can be made plausible by the following considerations. A viscoelastic material relaxes: at constant load, the deformation increases with time; with constant strain, the stress decreases to zero with time. In flow, a material is continually stressed and relaxing. The relaxation proceeds at a constant rate, determined by the properties of the material; the stressing proceeds at any arbitrary rate, determined by the experimental conditions. The balance between stressing and relaxation determines a condition of elastic stress, which is stationary in space and can be described in the way outlined above.

The possibility of an elasticity (shear modulus) is given by the "entropy elasticity"—the reaction of a random distribution of directions or shapes of particles determined by thermal motion and the orientation tendency of the applied force.

II. Theoretical Approach

Common to all the following derivations is the concept of a tensor rotated about the Z-axis, the amount of rotation generally not being known. However, experiments^{5b} have shown that the amount of rotation—the angle χ —is identical for the strain, stress, and polarizability tensors. Furthermore, the isotropic condition in the YZ-plane (usually termed $P_{22} = P_{33}$) has been proved experimentally for flowing solutions in laminar^{5b} flow. This simplifies the symmetry

conditions considerably and allows flow-birefringence measurements to be used for determining χ and therefore the elastic properties of the flowing solutions.

The approach, as before, was first to calculate the strain-ellipsoid starting from a deformed unit sphere and determine the strain tensor in plane simple shear with its principal axes. Then using the stress-energy function, the principal axes of strain are transformed into the principal values of stress. The stress tensor is then rotated into its proper position in space, which is parallel to the position of the strain tensor. The different "normal stresses" are obtained by derived geometrical relations from the angle of rotation and the values of the principal stress. As has been proved experimentally, the difference between the principal axes of stress is proportional to the birefringence, therefore to the difference of the polarizability in two directions according to the stress-optical law. Assuming that the polarizability-tensor is rotated only about the Z-axis, expressions for the difference of principal axes of the polarizability tensor (the birefringence) in the three coordinate planes are obtained, which check with the ones resulting from the multiplication of the difference of the normal stresses by the stress-optical coefficient in the same plane.

In comparing the symmetry conditions of the strain-ellipsoid, the strain tensor, the stress tensor, and the polarizability tensor, one must be careful not to go further in deduction than is warranted. The derivations, together with experimental results, show that the angle of rotation of all three tensors about the Z-axis is the same. However, the strain-ellipsoid starts from a unit sphere and describes its deformation: the unstressed condition is a unit sphere. The stress tensor starts from an arbitrary hydrostatic pressure and describes the changes with straining, not necessarily similar to the strain-ellipsoid. The polarizability tensor is nearly spherical: the birefringence is always very small compared to the index of refraction. Still, by comparing these tensors with the strain ellipsoid some qualitative conclusions regarding symmetry can be made and have been useful for discussing the phenomena incurred in laminar flow.

III. Some Mathematical Relations

As will be shown in the following treatment, it has been necessary to develop relations between tensors in a way different from the usual one. It is convenient to use tensor calculus for the problems

of birefringence and mechanical stresses because mechanically the stresses on planes, which are given by the boundary conditions of the experiment, are measurable. The position of the principal stresses in plane shear is determined by the material but they are not directly observable. In birefringence, however, in each observation plane the differences of the principal values of the refractive index and their position in space can be measured. These conditions can, of course, be analyzed by regular calculus in Cartesian coordinates or by the method of Rivlin,⁴ but tensor calculus is especially suited for conditions where the principal values in arbitrary directions appear.

A symmetrical tensor of the second order can be described by three components:

$$\begin{vmatrix} a_{11} & a_{12} \\ a_{12} & a_{22} \end{vmatrix} \quad (1)$$

a_{11} and a_{22} are the "diagonal values," a_{12} the "cross terms." This tensor can also be described in terms of its "eigen-values" or "principal values."

$$\begin{vmatrix} A_1 & 0 \\ 0 & A_2 \end{vmatrix} \quad (2)$$

One can always transform the second form into the first one using a rotation of the coordinate axis by an angle which we call χ . The transformation is performed by the rule of tensor calculus:

$$u \begin{vmatrix} A_1 & 0 \\ 0 & A_2 \end{vmatrix} u^T \quad (3)$$

where u is a matrix

$$\begin{vmatrix} \cos \chi & -\sin \chi \\ \sin \chi & \cos \chi \end{vmatrix} \quad (4)$$

u^T is its transpose:

$$\begin{vmatrix} \cos \chi & \sin \chi \\ -\sin \chi & \cos \chi \end{vmatrix} \quad (5)$$

Matrix multiplication is associative and distributive but not commutative.

$$|a_{ik}| |b_{ik}| = |c_{ik}|$$

$$c_{ik} = \sum_{j=1}^s a_{ij} b_{jk} \quad (6)$$

$s = 2$ for 2×2 matrix; $s = 3$ for 3×3 matrix.

The performance of the calculation according to this rule gives the following expression.

$$\begin{vmatrix} a_{11} & a_{12} \\ a_{12} & a_{22} \end{vmatrix} = \begin{vmatrix} A_1 \cos^2 \chi + A_2 \sin^2 \chi & \frac{A_1 - A_2}{2} \sin 2\chi \\ \frac{A_1 - A_2}{2} \sin 2\chi & A_1 \sin^2 \chi + A_2 \cos^2 \chi \end{vmatrix} \quad (7)$$

The inclination of the principal axis X or 1 to the coordinate axis is given by

$$\tan 2\chi = 2a_{12}/(a_{11} - a_{22}) \quad (8)$$

If, however, from this matrix one subtracts half the sum of the diagonal values: $(A_1 + A_2)/2 = (a_{11} + a_{22})/2$, one obtains:

$$\begin{vmatrix} a_{11} & a_{12} \\ a_{12} & a_{22} \end{vmatrix} = \frac{A_1 + A_2}{2} \begin{vmatrix} 1 & 0 \\ 0 & 1 \end{vmatrix} + \frac{A_1 - A_2}{2} \begin{vmatrix} \cos 2\chi & \sin 2\chi \\ \sin 2\chi & -\cos 2\chi \end{vmatrix} \quad (9)$$

This means the original tensor is transformed into a scalar first term $(A_1 + A_2)/2$ (their mean value) multiplied with a unit matrix and a second term in which $(A_1 - A_2)/2$ is multiplied with a trigonometric function as a tensor, whose principal values are:

$$\begin{vmatrix} +1 & 0 \\ 0 & -1 \end{vmatrix}$$

The difference of the principal values of this trigonometric tensor is 2, so that the difference of the principal values of the second term is $A_1 - A_2$, equal to that of the original tensor. The sum of the diagonal value of the first matrix is 2, the value for the first term is $A_1 + A_2$, equal to that of the original tensor. The second term of the transformed tensor can be described geometrically by a *vector* of the magnitude $A_1 - A_2$, *inclined* to the X-axis at an angle 2χ .

This transformation means that the magnitude of the components of a second-order symmetrical tensor in an arbitrary position in space

can be expressed by the difference of the principal values and the angle of rotation χ in a simple way:

$$\begin{aligned}a_{11} &= \frac{A_1 + A_2}{2} + \frac{A_1 - A_2}{2} \cos 2\chi \\a_{22} &= \frac{A_1 + A_2}{2} - \frac{A_1 - A_2}{2} \cos 2\chi \\a_{12} &= \frac{A_1 - A_2}{2} \sin 2\chi \\a_{11} - a_{22} &= (A_1 - A_2) \cos 2\chi = 2a_{12} \cot 2\chi\end{aligned}\tag{10}$$

Thus, the calculation of these components starting from the principal values is very much simplified as compared with the use of directional cosines as in coordinates calculations. In the physical cases of interest—flow-birefringence and mechanical stresses—the first term $(A_1 + A_2)$ is of secondary interest: in birefringence it is a constant equal to the mean index of refraction n_0 ; in the mechanical case it is a uniform hydrostatic pressure, that does not produce any deformations in the incompressible case treated later.

In the particular case of shear, the third direction in space (Z or 3) is not involved in a deformation; the rules set above apply in this case, with $a_{33} = A_3$. The tensor is therefore:

$$\begin{vmatrix} a_{11} & a_{12} & 0 \\ a_{12} & a_{22} & 0 \\ 0 & 0 & a_{33} \end{vmatrix}\tag{11}$$

In terms of the three principal values A_1 , A_2 , and A_3 and the angle of rotation χ the components of the tensor and their differences are:⁶

$$\begin{aligned}a_{11} &= \frac{A_1 + A_2 + A_3}{3} + \frac{1}{6} (A_1 + A_2) \\&\quad - \frac{1}{3} A_3 + \frac{A_1 - A_2}{2} \cos 2\chi \\a_{22} &= \frac{A_1 + A_2 + A_3}{3} + \frac{1}{6} (A_1 + A_2) \\&\quad - \frac{1}{3} A_3 - \frac{A_1 - A_2}{2} \cos 2\chi\end{aligned}$$

$$\begin{aligned}
 a_{33} &= \frac{A_1 + A_2 + A_3}{3} - \frac{1}{3}(A_1 + A_2) + \frac{2}{3}A_3 \\
 a_{12} &= \frac{A_1 - A_2}{2} \sin 2\chi \\
 a_{11} - a_{22} &= (A_1 - A_2) \cot 2\chi = 2 a_{12} \cot 2\chi \\
 a_{22} - a_{33} &= \frac{1}{2}(A_1 + A_2) - A_3 - \frac{A_1 - A_2}{2} \cos 2\chi \\
 &= \frac{1}{2}(A_1 + A_2) - A_3 - a_{12} \cot 2\chi \\
 a_{11} - a_{33} &= \frac{1}{2}(A_1 - A_2) - A_3 + \frac{A_1 - A_2}{2} \cos 2\chi \\
 &= \frac{1}{2}(A_1 + A_2) - A_3 + a_{12} \cot 2\chi
 \end{aligned} \tag{12}$$

The "isotropic" part of the tensor $(A_1 + A_2 + A_3)/3$ which as stated above is of less importance, is separated from the "deviator" components. Often, as is seen in the following, the *differences* are the experimentally observable effects, not the components themselves. Thus, the mathematical formulation for the three-dimensional transformation involving a rotation of a tensor with three arbitrary "eigenvalues" about the Z-axis has been developed. This kind of transformation will be used for the practically important case of plane simple shear. The transformation is a purely geometrical operation; inserting the actual values of the principal values as functions gives the physical effects.

The coordinate transformation described is a linear one: the values for A_1, A_2, A_3 are converted to the values along the reference axes by linear operations involving trigonometric functions.

The Validity of the Sadron Rule

In connection with the investigations of either flow birefringence or mechanical stresses, it is of great importance to know the law of superposition; that is, the relative effect of the various components of a system (e.g., the solvent and the polymer) with regard to both magnitude and direction in space. Such a rule was described by

Sadron in 1936⁷ for the birefringence of polydisperse systems. It is possible to show that it has a much more general validity and can be applied in special cases of tensor additivity. The form of the tensor development above can be used to add tensors—particularly symmetric plane tensors—according to the well-known rule:

$$|a_{ik}| + |b_{ik}| = |c_{ik}| \quad (13)$$

$$c_{ij} = a_{ij} + b_{ij}$$

Using the formula developed above one obtains:

$$\begin{aligned} \begin{vmatrix} C_{11} & C_{12} \\ C_{12} & C_{22} \end{vmatrix} &= \frac{A_1 + A_2 + B_1 + B_2}{2} \begin{vmatrix} 1 & 0 \\ 0 & 1 \end{vmatrix} \\ &+ \frac{1}{2} \begin{vmatrix} (A_1 - A_2) \cos 2\chi_a + (B_1 - B_2) \cos 2\chi_b & \\ & (A_1 - A_2) \sin 2\chi_a + (B_1 - B_2) \sin 2\chi_b \\ & (A_1 - A_2) \sin 2\chi_a + (B_1 - B_2) \sin 2\chi_b \\ & -(A_1 - A_2) \cos 2\chi_a + (B_1 - B_2) \sin 2\chi_b \end{vmatrix} \quad (14) \\ &= \frac{C_1 + C_2}{2} \begin{vmatrix} 1 & 0 \\ 0 & 1 \end{vmatrix} + \frac{C_1 - C_2}{2} \begin{vmatrix} \cos 2\chi_c & \sin 2\chi_c \\ \sin 2\chi_c & -\cos 2\chi_c \end{vmatrix} \end{aligned}$$

with:

$$\tan 2\chi_c = \frac{(A_1 - A_2) \sin 2\chi_a + (B_1 - B_2) \sin 2\chi_b}{(A_1 - A_2) \cos 2\chi_a + (B_1 - B_2) \cos 2\chi_b} \quad (15)$$

and

$$(C_1 - C_2)^2 = [(A_1 - A_2) \cos 2\chi_a + (B_1 - B_2) \cos 2\chi_b]^2 - [(A_1 - A_2) \sin 2\chi_a + (B_1 - B_2) \sin 2\chi_b]^2 \quad (16)$$

It has been shown above that the geometric interpretation of the second part of the tensor is a vector of the magnitude $(A_1 - A_2)$ inclined at an angle 2χ to the x-axis. This, of course, pertains also to the vector $(B_1 - B_2)$ and $(C_1 - C_2)$. The geometrical interpretation of the result of these calculations is that $(C_1 - C_2)$ is the result of a *vectorial addition* of $(A_1 - A_2)$ and $(B_1 - B_2)$ according to the *parallelogram rule*, using the double angles 2χ . (See Fig. 1.)

In the case of interest—birefringence and mechanical stresses—as has been shown above, the terms $A_1 + A_2$, $B_1 + B_2$, and $C_1 + C_2$ are not of primary importance. Therefore, for instance in the case of birefringence, introducing Δn_a instead of $A_1 - A_2$, etc., and expanding to an *i*-component system the following rule is obtained:

$$\Delta n^2 = \left[\sum_i \Delta n_i \cos 2\chi_i \right]^2 + \left[\sum_i \Delta n_i \sin 2\chi_i \right]^2 \quad (17)$$

and

$$\tan 2\chi = \sum_i \Delta n_i \sin 2\chi_i / \sum_i \Delta n_i \cos 2\chi_i \quad (18)$$

This is the Sadron rule.

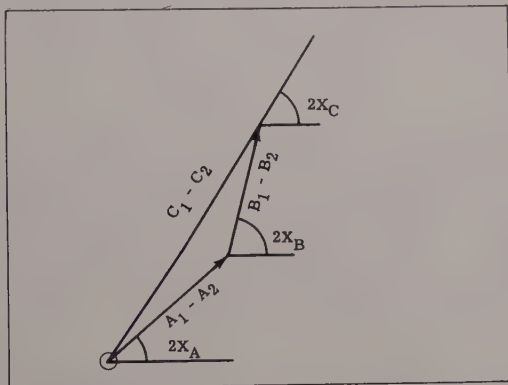


Fig. 1. Geometrical diagram of the Sadron rule.

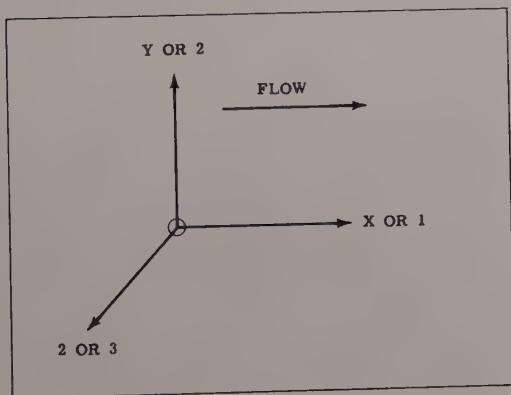


Fig. 2. Reference axes.

The application of the additivity of tensors to *birefringence* problems has to be confined to the case of dilute solutions where the results are only given by an addition of the polarizability tensors of the components excluding any possible optical interaction. It is

not possible to apply the Sadron rule for the case of superimposed birefringent plates calculating the resultant birefringence from the constants for each plate. However, in *mechanics* the additivity of stress *is* present and the additivity rule should be applicable without reservation.

The analysis of the corresponding three-dimensional case showed that the Sadron rule can be applied to three-dimensional cases, when, as for plane shear, only a rotation about the Z-axis is performed.

IV. The Strain Tensor

The experimental possibility of investigating flow birefringence in three directions of space necessitates a more elaborate theoretical investigation of the distribution of deformations, stresses, and birefringence in space.

The discussion of the strain distribution can be started, essentially in the same way as in a previous publication,⁵ from a unit sphere determined by the equation;

$$x^2 + y^2 + z^2 = 1 \quad (19)$$

The sphere is subjected to a deformation of the kind occurring in plane simple shear—namely in affine transformation of the kind⁸

$$\begin{aligned} x' &= x + sy \\ y' &= y \\ z' &= z \end{aligned} \quad (20)$$

The equation of the sphere is then changed into:

$$x^2 + (1 + s^2)y^2 + z^2 - 2sxy = 1 \quad (21)$$

This equation is the one of a triaxial ellipsoid inclined towards the XZ-plane, which can be written according to the rules of tensor calculus as:

$$\begin{vmatrix} 1 & -s & 0 \\ -s & 1 + s^2 & 0 \\ 0 & 0 & 1 \end{vmatrix} \quad (22)$$

the minus sign coming from the rotation in the mathematically negative sense (clockwise).^{*} From tensor calculus the inclination

^{*} If one introduces $(1 + \epsilon_{yy})v^{-2} = 1 + s^2$, then for small s : $\epsilon_{yy} = 1/2 s^2$, or, neglecting the sign, Love's expression is obtained.⁸

χ of the principal axis 1 of the ellipsoid towards the XZ-plane is determined as:

$$\tan 2\chi = -2s/(1 - 1 - s^2) = 2/s \quad (23)$$

$$s = 2 \cot 2\chi$$

This relation, which was introduced in the previous publication, is a direct consequence of the affine transform of a sphere in plane simple shear, as applied to incompressible materials.

The strain tensor can be transformed into principal axes using the rule:

$$u^T | \quad |u \quad (24)$$

where u and u^T have the same meaning as above. The performance of this multiplication results in (Appendix):

$$\begin{vmatrix} 1 + s_2 \sin^2 \chi - s \sin \chi & 0 & 0 \\ 0 & 1 + s^2 \sin^2 \chi + s \sin \chi & 0 \\ 0 & 0 & 1 \end{vmatrix} \quad (25)$$

The principal values, called respectively, $1/\lambda_1^2$ and $1/\lambda_2^2$, can be transformed by trigonometric rules into functions of s and 2χ :

thus

$$s = 2 \cot 2\chi = \cos \chi - \tan \chi$$

$$\cot^2 \chi - s \cot \chi - 1 = 0$$

$$\cot \chi = (s/2) + \sqrt{1 + (s^2/4)} > 0$$

$$\begin{aligned} \cot^2 \chi &= (s^2/4) + 1 - (s^2/4) + 2(s/2) \sqrt{1 + (s^2/4)} \\ &= 1 + (s^2/2) + s \sqrt{1 + (s^2/4)} \end{aligned} \quad (26)$$

$$\cos^2 \chi = 1 + (s^2/2) + (s/\sin 2\chi)$$

and similarly:

$$\tan^2 \chi = 1 + (s^2/2) - (s/\sin 2\chi) \quad (27)$$

Therefore introducing λ , the principal extension in shear:

$$\begin{aligned} \lambda_1^2 &= \cot^2 \chi = 1 + (s^2/2) + (s/\sin 2\chi) = \lambda^2 \\ \lambda_2^2 &= \tan^2 \chi = 1 + (s^2/2) - (s/\sin 2\chi) = 1/\lambda^2 \\ \lambda_3^2 &= 1 \end{aligned} \quad (28)$$

The transformation to principal values can also be performed solving the "eigenvalue equation" introducing the "eigenvalue Λ :"*

$$\begin{vmatrix} 1 - \Lambda & -s & 0 \\ -s & 1 + s^2 - \Lambda & 0 \\ 0 & 0 & 1 - \Lambda \end{vmatrix} \quad (29)$$

According to this rule, the following equation must be solved:

$$(1 - \Lambda) (1 - \Lambda) (1 + s^2 - \Lambda) - s^2 (1 - \Lambda) = 0 \quad (30)$$

The first solution is

$$\Lambda_1 = +1 \quad (31)$$

The next solutions are:

$$\begin{aligned} 1 - \Lambda + s^2 - \Lambda s^2 - \Lambda + \Lambda^2 - s^2 &= 0 \\ \Lambda^2 - 2\Lambda [1 + (s^2/2)] + 1 &= 0 \\ \Lambda_{2,3} &= 1 + (s^2/2) \pm \sqrt{[1 + (s^2/2)]^2 - 1} \\ \Lambda_{2,3} &= 1 + (s^2/2) \pm s\sqrt{1 + (s^2/4)} \end{aligned} \quad (32)$$

which are identical to the expressions above. This calculation gives the principal values much more directly than using the multiplication of matrices, but the discussion as to which Λ -value refers to which position is not so straightforward. Incidentally, the identity of λ_1 , and λ_2 in shear with $\cot \chi$ and $\tan \chi$ has been derived graphically in the previous publication.⁵

λ_1 , λ_2 , and $\lambda_3 = 1$ are the principal axes of the strain-ellipsoid which results from the deformation of a sphere in plane simple shear.

For considerations of symmetry discussed later, the shapes of the projections and traces of the strain-ellipsoid in the three coordinate planes are determined.

* For a tensor

$$\begin{vmatrix} a_{11} & a_{12} & 0 \\ a_{12} & a_{22} & 0 \\ 0 & 0 & a_{33} \end{vmatrix}$$

the "characteristic equation" is obtained by developing the determinate:

$$(a_{11} - \lambda) (a_{22} - \lambda) (a_{33} - \lambda) - a_{12}^2 (a_{33} - \lambda) = 0$$

where λ is the "eigenvalue."

The strain ellipsoid can now be *projected* onto the three coordinate planes, starting from eq. (21):

$$F = x^2 + (1 - s^2)y^2 + z^2 - 2xys = 1 \quad (33)$$

A tangent is defined by the total differential of F

$$dF = (\partial F/\partial x)dx + (\partial F/\partial y)dy + (\partial F/\partial z)dz \quad (34)$$

In the X direction, on the YZ-plane, a projection is determined by the tangent to the ellipsoid, therefore $dy = dz = 0$, or:

$$\partial F/\partial x = 0 \quad (35)$$

similarly for the other planes

$$\partial F/\partial y = 0$$

$$\partial F/\partial z = 0$$

The tangents determined by these conditions must also fulfill the equation for the ellipsoid; therefore one eliminates the x-coordinate by using the above relations for the tangent.

(1) *YZ-plane*

$$\partial F/\partial x = 2x - 2ys = 0$$

$$x = ys$$

$$y^2s^2 + (1 + s^2)y^2 + s^2 - 2y^2s^2 = 1$$

$$y^2 + z^2 = 1$$

The equation for this projection is the one of a *circle* of unit radius in XZ-plane.

(2) *XZ-plane*

$$\partial F/\partial y = 2y(1 + s^2) - 2xs = 0$$

$$y = xs/(1 + s^2)$$

$$x^2 + [x^2s^2/(1 + s^2)] + z^2 - [2x^2s^2/(1 + s^2)] = 1$$

$$[x^2/(1 + s^2)] + z^2 = 1$$

This is the equation of an *ellipse* with the axes $\sqrt{1 + s^2}$ and 1 parallel to the directions of the coordinates, the larger axis in the X direction.

(3) *XY-plane*

$$\partial F / \partial z = 2z = 0 \quad z = 0$$

$$x^2 + (1 + s^2)y^2 - 2xys = 1$$

This is the same equation that one obtains from the strain tensor neglecting the unit y in the third row. The solution has already been given: the axes of the ellipse are:

$$1 + s^2 \pm s\sqrt{1 + (s^2/4)}$$

inclined by the angle χ to the X-axis.

Another set of expressions is obtained by determining the "traces"—the intersections of the coordinate planes with the strain-ellipsoid. One obtains these from the tensor by setting the suitable rows and columns = 0, or directly from eqs. (21) or (33).

(1) *XY-plane*: 3 row and 3 column = 0

$$\begin{vmatrix} 1 & -s \\ -s & 1 + s^2 \end{vmatrix}$$

This is the equation of an ellipse with the axes $1 + (s/2) \pm s\sqrt{1 + (s^2/4)}$ inclined by χ to the X-axis.

(2) *XZ-plane*: 2 row and 2 column = 0

$$\begin{vmatrix} 1 & 0 \\ 0 & 1 \end{vmatrix}$$

This is the equation of a unit *circle*.

(3) *YZ-plane*: 1 row and 1 column = 0

$$\begin{vmatrix} 1 + s^2 & 0 \\ 0 & 1 \end{vmatrix}$$

This is the equation of an ellipse with the axes $1/\sqrt{1 + s^2}$ and 1 with its axes parallel to the direction of the coordinate axes, the larger axis in the Z-direction. Comparing these two sets of expressions it is seen that whereas the XY-plane give identical expressions in both cases (as the ellipsoid is rotated in this plane) the XZ- and YZ-planes are interchanged: for the trace the XZ-plane gives a circle, for the projection the YZ-plane.

In the following, one will see why these symmetry conditions have been calculated. It will be shown that the *projections* of the strain-

ellipsoid are similar to the symmetry conditions of the stresses; therefore, they can be used for qualitative deductions.

V. Stress-Tensor

The stress tensor will now be discussed.*

The following is well known, but repeated here to give a complete logical development without need of other references.

The calculation of the principal stresses from the strain-energy function W can be performed similarly to Mooney and Rivlin in the following way, *not involving any assumptions*: A unit sphere of isotropic, unstrained material (radius = 1, volume = $4/3\pi$) is deformed by 3 unequal, mutually perpendicular, uniform and constant stresses σ_1 , σ_2 , and σ_3 into a triaxial ellipsoid. The axes λ_1 , λ_2 , and λ_3 are determined by: $\lambda = (\text{deformed length})/(\text{initial length})$, this is usually called a deformation in "Cauchy measure." They are directed in the directions of the stresses, that are therefore principal stresses referred to the ellipsoid. The strain energy W is defined as energy per volume unit or ergs/cc. = dynes/cm.². Following Rivlin's procedure, a virtual increase $d\lambda_i$ in deformation in the three axes is introduced. The strain energy E of the initial unit sphere changes by dE due to this additional deformation. As the stresses are assumed to be constant, dE can only be caused by a change in volume induced by the additional deformation in each direction. The volume is a function of all three λ 's, therefore:

$$dE = 4/3\pi dW = (\partial W/\partial \lambda_1) d\lambda_1 \sigma_1 + (\partial W/\partial \lambda_2) d\lambda_2 \sigma_2 + (\partial W/\partial \lambda_3) d\lambda_3 \sigma_3 \quad (36)$$

The volume of the triaxial ellipsoid resulting from the deformation of the unit sphere is:

$$V = 4/3\pi \lambda_1 \lambda_2 \lambda_3 \quad (37)$$

Inserting this expression and cancelling the constant factor $4/3\pi$, the result is obtained:

$$dW = \lambda_2 \lambda_3 d\lambda_1 \sigma_1 + \lambda_3 \lambda_1 d\lambda_2 \sigma_2 + \lambda_1 \lambda_2 d\lambda_3 \sigma_3 \quad (38)$$

* In classical deformational mechanics all the stress-tensor components are calculated from the corresponding strain tensor components (for the incompressible case) by a simple multiplication with the shear modulus G (Lamé). This is, however, not true for finite deformations, where the principal axes have to be used.

The strain-energy W is an arbitrary function of the λ 's so quite generally the change dW can be expressed as a total differential.

$$dW = (\partial W / \partial \lambda_1) d\lambda_1 + (\partial W / \partial \lambda_2) d\lambda_2 + (\partial W / \partial \lambda_3) d\lambda_3 \quad (39)$$

As both these equations represent the identical value of dW and the magnitude of the $d\lambda_i$ are arbitrary, a comparison term for term gives an expression for the principal stresses σ_i :

$$\begin{aligned} \sigma_1 &= (1/\lambda_2\lambda_3)(\partial W / \partial \lambda_1) \\ \sigma_2 &= (1/\lambda_3\lambda_1)(\partial W / \partial \lambda_2) \\ \sigma_3 &= (1/\lambda_1\lambda_2)(\partial W / \partial \lambda_3) \end{aligned} \quad (40)$$

In this derivation dE has been, as Rivlin did, referred to the original volume of the sphere. If one, however, refers dE to the volume of the ellipsoid before dW is applied, i.e., one calculates the increase in strain-energy starting from the deformed state, then the expressions for the σ 's becomes equal to the ones for the incompressible case stated below. Practically, this difference is irrelevant as in the following only the incompressible case applicable to flowing solutions is treated. However, in the basic definitions it is important to know exactly the steps taken. Volume constancy requires the third invariant I_3 :

$$I_3 = \lambda_1^2 \lambda_2^2 \lambda_3^2 = 1 = \text{const.} \quad (41)$$

then

$$\begin{aligned} (3/4\pi) dV &= d(\lambda_1\lambda_2\lambda_3) = 0 \\ \lambda_2\lambda_3 d\lambda_1 + \lambda_3\lambda_1 d\lambda_2 + \lambda_1\lambda_2 d\lambda_3 &= 0 \\ (d\lambda_1/\lambda_1) + (d\lambda_2/\lambda_2) + (d\lambda_3/\lambda_3) &= 0 \end{aligned} \quad (42)$$

This limiting condition for choosing the λ 's is introduced into the expression for the total differential dW , multiplied with an arbitrary constant p_0 . Only when this relation is fulfilled does dW remain a total differential:

$$dW = (\partial W / \partial \lambda_1) d\lambda_1 + (\partial W / \partial \lambda_2) d\lambda_2 + (\partial W / \partial \lambda_3) d\lambda_3 + p_0 [(d\lambda_1/\lambda_1) + (d\lambda_2/\lambda_2) + (d\lambda_3/\lambda_3)]$$

or rearranged:

$$dW = \left(\frac{\partial W}{\partial \lambda_1} + \frac{p_0}{\lambda_1} \right) d\lambda_1 + \left(\frac{\partial W}{\partial \lambda_2} + \frac{p_0}{\lambda_2} \right) d\lambda_2 + \left(\frac{\partial W}{\partial \lambda_3} + \frac{p_0}{\lambda_3} \right) d\lambda_3$$

again comparing term for term with the expression for the principal stresses σ_i one obtains the expressions for the incompressible case (using the relation $\lambda_1\lambda_2\lambda_3 = 1$):

$$\begin{aligned}\sigma_1 &= \lambda_1(\partial W/\partial\lambda_1) + p_0 \\ \sigma_2 &= \lambda_2(\partial W/\partial\lambda_2) + p_0 \\ \sigma_3 &= \lambda_3(\partial W/\partial\lambda_3) + p_0\end{aligned}\quad (43)$$

or generally

$$\sigma_i = \lambda_i(\partial W/\partial\lambda_i) + p_0$$

For incompressible materials W can be introduced as *any* function of the invariants, not only as a sum used by Mooney:

$$W = f(I_1, I_2) \quad (44)$$

From the definition of the principal stresses of incompressible materials deduced above:

$$\sigma_i = (\partial W/\partial\lambda_i)\lambda_i + p_0$$

Therefore (Rivlin):

$$\sigma_1 = \frac{\partial W}{\partial I_1} \frac{\partial I_1}{\partial \lambda_i} \lambda_i + \frac{\partial W}{\partial I_2} \frac{\partial I_2}{\partial \lambda_i} \lambda_i + p_0$$

However, as defined for the incompressible case:

$$\begin{aligned}I_1 &= \lambda_1^2 + \lambda_2^2 + \lambda_3^2 - 3 \\ I_2 &= (1/\lambda_1^2) + (1/\lambda_2^2) + (1/\lambda_3^2) - 3\end{aligned}\quad (45)$$

Introducing:

$$\partial I_1/\partial\lambda_i = 2\lambda_i; \quad \partial I_2/\partial\lambda_i = -2/\lambda_i^3$$

The principal stresses for any deformation are⁹:

$$\sigma_i = 2\lambda_i^2(\partial W/\partial I_1) - (2/\lambda_i^2)(\partial W/\partial I_2) + p_0 \quad (46)$$

After deducing the conditions for any arbitrary deformation, the special case of plane simple shear—the laminar flow of viscoelastic liquids—will be considered.

The strain-invariants introduced as purely mathematical expressions have, especially in the incompressible case, a clear geometrical meaning. The first invariant I_1 is the square of the diagonal of the deformed cube, or in the case of the ellipsoid the diagonal of the cir-

cumscribed "cuboid." More precisely, it is the increase of the square of the length of this diagonal over the square of the initial one of the cube.³ The second invariant I_2 is the sum of the diagonal values of the strain-tensor (-3) . The third invariant I_3 is the volume of the deformed cube, which in the incompressible case remains constant. In the case of plane simple shear of an incompressible material $I_1 = I_2 = s^2$ and $I_3 = 1$. For large values of s : $s \sim \lambda_1$ and $I_1 \sim \lambda_1^2$ becomes the square of the principal extension. The question to be asked is: do the stresses for large deformations depend on I_1 (i.e., the dimensions of the strain-ellipsoid) or I_2 (the diagonal values of the strain-tensor)? Purely mathematically a decision cannot be made, only adequately performed experiments are decisive.

For polymer solutions the weight of evidence suggests a dependence on I_1 alone, i.e., the strain-ellipsoid. For vulcanized rubber Rivlin and Saunders^{9a} have produced evidence of *both* I_1 and I_2 determining the stresses, what makes the relations more complicated. A dependence on I_2 alone has not been as yet ascertained.

For simple plane shears, see eqs. (28); similarly for pure shear:

$$\begin{aligned}\lambda_1 &= \lambda; & \lambda_2 &= 1/\lambda; & \lambda_3 &= 1 \\ \sigma_1 &= 2\lambda^2(\partial W/\partial I_1) - (2/\lambda^2)(\partial W/\partial I_2) + p_0 \\ \sigma_2 &= (2/\lambda^2)(\partial W/\partial I_1) - 2\lambda^2(\partial W/\partial I_2) + p_0 \\ \sigma_3 &= 2\left(\frac{\partial W}{\partial I_1} - \frac{\partial W}{\partial I_2}\right) + p_0\end{aligned}\quad (47)$$

Further, as has been shown in eqs. (28) above, with s = amount of shear:

$$\begin{aligned}\lambda^2 &= \lambda_1^2 = 1 + (s^2/2) + (s/\sin 2\chi) \\ 1/\lambda^2 &= \lambda_2^2 = 1 + (s^2/2) - (s/\sin 2\chi) \\ \lambda_3^2 &= 1\end{aligned}$$

Inserting these values into the stress equations the final expressions for the principal stresses in plane simple shear are obtained:

$$\begin{aligned}\sigma_1 &= 2\left\{\frac{\partial W}{\partial I_1} + \frac{s^2}{2}\frac{\partial W}{\partial I_1} + \frac{s}{\sin 2\chi}\frac{\partial W}{\partial I_1} - \frac{\partial W}{\partial I_2}\right. \\ &\quad \left.- \frac{s^2}{2}\frac{\partial W}{\partial I_2} + \frac{s}{\sin 2\chi}\frac{\partial W}{\partial I_2}\right\} + p_0\end{aligned}$$

$$\sigma_1 = 2 \left\{ \left(\frac{\partial W}{\partial I_1} - \frac{\partial W}{\partial I_2} \right) \left(1 + \frac{s^2}{2} \right) + \frac{s}{\sin 2\chi} \left(\frac{\partial W}{\partial I_1} + \frac{\partial W}{\partial I_2} \right) \right\} + p_0 \quad (48)$$

$$\sigma_2 = 2 \left\{ \left(\frac{\partial W}{\partial I_1} - \frac{\partial W}{\partial I_2} \right) \left(1 + \frac{s^2}{2} \right) - \frac{s}{\sin 2\chi} \left(\frac{\partial W}{\partial I_1} + \frac{\partial W}{\partial I_2} \right) \right\} + p_0$$

$$\sigma_3 = 2 \left(\frac{\partial W}{\partial I_1} - \frac{\partial W}{\partial I_2} \right) + p_0$$

The "isotropic value" is:

$$p_i = p_0 + \frac{\sigma_1 + \sigma_2 + \sigma_3}{3} = 2 \left(\frac{\partial W}{\partial I_1} - \frac{\partial W}{\partial I_2} \right) \left(1 + \frac{s^2}{3} \right) + p_0 \quad (49)$$

Inserting these principal stress values into the system of mathematical relations for tensors rotated by an angle χ —as in plane simple shear—all the measurable stress components and stress differences are calculated:

$$\sigma_{11} = 2s^2 \frac{\partial W}{\partial I_1} + 2 \left(\frac{\partial W}{\partial I_1} - \frac{\partial W}{\partial I_2} \right) + p_0$$

$$\sigma_{22} = -2s^2 \frac{\partial W}{\partial I_2} + 2 \left(\frac{\partial W}{\partial I_1} - \frac{\partial W}{\partial I_2} \right) + p_0$$

$$\sigma_{33} = \sigma_3 = 2 \left(\frac{\partial W}{\partial I_1} - \frac{\partial W}{\partial I_2} \right) + p_0$$

$$\sigma_{12} = \tau = \frac{\sigma_1 - \sigma_2}{2} \sin 2\chi = 2s \left(\frac{\partial W}{\partial I_1} + \frac{\partial W}{\partial I_2} \right) \quad (50)$$

$$\sigma_{11} - \sigma_{22} = \tau s = 2s^2 \left(\frac{\partial W}{\partial I_1} + \frac{\partial W}{\partial I_2} \right)$$

$$\sigma_{22} - \sigma_{33} = -2s^2 \frac{\partial W}{\partial I_2}$$

$$\sigma_{11} - \sigma_{33} = 2s^2 \frac{\partial W}{\partial I_1}$$

Further introducing p_i , using eq. (49):

$$\sigma_{11} - p_i = \frac{2}{3} s^2 \left[2 \frac{\partial W}{\partial I_1} + \frac{\partial W}{\partial I_2} \right]$$

$$\sigma_{22} - p_i = -\frac{2}{3}s^2 \left[\frac{\partial W}{\partial I_1} + 2 \frac{\partial W}{\partial I_2} \right]$$

$$\sigma_{33} - p_i = -\frac{2}{3}s^2 \left[\frac{\partial W}{\partial I_1} - \frac{\partial W}{\partial I_2} \right]$$

Which set of equations is suitable for comparison with experimental results requires careful consideration.

Or introducing the shear modulus $G = \tau/s$ and a factor m according to Kotaka¹⁰:

$$G = 2 \left(\frac{\partial W}{\partial I_1} + \frac{\partial W}{\partial I_2} \right) \quad (51)$$

$$m = - \frac{\frac{\partial W}{\partial I_2}}{\frac{\partial W}{\partial I_1} + \frac{\partial W}{\partial I_2}} = \frac{\sigma_{22} - \sigma_{33}}{\sigma_{11} - \sigma_{22}} \quad (52)$$

$$\tau = Gs$$

$$\sigma_1 - \sigma_2 = 2\tau/\sin 2\chi \quad (53)$$

$$\sigma_{11} - \sigma_{22} = \tau s$$

$$\sigma_{22} - \sigma_{33} = m\tau s$$

$$\sigma_{11} - \sigma_{33} = (1 + m)\tau s$$

These results, except for $\sigma_1 - \sigma_2$, are identical with those of Rivlin,³ who used another mathematical treatment. The Weissenberg² assumption (in his notation) $P_{22} = P_{33}$ or $\sigma_{22} = \sigma_{33}$ is equivalent to standing $m = 0$ or $\partial W/\partial I_2 = 0$. Then W should depend only on I_1 . For shear $I_1 = I_2 = s^2$ so that, say, a power series of I_1 is equivalent to W being a power series with even exponents of s . A decision whether W is a function of I_1 alone is not possible from measurements of the "usual" normal stress ($P_{11} - P_{22}$) or ($\sigma_{11} - \sigma_{22}$), because for any W , its relation to the shear stress τ is only determined by s . However the "other" normal stresses are functions of each separate invariant: $\sigma_{22} - \sigma_{33}$ that of I_2 and $\sigma_{11} - \sigma_{33}$ that of I_1 .

In a recent paper [P. U. A. Grossman, *Kolloid-Z.*, **174**, 97 (1961)], Weissenberg's proof that $\partial W/\partial I_2 \equiv 0$ is given. Starting from eq. (46) and general "quasi-linear" relations between the stress and deformation tensor, it is shown (using the Cayley-Hamilton theorem) that $\partial W/\partial I_2 \neq 0$ leads to a dependence of σ_i on λ_i^4 . This is incompatible with the tensor properties of both the strain and stress that can only be a function of λ_i^2 . $\partial W/\partial I_2 = 0$ means geometrically that, as mentioned above, at constant deformed volume, W depends

only on the length of the space diagonal, not on how it is subdivided into the λ_i that change I_2 .

By this treatment the geometrical effect introduced by the rotation of the strain-tensor is clearly separated from the stresses set up by the strain energy function, which can also be a nonlinear function of the invariants, or stated differently these relations are valid, even when Hooke's law in shear is not valid, i.e., when G varies with τ . This has been also found experimentally.

This calculation also describes the stress-distribution in space, specifically the position of the shear stresses. In laminar flow the acting shear stress is caused by the boundary conditions—the pressure difference in the case of the capillary, the torque in the rotational viscometers—is directed in the direction of flow (X-axis). This is *not* influenced by the properties of the material, but only by the equilibrium of the forces applied.

As has been developed, the principal axis 1 is inclined by an angle χ to the direction of flow (X-axis). The shear stress is:

$$\tau = [(\sigma_1 - \sigma_2)/2] \sin 2\chi \quad (54)$$

which is a maximum when $\chi = 45^\circ$ to the direction of σ_1 not to the X-axis as in the case of small elastic deformations. Therefore $\tau_{max} = (\sigma_1 - \sigma_2)/2$ is inclined by $45^\circ - \chi$ in the mathematically negative sense (clockwise) to the X-axis.

The rate-of-deformation tensor is directed in the direction determined by $s \rightarrow ds$. As $s = 2 \cot 2\chi \rightarrow 0$, $\chi \rightarrow 45^\circ$. Therefore the principal axis of the rate-of-deformation tensor is inclined by 45° , the rate of shear (a component of the tensor) is directed along the X-axis. The frictional power N performed on the flowing liquid is:

$$N = \tau D$$

where D is the rate of shear. This is valid for *any* material since the components of the respective tensors are both oriented along the X-axis.

However, the maximum possible power is given by D and τ_{max} , should they be parallel to each other. This is obviously:

$$N_{max} = D\tau_{max} = N/\sin 2\chi = \tau D/\sin 2\chi$$

This "geometrical viscosity effect" is what Weissenberg¹¹ introduced, calculating η_{max} from τ_{max} and D , correcting the drop in vis-

cosity (non-Newtonian behavior) by $1/\sin 2\chi$.¹² However, this is generally not enough to compensate for the viscosity drop. Further it has been experimentally shown that the change of the angle χ with D is independent of the change of τ (or viscosity) with D .

Having now determined the stress-distribution in space, one can refer back to the discussion of the strain-ellipsoid. Isotropic conditions in the YZ-plane are identical with the circular symmetry of the projection of the ellipsoid ($m = 0$) in the same plane. Elliptical symmetry is present in both the XY- and XZ-planes for both cases, the first inclined under the same angle χ .

VI. Optical Tensor (Polarizability Tensor)

In the calculation of the conditions in flow-birefringence use is made, as in all similar calculations, of the polarizability P using the well-known Lorentz-Lorenz formula:

$$P = (n^2 - 1)/(n^2 + 2) = \frac{4}{3} \pi N_0 \alpha_m \quad (55)$$

(n , index of refraction; N_0 , Avogadro number; α_m , the mean polarizability per molecule) where for birefringence purposes the change of the polarizability in space is small (10^{-5}) as compared with the polarizability itself. Therefore one can use the differential expression with adequate precision:

$$\Delta P \sim dP = [6n/(n^2 + 2)^2] \Delta n \quad (56)$$

The polarizability in three-dimensional space is described by a tensor:

$$\begin{vmatrix} P_1 & 0 & 0 \\ 0 & P_2 & 0 \\ 0 & 0 & P_3 \end{vmatrix} \quad (57)$$

Now the reference coordinate system is rotated by an angle χ_0 in the mathematically positive sense around the Z-axis, using the $u|u^T$ system as before. One obtains:

$$\begin{vmatrix} P_1 \cos^2 \chi_0 + P_2 \sin^2 \chi_0 & \frac{1}{2} (P_1 - P_2) \sin 2\chi_0 & 0 \\ \frac{1}{2} (p_1 - p_2) \sin 2\chi_0 & p_1 \sin^2 \chi_0 + p_2 \cos^2 \chi_0 & 0 \\ 0 & 0 & P_3 \end{vmatrix} \quad (58)$$

The description of the polarizability as a tensor with three unequal axes places the flowing solutions in the class of biaxial crystals with rhombic symmetry, as seen from Born.¹³

According to Born¹⁴ the optical effects are determined by the intersections of the planes normal to the direction of observation and the polarizability tensor—which are called the *traces* of the tensor on the reference planes. These are now calculated for the different reference planes:

The XY-plane, the shear plane, or 1,2 plane. The trace is obtained by putting the 3 row and 3 column = 0

$$\begin{vmatrix} P_1 \cos^2 \chi_0 + P_2 \sin^2 \chi_0 & \frac{1}{2} (P_1 - P_2) \sin 2\chi_0 \\ \frac{1}{2} (P_1 - P_2) \sin 2\chi_0 & P_1 \sin^2 \chi_0 + P_2 \cos^2 \chi_0 \end{vmatrix} \quad (59)$$

This tensor according to the developments in the mathematical part can be rearranged into

$$P_0 + \Delta P_{12} = \frac{P_1 + P_2}{2} \begin{vmatrix} 1 & 0 \\ 0 & 1 \end{vmatrix} + \frac{P_1 - P_2}{2} \begin{vmatrix} \cos 2\chi_0 & \sin 2\chi_0 \\ \sin 2\chi_0 & -\cos 2\chi_0 \end{vmatrix} \quad (60)$$

Here some simplifications are possible. As the birefringence is small, the mean polarizability P_0 can be introduced:

$$P_0 = (n_0^2 - 1)/(n_0^2 + 2) = (P_1 + P_2 + P_3)/3 \sim (P_1 + P_2)/2 \quad (61)$$

When n_0 is the mean index of refraction:

$$\Delta P = P_1 - P_2 = \Delta n [6n_0/(n_0 + 2)^2] \quad (62)$$

and

$$\Delta P_{12} = \Delta n_{12} [6n_0/(n_0 + 2)^2] \quad (63)$$

Depending on the magnitude of P_1 and P_2 , Δn can be either positive or negative, assuming χ to be always $0 < \chi < 45^\circ$. Introducing the expression for P_1 , ΔP_{12} , and ΔP , and cancelling, one obtains:

$$\Delta n_{12} = \frac{\Delta n}{2} \begin{vmatrix} \cos 2\chi_0 & \sin 2\chi_0 \\ \sin 2\chi_0 & -\cos 2\chi_0 \end{vmatrix} \quad (64)$$

The trigonometric part is a tensor which can be described in principal axes as before:

$$\Delta n_{12} = \frac{\Delta n}{2} \begin{vmatrix} +1 & 0 \\ 0 & -1 \end{vmatrix} \quad (65)$$

The observed effect is the difference in principal axes, therefore:

$$\Delta n_{12} = \Delta n \quad (66)$$

According to the mathematical part, the above formulation resulted from a rotation of the coordinates by an angle χ_0 . Therefore in the XY-plane the observed birefringence Δn_{12} is inclined to the X-axis at an angle χ_0 in the mathematically positive sense, as the cross-terms are both positive.

The YZ-plane, normal to the shear planes and normal to the direction of shear or the 2,3-plane. The trace is obtained by putting the 1 row and 1 column = 0.

$$\begin{vmatrix} P_1 \sin^2 \chi_0 + P_2 \cos^2 \chi_0 & 0 \\ 0 & P_3 \end{vmatrix} \quad (67)$$

This tensor has its principal axes aligned along the directions of the coordinate axes as the cross-terms are both 0. The angle is 0 when m_0 and $(P_1 - P_2)$ have both the same sign, 90° when they have different signs. As above the difference in principal values is

$$\begin{aligned} \Delta P_{23} &= P_1 \sin^2 \chi_0 + P_2 \cos^2 \chi_0 - P_3 \\ &= m_0 (P_1 - P_2) \cos 2\chi_0 \end{aligned} \quad (68)$$

having introduced m_0 , similarly to m in the stress-tensor:

$$m_0 = \frac{P_1 \sin^2 \chi_0 - P_2 \cos^2 \chi_0 - P_3}{(P_1 - P_2) \cos 2\chi_0} \quad (69)$$

Therefore the observable birefringence in this plane, as shown, is:

$$\Delta n_{23} = m_0 \Delta n \cos 2\chi_0 \quad (70)$$

The XZ-plane, normal to the shear planes or 1,3-plane. The trace is obtained putting the 2 row and 2 column = 0.

$$\begin{vmatrix} P_1 \cos^2 \chi_0 + P_2 \sin^2 \chi_0 & 0 \\ 0 & P_3 \end{vmatrix} \quad (71)$$

Here again the cross-terms = 0 and the principal axes are oriented along the coordinate axes. The angle is 0° when Δn is positive, 90° when Δn is negative, referred to the direction of the maximum polarization. The difference in principal values is

$$\Delta P_{13} = P_1 \cos^2 \chi_0 + P_2 \sin^2 \chi_0 - P_3$$

or introducing m_0 as above:

$$\Delta P_{13} = (1 + m_0) (P_1 - P_2) \cos 2\chi_0 \quad (72)$$

Therefore the observable birefringence in the plane is

$$\Delta n_{13} = (1 + m_0) \Delta n \cos 2\chi_0 = \Delta n \cos 2\chi_0 + \Delta n_{23} \quad (73)$$

Another way of achieving the same result is assuming the proportionality between differences of principal values of stresses in the planes of observation and the birefringence using the stress-optical coefficient C :

$$\Delta n = C(\sigma_1 - \sigma_2) \quad (74)$$

Then from the stress-tensor in the XY-phase:

$$C(\sigma_1 - \sigma_2) = \Delta n_{12} = C(2\tau/\sin 2\chi) \quad (75)$$

inclined at χ towards the X-axis.

In the XZ-plane:

$$C(\sigma_{11} - \sigma_{33}) = \Delta n_{13} = C\tau s(1 + m) \quad (76)$$

In the YZ-plane:

$$C(\sigma_{22} - \sigma_{33}) = \Delta n_{23} = C\tau sm \quad (77)$$

or introducing Δn and $s = 2 \cot 2\chi_0$

$$\begin{aligned} \Delta n_{23} &= m \Delta n \cos 2\chi_0 \\ \Delta n_{13} &= (1 + m) \Delta n \cos 2\chi_0 = \Delta n \cos 2\chi_0 + \Delta n_{23} \end{aligned} \quad (78)$$

The equivalence of both ways of calculation (with $m = m_0$) is directly seen. This method gives identical results here, as the "normal stresses" are really "normal," i.e., they are directed along the co-ordinate axes. Only σ_1 is inclined at χ . The above treatment has shown clearly that the symmetry conditions would be vastly simplified if, as Weissenberg assumed, $(\sigma_{22} = \sigma_{33}) = P_{22} = P_{33}$ * or $m = m_0 = 0$. This proof has been attempted in the experimental papers, with the result that it seems highly probable that this relation is true for polymer solutions.

Then the obvious conclusion is that W is alone a function of s^2 as the first invariant only. One can also introduce a nonlinear relation and apply the Sadron rule in the three-dimensional case for laminar flow.

Previous experiments have already proved that $\sigma_{11} - \sigma_{22} = \tau s$

* Here P_{22} and P_{33} in the notation used by Weissenberg are stresses not polarizabilities.

is independent of the validity of Hooke's law in shear, supporting this theory.

The discussion of the polarizability tensor has resulted in identical expressions as those for projections of the strain-ellipsoid: an inclined ellipse in the 1,2-plane, a circular symmetry in the 2,3-plane, and an ellipse with axes in the direction of the coordinate in the 1,3-plane. Therefore a discussion of the optical symmetry conditions in flow can be performed using a model strain-ellipsoid, as has been shown before.

The whole treatment described starts from a special mechanical case: laminar shear. It is developed with a deliberate limitation to generality for the case of flowing materials, which are the ones of interest here. The calculations for particular cases of laminar flow, such as capillary flow and Couette flow, are comparatively simple, knowing the boundary conditions and using usual rheological methods of calculation. This will explicitly be done in the future should the need arise. What is still the unsolved question is: How is the rate of shear D connected with s on a model basis? There do not seem to be *mechanical* theories to account for the drop in viscosity with D in the range found experimentally. Weissenberg contributes it to a "disintegration process"—outside deformational mechanics, practically admitting that no solution of the purely mechanical problem is as yet found. So far one simply has to accept the non-Newtonian viscosity as an empirical fact. This means that *two independent* functions of D , i.e., η and s , as Coleman and Noll¹⁵ have already suggested, are necessary to describe a material at any D .

VII. Conclusions

In the foregoing treatment the problem of elastic deformation in flowing (viscoelastic) liquids has been treated using the theory of finite elastic deformations applying tensor calculus. Special emphasis has been placed on the three-dimensional distribution of stresses. The optical case has also been treated using the polarizability tensor, rotated in space about the Z-axis to a position parallel to the stress-tensor. The conditions are then developed which allow optical measurements to be used to explore mechanical symmetry conditions.

The author wishes to acknowledge the help of Mr. Roland Seneor for some of the mathematical treatment presented.

APPENDIX I. Calculation of the Principal Values of the Strain-Tensor

$$\begin{aligned}
 & u^T \begin{vmatrix} 1 & -s & 0 \\ -s & 1+s^2 & 0 \\ 0 & 0 & 1 \end{vmatrix} \cdot u = u^T \begin{vmatrix} 1 & -s & 0 \\ -s & 1+s^2 & 0 \\ 0 & 0 & 1 \end{vmatrix} \begin{vmatrix} \cos \chi & \sin \chi & 0 \\ -\sin \chi & \cos \chi & 0 \\ 0 & 0 & 1 \end{vmatrix} \\
 & = u^T \begin{vmatrix} \cos \chi + s \sin \chi & \sin \chi - s \cos \chi & 0 \\ -s \sin \chi - (1+s^2) \sin \chi & -s \sin \chi + (1+s^2) \cos \chi & 0 \\ 0 & 0 & 1 \end{vmatrix} \\
 & = \begin{vmatrix} \cos \chi & -\sin \chi & 0 \\ \sin \chi & \cos \chi & 0 \\ 0 & 0 & 1 \end{vmatrix} \begin{vmatrix} \cos \chi + s \sin \chi & \sin \chi - s \cos \chi & 0 \\ -s \sin \chi - (1+s^2) \sin \chi & -s \sin \chi + (1+s^2) \cos \chi & 0 \\ 0 & 0 & 1 \end{vmatrix} \\
 & = \begin{vmatrix} \cos^2 \chi - s \sin \chi \cos \chi - s \sin \chi \cos \chi + (1+s^2) \sin^2 \chi & & \\ -\sin \chi \cos \chi + s \sin^2 \chi - s \cos^2 \chi + (1+s^2) \sin \chi \cos \chi & & \\ & & 0 \end{vmatrix} \\
 & = \begin{vmatrix} -\sin \chi \cos \chi - s \sin^2 \chi + (1+s^2) \sin \chi \cos \chi & & 0 \\ \sin^2 \chi + s \sin \chi \cos \chi + s \sin \chi \cos \chi + (1+s^2) \cos^2 \chi & & 0 \\ & & 1 \end{vmatrix} \\
 & = \begin{vmatrix} 1+s^2 \sin^2 \chi - s \sin 2\chi & -s \cos 2\chi + \frac{s^2}{2} \sin 2\chi & 0 \\ -s \cos 2\chi + \frac{s^2}{2} \sin 2\chi & 1+s^2 \cos^2 \chi + s \sin 2\chi & 0 \\ 0 & 0 & 1 \end{vmatrix} = \begin{vmatrix} \tan^2 \chi & 0 & 0 \\ 0 & \cot^2 \chi & 0 \\ 0 & 0 & 1 \end{vmatrix} = \begin{vmatrix} 1/\lambda_1^2 & 0 & 0 \\ 0 & 1/\lambda_2^2 & 0 \\ 0 & 0 & 1 \end{vmatrix}
 \end{aligned}$$

Calculation of the Principal Values

$$\begin{aligned}
 c_{12} &= -s \cos 2\chi + \frac{s^2}{2} \sin 2\chi \\
 &= -2 \cot 2\chi \cos 2\chi + 2 \cot^2 2\chi \sin 2\chi \\
 &= -2 \frac{\cos^2 2\chi}{\sin 2\chi} + 2 \frac{\cos^2 2\chi}{\sin 2\chi} = 0
 \end{aligned}$$

$$\begin{aligned}
 c_{11} &= 1 + s^2 \sin^2 \chi - s \sin 2\chi \\
 &= 1 + 4 \frac{\cos^2 2\chi}{\sin^2 2\chi} \sin^2 \chi - 2 \cos 2\chi \\
 &= 1 - 2 \cos^2 \chi + 2 \sin^2 \chi + 4 \\
 &\quad \frac{\cos^4 \chi - 2 \cos^2 \chi \sin^2 \chi + \sin^4 \chi}{4 \sin^2 \chi \cos^2 \chi} \sin^2 \chi \\
 &= \frac{\cos^2 \chi - 2 \cos^4 \chi + 2 \sin^2 \chi \cos^2 \chi + \cos^4 \chi - 2 \cos^2 \chi \sin^2 \chi + \sin^4 \chi}{\cos^2 \chi} \\
 &= \frac{\cos^2 \chi + \sin^4 \chi - \cos^4 \chi}{\cos^2 \chi} \\
 &= \frac{\cos^2 \chi + (\sin^2 \chi - \cos^2 \chi) (\sin^2 \chi + \cos^2 \chi)}{\cos^2 \chi} \\
 &= \frac{\cos^2 \chi + \sin^2 \chi - \cos^2 \chi}{\cos^2 \chi} = \frac{\tan^2 \chi}{\cos^2 \chi}
 \end{aligned}$$

$$\begin{aligned}
 c_{22} &= 1 + s^2 \cos^2 \chi + s \sin 2\chi \\
 &= 1 + 4 \frac{\cos^2 2\chi}{\sin^2 2\chi} \cos^2 \chi + 2 \cos 2\chi \\
 &= 1 + 2 \cos^2 \chi - 2 \sin^2 \chi + 4 \frac{\cos^4 \chi - 2 \cos^2 \chi \sin^2 \chi + \sin^4 \chi}{4 \sin^2 \chi \cos^2 \chi} \cos^2 \chi \\
 &\quad \sin^2 \chi + 2 \sin^2 \chi \cos^2 \chi - 2 \sin^4 \chi + \\
 &= \frac{\cos^4 \chi - 2 \cos^2 \chi \sin^2 \chi + \sin^4 \chi}{\sin^2 \chi} \\
 &= \frac{\sin^2 \chi + \cos^4 \chi - \sin^4 \chi}{\sin^2 \chi}
 \end{aligned}$$

$$= \frac{\sin^2 \chi + (\cos^2 \chi - \sin^2 \chi - \sin^2 \chi) (\cos^2 \chi + \sin^2 \chi)}{\sin^2 \chi}$$

$$= \frac{\sin^2 \chi + \cos^2 \chi - \sin^2 \chi}{\sin^2 \chi} = \underline{\cot^2 \chi}$$

References

1. Mooney, M., *J. Appl. Phys.*, **11**, 582 (1940); *J. Colloid Sci.*, **6**, 96 (1951).
2. Weissenberg, K., Conf. Brit. Rheologists Club, 1946.
3. Rivlin, R. S., *Phil. Trans. Roy. Soc.*, **A240**, 459 (1948).
4. Rivlin, R. S., *Rheology*, Vol. I, F. Eirich, ed., Academic Press, New York, 1956, chapter 10.
5. Philippoff, W., *Trans. Soc. Rheology*, **1**, 95 (1957).
- 5a. Philippoff, W., J. G. Brodnyan, and F. H. Gaskins, *J. Appl. Phys.*, **28**, 1118 (1957).
- 5b. Roberts, J. E., *Proceedings 2nd International Congress Rheology*, Oxford, 1953, p. 91. N. Pilpel, *Trans. Faraday Soc.*, **50**, 1369 (1954); **51**, 1307 (1955). W. Philippoff, *Trans. Soc. Rheology*, **5**, 149 (1961).
6. Alfrey, T., and E. F. Gurnee in F. Eirich, *Rheology*, F. Eirich, ed., Academic Press, New York, 1956, chapter 11, p. 405.
7. Sadron, C., *J. phys. rad.* (7) **9**, 381 (1936).
8. Love, A. E. H., *A Treatise on the Mathematical Theory of Elasticity*, 4th ed., Dover, New York, 1944, 37, p. 70.
9. Rivlin, R. S., see Ref. 4, Volume I, pp. 365-367.
- 9a. Rivlin, R. S., and D. W. Saunders, *Phil. Trans. Roy. Soc.* **A243**, 251 (1957).
10. Kotaka, T., M. Kurata, and M. Tamura, *J. Appl. Phys.*, **30**, 1705 (1959).
11. Weissenberg, K., *Arch. Geneve*, **17**, 1 (1935).
12. Philippoff, W., *J. Appl. Phys.*, **27**, 984 (1956).
13. Born, M., *Optik*, Berlin, 1933, p. 232.
14. Born, M., *Optik*, Berlin, 1933, p. 227.
15. Coleman, B. D., and W. Noll, *Arch. Ratl. Mech.*, **3**, 289 (1959).

Synopsis

Using the assumption that a flowing viscoelastic liquid develops elastic stresses in steady laminar flow, the "normal stresses" in the three directions in space are determined using tensor calculus. The results conform with previous results using Cartesian coordinates. The idea used is the finite deformation of a unit sphere to a triaxial ellipsoid involving a rotation of the largest principal axis by an angle χ . Next the polarizability (and, therefore, the index of refraction) is treated in a similar way leading to expressions for the birefringence of a flowing liquid in the three reference places in space. These expressions are experimentally tested in an accompanying paper.

The theoretical treatment, together with the experimental results, show that this approach, which is consistent with Weissenberg's assumption of $P_{22} = P_{33}$, describes and predicts experimental effects adequately.

Flow Birefringence of Molten Polyethylene

F. D. DEXTER and J. C. MILLER, *Development Laboratory, Union Carbide Plastics Company, Division of Union Carbide Corporation, Bound Brook, New Jersey*, and W. PHILIPPOFF, *Esso Research and Engineering Company, Linden, New Jersey*

The flow birefringence of dilute polymer solutions, while perhaps not completely understood, has a firm background of experiment and theory.^{1,2} Stress birefringence techniques and theory have also advanced to the position where their usefulness in stress analysis of complex structures is well recognized.³ The birefringence of concentrated polymer solutions and linear polymer melts, however, has received essentially no attention either experimentally or theoretically until the last 10 years.⁴⁻⁶ No measurements in simple shear on whole polymers have been reported, and the flow birefringence of polymer melts is an unexplored field. This is not too surprising when the experimental difficulties are considered.

The flow birefringence data reported in this paper were obtained about 7 years ago in conjunction with the rotational viscometry of molten polyethylene. A simple, easily constructed experimental apparatus was used: a parallel plate type viscometer viewed perpendicular to the 1-3 plane as illustrated in Figure 1. λ_{12} is the applied shear stress.

The technique of measuring birefringence through the 1-3 plane presents interpretation difficulties. In polymer solutions with a few exceptions,^{7,8} birefringence measurements have been made viewing the 1-2 plane parallel to the shear plane, and interpretations have evolved from these experiments. Viewing perpendicular to the shear plane raises the problem that molecules are being oriented parallel to the 1-3 plane. The extinction angle in this case is always 0° , and the usual orientation angle, χ , cannot be observed. The results were useful qualitatively for understanding polymer flow, but quantitative applications were not feasible until the recent development of the

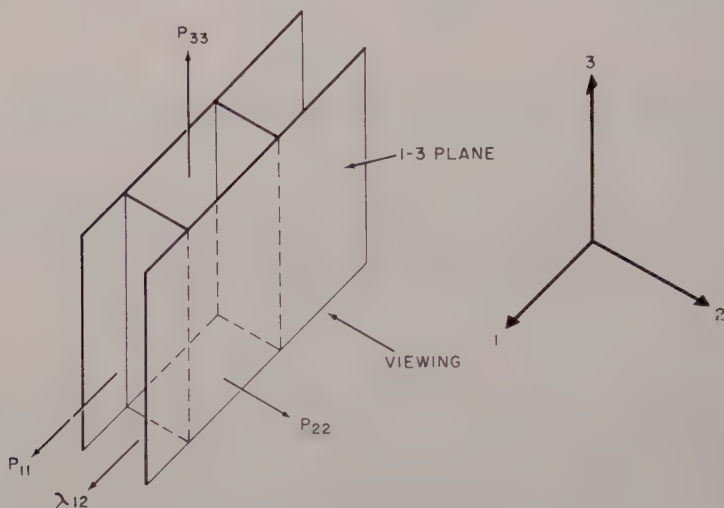


Fig. 1. Definition of axes and planes.

relations between optical and stress tensors⁹ and the finding that two of the principal stresses P_{22} and P_{33} are equal.¹⁰

Experimental

The flow birefringence of molten polyethylene was measured through the 1-3 plane with a standard circular polariscope³ and a parallel plate viscometer. A diagram of the birefringence equipment is shown in Figure 2. Light from a mercury vapor lamp source passes successively through a polarizing disc, a quarter-wave plate, the sample in the oven, another quarter-wave plate and polarizing disc, and to a photoelectric tube. Changes in the birefringence of the sample influence the intensity of the light reaching the photoelectric tube, and the changes in birefringence are converted to an electrical output. The output of the photoelectric tube was measured with a stabilized circuit¹¹ and fed through a linear potentiometer to reduce the voltage. The reduced output was recorded with a Brown recording potentiometer as a function of time. Dark currents from the photoelectric tube and light leaks through the polaroids were balanced out in the measuring circuit. The measuring beam of light was limited to a small section at the center of the viscometer to eliminate edge effects.

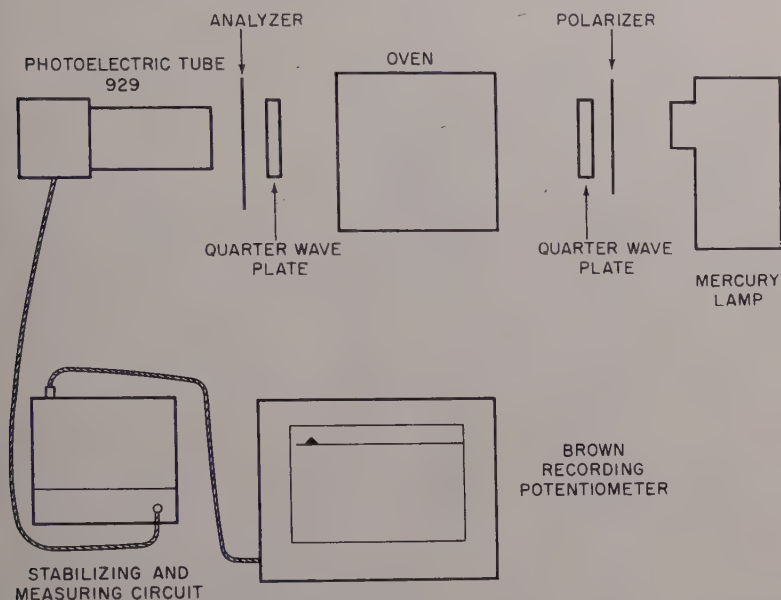


Fig. 2. Diagram of the birefringence apparatus.

Quantitative measurements of the birefringence were accomplished by first paralleling the polaroids with the sample at rest and setting the potentiometer to produce a value of 100 on the recorder. The polaroids were then crossed; a small adjustment was made for light leakage, a load or motion was applied to the viscometer, and the change in birefringence with time was recorded until equilibrium. The ratio of the equilibrium light intensity to the paralleled polaroids light intensity was used as the ratio of emergent to incident light and the birefringence calculated from the eqs. (1) and (2).³

$$I/I_0 = \sin^2 (\alpha/2) \quad (1)$$

$$\Delta n_{13} = (\lambda/2\pi d) \alpha \quad (2)$$

where I is the intensity of the emergent beam, I_0 is the intensity of the incident beam, α is the phase difference between the transmitted light in the principal directions, d is the sample thickness, λ is the wavelength of the light, and Δn_{13} is the birefringence viewing the 1-3 plane.

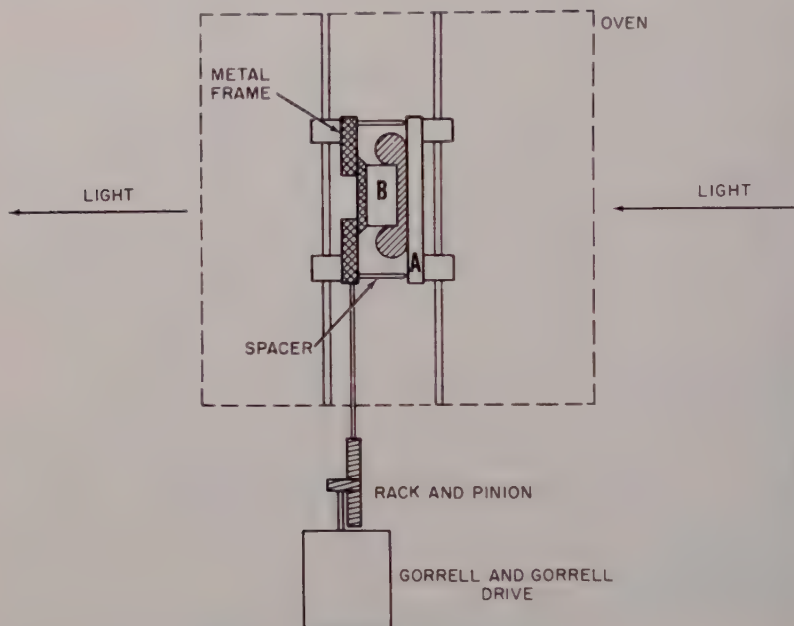


Fig. 3. Diagram of the viscometer.

The viscometer contained in the oven was a parallel plate arrangement of two glass plates *A* and *B* shown in Figure 3, one of which was held in a metal frame. Spacers on the metal frame determined the clearance between the plates at 50 mils. The viscometer was heated, assembled, and then forced into the framework. Either a constant load or constant velocity could be applied to the metal frame to produce simple shear. Some experiments were run at constant stress, but friction in the viscometer was high and most of the measurements were made at constant rate of shear using a gear drive to push the metal frame.

The oven was a conventional thermostated air oven in which temperature could be controlled to $\pm 2^\circ\text{C}$.

A number of low density (0.918–0.920 g./cc.) polyethylenes were investigated as a function of rate of shear at 150°C . One polyethylene, designated *A*, was thoroughly examined through the temperature range of 130 – 170°C . The recoverable shear data for polyethylene *A* were obtained on a rotational viscometer described previously.¹²

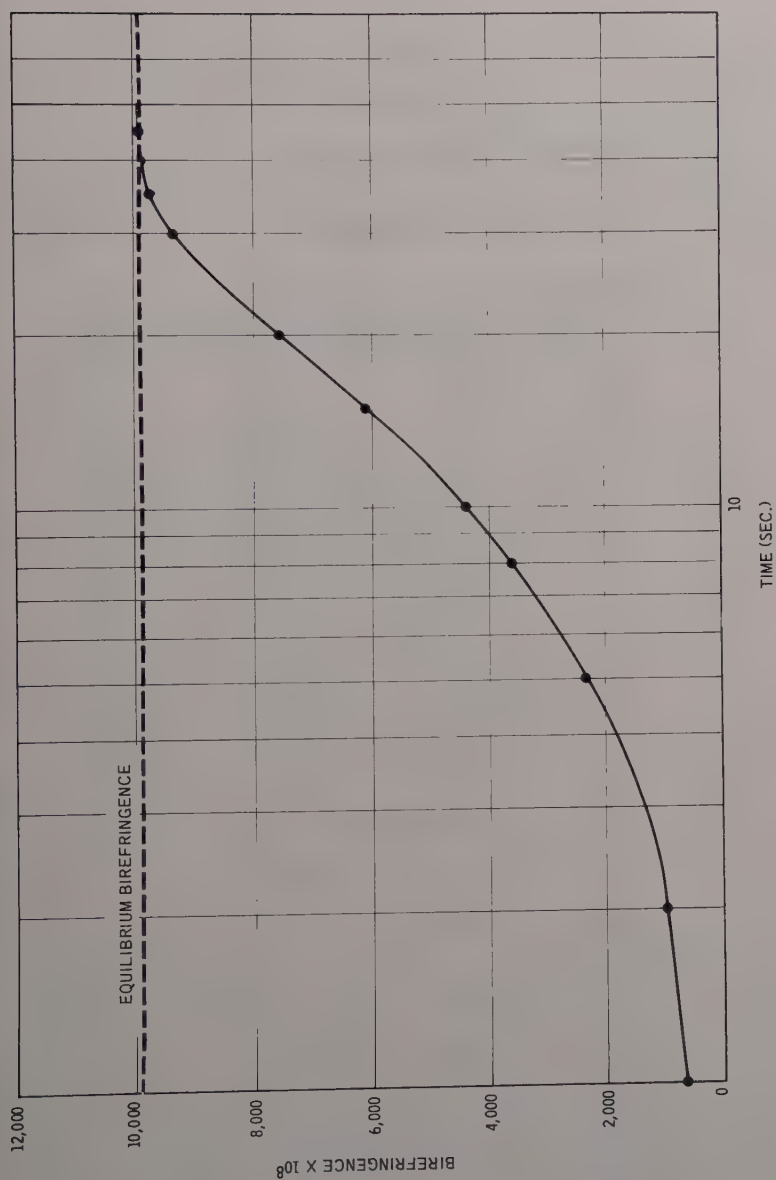


Fig. 4. Time-delayed birefringence of polyethylene A. Stress: 14×10^4 dynes/cm.², temperature: 150°C.

Results

A typical birefringence-time curve at constant stress is illustrated in Figure 4. This curve is not a simple exponential and, as might be expected, the time-delayed birefringence behavior is governed by a spectrum of retardation times.

The flow birefringence of polyethylene A, a polymer whose flow properties had been reported previously by Dexter,¹² is shown in Figure 5. In Figure 5 the birefringence through the 1-3 plane is

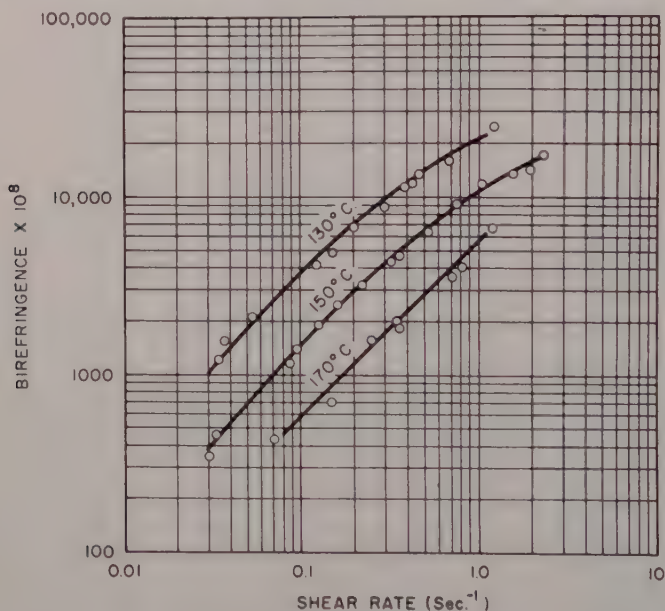


Fig. 5. Flow birefringence of polyethylene A.

plotted versus the rate of shear on log-log coordinates for three temperatures, 130, 150, and 170°C. At low rates of shear the birefringence is directly proportional to the rate of shear since the curves are inclined at 45°. Above 0.4 sec.⁻¹ the data at 130 and 150°C. show a large deviation from linearity. These curves are in sharp contrast to the stress-birefringence curve shown in Figure 6 for 150°C., where the birefringence shows a greater than proportional increase in birefringence with stress over the entire stress range.

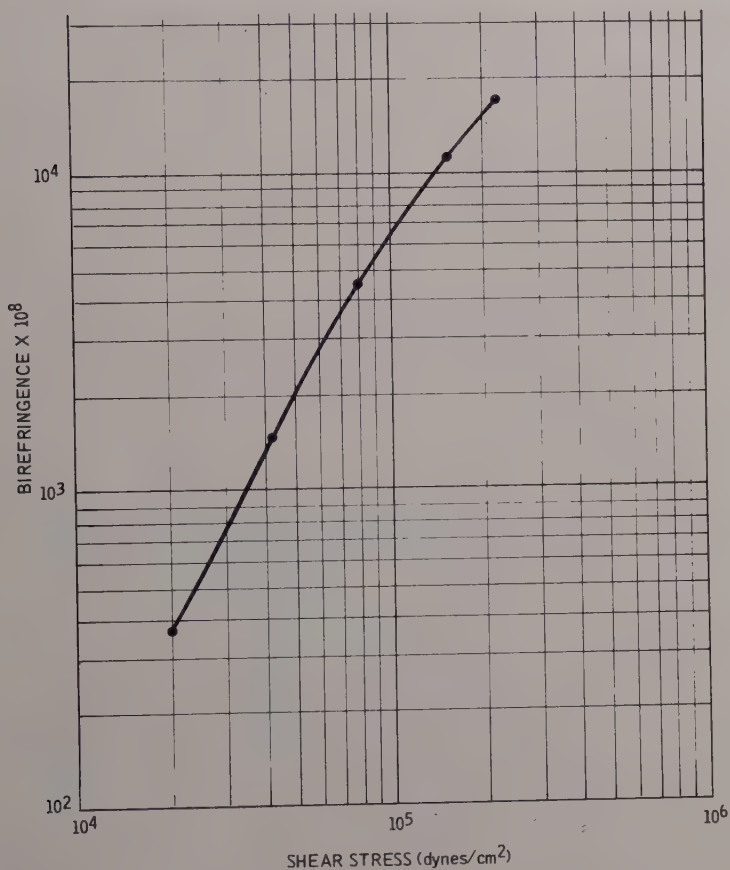


Fig. 6. Birefringence vs. stress. Polyethylene A at 150°C.

The birefringence-shear data for a number of polyethylenes of differing melt index are plotted on Figure 7. The birefringence decreases as the melt index increases (viscosity decreases).

Discussion

The birefringence data on polyethylene A combined with recoverable shear data obtained with a rotational viscometer can be used to test the mechanical theories of Weissenberg¹³ and Mooney¹⁴ and

the assumption that the flow birefringence is proportional to the difference in principal stresses^{6,9} for the flow of polymer melts.

Philippoff¹⁵ has given the equation relating the birefringence, Δn_{13} , through the 1-3 plane to the difference in principal stresses and the recoverable shear, s :

$$\Delta n_{13} = C(P_{11} - P_{33}) = C\tau_{12}s(m + 1) \quad (3)$$

where τ_{12} is the shear stress and C , the stress optical coefficient.

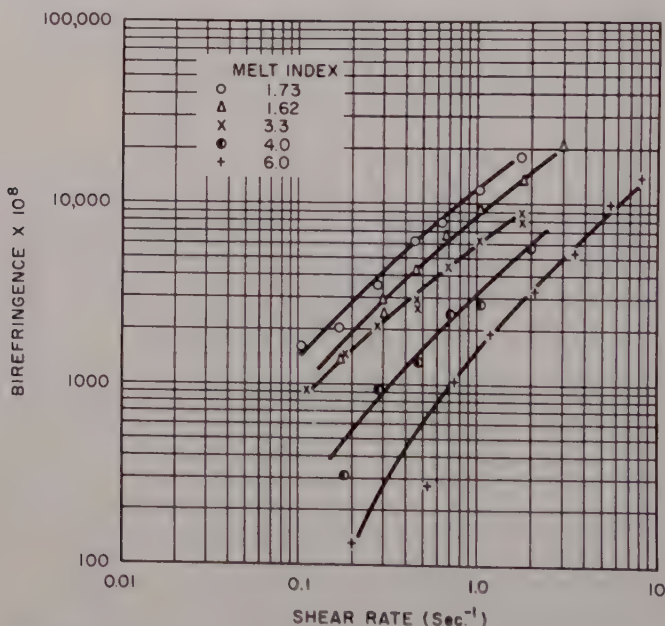


Fig. 7. Flow birefringence of various polyethylenes. Temperature: 150°C.

The value of m is defined as:

$$(P_{22} - P_{33})/(P_{11} - P_{22}) \quad (4)$$

and with the assumption of $P_{22} = P_{33}$, m becomes zero. Physically, this predicts no birefringence in the 2-3 plane. Experiments with polymer solutions⁴ have established that m is zero or at least a number small enough to be negligible.

Assuming m to be zero or negligible for polymer melts, eq. (3) rearranges to:

$$s = \Delta n_{13}/C\tau_{12} \quad (5)$$

From this equation the recoverable shear can be calculated from the birefringence results and compared to directly measured recoverable shears.

The value of C , the stress optical coefficient, was obtained from Saunders⁴ data on irradiated low density polyethylenes at 130°C. The tensile birefringence plotted against the radiation dose in arbitrary units is shown in Figure 8 where the value 2200 Br was obtained by a linear extrapolation to zero radiation dose.

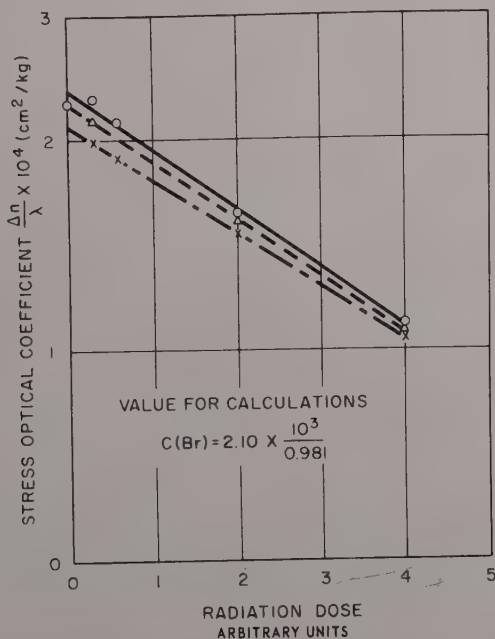


Fig. 8. Extrapolation of tensile birefringence data. [D. W. Saunders, *Trans. Faraday Soc.*, **52**, 242 (1956).]

Table I lists the experimental and calculated recoverable shears for a number of stresses of 130, 150, and 170°C. The data agree well at 150 and 170°C., but show a substantial difference at 130°C. This

could be explained by incomplete recovery data at this temperature or friction effects in the rotational instrument. This correlation of the birefringence and the recoverable shear data tends to confirm that the assumptions of eq. (5) are valid for the mechanical behavior of polymer melts in laminar shear. The precision of the measurements, however, is not sufficient to determine whether m is zero or a small number.

TABLE I
Comparison of Experimental and Calculated Recoverable Shears

Shear stress dynes/cm. ² , $\times 10^{-4}$	Rate of shear, sec. ⁻¹	$\Delta n_{12} \times 10^3$	Calculated recoverable shear strain	Experimental recoverable shear strain
130°C.				
8.22	0.20	6,700	3.4	1.9
12.1	0.41	12,000	3.8	2.0
16.4	0.65	16,000	4.2	2.9
20.4	0.96	20,000	4.4	3.1
150°C.				
4.1	0.1	1,500	1.5	1.2
8.2	0.3	4,300	2.3	1.8
16.4	1.0	10,600	3.1	2.9
24.5	2.1	15,800	3.1	3.8
170°C.				
4.1	0.20	1,150	1.3	1.1
8.2	0.63	3,600	1.9	2.1
12.2	1.12	6,200	2.2	2.6

Recently, recoverable shear data for molten polyethylene based on end corrections for a capillary viscometer were reported by Bagley.¹⁶ The relation between the capillary end correction and the recoverable shear is¹⁷:

$$s = 2(e - n)$$

where e is the total end correction and n the Couette correction. Bagley's results are plotted in Figure 9 along with the recoverable shear data from the rotational viscometer. The agreement is satisfactory since the polyethylenes were not identical and two different types of viscometers were used. A small difference in the moduli

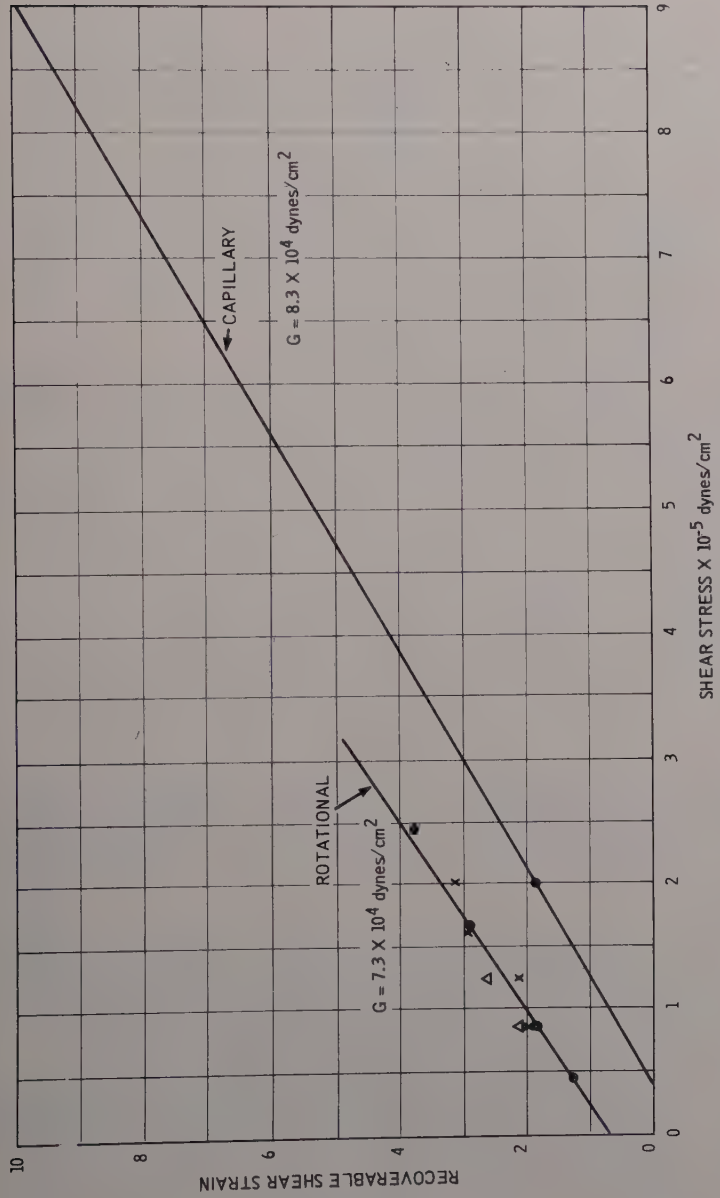


Fig. 9. Comparison of recoverable shear strain.

8.4×10^4 dynes/cm.² for the capillary and 7.3×10^4 dynes/cm.² for the rotational instrument could easily be the result of differences in molecular weight distribution.^{18,19}

References

1. Cerf, R., and H. A. Scheraga, *Chem. Revs.*, **51**, 185 (1952).
2. Eirich, F. R., ed., *Rheology*, Vol. I, Academic Press, New York, 1956.
3. Frocht, M. M., *Photoelasticity*, Wiley, New York, 1941.
4. Saunders, D. W., *Trans. Faraday Soc.*, **52**, 1425 (1956).
5. Nielsen, L. E., and R. Buchdahl, *J. Colloid Sci.*, **5**, 282 (1950).
6. Lodge, A. S., *Trans. Faraday Soc.*, **52**, 1425 (1956).
7. Philippoff, W., *Trans. Soc. Rheology*, **5**, 149 (1961).
8. Foreman, W. T., *J. Chem. Phys.*, **32**, 277 (1960).
9. Philippoff, W., *J. Appl. Phys.*, **32**, 984 (1956).
10. Roberts, J. E., *Proceedings of Second International Congress on Rheology*, Academic Press, New York, 1954.
11. Smith, E. F., and A. P. Wangsgard, *J. Polymer Sci.*, **5**, 169 (1950).
12. Dexter, F. D., *J. Appl. Phys.*, **25**, 1124 (1954).
13. Weissenberg, K., *Proceedings of First International Congress on Rheology*, North-Holland, Amsterdam, 1949.
14. Mooney, M., *J. Colloid Sci.*, **6**, 96 (1951).
15. Philippoff, W., *Trans. Soc. Rheology*, **5**, 163 (1961).
16. Bagley, E., *J. Appl. Phys.*, **31**, 1127 (1960).
17. Philippoff, W., *Trans. Soc. Rheology*, **2**, 263 (1958).
18. Leaderman, H., R. G. Smith, and R. W. Jones, *J. Polymer Sci.*, **14**, 48 (1954).
19. Van Holde, K. E., and J. W. Williams, *J. Polymer Sci.*, **11**, 243 (1954).

Synopsis

A simple viscometer which consisted of two glass plates and a circular polariscope were used to investigate the birefringence of molten polyethylene through the 1-3 plane. The birefringence was proportional to the shear rate at small rates of shear, but not at rates of shear exceeding 0.4 sec.^{-1} . Stress-birefringence curves show a greater than proportional increase in birefringence with stress over the range investigated.

Recoverable shear strains were calculated from the birefringence data by assuming tensorial distribution of stresses and optical properties. The calculated strains agreed favorably with recoverable shear strains obtained with a rotational viscometer. The results help to confirm the assumptions that $P_{22} = P_{33}$ and that the birefringence is proportional to the differences in principal stresses.

Comparison of the recoverable shear strain from the rotational viscometer with recoverable shear strain calculated from capillary viscometer end correction data showed good agreement. A small difference in shear modulus is attributed to molecular weight distribution differences.

The Rheology of Polyelectrolytes. I. Flow Curves of Concentrated Poly(acrylic Acid) Solutions

JOHN G. BRODNYAN and E. LLOYD KELLEY,
Rohm & Haas Co., Philadelphia, Pennsylvania

Introduction

The rheology of polyelectrolytes, both natural and synthetic, is of interest. These materials are used as thickeners, film formers, and dispersants in many commercial products. Also, many biologically important materials are polyelectrolytes.

Most of the reported investigations of their flow behavior have been on dilute solutions; the relationship of intrinsic viscosity to the shape and size of the polyelectrolyte has been investigated in great detail.¹ Only a few investigations have been reported on the more concentrated solutions which are of interest in industrial applications. In this report the investigation of such concentrated solutions of a model polyelectrolyte, poly(acrylic acid), will be given.

It has been recognized that the viscosities of the solutions depend upon the rate of shear of the measurement. Since in processing and use the solutions undergo rates of shear which may vary from low to very high, it was decided to investigate the flow behavior in as wide a range as possible. A biconical rotational viscometer was used at low rates of shear and a high-pressure capillary instrument was used at high rates of shear. The range covered was sufficient in most cases to give not only the low rate of shear Newtonian region but also the high rate of shear Newtonian region. In the case of both viscometers those values of apparent shear rate which were obtained in the shear thinning region were subjected to the necessary corrections.²

Recently the shear rate dependence of the viscosity of coiling polymers has been described in terms of molecular parameters. Several theories³⁻⁵ which agree in their basic essentials, i.e., that this apparent

change in viscosity is the result of the springlike behavior of coiling polymers as they are deformed and rotated under a shearing force, have been proposed. Our results have been evaluated in terms of Bueche's³ theory because it requires only the measurement of viscosity as a function of rate of shear. Pao's theory⁴ requires a detailed knowledge of the spectrum of retardation times. Takemura's result⁵ is similar to Bueche's, and a test of Bueche's is essentially a test of it also. An empirical modification of Bueche's theory has shown agreement with experimental data on poly(methyl methacrylate),⁶ polystyrene,⁶ and rubber solutions,⁷ defining a standard curve for those polymers.

The configuration or extension of the polymer changes as the acid is neutralized, i.e., as the charge on the polymer is changed, therefore data were gathered at several degrees of neutralization and with an excess of base.

Experimental Methods

The Biconical Rotational Viscometer

Our rotational viscometer utilizes the design of Mooney and Ewart⁸ as modified by Philippoff.⁹

The rotational viscometer is shown in Figure 1. The viscometer proper is suspended in a large thermostated bath by means of a rigid metal frame from which the viscometer can be easily detached for cleaning and filling with a sample. The rotating inner cylinder or bob is slightly conical at both ends, making an angle of $2^{\circ}50'$ with the stationary cup. Consequently, a uniform rate of shear is maintained in the gap and the end effects are extremely small since they are produced only at the rim and apex of each cone. The radii of the inner and outer cylinders are 3.963 and 4.166 cm., thus the gap is only 0.203 cm. The narrow gap permits (1) a relatively high maximum rate of shear compared to the overall size of the viscometer and (2) the use of small samples since the total liquid capacity is only ca. 50 ml. The cup has a removable cover which is sealed using an O-ring. In the middle of the cover there is a chimney-type opening. The narrow but long head of sample contained in the neck tends to (1) reduce the rate of evaporation and (2) insure that the gap remains filled with sample even where there is a noticeable Weissenberg effect.

The parts of the viscometer which contact the sample were made of

stainless steel to impart the chemical resistance necessary at an extreme pH, etc. Although the bob is hollow and the drum dial is made of aluminum, it was necessary to incorporate an air-bearing¹⁰ to minimize the force bearing on the steel point. A continuous stream of air forms a cushion between the two metal plates of the air-bearing, thus supporting the bob so that no weight is bearing on the steel point. When investigating liquids of low viscosity, we have reduced the friction to less than 0.01 g. by also removing the upper-shaft precision ball bearing altogether.¹¹

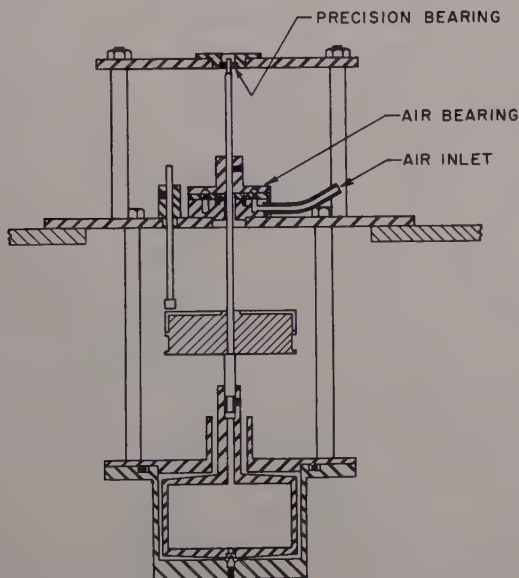


Fig. 1. Conicylindrical rotational viscometer.

An optical system was designed for investigations at extremely low rates of shear. Thus our limits of shear rate and shear stress using the rotational viscometer with its accessories and modification are from 1×10^{-7} to $2.5 \times 10^2 \text{ sec.}^{-1}$ in rate of shear (provided turbulence does not set in before the upper limit) and from 1×10^{-1} to 1×10^4 dynes/cm.² in shearing stress.

The rotational viscometer was calibrated with two standard viscosity oils obtained from the National Bureau of Standards. One was Oil M (Lot No. 28, $\eta_{20^\circ\text{C.}} = 3.464$ poise), the other was Oil OB (Lot

No. 17, $\eta_{20^\circ\text{C.}} = 297.5$ poise). The values obtained for the proportionality constant, K_s , between the shear stress and the measured weight less friction were 4.40 using Oil M and 4.44 using Oil OB, giving an average value of 4.42. The value of K_s calculated from the ge-

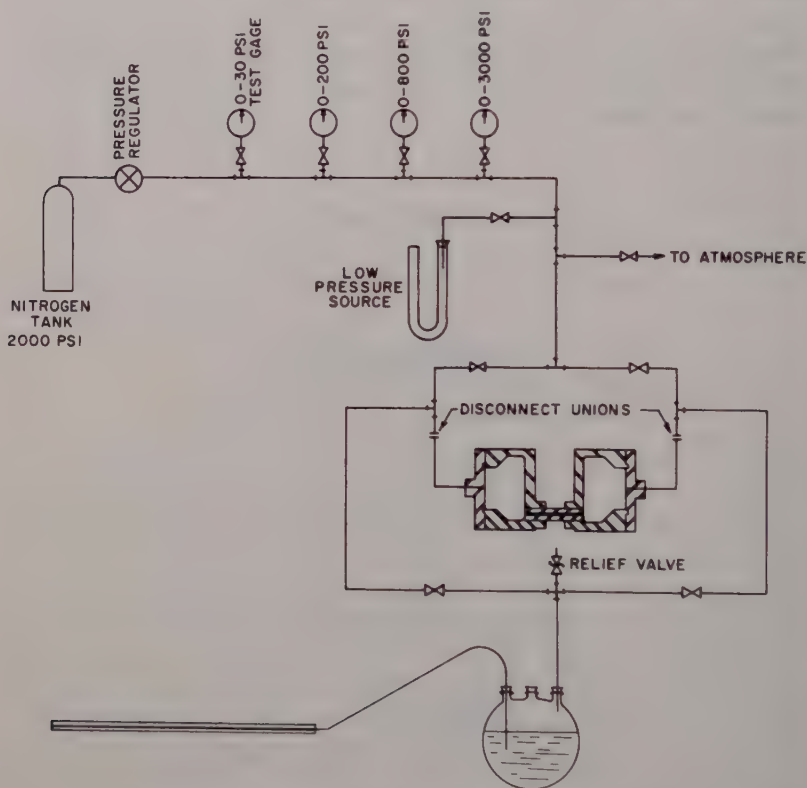


Fig. 2. Capillary viscometer, schematic arrangement.

ometry was 4.33; thus the experimental value differed by only 2% from the calculated value.

Water was measured in the instrument to ascertain (1) the lowest range of measurable viscosity and (2) the rate of shear at which turbulence begins. The shaft was used in lieu of the drum dial as lever arm. This enabled measurements using smaller torques. Excellent agreement was obtained with the literature for water. Further, the

critical rate of shear for the inception of turbulence was found experimentally to be 21.8 sec.^{-1} , differing by only 4.6% from the value of 20.8 sec.^{-1} calculated from the geometry.

The Capillary Viscometer

Our capillary viscometer is designed after the instrument of Philippoff.² The only modifications are the use of high-pressure stainless steel tubing throughout and the insertion of a relief valve to protect the glass monitoring assembly from surges of pressure. A diagram of the viscometer and its attendant parts for controlling and measuring the driving pressure and for monitoring the liquid flow rate is given in Figure 2. At present we have seven capillaries which can be used with the instrument. The values for length over radius for the capillaries are: 11.9, 63.0, 105, 124, 331, 581, and 897. The shear limits of the instrument are 5×10^{-1} to $3 \times 10^6 \text{ sec.}^{-1}$ in rate of shear (provided turbulence does not set in) and 10 to $6 \times 10^6 \text{ dynes/cm.}^2$ in shearing stress.

The same NBS oils used for calibrating the rotational viscometer were used to calibrate each capillary. The Couette¹² and Hagenbach¹³ corrections were taken into account. As a further check on the calibration, we experimentally determined the flow curve for water using the capillary dimensions obtained from the calibration. The resultant flow curve was in good agreement with the theoretical flow curve for water. Turbulence was found to set in at a Reynolds' Number of approximately 400.

Material Investigated

The poly(acrylic acid) used in these investigations was Acrysol A-5, a commercial product of Rohm & Haas Company. Stock solutions having different degrees of neutralization were prepared via the quantitative addition of reagent grade sodium hydroxide. The degree of neutralization, α , is the ratio of equivalents of sodium hydroxide per equivalent of acrylic acid. Lower concentrations were prepared by diluting the stock solutions with deionized water.

The viscosity-average molecular weight, M_v , of the poly(acrylic acid) was determined from the intrinsic viscosity in benzene of the poly(methyl acrylate) prepared by methylation of the polyacid with diazomethane; this method was a modification of the technique devised by Katchalsky and Eisenberg.¹⁴ A molecular weight of $2.2 \times$

10^5 was determined for the poly(methyl acrylate) from the intrinsic viscosity at 30°C . through the application of the relationship:¹⁵

$$[\eta] = 4.5 \times 10^{-5} M_v^{0.78}$$

That molecular weight of polyester corresponds to a molecular weight of 1.8×10^5 for the polyacid.

Experimental Results

The usual double logarithmic plots of rate of shear versus shearing stress, known as flow curves, are given on Figures 3–6 for the various concentrations of solutions having α equal to 0.0, 0.62, 1.0, and 1.8, respectively. The low rate of shear Newtonian region is given for all the solutions, but we were not able to reach the high rate of shear Newtonian region for all. Distinction is made on Figures 3–6 between the data obtained using the two viscometers.

In order to ensure that all samples examined had reached their equilibrium viscosity, flow data were gathered shortly after neutralization and again after a couple of months. All viscosities were constant.

For the solutions having α equal to 0.0 and 1.0, the flow data were gathered in an order which would reveal whether the polymer was susceptible to high shear degradation. The procedure was to gather the low rate of shear data (less than 1 sec.^{-1}) both before and after high rate of shear data were gathered. In all cases, subjecting the material to high rates of shear did not alter the value of η_0 , indicating that no shear degradation had occurred; η_0 is the Newtonian viscosity at low rates of shear.

The data were also plotted as $\log \eta$ vs. $\log D$ and then fitted to the standard curve of Bueche;⁶ η is the apparent viscosity at a given rate of shear D . From this curve fitting a relaxation time, τ , is obtained. A plot of η/η_0 vs. $\log D\tau$ should then give a master plot with the same shape as Bueche's standard curve (Fig. 7). It is seen on Figure 7 that the form of the polyelectrolyte curves is the same as the standard curve (the solid line) and therefore the same as the rate of shear dependence of poly(methyl methacrylate),⁶ polystyrene,⁶ and rubber⁷ solutions. The only differences are in the values of the relaxation times. The dotted line on Figure 7 gives Bueche's theoretical curve,³ but it predicts too abrupt a drop of viscosity with rate of shear. Bueche attributed this difference to the effect of molecular weight polydispersity.

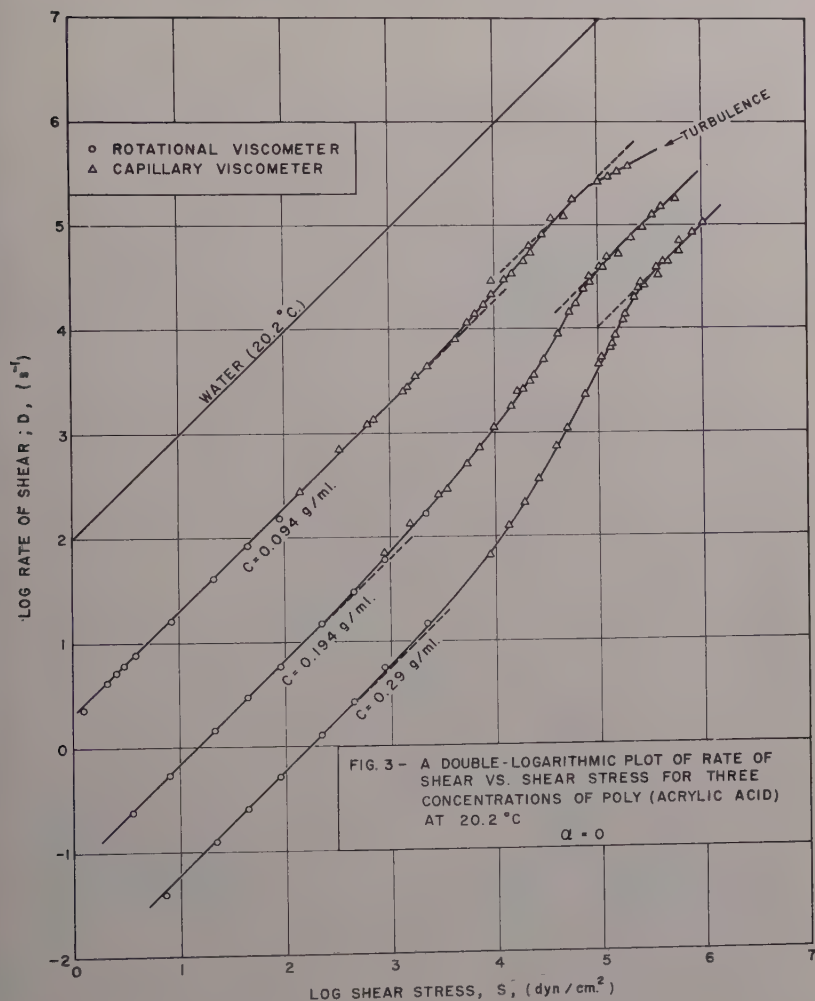


Figure 3.

From the relaxation time, the polymer concentration, the temperature, and the Newtonian viscosity at low rates of shear a molecular weight can be calculated.⁶

$$M = \pi^2 A k T c \tau / 12 \eta_0 \quad (1)$$

where A = Avogadro's number, k = Boltzmann's constant, and c = concentration (g./ml.).

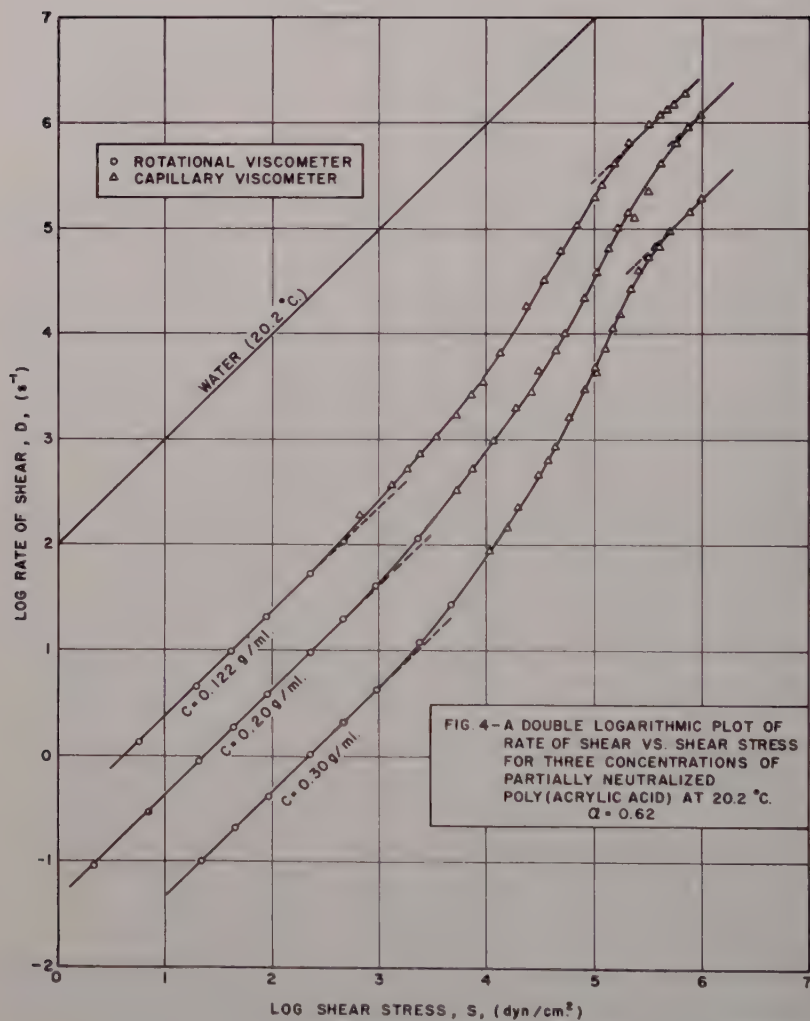


Figure 4,

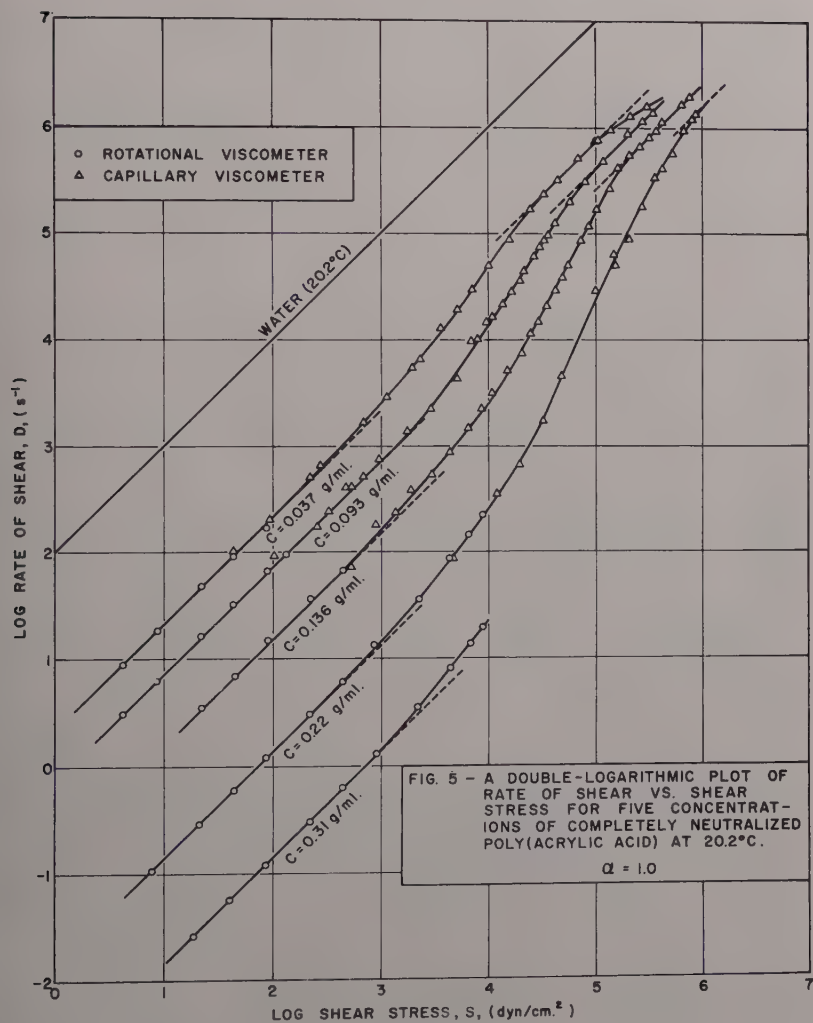


Figure 5.

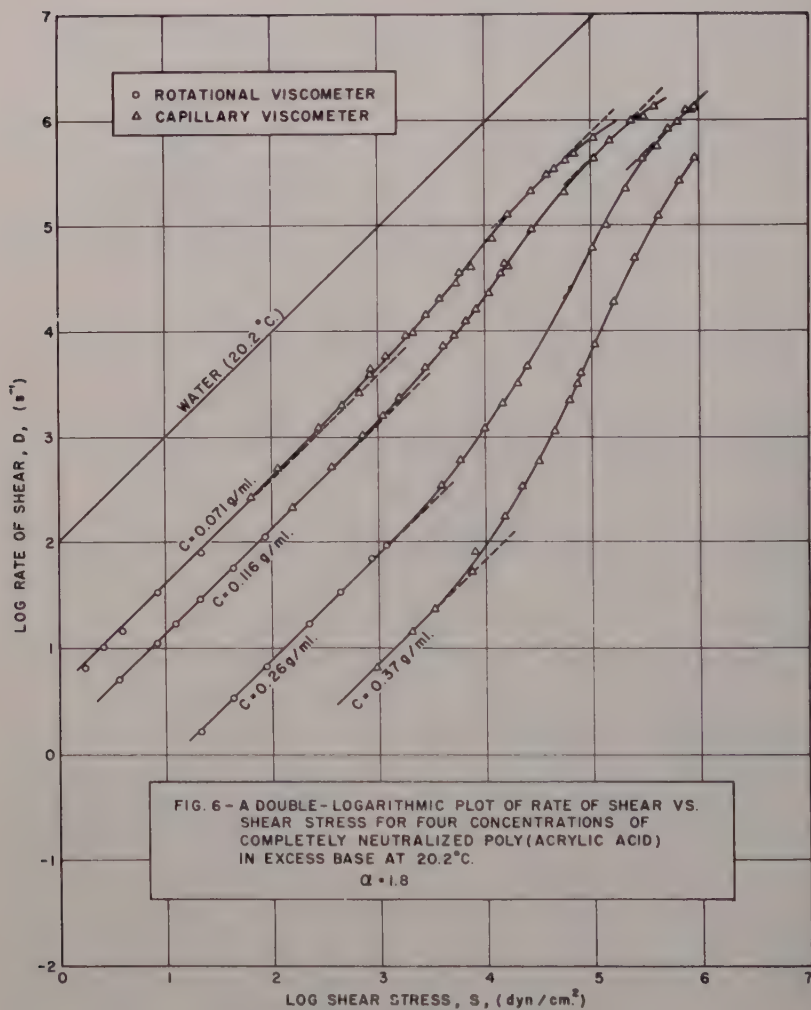


Figure 6.

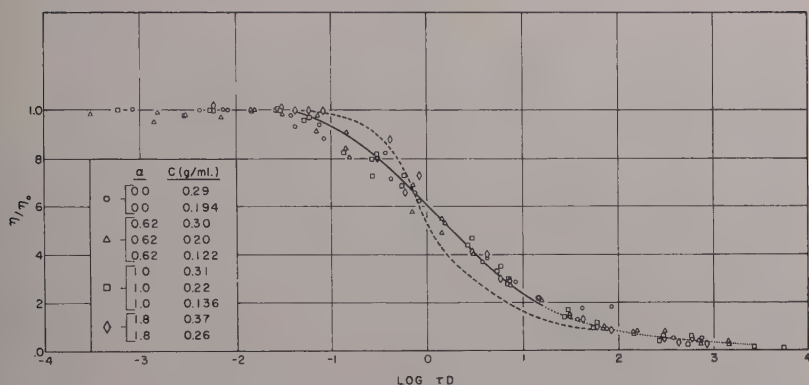


Fig. 7. Comparison of experimental data with Bueche's standard curve.

In Table I all these quantities are given. Only solutions with a concentration greater than 10% are used since Bueche's theory is valid only for such concentrated solutions³ where the molecules would exist as free draining coils.

The average value of 2.1×10^5 for the molecular weight when α equals zero is in good agreement with the value of 1.8×10^5 for the poly(acrylic acid) determined by the more standard method. The other average values are also in good agreement with the predicted values. This, however, may be fortuitous for α equal to 0.62 and 1.0 since it is expected that the polymer molecules are extended at these

TABLE I
The Calculation of Molecular Weights from Relaxation Times

α	Concentration, g./ml.	η_0 , poise	τ^{-1} , sec. ⁻¹	$M_{\tau} \times 10^5$	$\bar{M}_{\tau} \times 10^5$	$M_v \times 10^5$
0	0.29	170	133	2.6	2.1	1.8
0	0.194	14.8	1760	1.5		
0.62	0.30	220	64	4.3	2.8	2.2
0.62	0.199	24.3	620	2.7		
0.62	0.122	4.25	4600	1.27		
1.0	0.22	74	246	2.5	2.2	2.4
1.0	0.136	6.20	2500	1.8		
1.8	0.37	135	151	3.7	3.0	2.4
1.8	0.26	12.5	1800	2.3		

degrees of neutralization and might not fulfill the condition imposed on the model that it be free draining. The scatter about the average value of molecular weight is not much worse than that found by Bueche and Harding⁶ with poly(methyl methacrylate) and polystyrene solutions. It is apparent though that for all degrees of neutralization $M\tau$ decreases as the solution concentration decreases. This indicates that the relaxation time may not be inversely proportional to concentration to the first power but to some lower power.

On Figures 3-6 it appears that the solutions become shear thinning at approximately the same shearing stress. This behavior has been noted with other polymer solutions and it is a consequence of the mechanism which leads to the standard curve.³ Since η/η_0 is a known function of $D\tau$, $D\tau$ is a constant at any arbitrary value of η/η_0 at which a solution is defined to be shear thinning. In our work we have arbitrarily chosen $(\eta/\eta_0)_{st}$ equal to 0.90. From the definition of τ , eq. (1), it can be shown that:

$$\begin{aligned} D\tau = \text{constant} &= (12M/\pi^2 Ak)(D\eta_0/cT) \\ &= 12M/\pi^2 Ak(\eta_0/\eta)_{st}(D\eta/cT) \quad (2) \end{aligned}$$

Since $(\eta/\eta_0)_{st}$ is given, $D\eta/cT$, which is equal to S_{st}/cT , is a constant for a given molecular weight. The reason S_{st} appears to be constant is that T was held constant and the variation of c was within the range of our ability to estimate the curve shapes. The quantity S_{st}/c at $\eta = 0.90 \eta_0$ was determined for each solution above 0.1 g./ml. and the values are given in Table II.

The scatter about the average value of S_{st}/c for any degree of neutralization is not large. It is to be noted that the average values appear to go through a minimum as the polymer is progressively neutralized. Yang's work¹⁶ with poly- γ -benzyl-L-glutamate solutions in which he changed the configuration of the molecules from a random coil to a stiff rod (helix) by changing the solvent from dichloroacetic acid to *m*-cresol, indicates that S_{st}/c is much less for a rigid rod (a factor of five or more) than it is for a random coil even though the molecular weight is held constant. Therefore, the minimum in the average value for S_{st}/c at a degree of neutralization of 0.62 is probably due to the random coil extending until it is 60% neutralized, then going back to a random shape as the extra charges formed upon increase in the degree of neutralization suppress the electrostatic effects which caused the extension of the molecule.

TABLE II

The Effects of Degree of Neutralization and Concentration on the Poly(acrylic Acid) Solutions at 20°C.

α	Concentration, g./ml.	η_0 , poise	$(\eta_{sp}/c)_0$, $\times 10^3$	η_∞ , poise	$(\eta_{sp}/c)_\infty$, $\times 10^3$	S_{st}/c , $\times 10^3$	(S_{st}/c) , $\times 10^3$
0	0.29	170	58.5	9.50	3.27	13.8	9.5
0	0.194	14.8	7.6	2.80	1.44	5.2	
0	0.094	0.50	0.52	0.33	0.34	—	
0.62	0.30	220	73.3	5.20	1.73	7.7	6.3
0.62	0.199	24.3	12.2	0.79	0.39	5.6	
0.62	0.122	4.25	3.48	0.36	0.28	5.7	
1.0	0.31	727	235	—	—	5.0	7.4
1.0	0.22	74.0	33.6	—	—	6.1	
1.0	0.136	6.20	4.55	0.400	0.29	11.0	
1.0	0.093	1.35	1.44	0.245	0.25	—	11.4
1.0	0.037	0.455	1.20	0.133	0.33	—	
1.8	0.37	135	36.5	—	—	15.4	
1.8	0.26	12.5	4.80	0.64	0.24	12.7	11.4
1.8	0.116	0.730	0.62	0.232	0.19	6.2	
1.8	0.071	0.223	0.30	0.123	0.16	—	

Many of the solutions reach a constant viscosity at high rates of shear, η_∞ , and those that do not are obviously approaching such a limit. In Table II the zero rate of shear viscosity, the infinite Newtonian viscosity, and the values of their respective specific viscosities divided by concentration are given. Merrill¹⁷ has studied polyisobutylene in a number of solvents and found that the specific viscosity at high rates of shear divided by concentration is independent of concentration and solvent type and only dependent on the molecular weight. Although the infinite shear rate values are more constant than the zero shear rate values for our samples, one could consider them reasonably constant only for α equal to 1.0 and 1.8. The reason that the polyacid values would increase with concentration while the polysalt values do not is not clear. There are other data which show that a polyelectrolyte salt does give a constant value of $(\eta_{sp}/c)_\infty$. Sodium carboxymethyl cellulose in 6% sodium hydroxide has been investigated in a wide range of rates of shear by Schurz,¹⁸ and from

his curves it appears that $(\eta_{sp}/c)_{\infty}$ equals 207 ± 4 . This value is of the same order of magnitude as the value obtained for our poly(sodium acrylate) in sodium hydroxide (200 ± 30 for α equal to 1.8).

Discussion

Much thought has been given to the interpretation of flow curves in terms of molecular properties. Umstatter¹⁹ noted that there exists a relationship between the inflection point of a flow curve and the molecular weight of the solute in that the former is found at smaller shear gradients when the molecular weight is increased. Philippoff²⁰ indicated that useful information about the polydispersity of a given sample might be contained in the flow curves, and Meskat²¹ showed experimentally that there exists a connection between polydispersity and the shape of the flow curve. Schurz¹⁸ has recently reviewed his efforts to obtain empirically connections between experimental flow curves and molecular properties.

It is not necessary now to employ an empirical approach since a number of theories³⁻⁵ appear to be in general agreement with experimental results. They confirm theoretically Umstatter's observation, predicting that the rate of shear at the inflection point will be determined by the relaxation time which is directly proportional to the molecular weight of the solute. Bueche and Harding⁶ have shown how this can be used as a method of molecular weight determination. The molecular weights Bueche determined by this method were in good agreement with the molecular weights obtained by other methods for poly(methyl methacrylate),⁶ polystyrene,⁶ and rubber.⁷ Our results with poly(acrylic acid) confirm his findings and other confirmation can be obtained from the literature. The results obtained from the evaluation of flow curves of polyisobutylene in decalin^{22,23} and carboxymethyl cellulose in 6% sodium hydroxide¹⁸ are given in Table III and are seen to be in good accord with Bueche's theory.

TABLE III
Molecular Weights Calculated from Flow Curve (M_{τ}) Compared to Experimental Molecular Weights (M)

	M_{τ}	M
Polyisobutylene	1.15×10^6	$1.06 \times 10^{6.23}$
Sodium carboxymethyl cellulose	1.8×10^5	$2.1 \times 10^{6.18}$

The theoretical flow curve is not in perfect agreement with the experimental data, giving a more rapid drop of viscosity with rate of shear than observed. The theoretical curve, however, was derived for monodisperse polymers, and the deviation may be due to polydispersity. If this is so, it must be possible to determine the polydispersity from the shape of the flow curve as Philippoff has indicated.²⁰ It is surprising, though, that the standard curve of Bueche which is empirical fits so many polymers so well. It may be that they all are close to the most probable molecular weight distribution.

Bueche's theory has been criticized by others⁵ because his simple mechanical model may not be self-consistent from the viewpoint of statistical mechanics; it does not contain the term for the Brownian motion of molecules in its initial formulation. Nevertheless, it does agree with experimental data and essentially with other self-consistent theories⁵ and the basic utility of the model is evident.

Conclusions

(1) The flow behavior of concentrated solutions of poly(acrylic acid) and poly(sodium acrylate) in water does not differ qualitatively from the flow behavior of other more hydrophobic polymers in organic solvents. Only the relaxation time is changed by the change of the low rate of shear Newtonian viscosity.

(2) Bueche's standard curve can be used to determine the molecular weight of the solute if the flow curves are known.

(3) Conversely, Bueche's standard curve can be used to predict the flow curve of a polymer solution provided the molecular weight and concentration of the solute, the temperature, and the low rate of shear Newtonian viscosity are known. It does not give good results at low concentrations of solute where the coil may not be free draining.

(4) The molecular theories also give a rational explanation for the empirical observation that shear thinning appears to occur at a constant shear stress.

The authors would like to thank F. H. Gaskins and W. Philippoff for their suggestions which resulted in the incorporation of the air bearing in the rotational viscometer, M. Bechta for his fine design work, and M. Tomcowicz for the construction of both viscometers.

Also acknowledged is the methylation of the poly(acrylic acid) by L. Miller and the viscometric determination of molecular weight by H. Mason.

References

1. A recent review of the subject has been given by B. E. Conway and A. Dobry-Ducaux in *Rheology*, Vol. 3, edited by F. R. Eirich, Academic Press, New York (1960).
2. Gaskins, F. H., and W. Philippoff, *J. Appl. Polymer Sci.*, **2**, 143 (1959).
3. Bueche, F., *J. Chem. Phys.*, **22**, 1570 (1954).
4. Pao, Yoh-Han, *J. Chem. Phys.*, **25**, 1294 (1956); *J. Appl. Phys.*, **28**, 591 (1957).
5. Takemura, T., *J. Polymer Sci.*, **27**, 549 (1958).
6. Bueche, F., and S. W. Harding, *J. Polymer Sci.*, **32**, 177 (1958).
7. Bueche, F., *J. Appl. Phys.*, **30**, 1114 (1959).
8. Mooney, M., and R. H. Ewart, *Physics*, **5**, 350 (1934).
9. Brodnyan, J. G., F. H. Gaskins, W. Philippoff, and E. G. Lendrat, *Trans. Soc. Rheology*, **2**, 285 (1958).
10. Private communication from F. H. Gaskins.
11. Private communication from W. Philippoff.
12. Couette, M., *Ann. Chim. Phys.*, **21**, 433 (1890).
13. Hagenbach, E., *Ann. Phys.*, **109**, 385 (1860).
14. Katchalsky, A., and H. Eisenberg, *J. Polymer Sci.*, **6**, 145 (1951).
15. Private communication from E. Cohn.
16. Yang, J. T., *J. Amer. Chem. Soc.*, **80**, 1783 (1958).
17. Merrill, E. W., *J. Polymer Sci.*, **38**, 539 (1959).
18. Schurz, J., *J. Colloid Sci.*, **14**, 492 (1959).
19. Umstatter, H., *Strukturmechanik*, Steinkopff, Dresden and Leipzig, 1948.
20. Philippoff, W., *Viskosität der Kolloide*, Steinkopff, Dresden and Leipzig, 1942.
21. Meskat, W., *Chem. Ing. Tech.*, **14**, 333 (1952).
22. Brodnyan, J. G., F. H. Gaskins, and W. Philippoff, *Trans. Soc. Rheology*, **1**, 109 (1957).
23. Philippoff, W., *J. Appl. Phys.*, **27**, 984 (1956).

Synopsis

Flow curves of a poly(acrylic acid) of 1.8×10^5 viscosity-average molecular weight were obtained at four degrees of neutralization and several concentrations over a wide range of rates of shear. A biconical rotational viscometer was used at low rates of shear and a high-pressure capillary viscometer was used at high rates of shear. The range covered was sufficient in most cases to give not only the low rate of shear Newtonian viscosity but also the high rate of shear Newtonian region.

Plots of η/η_0 vs. $\log D\tau$ were found to fit Bueche's standard curve. The shapes of the polyelectrolyte flow curves, therefore, are the same as the shapes of the flow curves of the more usual polymers, e.g., poly(methyl methacrylate). The polymers differ only in the magnitudes of their relaxation times and low shear rate Newtonian viscosities. From the experimental relaxation times the molecular weight was calculated and found to agree with that determined by intrinsic viscosity measurements.

Yield Stresses and Flow Properties of Carboxypolymethylene-Water Systems

WILLIAM H. FISCHER, WALTER H. BAUER, and STEPHEN E. WIBERLEY, *Walker Laboratory, Rensselaer Polytechnic Institute, Troy, New York*

Introduction

For many systems, such as aqueous clay suspensions used for drilling fluids and metallic soaps dispersed in hydrocarbons to form lubricating greases, an important property is the yield stress to which the material may be subjected before permanent deformation takes place. Measurements of yield stress may give values dependent on the apparatus design as well as the nature of the test material,^{1,2} on the time scale of the test procedure,^{3,4} and on extrapolation from flow measurements.⁵ Conveniently for the uniform application of a shear stress, an arrangement in which the test sample is held between a rotatable cone and a fixed plate allows the determination of the first stress at which permanent deformation occurs, with specified conditions of time of application of stress and magnitude of flow.⁶ With a cone-plate apparatus, studies were made of the yield stresses for lithium stearate-hydrocarbon oil dispersions, showing that the results obtained were affected by the rate of increase of stress, and by the shear rate and time of flow to which the dispersions had been previously subjected.⁷⁻⁹ After sufficiently long periods of shearing, the lithium soap-oil dispersions exhibited reversibly restorable yield values only if the maximum shear rate applied to the sample previously had not been exceeded. For study of the relations between yield stresses and molecular properties, it appeared important initially to study systems showing independence of previous shear history. For such systems, yield stresses could be determined either by application of initial stress to cause flow or on the cessation of deformation after reduction of stress during flow. Systems of carboxypoly-

methylene and water, used in this investigation, were found to meet the requirement, since they exhibited reversible restoration of flow properties after shearing, within the time scale and range of shear rate in the tests. In addition, the use of a polyelectrolyte provided opportunity for change of molecular state and interparticle forces through the control of the extent of ionization of the carboxyl groups with added base.

Materials

The polymer, Carbopol (prepared by B. F. Goodrich Chemical Co.), which was used in this study, was a carboxypolymethylene. An infrared spectrum obtained from a 1% dispersion by weight in KBr showed absorption bands due to methyl, methylene, and carboxyl groups only. From the infrared measurements, the estimated ratio of CH_3 to CH_2 groups is three to one. It was concluded that the polymer molecule is highly branched with short side chains and with most of the carboxyl groups on the main chain of the molecule.¹⁰⁻¹² Tests for unsaturation with permanganate and bromine were negative.¹³ Neutralization experiments employing both ammonium and sodium hydroxide indicated the presence of one carboxyl group per two methylene and methyl groups.

Dispersions of the polymer in freshly boiled distilled water were made by addition of weighed portions of Carbopol, which had been dried over P_2O_5 . Gentle mechanical stirring was used to disperse the swelled polymer. Finally, addition of water was made to give the desired stock concentrations of 1, 3, or 5% by weight. Grams of polymer used per 100 g. of water were recorded. Dispersions were stored at 5°C. until use.

Test samples were prepared from weighed portions of one of the stock dispersions, mixed in an agate mortar with sufficiently freshly standardized ammonium hydroxide solution to give the desired pH.

The pH of the samples remained essentially constant throughout the test period. It was observed, however, that the pH changed slowly with time, those samples with the highest initial pH showing the most rapid change.

Experimental Methods

Yield Stress

In the viscometer used in this investigation,^{14,15} a cone of low angle was immersed in a sample of the test material on a flat plate, temperature-controlled, with thermocouples imbedded in insulating material in contact with the sample.¹⁶

In order to determine yield stress with the viscometer a torque was imposed on the cone, immersed in the sample, with the drive shaft locked. Successively increasing stresses were applied to establish the region of measurable deformation, indicated by rotation of the cone and consequent decay of stress. With appropriate transducers the stress was recorded versus time. Stress equilibrium was considered to have been attained when decay of stresses was not observed

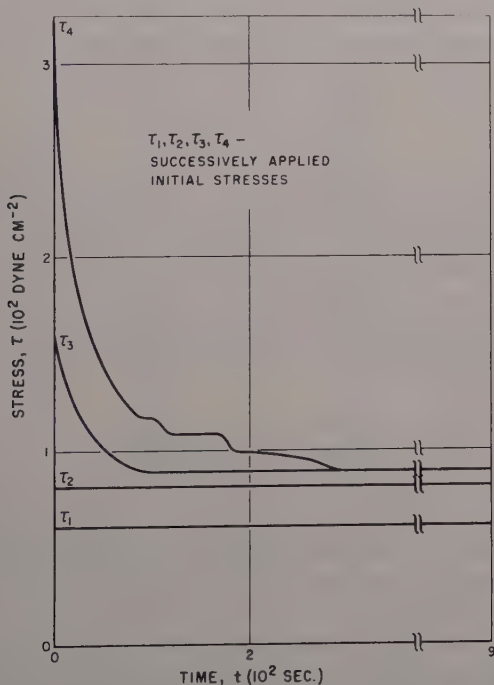


Fig. 1. Determination of yield stress for Carbopol-water dispersions with successive application of shear stress.

for 600 sec. In Figure 1, typical results are shown for a measurement of yield stress. An initial stress, τ_1 , was applied, and after no stress decay was observed for 600 sec., the stress applied was increased to τ_2 by further extension of a spiral spring attached to the cone drive shaft. This procedure was repeated until a stress decay on rotation of the cone, indicating permanent deformation of the test material, occurred within 600 sec., as, for instance, when τ_3 was applied. In this case rotation of the cone immersed in the test sample continued until no further stress decay occurred in a period of 600 sec., when equilibrium was established within the time scale of the experiment. Tests showed that the magnitude of the stresses applied had no effect on the yield stress finally measured, and the same value was reached from the successively applied stresses τ_3 and τ_4 . The yield stress equilibrium condition at 600 sec. could be approached from either quiescent or flow conditions, with results equal within the limits of reproducibility. Most of the measurements reported are based on equilibrium stress measurement after small deformation of the sample, because of the advantage of speed in measurement.

Flow Curves

For the study of flow properties of the Carbopol-water systems, shear stress was measured at selected values of shear rate when flow equilibrium had been reached, and flow curves, shear stress versus shear rate, were obtained. In programmed cycles of shear, the shear rate was uniformly increased to a maximum of 1200 sec.⁻¹ and reduced to zero in a period of 800 sec., with the use of the cone-plate viscometer and automatic control and recording as previously described.¹⁶

Experimental Results

Yield Stresses

Yield stresses were measured for a series of samples of concentrations of 1, 3, and 5% by weight of Carbopol in water, over a range of temperature, and at a series of pH values adjusted by addition of ammonium hydroxide, Table I. The yield stress at the temperatures of test, 15, 25, and 35°C. showed a maximum near pH 7 when plotted versus pH at each concentration, as illustrated by data obtained at 25°C., Figure 2.

TABLE I
Yield Stresses of Carbopol-Water Systems

pH ^a	τ_y^b		
	15°C.	25°C.	35°C.
	(a) 0.5% Carbopol ^c		
3.1	0	0	0
5.0	50	40	40
6.6	60	60	50
9.5	50	40	30
	(b) 1% Carbopol ^c		
2.8	15	0	0
4.8		80	
5.7	130	100	90
7.2		85	90
7.4	120		
8.5		80	60
9.4	90	60	40
	(c) 3% Carbopol ^c		
2.6	190	140	140
4.2		420	
4.9	540	470	430
6.0		470	420
7.3	530	430	
9.0		340	310
9.6	360	290	270
	(d) 5.5% Carbopol ^c		
2.3	750	650	660
3.5		1,090	
4.9	1,590	1,320	1,080
6.5	1,690	1,370	1,200
8.0	1,630	1,290	
8.6		1,260	960
9.3	1,420		
9.6		910	800
10.1		850	

^a Average pH during testing period.

^b τ_y = average yield stress in shear in dynes-cm.⁻².

^c Nominal Carbopol concentration in grams Carbopol per 100 g. water.

Flow Properties

From the flow curves obtained for the Carbopol-water systems at several values of pH, at 1, 3, and 5% concentration, and 15, 25, and 35°C., apparent viscosities, η_a , were calculated, where η_a is τ/D , τ is

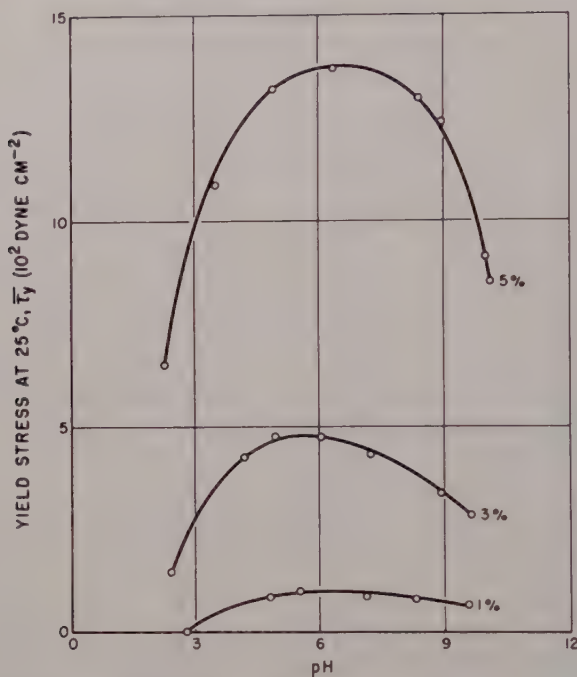


Fig. 2. Dependence of yield stress on pH. Concentrations in per cent by weight, Carbopol-water dispersions, cone-plate viscometer.

the shearing stress at the rate of shear, D . The results shown in Figure 3, at $D = 1140 \text{ sec.}^{-1}$, are typical of the variation of η_a with pH.

It was found that flow equilibrium was very rapidly established at any rate of shear reached in the range tested, up to 1140 sec.^{-1} . Flow curves, τ versus D , obtained in programmed cycles of shear, showed little or no difference between the curves for increasing and those for decreasing shear rate. It was found for each of the fifty samples studied that the equation¹⁷

$$\tau - \tau_y = AD^N$$

where τ_y is the yield stress and A and N are constants for a particular sample, applied. Examples of the fit of the data are shown in Figure 4, exhibiting the linear variation of $\log(\tau - \tau_y)$ with $\log D$ for typical

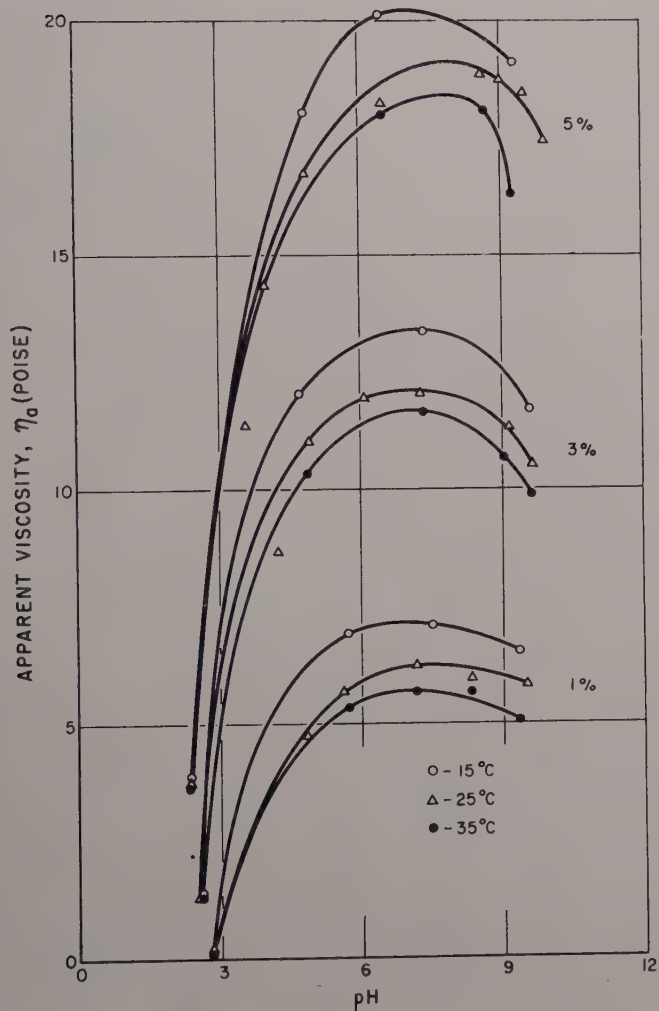


Fig. 3. Apparent viscosity, τ/D , at $D = 1140 \text{ sec.}^{-1}$, as a function of pH, for Carboxypol-water dispersions, at various concentrations and temperatures.

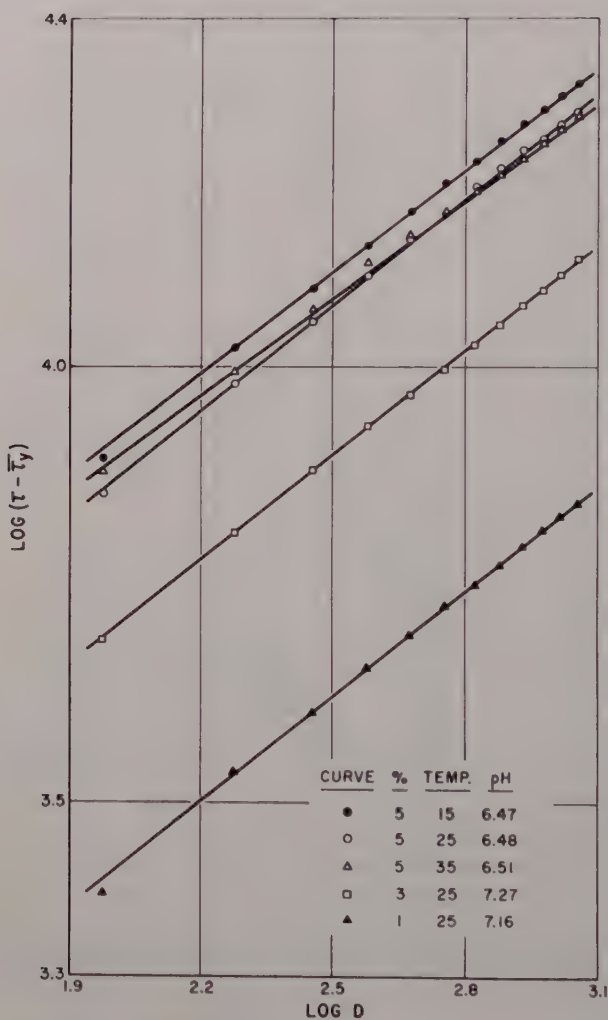


Fig. 4. Typical flow curves, $\log(\tau - \tau_y)$ versus $\log D$, for Carbopol-water dispersions. τ expressed in dyne-cm.⁻², D in sec.⁻¹.

samples. Since the logarithmic presentation of the data was linear over the range tested, the results of the study of the flow properties are most readily presented in terms of A and N , termed the consistency variable and the index of non-Newtonian behavior. The values found are given in Table II, in which A has been calculated for D/D_{400} instead of D , in order to avoid extrapolation beyond the range of the experimental data.

Variation of Viscosity and Yield Value with Temperature

It was found that the viscosities, η_a , calculated at selected rates of shear and values of pH, for the Carbopol-water systems studied

TABLE II
Characteristic Constants in Flow for Carbopol-Water Systems

pH	15°C.		25°C.		35°C.	
	N	A	N	A	N	A
(a) 1% Carbopol						
2.8	0.7	100	0.8	90	0.7	90
4.8			0.4	3,400		
5.7	0.4	5,200	0.4	4,100	0.4	4,000
7.2			0.4	4,600	0.4	4,200
7.4	0.4	5,400				
8.5			0.4	4,400	0.4	4,200
9.4	0.3	5,300	0.4	4,300	0.4	3,800
(b) 3% Carbopol						
2.6	0.5	800	0.5	950	0.4	800
4.2			0.5	5,800		
4.9	0.4	8,500	0.4	7,700	0.4	7,600
6.0			0.4	8,600	0.4	8,400
7.3	0.4	9,600	0.4	8,700		
9.0			0.4	8,100	0.4	7,800
9.6	0.4	8,300	0.4	7,500	0.4	7,300
(c) 5% Carbopol						
2.3	0.5	2,200	0.5	2,100	0.4	2,200
3.5			0.4	7,700		
4.9	0.4	12,000	0.4	9,500	0.4	11,000
6.5	0.4	14,000	0.4	11,000	0.4	13,000
8.0	0.4	15,000	0.4	13,000		
8.6			0.4	14,000	0.4	14,000
9.3	0.4	14,000				
9.6			0.4	14,000	0.4	12,000
10.1			0.4	14,000		

varied with temperature approximately according to the relationship

$$\eta_a = Be^{Q_n/RT}$$

where B and R are constants, T is the Kelvin temperature, and Q_n is a nominal heat of activation for flow. A similar relation was found at selected values of pH for the relation between yield stress and temperature,

$$\tau_y = B^1 e^{Q_y/RT}$$

where B^1 and R are constants, and Q_y is a nominal heat of activation for initial deformation. When $\log Q_n$ and $\log Q_y$ were plotted against $1/T$ for the Carbopol-water systems, it was found that the curves obtained were not linear, but were slightly concave upwards, as has been previously reported for polymers and polyelectrolytes.^{8,19} From the average slope estimated for the various samples, values of Q_n and Q_y were calculated, with the results given in Table III.

TABLE III
Apparent Heats of Activation for Yield and Flow

gram Carbopol		pH	Q_y , kcal.	Q_{η} , kcal.
100 g. H ₂ O				
1	4	—	3.4	
	6	—	2.2	
	8	—	1.6	
3	4	2.1	1.9	
	6	2.5	1.3	
	8	2.6	1.3	
5	4	3.6	1.1	
	6	3.2	1.5	
	8	3.3	0.9	
H ₂ O		—	—	4.1

Discussion

Flow Properties

At all concentrations studied, Carbopol-water dispersions exhibited shear rate thinning and unexpectedly high flow resistance, though

yield stresses were clearly established only above 0.5% Carbopol. In investigations of Carbopol-water systems, Metzner and Dodge²⁰ have found that the flow properties are described by the relation of the type

$$\tau = AD^N$$

reporting values of N ranging from 0.7 to 0.4 for polymer concentrations of 0.2 to 0.5%. Similar shear rate thinning was found for the Carbopol-water dispersions of 0.5 to 5% Carbopol studied in this investigation, with rapid establishment of flow equilibrium at any rate of shear. At high shear rates, the flow was described by the equation used by Metzner, with values of N as low as 0.3 for some systems. At low shear rates, however, the simple exponential relationship failed to apply.

For many polymer-solvent systems, the double logarithmic plot of shear rate versus shear stress shows a region of constant viscosity at low shear rates, where a limiting value of η_0 is reached, as reported by Philippoff²¹ and others. No approach to such a limiting viscosity was found for Carbopol dispersions in water. Instead, as the shear rate was reduced in flow tests, a constant value of shear stress was reached as a limit, with the curve of log shear rate versus log shear stress showing rapid curvature, tending to be parallel to the shear rate axis as the shear rate was reduced. Approach to the yield stress at very low rates of shear was observed through stress decay measurements, but the flow behavior found was not Newtonian. If a region of flow at constant viscosity, η_0 , exists for the Carbopol-water systems, it must appear in a creep type of flow with time scales extending far beyond those of this investigation. Water dispersions of polyacrylic acids, similar to Carbopol except for the absence of chain branching, exhibit the expected low rate of shear behavior without the appearance of yield stresses of importance.¹⁹ The high degree of molecular interaction causing the resistance to flow under a limiting stress, shown by the Carbopol, is ascribed therefore to the presence of the chain branching in the Carbopol molecule, absent in the usual polyacrylic acids.

At high shear rates, no trend toward a constant limiting viscosity was found for the Carbopol-water dispersions, although in a number of tests shear rates of 10^4 sec.^{-1} were reached. The region of limiting viscosity, η_∞ , which is presumed to exist, must be at shear rates

beyond the limits set by the experimental arrangement used. Further investigations are planned with a capillary viscometer better suited to high shear rate studies.

The exponential relationship between shear rate and shear stress, used by Metzner²⁰ in flow calculations, is adequate for high shear rate use to describe flow of Carbopol-water dispersions from 0.1 to 5%. However, for applications involving initial stirring rates, flow of drilling fluids,²² and in other conditions with flow at low shear rates, an added parameter, the yield stress, τ_y , must be considered. Over the complete range of conditions of flow studied, the three parameter relation of Herschel and Bulkley¹⁷

$$\tau - \tau_y = AD^N$$

was found to be adequate. The values of yield stress and of the consistency variable, A , referred to D/D_{400} , varied with the concentration, pH, and temperature, but the index of shear rate thinning, N , as shown in Table II, was 0.4 in almost all cases. Comparisons of N for solutions of polymers which differ primarily in the degree of branching may show that the value of N is a function of the degree of branching.

Effect of Ionization on Flow

From the variation of apparent viscosities, τ/D , of the Carbopol-water dispersions at any particular rate of shear, such as shown in Figure 3 for $D = 1140 \text{ sec.}^{-1}$, the flow properties vary with the extent of ionization as would be expected for polyelectrolyte-water systems. At low values of pH, the viscosity is lowest, corresponding to a condition of maximum intramolecular cohesion and of coiling for the molecule. As the carboxyl groups are progressively ionized, intramolecular repulsion of the charges should dilate and extend the coils, with a resulting maximum viscosity near a pH of 6 to 7, as was the case. The decrease found in the viscosities as further addition of base was made may be ascribed to the increase of ionic strength and shielding reducing the intramolecular repulsion of the charged carboxyls, thus compressing the molecule.

The flow behavior of the Carbopol-water systems as the degree of ionization increases is thus similar to that exhibited by other polyelectrolytes such as polyacrylic acid. In marked contrast to the polyacrylic acid-water dispersions, however, the Carbopol-water dis-

persions exhibit relatively high viscosities under similar concentration, pH, and shear rate conditions, of the order of fifty times larger than found for polyacrylic acids.

Since, as far as is known, the two molecular structures differ only in that the Carbopol has numerous short branches, possibly carrying carboxyl groups, the higher viscosities exhibited by the Carbopol-water systems are thought to be a result of the influence of this branched structure. Even though the unionized polymer molecule may be somewhat coiled, it is most likely more extended than would be expected for the unionized case, due to the steric hindrance of coiling because of the branches.

Yield Stresses

For the Carbopol-water dispersions, the yield stress at which permanent deformation occurs in plane shear was found to be a clearly defined property in the stated conditions of time of test and method of application of stress. It was rapidly and reversibly restored after deformation in flow. Measurement in a cone-plate apparatus is believed to be free from effects of yield in compression and undefined flow which are involved when penetrometer types of experimental arrangements are used.

The variation of the yield stress with conditions of polymer ionization, concentration, and temperature resembles that found for the viscosity, and the changes may be explained in terms of extension of the polyelectrolyte according to the degree of ionization and the ionic strength. It is, however, difficult to understand the origin of the extremely large molecular interactions which immobilize 5% Carbopol-water dispersions at shear stresses up to 1600 dynes cm.^{-2} . The presence of carboxyl groups along the Carbopol chain is not sufficient to explain the yield stress results, since carboxyl groups are also present in polyacrylic acid, for which flow occurs in water dispersions under very low shear stresses. Again, the limiting yield stress may arise from the branching of the chain, which would be expected to reduce flexibility and extent of coiling of the unionized polymer, and restrict the freedom of translational motion of chain segments in contact. Extension of the unionized polymer must be incomplete, since on ionization the yield value is almost doubled, indicating further uncoiling.

Conclusions

1. Yield stresses of Carbopol-water dispersions required for permanent deformation may be related to the presence of chain branching in the carboxypolyethylene molecule.

2. Large variations of yield stress with degree of ionization of the Carbopol molecules parallel the change of viscosity of polyelectrolyte-water systems with ionization, and are similarly explained in terms of molecular extension based on charge repulsion and ionic strength.

3. At all conditions of pH, concentration, and temperature applied, and over the range of shear rate, up to 10^4 sec.^{-1} , in this investigation, an empirical equation,

$$\tau - \tau_y = AD^n$$

where the yield stress τ_y is one parameter, was found to describe the relation of the shear stress and the shear rate in flow.

This investigation was supported in part by grants from the Socony Mobil Oil Company, Inc. to the friction and lubrication program, Research Division, and from the Esso Education Foundation to the Chemistry Department, Rensselaer Polytechnic Institute. Acknowledgment is made of the assistance of Roger G. Mazlen and Edward M. Glannon in the initial phases of this work.

References

1. Dukes, W. A., *Rheology of Disperse Systems*, Pergamon, New York, 1959.
2. Singleterry, C. R., and E. E. Stone, *J. Colloid Sci.*, **6**, 171 (1951).
3. Renshaw, T. A., *Ind. Eng. Chem.*, **47**, 834 (1955).
4. Brown, G. L., and B. S. Garrett, *J. Appl. Polymer Sci.*, **1**, 283 (1959).
5. Weltman, R. N., *NLGI Spokesman*, **20**, No. 3, 34 (1956).
6. Bruss, H., *Schmieretechnik*, No. 3, 6 (1957).
7. Bauer, W. H., A. P. Finkelstein, D. O. Shuster, and S. E. Wiberley, *NLGI Spokesman*, **23**, 15 (1959).
8. Bauer, W. H., D. O. Shuster, and S. E. Wiberley, *Trans. Soc. Rheol.*, **2**, 315 (1960).
9. Bauer, W. H., A. P. Finkelstein, and S. E. Wiberley, *Trans. ASLE*, **2**, No. 3, 215 (1961).
10. Guertin, D. L., S. E. Wiberley, and W. H. Bauer, *J. Am. Oil Chemists' Soc.*, **33**, 172 (1956).
11. Swern, D., and O. D. Shreve, *Anal. Chem.*, **22**, 1498 (1950).
12. Freeman, N. K., *J. Am. Chem. Soc.*, **74**, 2523 (1952).
13. McElvain, S. M., *The Characterization of Organic Compounds*, Macmillan, New York, 1949, pp. 82-85 and 130-131.
14. McKennell, R., *Proc. Second Intern. Congr. Rheol.*, Oxford, **1953**, 350 (1954).
15. McKennell, R., *Anal. Chem.*, **28**, 1710 (1956).

16. Bauer, W. H., A. P. Finkelstein, C. A. Larom, and S. E. Wiberley, *Rev. Sci. Instr.*, **30**, 167 (1959).
17. Herschel, W. H., and R. Bulkley, *Kolloid-Z.*, **39**, 291 (1926).
18. Ferry, J. D., L. D. Grandine, Jr., and D. C. Udy, *J. Colloid Sci.*, **8**, 529 (1953).
19. Heckler, G. E., T. E. Newlin, D. M. Stern, R. A. Stratton, J. R. Witt, and J. D. Ferry, *J. Colloid Sci.*, **15**, 294 (1960).
20. Dodge, D. W., and A. B. Metzner, *A.I.Ch.E. Journal*, **5**, 189 (1959).
21. Philippoff, W., and F. H. Gaskins, *Trans. Soc. Rheol.*, **2**, 263 (1958).
22. Rogers, W. F., "Rheological and Wall-Building Properties of Drilling Fluids" (Chap. 7, pp. 228-277), in *Composition and Properties of Oil Well Drilling Fluids*, Gulf Publication Co., Houston, Texas, 1953.

Synopsis

Dispersions of carboxypolymethylene (Carbopol) in water were found to exhibit sharply defined yield stresses, rapidly restored after imposed flow, as shown by stress relaxation measurements made with a cone and plate viscometer. Flow curves, rate of shear versus shearing stress, exhibited marked shear rate thinning, with little or no hysteresis. Effects of variation of concentration, pH, and temperature were investigated. A relation between shear stress and rate of shear involving yield stress as a parameter is discussed.

Upper Newtonian Regime in Polymer Solutions.

I. Polystyrenes in Toluene

E. W. MERRILL, H. S. MICKLEY, A. RAM, and G. PERKINSON,

*Department of Chemical Engineering, Massachusetts Institute of
Technology, Cambridge, Massachusetts*

Introduction

Philippoff¹ was the first to show that in solutions of polymers of moderate concentration, the apparent viscosity (defined as shear stress/shear rate) decreases with increase of shear rate, until at sufficiently high rates of shear (ca. 10^5 sec.^{-1}) it becomes constant in the upper Newtonian regime. In the publications¹ cited, one finds reference only to polymer solutions in which the macromolecules are solvated random coils (in contradistinction to rigid rodlike particles), and only to polymers of a molecular weight which would be commonly recognized as "medium" to "high."

From analysis of data obtained by Brodnyan, Gaskins, and Philippoff² on a commercial high-molecular weight grade of polyisobutylene dissolved in solutions of various concentrations in decalin, it was discovered³ that in the upper Newtonian regime the viscosity of a solution of any one of several concentrations was such that the upper Newtonian viscosity number* (UNVN) was constant, independent of the concentration.

Constancy of UNVN indicates that the macromolecules are contributing individually (i.e., additively) to the whole viscosity of the solution, and for this reason, if for no other, the upper Newtonian viscosity regime would appear to be important to polymer physics. In the range of low concentrations of polymer solutions accessible to

* η = solution viscosity; η_s = solvent viscosity; $\eta_{sp} = (\eta - \eta_s)/\eta_s$ = specific viscosity; η_{sp}/c = viscosity number, where c = concentration of polymer in g./dl.; $[\eta] = \lim_{c \rightarrow 0} (\eta_{sp}/c)$ = intrinsic viscosity.

examination in Ubbelohde or Ostwald capillary viscometers (for the purpose of extrapolating to zero concentration, thereby obtaining the intrinsic viscosity, and from this the molecular weight), the viscosity number is never found to be independent of the concentration. Further, in these conventional instruments for intrinsic viscosity determination, there is some question as to whether the polymer solution is in Newtonian flow. In several recent papers, the practice of double extrapolation, not only to zero concentration but also to zero shear rate, is advocated. Claesson¹ in a meticulous study of *very dilute* solutions down to shear rates as low as 10^{-3} sec.⁻¹ (compared to the usual capillary values of 10^2 to 10^3) found no definite evidence of the lower Newtonian regime. The lower Newtonian regime, so clearly evident in the various papers of Philippoff, appears in conjunction with levels of concentration under which network association of crowded polymer molecules seems likely. As shown by Lodge,⁵ the rheology of a liquid, the flow of which is controlled by the destruction and rebuilding of network aggregates, should be Newtonian below a certain value of shear stress. No such definite limit, below which Newtonian flow is to be expected, can be cited from theory for *individual* random coiling macromolecules in solution, i.e., in concentrations so low that the macromolecules act effectively as solvated spheres separated from each other by pure solvent.

Experimental

Viscometry

The polystyrene solutions were studied at shear rates up to 96,000 sec.⁻¹ on a coaxial cylinder viscometer,⁶ whereas previous investigators have used high pressure capillary instruments. In the coaxial cylinder viscometer used,⁶ the bottomless gap between cylinders is so narrow that the fluid under test drains slowly into the annular gap and keeps it full, the excess overflowing at the top and the bottom. The quantity of liquid in the gap at any time is about 0.6 ml. Because of the small width of the gap (compared to the cylindrical radius) the shear stress and shear rate are respectively uniform (to within $\pm 0.6\%$) in all elements of the fluid.

The shear stress is detected electrically through a strain cell torque transducer connected to the stationary cylinder, and the shear rate is detected as the signal from a tachometer generator geared to the

rotating cylinder. These signals are supplied to an x-y recorder. The viscometer operates automatically. The curve of shear stress versus shear rate is plotted from 0 to 96,000 sec.^{-1} of shear rate in 9.6 sec., and returns to 0 in another 9.6 sec. (shear rate increases or decreases at the rate of 10,000 $\text{sec.}^{-1}/\text{sec.}$).

The temperature of the liquid under test in the annular gap of the coaxial cylinder viscometer is within 1°C. of the temperature of the thermostatted coolant pumped through rotor and stator cylinders in circumferential channels separated from the annulus by 0.060-in. metal walls.

It was anticipated from the studies of G. I. Taylor that instability in the laminar flow of liquid in the annulus of the particular coaxial cylinder viscometer used in these studies would occur at shear rates exceeding 2.36×10^6 times the kinematic viscosity (in stokes). By direct experiment on simple Newtonian solvents (water, cyclohexane, benzene, decalin, 1,2-dichlorobenzene, MEK), it was found that instability occurred with remarkable uniformity when the shear rate exceeded 2.76×10^6 times the kinematic viscosity. In the case of these Newtonian solvents, above the critical shear rate, the shear stress versus shear rate relation (1) increases abruptly in slope by a factor of about 3.5 (times the slope in the laminar flow regime) and (2) remains almost linear, extrapolating back to a large negative value of shear stress at zero shear rate.

For polymer solutions, the onset of turbulence was found to show up in the same way, viz., sudden increase of slope of the shear stress-shear rate relation, forming with higher shear rates a straight line passing well below the origin.

The Polystyrenes

Of the nine polystyrenes listed in Table I, six were synthesized anionically (and thus with a narrow molecular weight distribution) and were supplied by Dow Chemical Company. These are listed with the Dow S-prefixed numbers. Monsanto Chemical Co. supplied two whole polymers, identified in Table I as RL-35-K3 and Erin 2CL/HS, and a fractionated polymer, identified as fp.

In general the procedure for making a solution of the polymer for viscometric testing consisted of the following steps in sequence: weighing out an appropriate amount of polymer, placing this in a volumetric flask, adding about two-thirds of the required reagent grade

TABLE I

Polystyrene Designation	$[\eta]_0^a$	\bar{M}_n^c	\bar{M}_v^b	\bar{M}_w^e	$[\eta]_{0.01}$	$\frac{d[\text{LSVN}]}{dc}$	$\frac{d[\text{UNVN}]}{dc}$	Huggins' k^e from LSVN	Huggins' k^e from UNVN
S103	0.52	118,000	113,500	123,000	0.47	0.11	0.11	0.406	0.406
S105	0.61	147,500	141,900	152,000	0.52	—	—	—	—
S109	0.70	182,000	171,800	193,000	0.67	—	—	—	—
Erin 2CL HS	0.78	—	201,000	220,000 ^d	0.74	0.24	0.17	0.394	0.288
S108	0.87	247,000	234,000	261,000	0.84	0.31	0.22	0.406	0.288
RL-35-K3	1.16	—	351,000	390,000 ^d	1.12	0.55	0.25	0.41	0.186
fp	(2.605)	—	1,100,000 ^d	—	2.3 ^f	—	—	—	—
S12	2.75	1,002,000	1,175,000	1,197,000	2.55	—	0	—	0
S114	6.32	2,820,000	3,730,000	3,500,000	3.55	—	0	—	0

^a Measured in toluene at 25°C.^b From "g" using: $[\eta]_0 = 1.34 \times 10^{-4} \bar{M}_v^{0.71}$.^c As reported by Dow Chemical Co., except as otherwise noted.^d As reported by Monsanto Chemical Co.^e Calculated as: $k = \frac{d(\eta_{sp}/c)/dc}{[\eta]^2}$.^f Accuracy very poor, due to lack of points.

toluene (Baker's), sealing the flask, letting it stand 2 days, rotating the flask end over end on a mechanical frame 30 times per minute for 24 hr., adding solvent to bring to the mark, and mixing by hand manipulation of the flask. No propeller stirring or other high shear means of preparation was used.

The high shear rate viscometry was performed in all cases with coolant circulating through rotor and stator of the coaxial cylinder viscometer. Because the solution is forced through a tube flushed externally with the thermostatted coolant, in its passage from the filling syringe on the stator cylinder to the annular gap, it arrives at the gap at the temperature of the coolant. The heat capacity of the coolant streams and of the brass rotor and stator is so large relative to that of the liquid under test that the test liquid is brought to its test temperature before it arrives in the annulus regardless of the temperature at which it is supplied to the reservoir.

Low shear rate viscometry was carried out in Ubbelohde-type dilution viscometers, made according to a design of Prof. P. M. Doty and described elsewhere.⁷

All viscometry reported herein was carried out at 25°C., at which temperature the viscosity of the pure solvent (toluene) was taken as 0.55 cps.

Results

Figure 1 shows an original recorder plot of shear stress versus shear rate. From the upper Newtonian viscosity, η_{un} measured as the slope of the straight line that coincides with the straight section of the

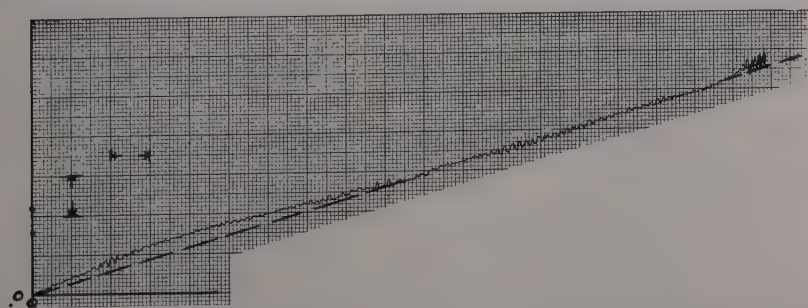


Fig. 1. Original recorder plot of shear stress (ordinate) versus shear rate (abscissa). Ordinate division shown = 500 dynes/cm.². Abscissa division shown = 5000 sec.⁻¹.

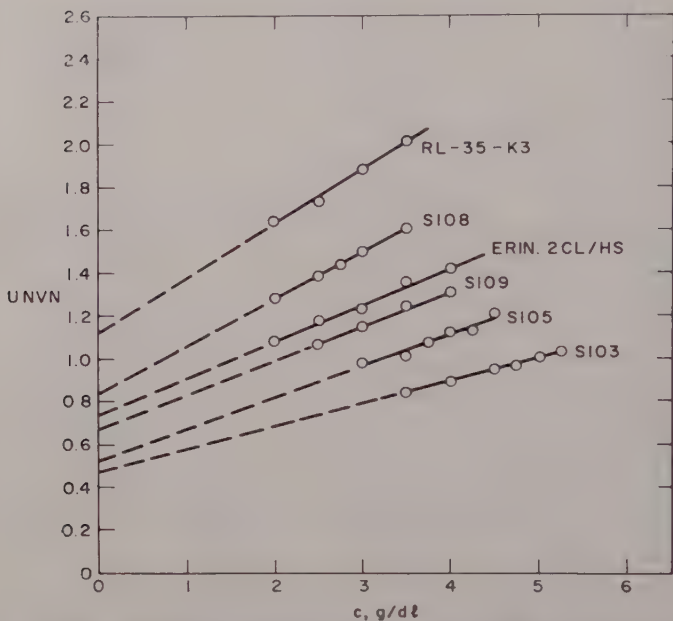


Fig. 2. Upper Newtonian viscosity number UNVN versus concentration of polystyrene in toluene, g./dl. at 25°C. Number against each curve refers to designation of species in Table I.

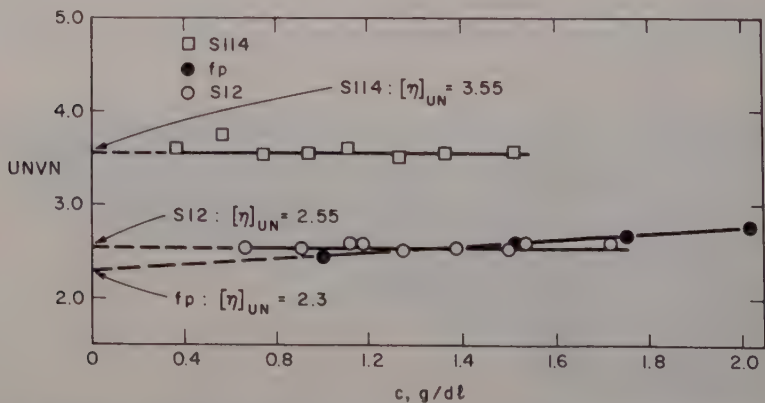


Fig. 3. Upper Newtonian viscosity number UNVN versus concentration of polystyrene in toluene, g./dl., at 25°C. Designations S12, S114, and fp from Table I.

experimental curve and extrapolates *through the origin*, the upper Newtonian specific viscosity and viscosity number are calculated as, respectively:

$$\text{UNSP} = (\eta_{\text{un}} - \eta_s)/\eta_s$$

and

$$\text{UNVN} = (\eta_{\text{un}} - \eta_s)/\eta_s c$$

where c = polymer concentration in g./dl. and η_s = solvent viscosity.

Figures 2 and 3 show the variation of UNVN with c , computed from recorder plots similar to that of Figure 1.

Contrary to expectation,³ the polystyrenes of molecular weight 390,000 and less show a definite decrease of UNVN with c , whereas the two high molecular weight anionic polymers S12 and S114 show no variation of UNVN with c . In Table I, the intrinsic viscosities $[\eta]_{\text{un}}$ of the upper Newtonian regime, obtained by extrapolation of the data of Figure 2 to $c = 0$, and as the mean values of UNVN in Figure 3, are compared with the conventional intrinsic viscosities. The values of $[\eta]_{\text{un}}$ are plotted in Figure 4 in relation to the equation from which the viscosity-average molecular weights of polystyrene in toluene at 25°C. was calculated, viz:

$$[\eta]_0 = 1.34 \times 10^{-4} \bar{M}_v^{0.71}$$

Contrary to expectation,³ the polystyrenes up through S12 (1,175,000 MW) show an upper Newtonian intrinsic viscosity $[\eta]_{\text{un}}$ that is almost identical to that for the low shear regime $[\eta]_0$. Thus $[\eta]_{\text{un}}$ varies as the 0.7 power of \bar{M}_v , approximately, not the 0.5 power as anticipated.³ The highest molecular weight species, S114, shows a much lower $[\eta]_{\text{un}}$ than $[\eta]_0$.

Without further data at hand it is fruitless to speculate on how $[\eta]_{\text{un}}$ varies with \bar{M}_v when \bar{M}_v exceeds 1.2×10^6 (anionic type S12).

The experiments reported are sufficiently complete, however, to establish clearly that the Huggins' constant k , while remaining constant at 0.40 as evaluated from *Ubbelohde data*, decreases progressively from 0.40 for the lowest molecular weight species (113,500 MW) to zero, when evaluated from $[\eta]_{\text{un}}$ and the tangent slopes $d(\text{UNVN})/dc$ at $c = 0$ in Figures 2 and 3. (The limited data given in Fig. 3 on the fractionated polymer fp, the average molecular weight of which is nearly identical to that of S12, suggest a concentration dependence of UNVN on c . This poses the question, which cannot be answered

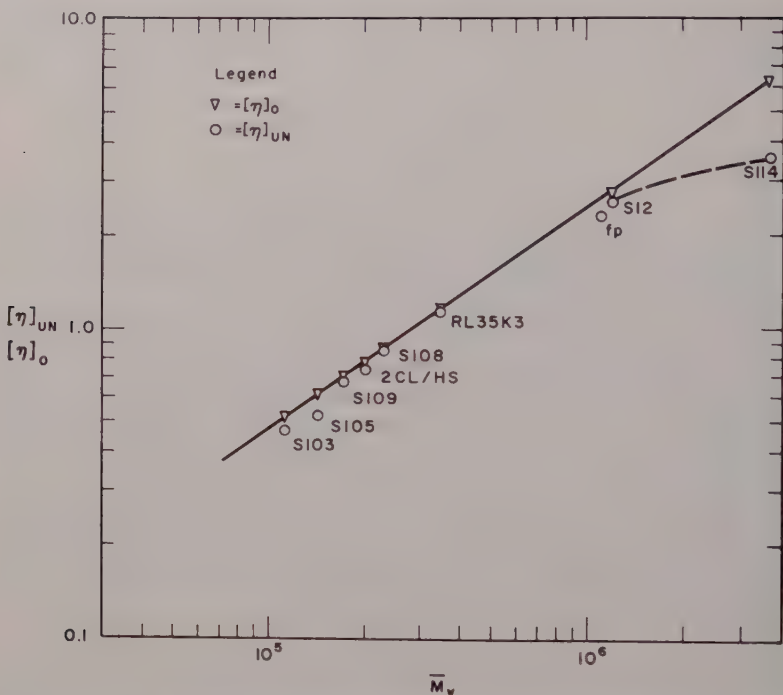


Fig. 4. Upper Newtonian intrinsic viscosity $[\eta]_{un}$ and conventional low shear intrinsic viscosity $[\eta]_0$ versus viscosity-average molecular weight M_v for polystyrenes in toluene at 25°C.

without further experiment, as to whether the fractionated polymer in fact contains sufficient low molecular weight species to introduce the UNVN dependence on c exhibited by the species shown in Fig. 2. The *anionic* polymer S12 should contain a completely negligible amount of polymer less than 1.0×10^6 in molecular weight.)

These results have led us to make a detailed re-examination of the viscosities of polyisobutylenes in the upper Newtonian regime, which has been thwarted in part by the complications of finding a true intrinsic viscosity $[\eta]_0$ on the high molecular species.⁷ It is possible, nonetheless, to report two facts that are in contradiction to the data originally reported.³ These are:

(1) The low molecular weight polyisobutylenes (Vistanex grades LMMS and LMMH, ca. 50,000 MW) show a decrease of UNVN with

decrease of c , which was missed in the original observation. For these low molecular weight species, the value of $[\eta]_{\text{un}}$ obtained by extrapolation of UNVN vs. c to $c = 0$, turns out to be about equal to the standard value $[\eta]_0$ (approximately 0.48) in the same solvent at the same temperature.

(2) It is clearly established that the value of the $[\eta]_{\text{un}}$ varies, for a given polymer, from solvent to solvent, though to a lesser degree than the values of $[\eta]_0$ between the same solvents. The original intercomparison of data³ that led to identity of $[\eta]_{\text{un}}$ for various polyisobutylenes in different solvents proved to be erroneous in one part (*o*-dichlorobenzene and hexadecane) because of a misreported capillary diameter in one of the references. The other parts of the intercomparison still stand, but are thrown in doubt because of our inability to find experimentally the values obtained by Brodnyan² for a polyisobutylene in decalin, and by the phenomena observed in benzene solutions of polyisobutylene, which conceivably may be a manifestation of turbulence.

Discussion

The data obtained on polystyrenes, reported herein, are partly in accord with, and partly contrary to, previous findings. Extensive further experimental study appears desirable. On our part, the immediate areas of investigation are the variation of $[\eta]_{\text{un}}$ with solvent for polystyrenes, polyisobutylenes, and other linear polymers, the transition from dependence to independence of UNVN on c , and the variation of $[\eta]_{\text{un}}$ with M above this transition.

We wish to acknowledge with pleasure the comments of Dr. Philippoff, after whom the upper Newtonian regime should appropriately be named. Dr. Philippoff reports⁸ that in his experimental work on low molecular polymers (such as the polyisobutylenes of Ref. 3 of ca. 50,000 MW), he was unable to demonstrate the existence of the upper Newtonian regime and makes the criticism, which appears entirely correct, that the limited range of shear rate over which the upper Newtonian region was observed on the low molecular weight polymers may introduce an experimental artifact that would be resolved if the range of shear rate measurement were extended over a decade.

Brodnyan⁹ observed for polyacrylic acid of 180,000 MW, in varying degrees of neutralization, a clearly defined UNVN which decreased with c , and called our attention to the similarity of this trend

in polyacrylic acid solutions to that noted herein for polystyrene of approximately the same chain length (e.g., S109).

The generous aid of E. I. du Pont Film Division is gratefully acknowledged, as is the continuing cooperation of Dow Chemical Co., Enjay Co., Rohm & Haas, and Monsanto Chemical Co. in supplying fractionated, anionic, and other well-characterized polymers.

References

1. Philippoff, W., and K. Hess, *Z. physik. Chem.*, **B31**, 237 (1936).
2. Brodnyan, J. G., F. H. Gaskins, and W. Philippoff, *Trans. Soc. Rheology*, **1**, 109 (1957).
3. Merrill, E. W., *J. Polymer Sci.*, **38**, 539 (1959).
4. Claesson, S. (Uppsala). Lecture sponsored by Department of Chemistry, M.I.T., at M.I.T., March, 1960.
5. Lodge, A. S., *Trans. Faraday Soc.*, **52**, 120 (1956).
6. Merrill, E. W., "Viscometry of Polymer Solutions in a Coaxial Cylinder Viscometer Under High Rates of Shear," to be published in Proceedings of ASTM Symposium on Non-Newtonian Viscometry, Washington, 1960.
7. Merrill, E. W., "Effect of Shear on the Intrinsic Viscosity of a Whole Polymer in Solution," *J. Polymer Sci.*, in press.
8. Philippoff, W., private communication.
9. Brodnyan, J. G., private communication, and with E. L. Kelley, this volume, p. 205.

Synopsis

Polystyrenes of various molecular weights were dissolved in toluene, at various concentrations, and the viscosity number of each solution was determined as a function of concentration by (1) a conventional Ubbelohde capillary viscometer and (2) from the constant viscosity observed in the upper Newtonian regime (shear rate ca. $100,000 \text{ sec.}^{-1}$) by means of a coaxial cylinder viscometer.

It was found that the intrinsic viscosities (viscosity number extrapolated to zero concentration) for a given polymer, determined respectively from the Ubbelohde viscometer and in the upper Newtonian regime, were nearly identical up to a molecular weight of ca. 1.1×10^6 but significantly diverged for a species of 3.7×10^6 MW, the upper Newtonian intrinsic viscosity being about half the Ubbelohde value. Further, as molecular weight increased, the Huggins' constant k , determined from the upper Newtonian regime data, decreased as molecular weight increased and became zero for anionic polystyrenes of 1.1×10^6 and 3.7×10^6 MW.

An Equation for Non-Newtonian Flow

RALPH SHANGRAW, WAYNE GRIM, and ALBERT M. MATTOCKS, *College of Pharmacy, University of Michigan, Ann Arbor, Michigan*

The M-2 Viscometer

It was the purpose of this work to investigate non-Newtonian flow and to obtain information which would be useful to the formulation of pharmaceutical suspensions and emulsions. Experience with several commercially available viscometers indicated that a rotating-bob instrument would be most useful for such systems, and a machine of this type was designed and built in these laboratories. The instrument, called the M-2 Viscometer, is shown in diagrammatic sketch in Figure 1. The cup is driven by a d.c., thyatron-controlled motor, the speed of which is regulated by a potentiometer. A tachometer generator connected to the motor transmits a d.c. signal proportional to the rate of shear to the Y-axis of an X-Y recorder. Torque on the bob is transmitted from a lever arm to a force transducer, thence through a d.c. amplifier and filter to the X-axis of the recorder. A control unit is used to change the speed of cup rotation automatically, normally increasing speed from zero to some predetermined value then decreasing it again to zero at a constant rate of change. This is achieved through the use of a small synchronous motor connected by gears to a shaft attached to the speed-controlling potentiometer. On the shaft is a pair of metal "fingers" which contact a microswitch to reverse direction of the synchronous motor. By changing the gears linking the potentiometer shaft and synchronous motor the rate of change of shear can be varied. In addition to the X-Y recorder, a digital print-out system is frequently used. In this case, the X and Y signals are also coupled with two digital voltmeters (Model 20-C, F. L. Moseley Co.) and a numerical data printer (Model 1900, Clary Corp.), and a suitable switch is connected to the potentiometer shaft to activate the print-out system.

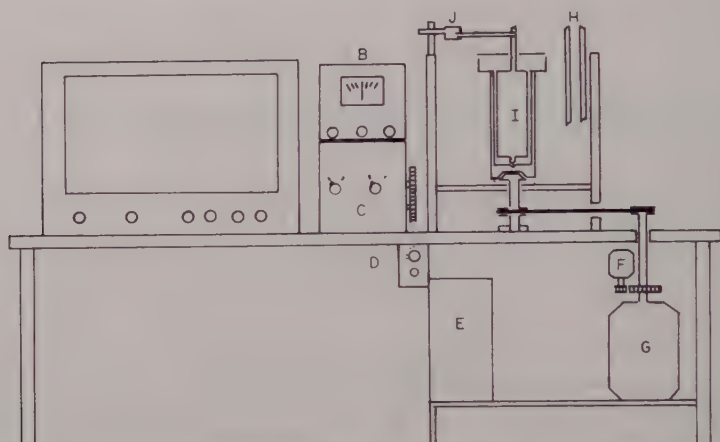


Fig. 1. Diagrammatic sketch of M-2 Viscometer. (A) Recorder; (B) amplifier; (C) control box; (D) manual potentiometer; (E) thyatron control; (F) tachometer; (G) motor; (H) temperature control unit; (I) cup and bob unit; (J) strain gage.

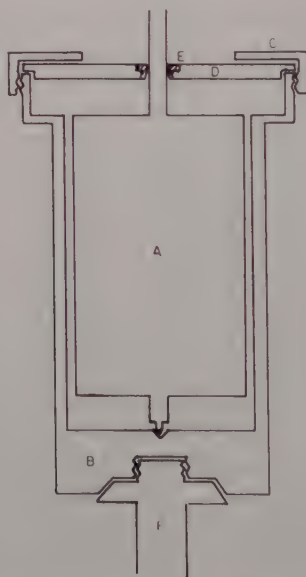


Fig. 2. Detail sketch of cup and bob and drive assembly. (A) Bob; (B) cup; (C) screw cap; (D) lid; (E) Oilite bushing; (F) drive shaft.

A more detailed sketch of the cup and bob is presented in Figure 2, and one of the control unit is shown in Figure 3. A list of components of the viscometer is given in Table I. Accurate cup and bob dimensions and "working constants" for converting r.p.m. to rate of shear and torque to stress are given in Table II.

TABLE I
Components of the M-2 Viscometer

Part	Description	Supplier
Motor	Master Speedranger motor, $\frac{1}{4}$ h.p., style 252945, with thyatron control and feedback system (0-500 r.p.m.)	Master Electric Co., Dayton, Ohio
Tachometer	Weston d.c. tachometer generator, type 750-A output 0-12 v.	Weston Electric Co., Newark, N. J.
Strain gages	Statham Model G-1 transducers, 1.5, 4, 8, 16, 32, and 80 oz. capacities.	Statham Instruments, Hato Rey, Puerto Rico
Amplifier	D.c. bridge amplifier and meter, model BAM-1, 12 v. bridge supply.	Ellis Associates, Pelham, N. Y.
Recorder	Librascope X-Y recorder, model 200-B.	Librascope, Inc., Glendale, Calif.
Potentiometer motor	Bodine synchronous motor, 9.3 r.p.m., 110 v., A.C.	Bodine Electric Co., Chicago, Ill.
Microswitch	Reversible Microswitch, Model BZ-RSX	Microswitch Co., Freeport, Ill.
Temperature controller	Sargent Laboratory relay, merc-to-merc regulator and 300-w. immersion heater.	Eberbach Laboratory Supply Co., Ann Arbor, Mich.

It should be noted that three equations are available for converting rotational velocity to average rate of shear. The first of these, called the Average Equation, calculates the rate of shear for the layer of liquid next to the cup and that next to the bob and averages the two. The second is that presented by Fischer¹ who integrated the expression for change of shear with radius of the layer and divided by the change in radius from cup to bob. This amounts to a summation of the rates of shear over individual layers divided by the number of

TABLE II
Cup and Bob Dimensions and Instrument Constants

Dimension or constant	Value
Inside radius of cup	4.6025 cm.
Radius of bob	4.5199 cm.
Height of bob	19.4310 cm.
Lever arm	11.3488 cm.
K_s	5.7857 ^a
K_f	$3.937 \times 10^{-4} \text{ cm.}^{-2}$

^a Dimensionless.

layers. The third equation is that of Andrade² who summed the shear over the total area and divided by the sum of the areas. The three equations are as follows:

Average Equation:

$$S = \frac{R_b^2 R_c^2}{R_c^2 - R_b^2} \left[\frac{1}{R_c^2} + \frac{1}{R_b^2} \right] \Omega \quad (1)$$

Fischer's Equation:

$$S = \frac{2R_c R_b}{R_c^2 - R_b^2} \Omega \quad (2)$$

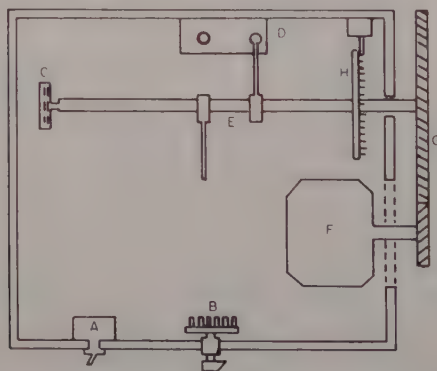


Fig. 3. Sketch of control unit for M-2 viscometer. (A) Motor switch; (B) manual-automatic selector switch; (C) potentiometer for automatic speed control; (D) motor reversing microswitch; (E) adjustable microswitch contacts; (F) synchronous motor; (G) changeable gears; (H) print-out switch.

Andrade's Equation:

$$S = \frac{4R_b^2 R_c^2}{(R_c^2 - R_b^2)^2} \ln R_c/R_b(\Omega) \quad (3)$$

where S is average rate of shear, Ω is rotational velocity, and R_c and R_b are radius of cup and bob, respectively. Of these, the equation of Andrade appears to be the one of choice, since force is transmitted proportionally to areas of adjacent layers. With sufficiently small gaps between cup and bob, however, as was the case with the M-2 viscometer, the three equations give essentially the same values for shear constants.

A similar constant was used to relate torque to average stress within the gap. One equation, derived by Samyn,³ sums the force per unit area over the various layers and divides it by the number of layers. A second, derived by Shangraw,⁴ sums the total force on individual layers and divides this by the sum of individual areas. The two equations are:

Samyn's Equation:

$$F = \frac{T}{2\pi h R_c R_b} \quad (4)$$

Shangraw's Equation:

$$F = \frac{T \ln R_c/R_b}{\pi h (R^2 - R_b^2)} \quad (5)$$

where T is torque, h is height of bob, and R_c and R_b are radius of cup and bob, respectively. Shangraw's equation is thought to be better for the same reason Andrade's equation was selected, but again it was found that for small annulus the values were nearly identical.

Tests for end-effect were conducted by measuring standard glycerin samples, and the deviations obtained were so small as to be negligible; thus shear and stress constants were used as indicated without corrections. As a result of experience with other instruments, possible accumulation of heat within the layer of liquid being sheared was of some concern, and a series of tests was performed to see if this might occur in the M-2 Viscometer. Glycerin samples were sheared at high rates over a period of 1 hr., with frequent up- and downcurves being run. Deviations between the curves were negligible; thus no heat

accumulation was detected. Tests of this sort have been made at numerous times, both with Newtonian and non-Newtonian materials, with the same results.

Shear-Stress Data

A large number of solutions of suspending agents, suspensions of solids in various aqueous media, and emulsions have been measured, and the shear-stress data are available.⁴⁻⁶

Selection of an Equation

Numerous empirical equations and several with a theoretical basis have been proposed to describe non-Newtonian flow, and these were examined as to applicability to several sets of shear-stress data. The exponential equation which has been used,⁷ $S = aF^b$, and a polynomial equation, $F = b_1S + b_2S^2$, fitted only limited segments of the curve. A polynomial with constant term, $F = b_0 + b_1S + b_2S^2$, fitted a larger portion of the curve, but still was not adequate. The Ree-Eyring Equation⁸ was tested graphically, but the plot of η_a vs. $1/S$ showed increasing curvature at low values of $1/S$, making extrapolation to zero to obtain a value for η_a unreasonable. When a value of η_a was approximated and plotted vs. S , this curve was also nonlinear throughout, making extrapolation difficult. The method of Maron and co-workers⁹ was attempted, in which arbitrary values for one of the constants are tested with a linear form of the Ree-Eyring equation until a value is found which gives a linear plot. By this method it was found that little changes in slopes occurred with large changes in arbitrary value, so that the procedure was not satisfactory for these data.

The Williamson Equation,¹⁰ $F = [fS/(s + S)] + \eta_a S$, where f , s , and η_a , are constants, was of considerable interest, since it had been noted to have physical meaning.¹¹ The methods proposed for evaluating its constants, however, depended either on having measurements at extreme shear rates from which f and η_a could be obtained graphically, or on the use of three data points to evaluate the three constants. As might be expected, the use of the latter method yielded constants considerably different with different sets of data points. In order to utilize all of the flow data in evaluating the constants of Williamson's Equation, it was converted to the linear form:

$$F = f + \eta_\alpha s + \eta_\alpha S - sF/S \quad (6)$$

or

$$F = b_0 + b_1 S + b_2 F/S \quad (7)$$

where b_0 is $f + \eta_\alpha s$, b_1 is η_α , and b_2 is $-s$. In this form the constants can be readily evaluated by least squares. The equation, evaluated in this manner, was found to fit a large number of flow curves exceedingly well, standard errors of estimate being within 1% in practically all cases.

In spite of the excellence of fit of the Williamson Equation, there were three objections to its use. (1) The expression for viscoelastic resistance, F_1 , which is.

$$F_1 = fS/(s + S) \quad (8)$$

was selected arbitrarily as a simple hyperbolic function without physical reason. (2) The asymptote to the curve, described by.

$$F_2 = f + \eta_\alpha S$$

appeared to be too far removed from the curve when compared to actual flow curves. (3) The constants of the equation did not vary in an orderly fashion as one increased the concentration of a suspended solid or thickening agent. For these reasons, a more critical examination was made of the hyperbolic portion of the equation.

The resistance to viscoelastic flow can be calculated from the Williamson Equation as follows:

$$F_1 = fS/(s + S) = F - \eta_\alpha S \quad (9)$$

and the hyperbolic equation may be converted to linear form:

$$1/F_1 = 1/f + (s/f)(1/S) \quad (10)$$

Thus, a plot of $1/F_1$ vs. $1/S$ should be linear. A graph of this type is illustrated in Figure 4, where it is seen that experimental values in upper and lower regions of shear show a trend away from linearity. This indicates that the hyperbolic representation of viscoelastic resistance is not an accurate representation of the data, and a new function is needed.

The linear portion of the flow curve, at high shear rates, is not adequately described by a single constant, since it would not ex-

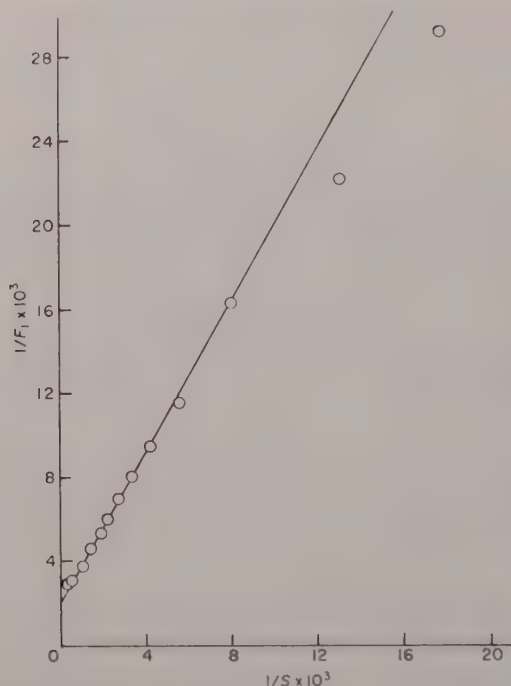


Fig. 4. Viscoelastic resistance to flow as shown by the Williamson equation; 20.18% v/v salicyalimide in 0.87% w/w methyl cellulose 1500 cps.

trapolate to the origin. It was decided to represent this portion of the curve by the equation for a plastic:

$$F_2 = f + \eta_a S \quad (11)$$

This represents the ultimate flow curve obtained after overcoming viscoelastic resistance. Viscoelastic resistance decreases with increasing rate of shear, and may be said to decrease at a rate proportional to the amount of resistance yet present; thus:

$$dF_1/dS = -aF_1 \quad (12)$$

where a is the constant of proportionality. Rearranging and integrating gives:

$$\ln F_1 = -aS + I \quad (13)$$

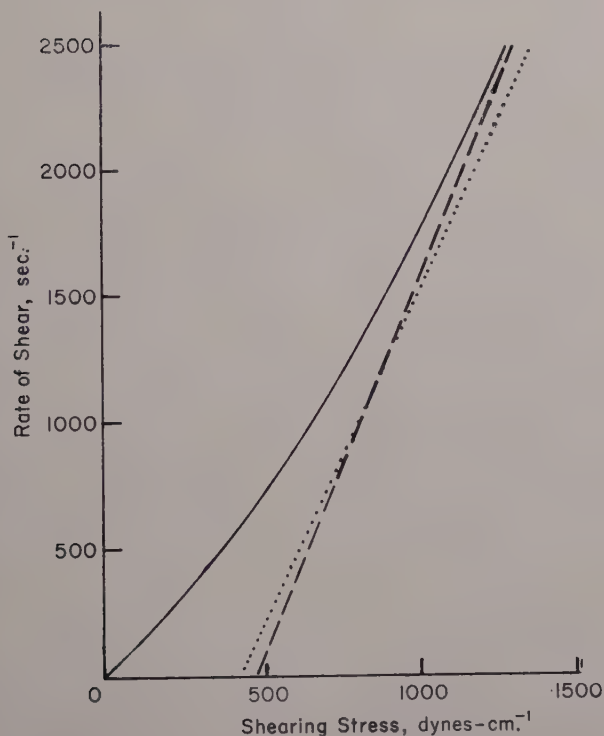


Fig. 5. Relationship of the asymptotes of the Williamson and Structure Equations to the experimental flow curve; 20.18% v/v salicylamide in 0.87% methylcellulose 1500 cps. (—) Experimental flow curve. (--) Asymptote from the Structure Equation. (··) Asymptote from Williamson's Equation.

or:

$$F_1 = b_e e^{-aS} \quad (14)$$

where b_e is called the coefficient of viscoelastic resistance. Combining the two functions one obtains:

$$F = F_1 + F_2 = f + \eta_a S - b_e e^{-aS} \quad (15)$$

which is called the Structure Equation.

The Structure Equation would be difficult to evaluate without knowing the value for a . An arbitrary value of 0.001 has been used, this being essentially fixed in order that values of e^{-aS} have a useful magnitude.

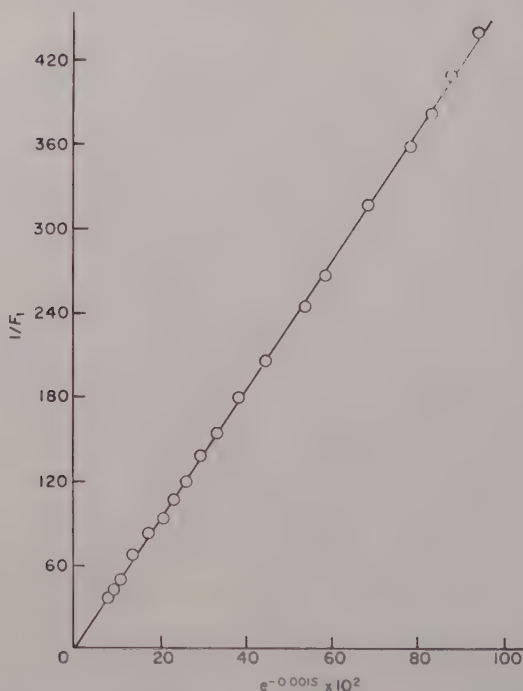


Fig. 6. Viscoelastic resistance to flow as shown by the Structure Equation; 20.18% v/v salicylamide in 0.87% w/w methyl cellulose 1500 cps.

Applying the Structure Equation to experimental data, using least squares, excellent fit was obtained. Over a large amount of data the standard error of estimate has consistently been 1% or less. The fit of the asymptote to the curve is much more satisfactory than with the Williamson equation, as illustrated in Figure 5, and the function for viscoelastic resistance appears to be an accurate representation of the data (Fig. 6). Further, the constants of the equation consistently increase with increases in concentration of suspending agent or solid in suspension. Constants for a typical set of suspensions⁵ are listed in Table III.

The Structure Equation can be used to calculate yield values for nonlinear flow curves:

$$\text{Yield Value} = \lim_{S \rightarrow 0} F = f - b_0 \quad (16)$$

TABLE III
 Constants of the Structure Equation [$F = f + \eta_{\infty}S - b_{\nu}e^{-0.001S}$]
 Suspensions of Salicylamide in
 Methyl Cellulose 1500 cps.^a

Concen- tration of salicyl- amide, % v/v	f	η_{∞}	b_{ν}	Concen- tration of salicyl- amide, % v/v	f	η_{∞}	b_{ν}
0.19% w/w ^b				1.16% w/w ^b			
0.0		0.03075		0.0	555.9	0.2420	0522.8
5.05		0.03180		5.78	679.4	0.2608	0641.5
10.32		0.03692		11.14	759.4	0.2898	0721.9
16.16		0.04376		15.79	938.8	0.3423	0882.8
21.13		0.05000		21.81	1268	0.4080	1202
27.43		0.06944		27.25	1431	0.5751	1344
0.43% w/w ^b				32.71	1993	0.7292	1876
0.0		0.07692		37.62	2875	1.074	2737
5.08		0.08623		43.28	5574	1.567	5375
10.53		0.09822		45.58	6949	1.810	6824
15.32		0.1171		1.59% w/w ^b			
19.80		0.1393		0.0	1634	0.2800	1507
26.10		0.1748		5.40	1981	0.2965	1806
31.12		0.2210		10.29	2205	0.3624	1985
0.87% w/w ^b				14.59	2766	0.3611	2509
0.0	220.0	0.1160	0212.7	19.69	3511	0.3937	3199
5.28	268.0	0.1922	0260.0	24.21	3773	0.5492	3415
10.36	308.0	0.2257	0294.5	28.07	5021	0.7281	4528
14.98	395.8	0.2571	0381.4	34.39	7454	0.9837	6754
20.18	474.2	0.3401	0458.3				
26.35	608.0	0.4482	0587.5				
30.43	741.2	0.5520	0721.1				
34.36	1345	0.9205	1319				
39.37	2402	1.370	2404				

^a Note: Suspensions in 0.19 and 0.43% methyl cellulose were Newtonian.

^b Methyl cellulose concentration.

since e^{-aS} approaches 1. Yield values calculated in this manner appear to fit experimental curves.

The limiting viscosity at low rates of shear, η_0 , which is of interest in applying the basic equations of Einstein, Taylor, and others, can be expressed as follows:

$$dF/dS = \eta_{\alpha} + ab_e e^{-aS} \quad (17)$$

and:

$$\lim_{S \rightarrow 0} dF/dS = \eta_{\alpha} + ab_v \quad (18)$$

Values of η_0 , so obtained, have been found to fit a reciprocal type of plot and fall on the same line with measured viscosities of the same system at lower concentrations where the flow is Newtonian (see Fig. 7). Thus, they follow the relationship pointed out by Ford:¹²

$$\phi/\phi_0 = 1 - aC_v$$

where a is Einstein's constant and C_v is the effective concentration times voluminosity, the latter term including a shape factor. The voluminosity obtained in this manner for the data in this paper varied with concentration of suspending agent, as shown in Table IV.

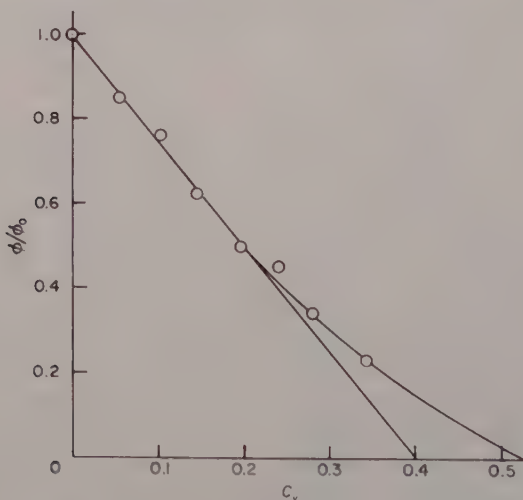


Fig. 7. Relative fluidity vs. volume concentration, suspensions of salicylamide in 1.597% methyl cellulose 1500 cps.

Further investigations into the relationship of η_0 from the Structure Equation to volume concentration of particles will be presented in a later paper. It appears, however, that use of the Structure Equation has promise in extensions of basic rheological concepts to non-Newtonian systems.

TABLE IV

Concentration, %, methyl cellulose	Voluminosity
0.19	0.872
0.43	0.889
0.87	0.909
1.16	0.889
1.59	1.000

The authors wish to acknowledge the contribution of Dr. T. Higuchi, University of Wisconsin, who suggested the logarithmic form for viscoelastic resistance.

References

1. Fischer, E. K., *Colloidal Dispersions*, Wiley, New York, 1950, p. 165.
2. Andrade, E. N. daC., *Viscosity and Plasticity*, Heffer, Cambridge, England, 1947, p. 41.
3. Samyn, J., *Rheology of Pharmaceutical Suspending Agents*, Ph.D. Dissertation, University of Michigan, 1957.
4. Shangraw, R., *Rheology of Methylcellulose Solutions*, Ph.D. Dissertation, University of Michigan, 1959.
5. Grim, W., *Rheology of Pharmaceutical Suspensions*, Ph.D. Dissertation, University of Michigan, 1959.
6. Sheth, B. B., *Rheology of Pharmaceutical Emulsions*, Ph.D. Dissertation, University of Michigan, 1960.
7. Fischer, E. K., and C. H. Lindsey, *J. Colloid Sci.*, **3**, 111 (1948); Farrow, F. D., et al., *J. Textile Inst.*, **19**, 18T (1928).
8. Ree, T., and H. Eyring, *J. Appl. Phys.*, **26**, 793 (1955).
9. Maron, S. H., and P. E. Pierce, *J. Colloid Sci.*, **11**, 80 (1956).
10. Williamson, R. V., *Ind. Eng. Chem.*, **21**, 1108, 1111 (1929).
11. *First Report on Viscosity and Plasticity*, Nordemann, New York, 1938, p. 169.
12. Ford, T. F., *J. Phys. Chem.*, **64**, 1168 (1960).

Synopsis

A rotating-cup viscometer, equipped with automatic program controls and two types of recording, an X—Y recorder and digital print-out, was developed. Using this equation numerous non-Newtonian systems have been measured, and various equations for describing non-Newtonian flow have been tested. The available equations were found inadequate, and a new equation, called the Structure Equation, was developed. The equation is as follows:

$$F = f + \eta_{\alpha}S - b_e e^{-a_s}$$

where F is shearing stress, S is rate of shear, f , η_α , b_r , and a are constants for a given system. The asymptote to the flow curve at high rates of shear is defined by its intercept, f , on the stress axis and its slope, η_α . Yield value is interpreted as $f - b_r$; a is an undefined constant which has the value of 0.001 for all systems yet studied. The viscosity at extremely low shear is defined as $\lim dF/dS$ which is $\eta_\alpha + ab_r$. Application of this equation to aqueous suspensions are presented.

The Frequency and Temperature Dependence of the Dynamic Mechanical Properties of a High Density Polyethylene

H. NAKAYASU,* H. MARKOVITZ, and D. J. PLAZEK, *Mellon
Institute, Pittsburgh, Pennsylvania*

In this report, the first on a series of proposed studies of the mechanical properties of crystalline polymers, we present data on the viscoelastic behavior of a high density polyethylene over a wide time scale and a considerable span of temperature. In the existing literature¹ on the subject, almost without exception² the data on dynamic mechanical properties on such materials have been obtained as a function of temperature by forced oscillation measurements³⁻⁵ at one frequency (or at most a limited number of frequencies) or by free vibration techniques⁶⁻⁹ at somewhat varying frequency. In addition, some investigations of stress relaxation have been reported.^{10,11}

We have paid special attention to the question whether, over the range of variables covered, the material exhibits linear viscoelastic behavior; i.e., whether its behavior is in accordance with that expected from the Boltzmann superposition principle.¹² We have also concerned ourselves with the question of how to adapt to our measurements the temperature-time equivalence principle which has been so useful in the study of amorphous polymers.^{13,14}

Experimental

Our polyethylene sample was prepared from Marlex 50 (Phillips Chemical Co., Bartlesville, Oklahoma) commercial pellets, which were placed in an open cavity mold in a vacuum oven. After replacing the air with nitrogen and evacuating, the oven was heated to 150°C. for

* Present address: Research Laboratory, Kurashiki Rayon Co., Sakazu, Kurashiki, Okayama, Japan.

about 5 hr. and then allowed to cool under vacuum. The open mold was then removed from the oven, covered, and placed in a press whose platens had been heated to 150°. After coming to temperature, a pressure of 1000 p.s.i., was applied to the mold which was then allowed to cool slowly (over a period of several hours). A strip 0.100 cm. wide, 0.093 cm. thick (both of these dimensions uniform to within $\pm 1.2\%$), and 3.61 cm. long was used for these measurements. The density was measured to be 0.9649 g./cm.³ at 23°C. by a density gradient tube method at the W. R. Grace & Co. Research Division through the kind courtesy of Mr. Louis Zapas.

Creep and dynamic mechanical properties were measured in torsion with the torsion pendulum instrument of Morrisson, Zapas, and DeWitt¹⁵ after some modifications were made. Because of the low loss of the material under investigation, it was especially important to reduce externally excited vibrations and to measure accurately the small phase angles between the driving current and the resultant torsional oscillation during forced dynamic measurements. To achieve the accuracy required, the method of measuring the phase angle was changed from that previously described. Using a technique similar to that developed elsewhere,¹⁶ the light beam reflected from the mirror attached to the top of the sample fell on a barrier-type photocell, the sinusoidal electrical output of which was fed to a galvanometer in a Model 621 direct recording oscillograph (Midwestern Instruments Inc., Tulsa, Oklahoma). The driving current went through another galvanometer in the same recorder. To avoid errors due to the slight variations in speed of the chart drive, timing signals (0.1, 1.2, 10, or 60 sec.) were recorded simultaneously with the other two on the chart paper whose speed could be varied from 0.2 to 3600 in./min. The frequency range of 1 cycle/hr. to 3 cycles/sec. could be covered. The instrument constants were obtained to a precision of about $\pm 1\%$. Free oscillation measurements were also made at each temperature from the recording of the damped sine wave. Thus dynamic measurements extended over almost five decades on the frequency scale.

For creep measurements, the deformation resulting from a constant current applied through the driving coil was recorded on a Beckman Photopen Recorder (National Technical Laboratories, South Pasadena, California), the pen of which followed the light beam reflected from the mirror which was connected rigidly to the top of the sample. The 35 cm. long, 0.001 in. tungsten wire which supported the coil form

required less than 1% of the torque used to twist the polyethylene strip. Data were obtained from a few seconds up to 3 days and thus covered five and one-half decades on the time scale for three of the temperatures.

As has been reported previously,^{17,18} the torsional response can be affected by the tension applied to the sample. An unbonded strain gage (Statham Laboratories, Inc., Los Angeles, California) was mounted in such a way that the longitudinal force on the sample could be adjusted and measured.

The length of the sample was measured in the apparatus at the various temperatures. These data together with published information¹⁹ on the variation of density with temperature was used to calculate the sample coefficient for each run.

In other respects the techniques, operating procedure, and calculations were carried out essentially as indicated in the original paper.¹⁵ In particular it should be noted that both creep and dynamic measurements could be performed on the same sample without removing it from the instrument.

The temperature, measured with a calibrated thermocouple placed next to the sample, was kept constant to within 0.5°C.

Results

The creep data, obtained at five temperatures, are presented in Figure 1 as a logarithmic plot of the time dependence of the creep compliance, $J(t)$. Although the curves for the higher temperatures are almost straight lines in this graph, the minor variations in slope are significant and, indeed, are required for consistency with the dynamic measurements.

The open points in Figures 2 and 3, showing the storage compliance, $J'(\omega)$, and loss compliance, $J''(\omega)$, respectively, as a function of the pulsance, $\omega = 2\pi$ times the frequency, are results of the forced oscillation dynamic measurements at ten temperatures from -30 to 80°C. The half-filled circles indicate results for free oscillation measurements. The agreement between the results of the free and forced vibration runs give us some confidence in the consistency of our instrument constants, since the former depend mostly on the moment of inertia of the oscillating system while the latter are mainly determined by the electromagnetic factors.

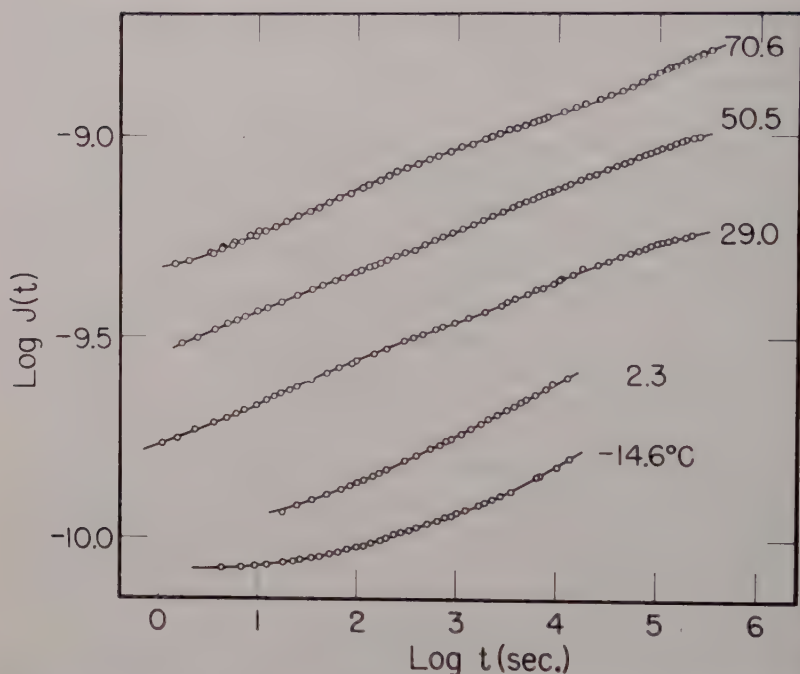


Fig. 1. Creep compliance, $J(t)$ (cm.²/dyne), for five temperatures plotted logarithmically against time (sec.).

Since our sample exhibited rather low loss, the phase angle between the current and motion was rather small, especially at the lower temperatures. For example, for the entire run at -29°C . the phase lag was less than 4.5° . Because of these small angles, the percentage error in their determination is correspondingly higher. This leads to greater uncertainties in $J''(\omega)$ from forced oscillations as indicated by the greater scatter of points at lower temperatures. Hence, in this region, we place more confidence in the points obtained from free vibration measurements since these are considerably more accurate. It is because of the increasing error in $J''(\omega)$ that data were not obtained at still lower temperatures.

Comparison of Creep and Dynamic Data

If a material exhibits linear viscoelastic behavior, the interrelationships among the various time-dependent properties are known. In

particular it should be possible to calculate the corresponding dynamic mechanical properties from creep data. Conversely, if such a calculation is made and agreement is found with measured values, this constitutes evidence of the validity of the Boltzmann superposition principle for that material over the range of variables investigated. The results of such computation are indicated by the completely filled circles in Figures 2 and 3. It is seen that the agreement is rather good for the two to two and one-half decades of overlap ob-

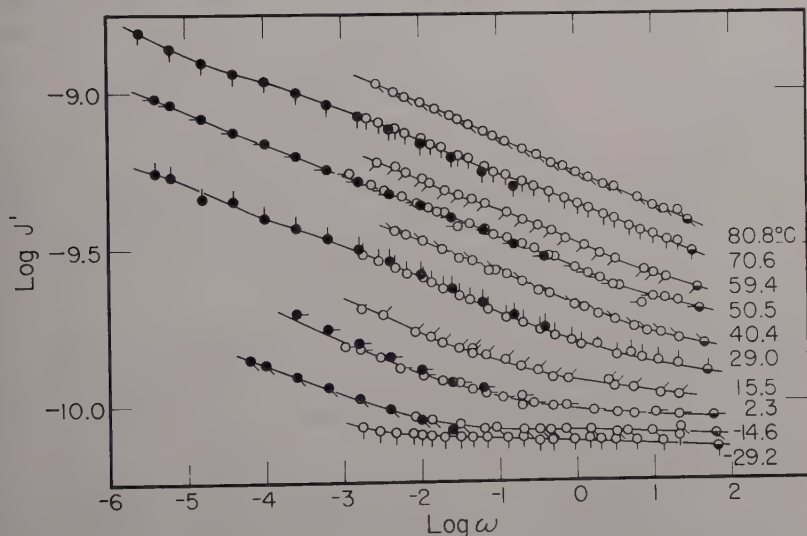


Fig. 2. Logarithmic plot of the in-phase component, $J'(\omega)$ in cm^2/dyne , of the complex dynamic compliance as a function of the pulsance, ω in radians/sec. (○) From forced oscillation; (◐) from free vibration; (●) calculated from $J(t)$. Temperatures as indicated.

tained for almost all of the temperatures at which both creep and dynamic measurements were made, and that as many as seven decades of the time scale have been covered. Since the same sample was used for both types of measurements without being removed from the apparatus, the same sample coefficients were used in calculating the results of Figures 1, 2, and 3. Hence uncertainties caused when it is necessary to change samples have been eliminated. Except for a few points, the computed and measured values are within 5% for $J'(\omega)$ and 7% for $J''(\omega)$.

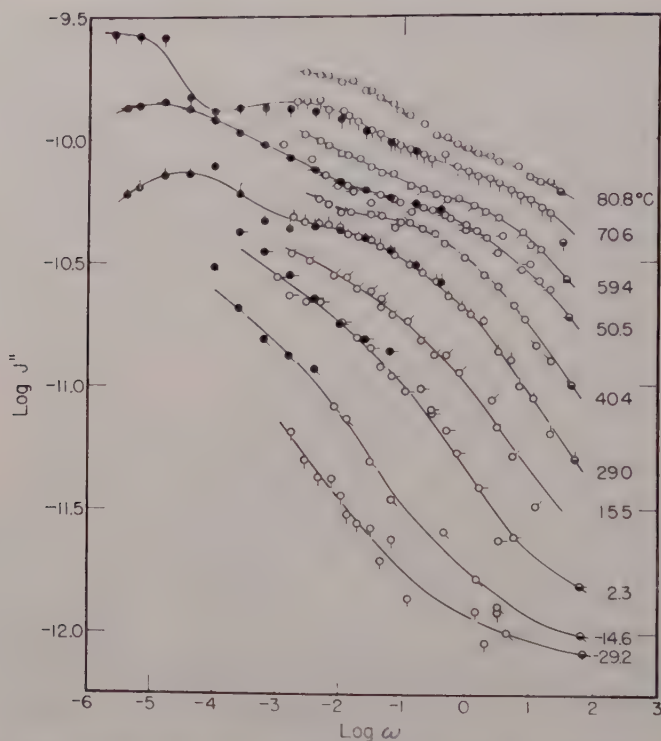


Fig. 3. Out-of-phase component, $J''(\omega)$ in cm^2/dyne , of the complex dynamic compliance plotted in same manner as $J'(\omega)$ in Fig. 2.

To carry out the above computations the retardation spectrum, $L(\tau)$, to be exhibited later, was first determined from the creep curves with the Stern²⁰ modification of the Ferry-Williams²¹ second approximation method

$$L(\tau) = M(-m) J(\tau) (d \log J(t)/d \log t)_{t=\tau}$$

where $M(-m)$ is a given function of the slope, m , of the logarithmic time plot of $dJ(t)/d \ln t$. $J'(\omega)$ was then calculated from the formula obtained by Smith²² (a modification of the similar Catsiff-Tobolsky²³ approximation involving moduli)

$$J'(\omega) = J(t) + L(t)\psi'(m)$$

where $\psi'(m) = (\pi/2) \csc(m\pi/2) + \Gamma(-m)$ and ω takes the value of

t^{-1} here as well as in the two formulas below. $J''(\omega)$ was computed by use of the Smith²² approximation assuming no flow,

$$J''(\omega) = [(\pi/2) \sec (m\pi/2)] L(t)$$

The Ferry-Williams²¹ relationship

$$J''(\omega) = L(t)/B(1-|m|)$$

gave agreeing results for the several runs which were calculated by both formulas. Because of the strong dependence of the calculation of $J''(\omega)$ on the slope of the creep curve, it is not surprising that the errors in $J''(\omega)$ should be greater. The above approximations are also not expected to hold in the neighborhood of large changes in slope. It is to this, rather than to the properties of our sample, that we ascribe the sharp changes in curvature in the 70° run and some of the details of the J'' curves at low frequencies as calculated from creep. The formulas also broke down at the short time part of the -16° run because of its small slope.

Thermal History

Another problem which is of special importance with crystalline polymers is the fact that the method of preparation, especially the thermal history, can seriously affect their mechanical properties.^{5,24} A sample of polyethylene, prepared by a method similar to ours, underwent an irreversible change in mechanical properties on being heated above 80°²⁵ and therefore no data were obtained at higher temperatures. During the course of our measurements, frequent check runs were made at 29° with results agreeing closely with the original run. Furthermore, all of the creep runs were made after we had obtained the dynamic data during which the sample had been kept at 80° for about 1 day. The agreement between the results of the two measurements—as indicated by the open and filled circles of Figures 2 and 3—is a further indication that our sample did not change significantly during the course of our measurements.

Test of Linearity

It has been pointed out that the mechanical properties of polyethylene become nonlinear at quite small strains.^{4,11} We therefore felt that it was important to check the effect of the amplitude of vibration in our dynamic data and the stress level in our creep studies.

The maximum strains in the sample, as calculated from the theory of the torsion of elastic prisms,²⁶ during most of our measurements was about 0.001 in the forced oscillations and 0.002 in creep. Increasing the latter by a factor of 2.5 gave creep compliance data which differed by at most a few tenths of a per cent. Amplitude effects were sought in the dynamic experiments throughout our study. In the most extensive series at 60°C., J' and $\tan \delta$ both changed by less than 1% as the amplitude of strain decreased to 0.0003 in forced vibrations. Furthermore, the free vibration experiments were performed at maximum deformations less than 0.1 of those used for imposed oscillations with results in good agreement for both J' and J'' as indicated in Figures 2 and 3.

Effect of Tension

For most of our measurements a tension of 30 g. or less was applied to our sample. The effect of varying this longitudinal force was studied. For example at 60°C., varying the tension over the range from 3.6 to 47 g. gave values of J' within a few tenths of a per cent and of $\tan \delta$ within 1% of one another. With an increase to a 60-g. load, J' increased by 1.5% and $\tan \delta$ by 2%. Thus, we have reason to believe that the tensile stresses which we applied, in the order of 3×10^6 dynes cm.², are in the region where they produce no appreciable effect on our results.

Another possible effect of the tension is that some permanent deformation might result because of longitudinal creep. If such a change did occur, it affected our length by less than 0.1% during the series of measurements reported here.

Temperature-Time Relationship

Close examination of Figure 2 makes it clear that it is not possible to superpose the $J'(\omega)$ curves with horizontal shifts along the logarithmic frequency scale. Performing the vertical shift indicated by the usually^{13,14} defined reduced storage compliance ($J'_p = J'T/T_0$) spreads the curves further apart and lessens the possibility to achieve superposition by a horizontal shift. Thus the application of this simple form of temperature-time equivalence which has been successful for amorphous polymers does not seem to be useful here.

The points of inflection in the $J''(\omega)$ plots of Figure 3 lead one to suspect the existence of possibly three mechanisms in the range

covered by the data. However, the $J''(\omega)$ curves for the lower temperatures can be superposed by horizontal shifts along the logarithmic frequency axis. The amount of these shifts is called $\log a_{T,I}$ where we have taken 29° as the base temperature. The result of this reduction is shown in Figure 4 where some of the runs have been omitted for the sake of clarity. A plot of $\log a_{T,I}$ against the reciprocal of the absolute temperature gives a straight line, as indicated in Figure 5, for those runs which have at least some superposable portion, those at tempera-

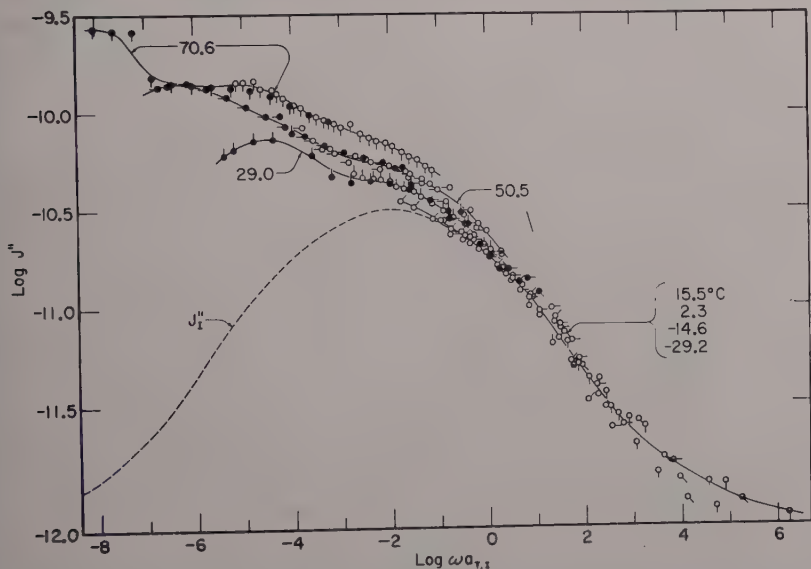


Fig. 4. Most of loss compliance values from Fig. 3, plotted logarithmically against $\omega a_{T,I}$, showing partial reduction. Dashed line indicates assumed contribution of mechanism I.

tures of 40° and lower. This curve was extrapolated to get the shift factors used for the higher temperatures in Figure 4. It is seen that the data for 15.5°C . and below fall together rather well, with the high temperature runs beginning to feather off from the reduced curve at a value of $\log \omega a_{T,I}$ of +1. In the region of superposition, extending over seven decades, the contribution of a single mechanism, which shall be referred to by the symbol I , is exhibited with comparatively little influence from others.

If the contributions of other mechanisms are to be examined, it is desirable to first eliminate the effect of I . To accomplish this, it is necessary to make some assumptions which we base on previous experience in polymer systems. In assessing the contribution of a mechanism to the viscoelastic properties, the compliances are taken to be additive.²⁷⁻³⁰ We also assume that $J''_I(\omega)$, the contribution of I to $J''(\omega)$, is symmetric³¹⁻³³ about a vertical axis at its maximum when plotted on a log-log plot. Figure 4 also displays $J''_I(\omega)$ as we have assumed it to be. At values of $\log \omega a_{T,I}$ above -1 we take $J''_I(\omega)$ to be equal to $J''(\omega)$ as obtained from the low temperature data which were superposed. An extrapolation of about a decade was required to reach the maximum we have chosen at $\log J''_I = -10.5$

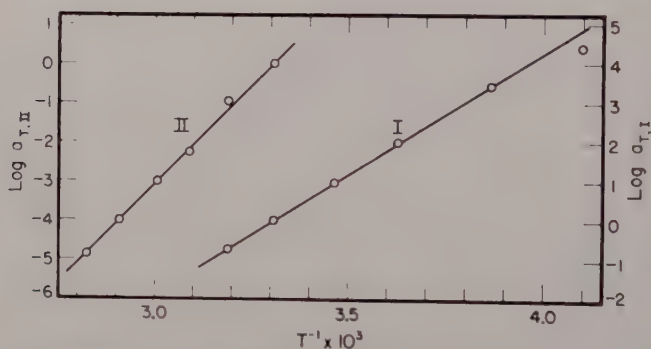


Fig. 5. Logarithms of shift factors $a_{T,I}$ and $a_{T,II}$ presented as functions of the reciprocal absolute temperature.

and $\log \omega a_{T,I} = -2.0$. The criterion for a suitable $J''_I(\omega)$ is that the point of inflection which $\log J''(\omega)$ has for the higher temperature runs in the neighborhood of $\log \omega a_{T,I} = -2$ not be present in $\log (J''(\omega) - J''_I(\omega))$. If the maximum in $\log J''_I(\omega)$ were taken as -10.45 at $\log \omega a_{T,I} = -2.5$, for example, this criterion would not have been met. Thus, although there is some degree of arbitrariness in our $J''_I(\omega)$, a choice not too far removed from it would give an undesirable result. The exact nature of $J''_I(\omega)$ on the low frequency side of the peak is only important in the neighborhood of the maximum. At frequencies not too far removed, the contribution becomes small and its precise value is not too important in the following analysis.

The part of $J''(\omega)$ which remains after subtraction of the contri-

bution $J''_I(\omega)$ is graphed in Figure 6 for the runs at higher temperatures. These curves can be superposed over more than four decades of frequency by a horizontal translation to the 29° data by an amount, $\log(a_{T,II}/a_{T,I})$ —the total shift from the original data being called $\log a_{T,II}$ —with the result shown in Figure 7 in the curve labeled $J'' - J''_I$. The superposed portion has no detectable contribution from other mechanisms and can be considered to be very nearly

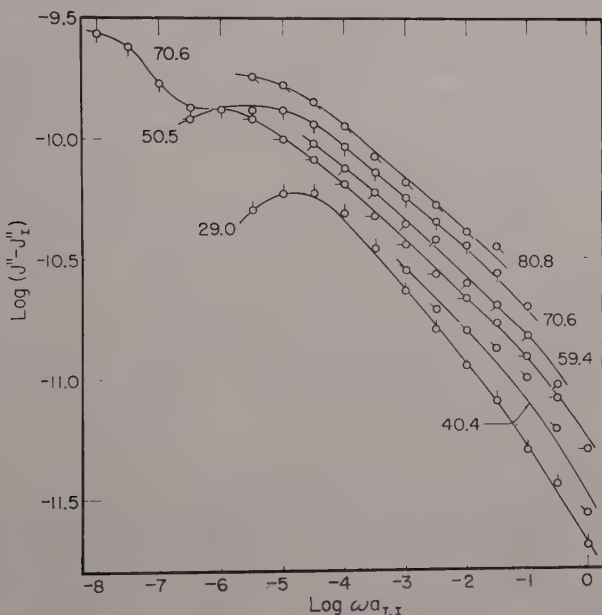


Fig. 6. Remainder of loss compliance after subtraction of contribution of mechanism I, $J''_I(\omega)$, plotted logarithmically versus the reduced frequency $\omega a_{T,I}$.

$J''_{II}(\omega)$. It is clear that there is at least one more dispersion at still lower frequencies as indicated by the feathering off of the various runs. We note that its a_T has a higher temperature coefficient than I or II. The range of the present data preclude making any quantitative statements concerning it. In fact considerable patience would be required to extend the data to sufficiently long times to obtain the necessary information. The usual procedure of accomplishing this by making measurements at higher temperatures cannot be used here

since it is known that the mechanical properties change irreversibly within the required time for performing these experiments at those temperatures.

The solid line in Figure 7 represents the 29° data which have been extended at the high frequency end by superposition from lower temperature curves using values of $a_{T,I}$. It is seen how these data are decomposed into the two contributions previously described.

The values of $a_{T,I}$ and $a_{T,II}$ thus far obtained from $J''(\omega)$ would be of no value unless they were also applicable to $J'(\omega)$. As indicated above, however, no simple horizontal shifts will superpose $J'(\omega)$. This is most readily seen by noting that the J' data of various tem-

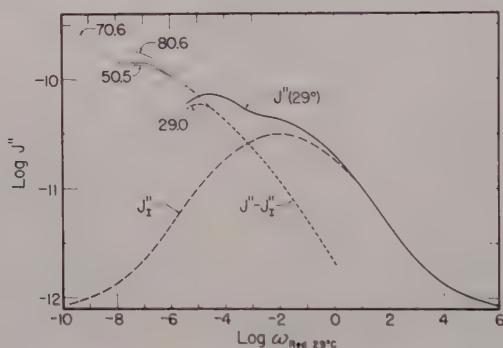


Fig. 7. Total 29°C. loss compliance (—) and components of same presented logarithmically against the reduced frequency as defined in text. (---) Mechanism I; (- -) mechanism II; (...) include incompletely reduced contributions of mechanism III.

peratures tend to different levels at high frequencies. The difference between this level for a given temperature and that for 29° will be designated by $\Delta J'_I$.

The contribution, $J'_I(\omega)$, of mechanism I to $J'(\omega)$, of course, has to be consistent with the function $J''_I(\omega)$ obtained above. In fact, to within an additive constant, we can calculate $J'_I(\omega)$ from $J''_I(\omega)$ using the theory of linear viscoelasticity and the various approximation methods which have been developed in connection with it. From $J''_I(\omega)$ we first calculate the corresponding contribution to the retardation spectra, $L_I(\tau)$ using the Ferry-Williams²¹ and Ninomiya-Ferry³⁴ second approximation methods, which gave results in good agreement

except near the maximum in $J''_I(\omega)$, where we accepted the results from the latter. Since, according to the Ferry-Williams second approximation formula

$$L(\tau = 1/\omega) = AJ'[(d \log J')/(d \log \omega)]$$

we can write

$$dJ' = (L/A) d \ln \omega$$

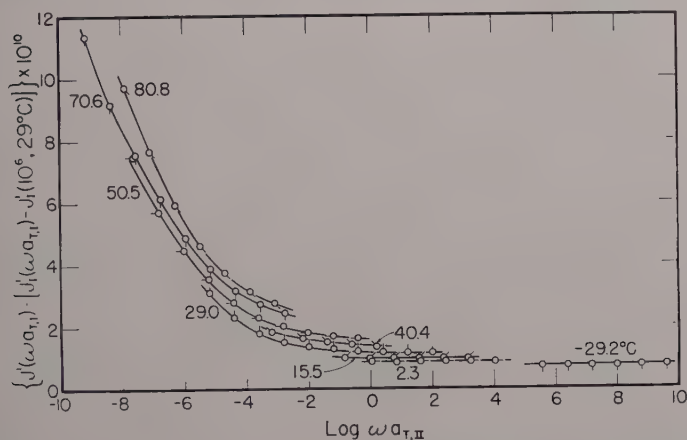


Fig. 8. Storage compliance differences obtained from curves in first reduction position and plotted here semilogarithmically in second reduction position. Vertical displacements from 29°C . curve are measure of $\Delta J'_I$. See text for details.

By integrating between a fixed frequency ω_1 and a variable frequency ω , we obtain

$$J'(\omega) - J'(\omega_1) = \int_{\omega_1}^{\omega} (L/A) d \ln \omega$$

In the present instance J' and L refer to J'_I and L_I , respectively, the argument of L is taken as $\tau = 1/\omega$, A is the tabulated function of the slope of the $\log L$ - $\log \tau$ curve, $\omega a_{T,I}$ replaces ω , and $\omega_1 a_{T,I}$ is taken as 10^6 where L has a very small value and $J'_I(\omega a_{T,I})$ is varying only slightly with frequency. The integration was performed numerically.

There remains the task of evaluating the limiting value of J'_I as a function of temperature. This was done by using a semi-log plot of $J'(\omega a_{T,I}, T) - [J'_I(\omega a_{T,I}, 29^\circ) - J'_I(\omega_1 a_{T,I}, 29^\circ)]$ against $\log \omega a_{T,I}$

as shown in Figure 8 where $a_{T,I}$ is obtained from the J'' data. If $\Delta J'_I$ were zero, these curves would superpose at the higher frequencies, as was the case with J'' (cf. Figs. 6 and 7). However, after such a shift is completed, a vertical translation on the semi-log plot is required. The amount of this vertical transposition to achieve superposition with the 29° curve is just $\Delta J'_I$, the temperature dependence of which is shown in Figure 9. Since $J'_I(10^6, -29^\circ)$, which is in a rather level part of the curve, and $\Delta J'_I$ for -29° are both known,

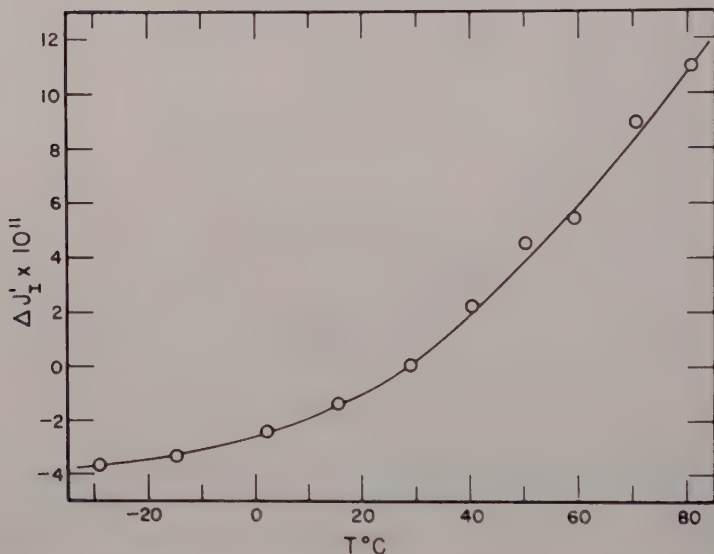


Fig. 9. Temperature variation of the frequency independent vertical shift term, $\Delta J'_I$.

$J'_I(10^6, 29^\circ)$ is found to be $1.13 \times 10^{-10} = 10^{-9.95}$ cm.²/dyne by addition of these two numbers.

Having determined the value of $J'(\omega a_{T,I})$ at high frequencies, we can now complete a test of consistency of the temperature shift factors obtained from $J''(\omega)$. Figure 10, a logarithmic plot of $\log(J'(\omega a_{T,I}) - \Delta J'_I)$ as a function of $\log \omega a_{T,I}$, shows that the lower temperature data can be superposed over the same range as was possible for $J''(\omega a_{T,I})$ in Figure 4 with feathering off of the higher temperature data again at about $\log \omega a_{T,I}$ equal to 1. After the total contribution of

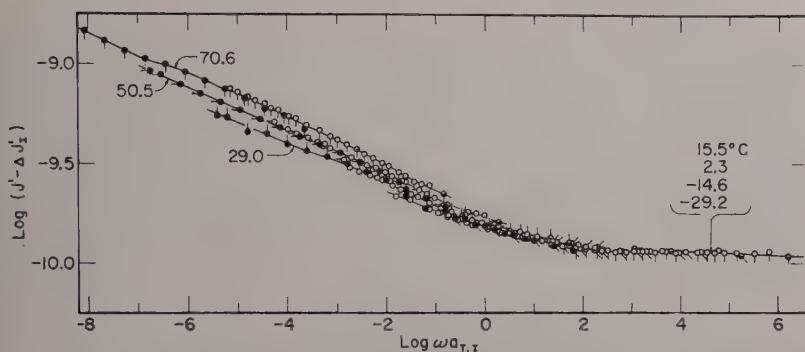


Fig. 10. Logarithmic plot of partially reduced storage compliance values as function of $\omega a_{T,I}$. Data from some temperatures omitted for sake of clarity.

mechanism *I* is subtracted, the further shift of $\log (a_{T,II}/a_{T,I})$ —making a total shift of $\log a_{T,II}$ —gives superposition as indicated by the curve labeled $J' - J'_I$ in Figure 11. This figure also exhibits $J'_I(\omega a_{T,I})$ and shows how the two components add up to the experimentally determined $J'(29^\circ)$ as extended at the high frequency end by superposition involving $\Delta J'_I$ and $a_{T,I}$.

Thus, by use of the assumption concerning $\Delta J'_I$, it is possible to decompose both $J'(\omega)$ and $J''(\omega)$ into two components, each compatible with the relations of linear viscoelasticity and with consistent sets of temperature shift factors.

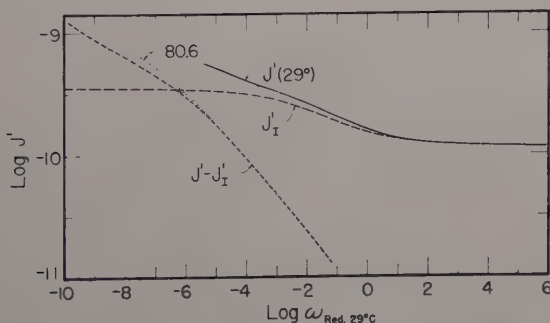


Fig. 11. Total $29^\circ\text{C}.$ storage compliance (—) and components of same presented logarithmically against reduced frequency as defined in text. (--) mechanism *I*; (- · -) principally mechanism *II* (· · ·); includes incompletely reduced contribution of mechanism *III*.

The exact interpretation of the quantity $\Delta J'_I$ is not clear to us. It cannot, however, readily be ascribed to the effect of another simple viscoelastic mechanism, say mechanism *B*, at higher frequencies:

(1) If such a mechanism occurred, for all of our temperatures, at frequencies so much higher than the range which we cover that only the low frequency asymptotic values of J' of *B* were effective in our portion of the time scale and if the temperature dependence of *B* were the usual shift along the frequency axis, then $\Delta J'_I$ would be zero.

(2) If *B* is not so far removed on the time scale, if we assume that $\Delta J'_I$ actually does have some slight time dependence, and if (a) has a lower effective heat of activation than mechanism *I*, the apparent asymptotic value of our measured $J'(\omega)$ would then be expected to decrease with increasing temperature and this is contrary to the experimental fact; moreover, on the other hand, if (b) mechanism *B* is near its maximum contribution to J' and has the higher effective heat of activation, as the temperature increased the contribution of *B* would be increasing but with a decreasing rate since portions further from its higher asymptotic limit would be effective. Then $\Delta J'_I$ would be expected to have a curvature opposite to that shown in Figure 9.

Thus, unless one wishes to admit more complicated types of behavior, another source, perhaps elastic rather than viscoelastic, for $\Delta J'_I$ must be sought. A possible explanation is that this term indicates an increasing compliance of the crystalline portions as the temperature rises. Evidence concerning this conjecture will be sought in our future studies on other polyethylenes and other hydrocarbons.

Temperature Dependence of Shift Factors

The values of $a_{T,I}$ and $a_{T,II}$ are listed in Table I and plotted in Figure 5 as a function of the reciprocal of the absolute temperature. The slopes correspond to heats of activation of 28 and 46 kcal./mole,

TABLE I
Temperature Shift Factors

Temp., °C.	-29.2	-14.6	2.3	15.5	29.0	40.4
log $a_{T,I}$	4.38	3.36	2.00	0.97	0.00	-0.77
Temp., °C.	29.0	40.4	50.5	59.4	70.6	80.8
log $a_{T,II}$	0.00	-0.20	-0.82	-1.16	-1.56	-1.90

respectively. This compares with a value of 30 kcal./mole reported by Faucher¹¹ on the basis of simple horizontal translation. In this calculation he emphasizes his points at lower temperatures and thus agreement with $a_{T,I}$ would be expected. The analysis by Sandiford and Willbourn^{1c} of the temperature effect on loss tangent maxima—in this region based mostly on the data of Oskin and Maxwell²—gives a value of 25 kcal./mole. These compare with the value of 38 kcal./mole ascribed to the β maximum and 11 to 15 kcal./mole to the γ peak.^{1c}

Ferry f-Shift

The appearance of Figure 4 is strongly reminiscent of the same type of plot presented by Berge, Saunders, and Ferry³⁵ for poly-*n*-octyl methacrylate. In that case the authors achieve superposition by a further translation of their curves along a slope of $-1/2$ which corresponds to multiplication of the frequency by f^{-2} and the compliance (both J' and J'') by f where f is the factor by which the number of network strands is multiplied in going between the two temperatures being compared. This f -shift is attributed to a change in the number of entanglements with temperature. If one follows the above formula with respect to the $J''(\omega a_{T,I})$ plot of Figure 4 and the corresponding logarithmic plot of $J'(\omega a_{T,I})$, we find that, indeed, superposition can be achieved. However, when $\log f$ is plotted against T^{-1} , a strongly curved plot is obtained. Furthermore, the amount of the translation corresponds to a decrease by a factor of about 2 in the number of network strands as the temperature increases from 15 to 70°C. Although it is difficult to imagine the large changes required in the number of such entanglements as may exist in the amorphous region of such a highly crystalline polymer, one might then hypothesize that detachment of chains from crystallites could decrease the number of chains. However, one would not expect to find the crystallinity decreasing at temperatures more than 150° below the melting point, and certainly not the large changes in amount of crystallinity required by this f -shift. Although some nuclear magnetic resonance data have been interpreted³⁶ to imply changes in crystallinity even at low temperatures, the changes are not as great as needed here. Furthermore, doubt has been cast³⁷ on the interpretation of NMR results and other^{38-40,11} methods do not allow much change below about 80°C.

Shift Due to Crystallinity Changes

Takemura⁴¹ has proposed that the ordinate be multiplied by an additional factor to achieve reduction when crystallinity changes with temperature. On applying this shift, unjustifiably we believe, to the stress relaxation data obtained by Catsiff and Tobolsky¹⁰ on Marlex 50 at strains as large as 2.7%, he successfully reduced their curves. Even if we empirically used the factors thus obtained, our data would not fall on a common curve.

Simple Horizontal Shift

Faucher,¹¹ in his stress relaxation measurements which cover somewhat less than $2^{1/2}$ decades of time, was able to achieve superposition by simple horizontal translation. Above about 20°C. his plot of $\log a\tau$ vs. T^{-1} is no longer straight and indicates a trend to higher ΔH . This, we believe, is a reflection of the influence of mechanism II. A curve with similar features was exhibited by Nagamatsu and Yoshitomi⁴² for polytrifluorochloroethylene which is also known to have more than one mechanism contributing to its viscoelastic behavior.

Other Viscoelastic Functions

Retardation Spectrum

Figure 12 shows the retardation spectra $L(\tau)$ as calculated from $J(t)$ by the Ferry-Williams²¹ second approximation method and from $J'(\omega)$ and $J''(\omega)$ by the Ninomiya-Ferry³⁴ second approximation formula. The agreement between values calculated from the creep and the two components of the dynamic data again reflect consistency with the expectations of linear viscoelasticity theory. The extension of this concordance to shorter times is obtained by the demonstrated agreement between the spectra calculated from $J'(\omega)$ and $J''(\omega)$.

Temperature reduction of $L(\tau)$ is not shown here since it would differ only slightly from the reduction of $J''(\omega)$ which is a zeroth order approximation to $L(\tau)$ when there is no viscosity contribution, as is the case here.

Moduli

Since our material has a rather low loss, $1/J(t)$ is a rather good approximation for $G(t)$, the relaxation modulus, and $1/J'(\omega)$ is a rather good approximation to $G'(\omega)$, the storage modulus.

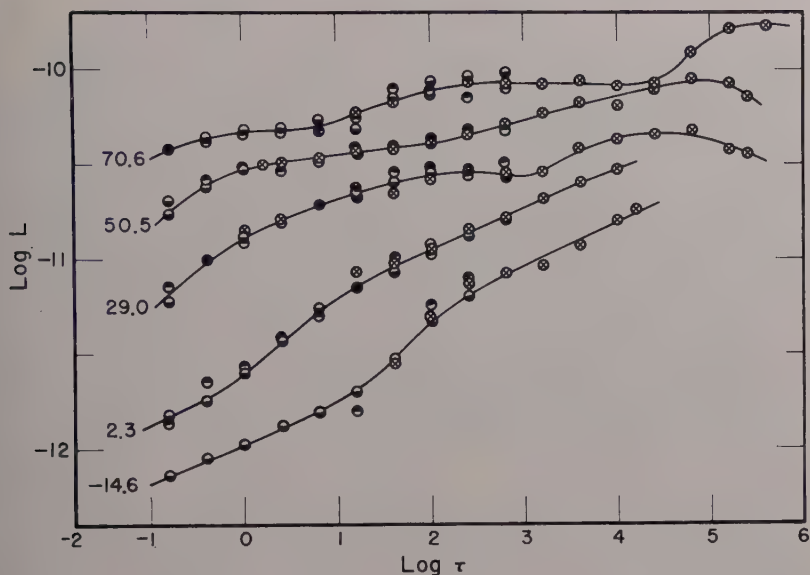


Fig. 12. Logarithmic plot of retardation spectra versus retardation time. (\otimes) From creep; (\oplus) storage compliance; (\ominus) loss compliance.

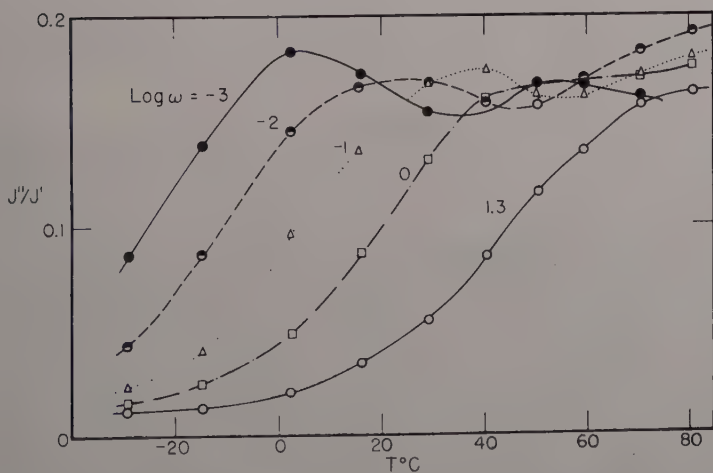


Fig. 13. Temperature dependence of the loss tangent at five selected frequencies.

Loss Tangent

Although $J'(\omega)$ and $J''(\omega)$ can be considered a sum of contributions from individual mechanisms, the loss tangent, $\tan \delta = J''(\omega)/J'(\omega)$, being then a ratio of sums is mathematically a more complicated quantity. Nevertheless it has become a rather popular method of expressing the results of viscoelastic experiments for a variety of reasons. It is relatively easily obtained from some measurements, especially the free vibration technique. In fact, sample dimensions

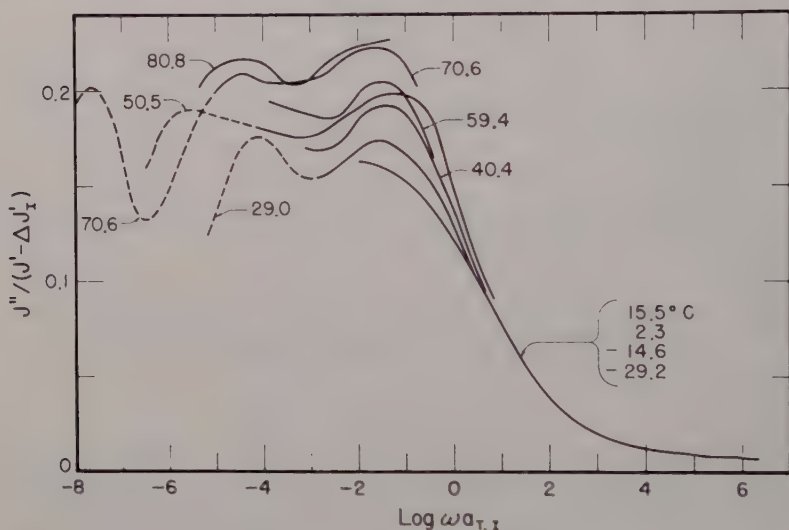


Fig. 14. Modified partially reduced loss tangent behavior plotted semilogarithmically against $\omega a_{T,1}$. (—) Derived from dynamic measurements; (---) calculated from creep.

and instrument parameters play no part in its evaluation in many cases. Also the presence of various mechanisms reveal themselves most clearly through $\tan \delta$ since they often give rise to very pronounced maximum in this function. In fact, the appearance of $\tan \delta$ versus temperature curves has brought forth the term "mechanical spectroscopy." In making use of such plots it is important to bear in mind, however, the viscoelastic and hence frequency dependent nature of $\tan \delta$. This is indicated in Figure 13 where the loss tangent is plotted against temperature for various frequencies. It is seen that the maxi-

imum value, as well as the temperature where it occurs, depends markedly on the frequency of measurement. In fact at the higher frequencies, in this case, there is no maximum in this region at all. This type of behavior is to be expected whenever there is more than one contributing mechanism with different dependence on the temperature.

Within our temperature range all of the measured loss peaks had values between 0.175 and 0.190. However, if $\Delta J'_T$ really represents a nonviscoelastic contribution to the compliance, it causes changes in the shape of the loss tangent curve because it is temperature dependent. The partially reduced modified loss tangent behavior obtained from the parameters plotted in Figures 4 and 10 is shown in Figure 14, plotted against $\log \omega a_{T,T}$. If the disturbing influence of $\Delta J'_T$ had not been eliminated, the lower temperature measurements would not be superposed.

The apparent increase with temperature in loss tangent magnitude is a manifestation of the lower frequency mechanism overtaking those at higher frequencies. Therefore, in spite of the misleading appearance the data are consistent with individual loss tangent curves whose amplitudes are independent of temperature. Furthermore, though the peaks of the mechanism are merging at higher temperatures, they appear not to merge because of the mutual interference. The 50° curve at low frequencies does not seem to fit the general trend here and elsewhere, and we feel the creep run made at this temperature must be in slight error.

Further Discussion

The dispersions with which we deal here can be identified with what most authors find as a single $\tan \delta$ peak which has usually been labeled the " α -transition." Except for one author⁶ who ascribes this mechanism to the amorphous region, there appears to be universal agreement that it is due to the melting of the crystals.^{3,8,9,43} We, however, find it hard to believe that the effects of melting can be seen more than 150° below the melting point. The evidence for this attribution is mainly data obtained on polymers which differ chemically from one another—with different degrees of branching, irradiation products, or copolymers. Thus it may be too early to assign a definite cause to this transition. We plan to seek more evidence on this point

by obtaining data on samples with the same chemical structure but differing amounts of crystallization.

References

1. Some recent review articles which discuss the mechanical properties of polyethylene include: (a) A. E. Woodward and J. A. Sauer, *Adv. Polymer Sci.*, **1**, 114 (1958); (b) I. L. Hopkins and W. O. Baker in F. R. Eirich, ed., *Rheology. Theory and Applications*, Vol. 3, Academic Press, New York, 1960, p. 388; (c) D. J. H. Sandiford and A. H. Willbourn in A. Renfrew and P. Morgan, ed., *Polythene*, Iliffe, London, 2nd ed., 1960, p. 167.
2. Oskin, E. T., and B. Maxwell, *Plastics Laboratory Technical Report 44A* (1957).
3. Sauer, J. A., and A. E. Woodward, *Revs. Mod. Phys.*, **32**, 88 (1960).
4. Sandiford, D. J. H., in *The Physical Properties of Polymers*, Society of Chemical Industry, London, 1959, p. 213.
5. Willbourn, A. H., *Trans. Faraday Soc.*, **54**, 717 (1958).
6. McCrum, N. G., *Makromol. Chem.*, **34**, 50 (1959).
7. Hellwege, K. H., R. Kaiser, and K. Kuphal, *Kolloid-Z.*, **147**, 155 (1956).
8. Wolf, K., and K. Schmieder, *Ricerca sci.*, **25A**, 732 (1955).
9. Nielsen, L. E., *J. Appl. Phys.*, **25**, 1209 (1954).
10. Catsiff, E. A., and A. V. Tobolsky, *ONR Technical Report RLT-19* (1956).
11. Faucher, J. A., *Trans. Soc. Rheology*, **3**, 81 (1959).
12. See for example, B. Gross, *Mathematical Structure of the Theories of Viscoelasticity*, Herman and Cie., Paris, 1953.
13. See for example, A. J. Staverman and F. Schwarzl in H. A. Stuart, ed., *Die Physik der Hochpolymeren*, Vol. 4, Springer, Berlin, 1956, p. 1.
14. Ferry, J. D., *ibid.* p. 373.
15. Morrisson, T. E., L. J. Zapas, and T. W. DeWitt, *Rev. Sci. Instr.*, **26**, 357 (1955).
16. Plazek, D. J., M. N. Vrancken, and J. W. Berge, *Trans. Soc. Rheology*, **2**, 39 (1958).
17. Kuhn, W., and O. Künzle, *Heiv. Chim. Acta*, **30**, 839 (1947).
18. Nielsen, L. E., *Rev. Sci. Instr.*, **22**, 690 (1951).
19. Quinn, F. A., Jr., and L. Mandelkern, *J. Am. Chem. Soc.*, **80**, 3178 (1958).
20. Stern, D. M., Ph.D. Thesis, University of Wisconsin, 1957.
21. Ferry, J. D., and M. L. Williams, *J. Colloid Sci.*, **7**, 347 (1952).
22. Smith, T. L., *Trans. Soc. Rheology*, **2**, 131 (1958).
23. Catsiff, E., and A. V. Tobolsky, *J. Colloid Sci.*, **10**, 375 (1955).
24. Nielsen, L. E., and F. J. Lection, data exhibited in R. Buchdahl, R. L. Miller, and S. Newman, *J. Polymer Sci.*, **36**, 215 (1959).
25. Chiang, R., unpublished results.
26. Timoshenko, S., *Theory of Elasticity*, McGraw-Hill, New York, 1934, p. 248.
27. Ferry, J. D., and E. R. Fitzgerald, *J. Colloid Sci.*, **8**, 224 (1953).
28. Ferry, J. D., W. C. Child, Jr., R. Zand, D. M. Stern, M. L. Williams, and R. F. Landel, *J. Colloid Sci.*, **12**, 53 (1957).
29. Plazek, D. J., *J. Colloid Sci.*, **15**, 50 (1960).

30. Plazek, D. J., W. Dannhauser, and J. D. Ferry, *J. Colloid Sci.*, accepted for publication.
31. Landel, R. F., *J. Colloid Sci.*, **12**, 308 (1957).
32. Williams, M. L., and J. D. Ferry, *J. Colloid Sci.*, **10**, 474 (1955).
33. Birnboim, M., Ph. D. Thesis, University of Wisconsin, 1961.
34. Ninomiya, K., and J. D. Ferry, *J. Colloid Sci.*, **14**, 36 (1959).
35. Berge, J. W., P. R. Saunders, and J. D. Ferry, *J. Colloid Sci.*, **14**, 135 (1959).
36. Collins, R. L., *J. Polymer Sci.*, **27**, 75 (1958).
37. Rempel, R. C., H. E. Weaver, R. H. Sands, and R. L. Miller, *J. Appl. Phys.*, **28**, 1082 (1957).
38. Swan, P. R., *J. Polymer Sci.*, **42**, 525 (1960).
39. Nakane, R., *J. Phys. Soc. Japan*, **15**, 1040 (1960).
40. Wunderlich, B., and M. Dole, *J. Polymer Sci.*, **24**, 201 (1957).
41. Takemura, T., *J. Polymer Sci.*, **38**, 471 (1959).
42. Nagamatsu, K., and T. Yoshitomi, *J. Colloid Sci.*, **14**, 377 (1959).
43. Nielsen, L. E., *J. Polymer Sci.*, **42**, 357 (1960).

Synopsis

Dynamic mechanical measurements were carried out on an unannealed sample of a high-density polyethylene with a torsion pendulum instrument in both forced and free oscillations. Data were obtained at frequencies between 2×10^{-4} and 9 cycles/sec. and at 10 temperatures between -30 and 80°C . above which significant irreversible changes in the sample occur. Creep measurements were made in the same instrument from a few seconds up to 3 days for five of these temperatures. As many as seven decades of the time scale were thus covered isothermally. Not only were the dynamic properties independent of amplitude and the creep compliance independent of stress level, but also the creep and the two components of the dynamic mechanical properties were compatible with the Boltzmann superposition principle over the range of variables covered. A simple temperature superposition is not successful with these data. It was possible to decompose the compliance into a sum of a frequency independent component and two viscoelastic mechanisms, each compatible with the Boltzmann superposition principle and with consistent temperature factors, $a_{T,I}$ and $a_{T,II}$. The temperature dependence of these factors correspond to heats of activation of 28 and 46 kcal./mole, respectively. The third dispersion which is also seen in our data has a higher energy of activation. The range which we cover here is that which the literature refers to as a single α -mechanism. We find the assignment of this peak to melting of crystals both premature and highly doubtful.

Bulk Creep and Recovery in Systems with Viscosity Dependent upon Free Volume

A. J. KOVACS, *Centre de Recherches sur les Macromolécules, Strasbourg, France, and Department of Chemistry, University of Wisconsin, Madison, Wisconsin*

Information on viscoelastic behavior in bulk is rather scarce in the rheological literature. Most of it concerns experiments in the acoustical or ultrasonic field, where the amplitude of the local volume deformation can be considered as infinitesimal. Some of these studies show that the bulk modulus has its own dispersion region, but the ratio of its extreme values in the high and the low frequency range is generally less than ten.¹

We would like to show here that in a transient experiment, such as creep, recovery, or relaxation, where the amplitude of the bulk deformation (the relative volume change) is finite, viscoelastic materials may have also a *specific nonlinear behavior* if their bulk viscosity depends on free volume as in shear.

Some calculations will be presented for the time-dependent volume change when a constant hydrostatic pressure is applied on such a system. Although Jenckel and Gehrke have carried out such experiments on polymers,² their results are not yet available for comparison. However, experimental manifestations of these specific features may be produced in many other ways involving time-dependent volume changes. In fact, some evidence of the nonlinear bulk behavior which will be described has been found by studying the isothermal volume changes of supercooled liquids³ below the glass-transition temperature, T_g . Furthermore, the anomalous absorption of small molecules by polymers⁴ below T_g may also be related to a similar behavior. Some other experimental manifestations will also be anticipated.

Bulk Creep and Recovery

Let us consider a special Kelvin body composed of a Hookean spring, K_f , in parallel with a free volume dependent dashpot η_f . For real materials it would be necessary to add also a Hookean spring, K_g , in series, which symbolizes the instantaneous elastic deformation occurring when the pressure is suddenly changed. Figure 1 represents such a model, where the dashpot is drawn in an unusual manner as a deformation-dependent element.

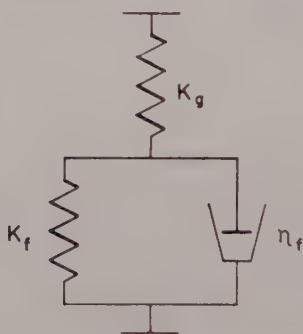


Fig. 1. Three-parameter mechanical model with a deformation dependent viscosity.

We assume that this body is in equilibrium at some constant temperature T_1 under an initial hydrostatic pressure P_1 with a specific volume v_1 . Then the pressure is changed isothermally at zero time by an amount ΔP , which can be positive or negative, and the subsequent relative volume change, $(v - v_1)/v_1$, is measured as a function of time, t . However, as observation cannot be made before some time t_i necessary for an isothermal pressure change, we assume here that the initial deformation at this time, $(v_i - v_1)/v_1$, is purely elastic and it corresponds to the deformation of the spring K_g . Under the new pressure $P_2 = P_1 + \Delta P$ the body will reach after some time a new equilibrium volume $v_2 = v_1 + \Delta v$.

If the total relative volume change $\Delta v/v_1$ is no greater than a few per cent we can write alternatively without appreciable error:

$$P = P_2 - P_1 = -K_g[(v_i - v_1)/v_1] = -K_f[(v_2 - v_i)/v_1] = -K[(v_2 - v_1)/v_1] \quad (1)$$

where K is the equilibrium bulk modulus, which equals the reciprocal of the thermodynamic compressibility: $\beta = -(1/v)(\partial v/\partial P)_T$. The two partial bulk moduli K_g and K_f are related to K by the well-known relation which comes out from eq. (1):

$$\beta = 1/K = 1/K_g + 1/K_f \quad (2)$$

The retarded elastic response of the model will be governed at any time $t \geq t_i$ by:

$$-\eta_f \frac{1}{v_i} \cdot \frac{dv}{dt} - K_f \frac{v - v_i}{v_i} = -K_f \frac{v_2 - v_i}{v_i} \quad (3)$$

which can be written

$$dv/(v - v_2) = -(K_f/\eta_f)dt \quad (4)$$

where the actual volume v is always encompassed by v_i and v_2 .

We assume now that the viscosity η_f is a function of the fractional free volume defined* by $f = (v - v_0)/v_0$, where v_0 is the specific "occupied" volume, which may be a function of temperature or pressure, but is independent of time. That means physically: the crystal-like lattice contraction (or expansion) associated with the changes of v_0 is a quasi-instantaneous process as compared to the variation of free volume involving local configurational rearrangements of structural units and holes. Furthermore, we assume that η_f and f are related by the Doolittle's free space equation⁵

$$\ln \eta_f = \ln A + B/f \quad (5)$$

where A and B are specific constants, the latter near to unity.

If we write for η_f for any time $t \geq t_i$, when the fractional free volume is f ,

$$\eta_f = \frac{\eta_f(t)}{\eta_f(\infty)} \cdot \eta_f(\infty) = \frac{\eta_f}{\eta_{f_2}} \cdot \eta_{f_2} \quad (6)$$

and introduce a new parameter s defined by

$$s = \ln \frac{\eta_{f_2}}{\eta_f(t)} = B \left(\frac{1}{f_2} - \frac{1}{f} \right) = B \frac{(v - v_2)v_{02}}{(v_2 - v_{02})(v - v_{02})} \quad (7)$$

* The above expression for f is slightly different from the usual definition of the fractional free volume⁸: $v_f/v = (v - v_0)/v$, which would involve more complicated mathematical formulations.⁹ From a practical point of view the ratio $v_f/v = v_0/v = (1 + f)^{-1} = (v - v_f)/v$, can always be approximated by unity in this paper, which involves an error generally less than 3%.

assuming a constant occupied volume after the time t_i , one can obtain from eqs. (4), (6), and (7)

$$\exp \{-s\} dv / (v - v_2) = -dt / (\eta_{f_2} / K_f) = -dt / \tau_2 \quad (8)$$

where τ_2 is the characteristic retardation time in the vicinity of the final equilibrium state.

Table I summarizes the characteristic parameters during the entire deformation process.

TABLE I

Time	0	t_i	$t > t_i$	∞
Pressure	P_1	P_2	P_2	P_2
Specific volume	v_1	v_i	v	v_2
Specific occupied volume	v_{01}	v_{02}	v_{02}	v_{02}
Fractional free volume	f_1	f_i	f	f_2
Parameter s	s_1	s_i	s	0

After suitable transformation, eq. (8) may be written

$$\left[\exp \{-s\} / s \left(1 - \frac{f_2}{B} s \right) \right] ds = -dt / \tau_2 = -dt / a_P \tau_1 \quad (9)$$

where a_P is the pressure shift factor defined first by Ferry and Stratton⁶ as:

$$\eta(P_2) / \eta(P_1) = \eta_{f_2} / \eta_{f_1} = \tau_2 / \tau_1 = a_P = \exp \{ B[(f_1 - f_2) / f_1 f_2] \} \quad (10)$$

We will show later that $f_2 s / B$ is generally much less than 1, so we can write with a very good approximation,⁹ taking as usual, $B = 1$:

$$[\exp \{-s\} / s] ds + f_2 \exp \{-s\} ds = -dt / a_P \tau_1 = -\varphi'(s) ds \quad (11)$$

which is the final differential equation to be integrated. However, the integral expression depends upon the sign of the parameter s , and we can consider two possibilities.

(1) If $v \geq v_2$, that is, if the volume is decreasing under the new pressure $P_2 > P_1$, we have $s \geq 0$. This is the case of *creep under compression*. Subsequently $f_1 > f_2$ and a_P is greater than 1.

Since we are only interested in the time-dependent volume change, we have to integrate between the initial time t_i , when $s = s_i$, and some indefinite time $t > t_i$ corresponding to $s < s_i$. Then we obtain from eq. (11):

$$\begin{aligned}\varphi_c(s, s_i) &= Ei(-s_i) - Ei(-s) + f_2[\exp\{-s\} - \exp\{-s_i\}] \\ &= (t - t_i)/a_P\tau_1\end{aligned}\quad (12)$$

where $Ei(-s) = \int_{\infty}^s \exp\{-u\}(du/u)$ is the tabulated⁷ (negative) exponential integral.

(2) On the other hand, when $P_2 < P_1$, and so $v \leq v_2$, we have $s \leq 0$, and subsequently $a_P < 1$. This is the *recovery* case when *pressure is released*.

Calling s' the absolute value of the parameter s : $s' = -s = |s|$ we can obtain from (11) in the same way as above:

$$\begin{aligned}\varphi_r(s', s_i') &= Ei(s_i') - Ei(s') + f_2[\exp\{s'\} - \exp\{s_i'\}] \\ &= (t - t_i)/a_P\tau_1\end{aligned}\quad (13)$$

where $Ei(s') = \int_{-\infty}^{s'} \exp\{u\}(du/u)$ is the tabulated (positive) exponential integral.⁷

Equations (12) and (13) are the final implicit solutions of the *creep* and *recovery* behavior of the proposed model; they may be used for all practical purposes without involving appreciable error for moderate pressure changes as we will see later.

Discussion

It is obvious that the time scale of these phenomena, defined by the retardation time τ_2 near the final equilibrium, must be greater than the t_i necessary for producing the isothermal pressure change ΔP . If $t_i > \tau_2$, the body will exhibit merely pure elasticity of modulus K . Practically, the time t_i cannot be much less in real experiments than 1 sec. As presumably⁶ K_f is of the order of 10^{11} dynes/cm.², η_f must be at least of the same order of magnitude in poises. Such a viscosity may be exhibited in shear by supercooled liquids near T_g under atmospheric pressure. If viscosity depends only on free volume, as assumed, one can obtain such a high value even *above* T_g under some higher pressure P_1 when the corresponding f_1 value is the order of, or less, than the fractional free volume f_g at T_g . It is reasonable to assume that these deductions may be applied even for the bulk viscosity η_f . Then f_2 must be the order of 0.025, or less, as can be deduced from the WLF equation.⁸ So, the simplification introduced above in (9) is quite accurate when $s \lesssim 10$ which corresponds to a moderate pressure change. Fortunately this is the pressure range when materials exhibit Hookean compressibility assumed by (1).

With these restrictions one can easily calculate the viscoelastic bulk deformation for a given pressure change, if the value of the fractional free volume in some reference equilibrium state, for instance f_1 , and its pressure coefficient $\beta_f = -(\partial f / \partial P)_T$ are known. To express the time dependent volume change on an absolute time scale, the retardation time τ_1 (or τ_2) must also be given. The other parameters, f_2 and s_t , present in the above integral equations may be derived from these values using the following relations:

$$f_2 - f_1 = -\beta_f(P_2 - P_1) \quad (14)$$

which defines β_f in the Hookean range; and

$$f_2 - f_t = [(v_2 - v_t)/v_t](1 + f_t) \quad (15)$$

which assumes that the occupied volume at time t_i is the same as in the final equilibrium (Table I). Then s_t may be derived from (7) and (15), we have:

$$-s_t = \frac{(v_2 - v_t)(1 + f_2)}{f_2[v_t(1 + f_2) - v_2]} \quad (16)$$

The actual viscoelastic deformation is related to s by:

$$\begin{aligned} \frac{v - v_t}{v_t} &= \frac{f - f_t}{1 + f_t} = \frac{f_2 - f_1}{1 + f_t} + \frac{f f_2 s}{1 + f_t} \\ &= \frac{v_2 - v_t}{v_t} + \frac{v_2 f_2^2 s}{v_t(1 + f_2)(1 - f_2 s)} \end{aligned} \quad (17)$$

which contains only known parameters, and so one can calculate, using (12) or (13), the time $(t - t_i)/\tau_1$, scaled by τ_1 , when it will be reached. The last three relations can be applied for either sign of s . However, for a given pressure change ΔP the absolute magnitude of s_t depends on the sign of ΔP , though the amplitude of the deformation is the same.

Let us now illustrate these features by a few numerical examples assuming some mean values of reasonable order of magnitude obtained in shear by Ferry et al.^{6,8} Suppose $\beta_f = 10^{-11}$ cm.²/dyne, and $f_1 = 0.025$. Table II lists the values of parameters needed for the calculation of the viscoelastic bulk deformation when this hypothetical material is submitted to some moderate pressure change. We have assumed here for simplicity that $f_t = f_1$, so that the "instantaneous"

TABLE II

$10^{-8} \Delta P$ dyne/cm. ²	$10^3(f_2 - f_i)$	$10^2 f_2$	s_i	$a_P = \tau_2/\tau_1$	Ref
+5	-5.000	2.000	+10.000	2.203×10^4	<i>a</i>
-5	+5.000	3.000	-6.667	1.273×10^{-3}	<i>a'</i>
+1.19	-1.190	2.381	+2.000	7.389	<i>b</i>
-1.19	+1.190	2.619	-1.820	0.162	<i>b'</i>
± 0	± 0	2.500	± 0	1	<i>c</i>

volume change is nearly the same (though not exactly) as that of the occupied volume: $(v_1 - v_i)/(v_{01} - v_{02}) = 1 + f_i = 1.025$. Consequently we have $a_P = \exp\{s_i\}$.

Figure 2 shows three *creep* curves ($\Delta P > 0$), where we have represented the relative time dependent bulk contraction: $-(v - v_i)/(v_2 - v_i)$, as a function of the logarithm of time scaled by τ_1 . Curve (*a*) is obtained for the highest value of ΔP , and curve (*b*) for the lower one (Table II). The last curve (*c*) is the classical exponential function obtained from (4) with a constant viscosity η_f . It corresponds also to the limiting case of (12) when s_i approaches zero. One can see that the free volume dependent viscosity may extend the experimental

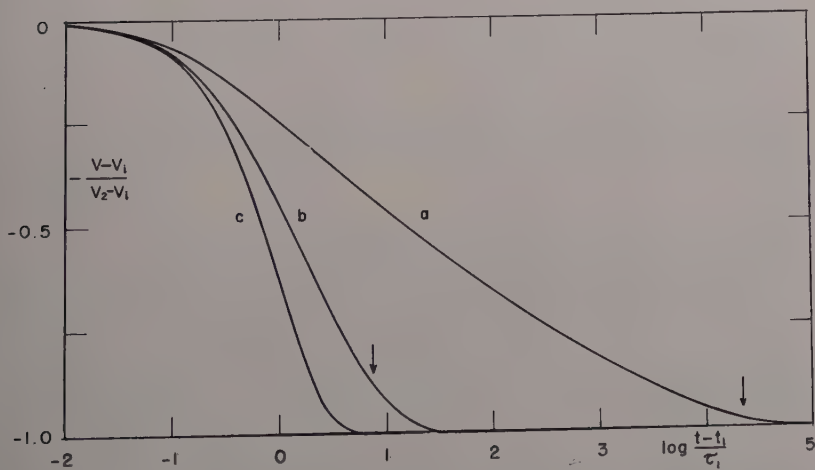


Fig. 2. Bulk creep. Relative volume contraction under constant pressures versus $\log(t - t_i)/\tau_1$.

time scale in a creep experiment by several powers of ten even for a moderate pressure change. Furthermore, the time dependent volume contraction becomes nearly linear with respect of the log of time over several decades, and could be approximated by some "box" distribution of the retardation times between two limits of the order of τ_1 and τ_2 . The abscissae $\log(\tau_2/\tau_1) = \log a_P$ are indicated by arrows.

Figure 3 represents the *recovery* curves (a' , b') for the same amounts of negative pressure change (Table II), but here the relative time dependent bulk expansion is plotted as a function of time (linear rather

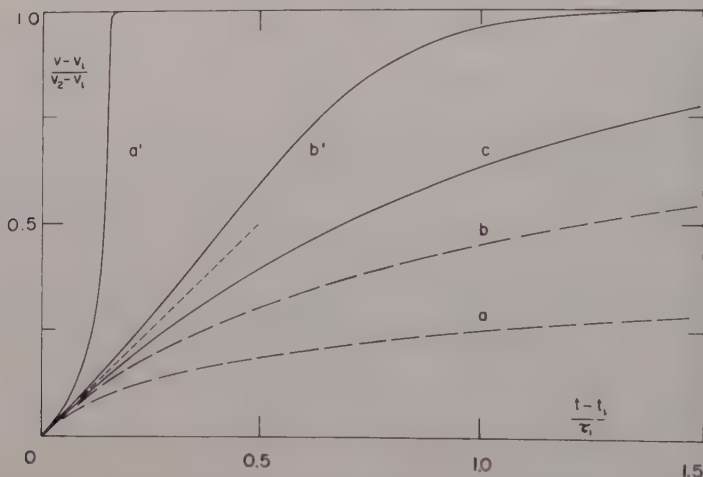


Fig. 3. Bulk recovery and creep. Relative expansion after released pressure (solid lines); relative contraction under constant pressure (dashed lines) versus $(t - t_i)/\tau_i$. Dotted line: Initial tangent.

than logarithmic), scaled by τ_1 . Curve (c) is, as in Figure 2, the classical exponential expression, which is also the limiting case of eq. (13) when s_i' approaches zero. Furthermore, we have represented in this figure the early parts of the previous creep curves (a, b) for comparison (dashed lines), and the initial tangent (dotted line) which is the same for the whole family of creep and recovery curves, provided that $f_i = f_1$.

We can easily see that in the recovery case (a', b') the free volume dependent viscosity has an accelerating, autocatalytic effect. Such curves cannot be obtained by a real distribution of retardation times.

But an expression of the type $1 - \exp\{-k(t - t_i)^n\}$ may be a quite accurate approximation if the exponent n is greater than 1* and increases rapidly with s_i' .

Figures 2 and 3 show the very asymmetrical response of this body with respect of the sign of pressure change, which is the direct consequence of the free volume dependent viscosity. If expressions other than that of Doolittle are used this asymmetrical behavior will still remain if η_f decreases with increasing free volume and vice versa, which is the general behavior one can expect. Therefore creep and recovery experiments in bulk are probably the most sensitive investigations to relate viscosity to free volume.

The above calculations may be easily extended for *pressure relaxation* experiments using some equivalent model. But such investigations in bulk are much more difficult to perform than creep or recovery. Besides a constant pressure (or volume) change, one can consider also a periodic excitation of circular frequency ω , $\Delta P_0 \sin \omega t$, and expect a subsequent out-of-phase bulk deformation which may even no longer be sinusoidal if $2\pi/\omega \approx \tau_1$, and the actual volume strain cannot be considered as infinitesimal. This problem may be studied as above by using complex variables, though the calculations are more complicated.

One can also compare creep and recovery at different constant temperatures for the same pressure change, and test by this manner the temperature coefficient⁸ of f : $\alpha_f = (\partial f / \partial T)_P$. On the other hand, if polymer samples with different amounts of plasticizers are compared at constant T and ΔP , one can test the concentration (c) coefficient of the free volume: $\gamma_f = (\partial f / \partial c)_{P,T}$ introduced by Ferry and Stratton.⁶

Indirect Experimental Manifestations

Isothermal volume changes of glass-forming systems at constant pressure give some experimental evidence of the described bulk behavior below T_g . We found recently that the model of Figure 1 is quite accurate for interpreting some of the early experimental observations in this field in a quantitative manner.⁹ The main difference between these phenomena and the ones described above arises from the nature of the applied pressure ΔP . In the present

* Note that such functions have no Laplace transforms.

treatment it is a real external pressure, but in case of quenched glasses we must assume an *effective internal pressure* produced by the sudden change of temperature $\Delta T = T_2 - T_1$. If this difference is negative (cooling) the sample will contract as in a creep experiment (Fig. 2), if it is positive (heating) an autocatalytical expansion may be observed, as in a recovery experiment (Fig. 3). Ritland, who described this behavior with a borosilicate Crown Glass¹⁰ at the same time when we made our similar investigations with polymers,³ has given two empirical formulae which are only slightly different from (12) and (13), but which contain five adjustable parameters, related to the "fictive temperature" concept of Tool.¹⁵ So it seems that free volume dependent bulk viscosity may explain some peculiar observations made with glasses, whatever their chemical composition. We will discuss the validity of these statements in a future paper.⁹

Besides real and internal pressure induced by temperature change, one can also produce a volume change by swelling pressure when small molecules can diffuse into such a viscoelastic medium. In fact, many authors have observed with glassy polymers^{4,11-14} an anomalous, non-Fickian behavior of some autocatalytic type during the sorption process. If successive interval sorption experiments are carried out where the difference between the initial and final concentration is small, there is a range of concentration where polymers exhibit a two-stage absorption process.^{11,12} It has been demonstrated that the first stage is a purely Fickian diffusion, which is followed by a slower "sigmoidal" increase of concentration. Long and Watt¹³ have shown that during the second stage of sorption there is no gradient in concentration inside the sample and so Fickian diffusion can no more be involved. Several investigators¹¹⁻¹⁴ agree that this process is governed by some configurational changes of the polymer network produced by the swelling pressure of the initial amount sorbed. Since the sorption process tends to maintain this pressure, Newns¹² has even concluded that the second stage may be compared to some creep process under constant stress. More precisely, we suggest that the above calculation on *recovery* may be applied to this second stage of sorption, and the subsequent swelling process, assuming an equivalence between the negative pressure change ΔP and the swelling pressure, related to the variation of the vapor pressure (activity) of the penetrant.

However, in general, and especially when the vapor pressure dif-

ference is great, these two sorption processes overlap and so the swelling involves a time-dependent pressure change which is a function of the spatial coordinates too. Such a combined diffusion-recovery process may produce many peculiar features¹⁴ where generally the autocatalytic swelling prevails over the Fickian diffusion as long as the sample is glassy, i.e., until its fractional free volume is less than some critical value comparable to f_g .

Other phenomena involving volume changes, such as isothermal crystallization of viscous melts or orientation of chainlike molecules, may show also such anomalous time effects when the fractional free volume is less than some critical value.

As a concluding remark we would like to point out that the viscoelastic bulk behavior may give much interesting information on the hole structure of liquidlike material, especially in the supercooled and glassy region.

This work was partly supported by a grant from the National Science Foundation, G12871. We are much indebted to Professor J. D. Ferry for the many helpful suggestions he made while the above concept was elaborated into this present form, and to Dr. R. S. Marvin for the pertinent remarks he made for clarifying the manuscript.

References

1. McKinney, J. E., H. V. Belcher, and R. S. Marvin, *Trans. Soc. Rheol.*, **4**, 347 (1960).
2. Jenckel, E., and P. Gehrke, Private communication (1959).
3. Kovacs, A. J., Thesis, Fac. Sci. Paris, 1954.
4. Park, G. S., *J. Polymer Sci.*, **11**, 97 (1953); *J. chim. phys.*, **55**, 134 (1958).
5. Doolittle, A. K., *J. Appl. Phys.*, **22**, 1471 (1951).
6. Ferry, J. D., and R. A. Stratton, *Kolloid-Z.*, **171**, 107 (1960).
7. *British Assn. Adv. Sci. Mathematical Tables*, Vol. I, University Press, Cambridge, 1946, pp. 31-33.
8. Williams, M. L., R. F. Landel, and J. D. Ferry, *J. Am. Chem. Soc.*, **77**, 3701 (1955).
9. Kovacs, A. J., *J. Polymer Sci.*, to be submitted.
10. Ritland, H. R., *J. Am. Ceram. Soc.*, **37**, 370 (1954).
11. Bagley, E., and F. A. Long, *J. Am. Chem. Soc.*, **77**, 2172 (1955).
12. News, A. C., *Trans. Faraday Soc.*, **52**, 1533 (1956).
13. Long, F. A., and I. Watt, *J. Polymer Sci.*, **21**, 554 (1956).
14. Kishimoto, A., H. Fujita, H. Odani, M. Kurata, and M. Tamura, *J. Phys. Chem.*, **64**, 594 (1960).
15. Tool, A. Q., *J. Res. Natl. Bur. Stand.*, **37**, 73 (1946).

Synopsis

Viscoelastic bulk deformation under pressure is calculated for a special Kelvin body which consists of a dashpot whose viscosity depends on the free volume, and a Hookean spring in parallel with a constant bulk modulus. Starting with Doolittle's formula relating the bulk viscosity to the fractional free volume, we have shown that the time dependence of the bulk deformation of this body is wholly asymmetrical with respect to the sign of the hydrostatic pressure change. If pressure is applied abruptly, the decrease of volume, instead of being exponential, is approximately linear with respect to the logarithm of time (except for the initial and the final part of the deformation, near the equilibrium). By contrast, if pressure is suddenly removed the volume increase will be a recovery of an autocatalytic type. Some examples of these typical features are illustrated by the behavior of supercooled liquids near the glass transition temperature. Tentatively the anomalous diffusion of small molecules through polymers can also be related to the same phenomena.

A Theory for the Occurrence of Intrinsic Resonances in Stressed Solid Materials*

S. R. BODNER, *Brown University, Providence, Rhode Island*

Introduction

Measurements of the frequency dependence of the complex modulus of crystalline solids in the audio range have yielded unusual results when the specimens are subjected to external loading or contain residual stress. The most interesting of these is the occurrence of resonances which appear to be intrinsic in the material, i.e., they are of microscopic origin and are independent of the sample dimensions. These resonances were first observed by Fitzgerald,¹⁻⁵ and corroborating findings have been made by the author⁶ and by Tombouliau.⁷

The present paper gives a brief review of the conditions under which the unusual results (in particular, the extra resonances) are observed. In the author's previous paper,⁶ he showed how extraneous resonances could arise from the testing technique, although there was strong evidence that some of the observed resonances were of microscopic origin. The experimental procedure of ref. 6 has been modified to eliminate those resonances which arise from the method of applying the static load on the specimen. Results of new experiments are presented which demonstrate the intrinsic material nature of the remaining resonances. The recent tests consist of measurements of the resonances and damping of aluminum specimens (commercial purity, 2S) while the specimen is under load. The special features of these test results are the occurrence of resonances in addition to the natural frequency spectrum, and the measurement of sharp damping peaks at frequencies corresponding to the Fitzgerald resonances of aluminum.

Other than the experiments of Fitzgerald and the author, there

* Supported by the Office of Naval Research, U.S. Navy, under contract Nonr 562(20), Task Order NR-064-424 with Brown University.

appear to be no measurements available of the audio frequency dependence of the complex modulus of materials subjected to external loads. A large number of tests have been made on prestressed specimens to determine the effect of cold working on the damping and modulus. The specimens were, however, unloaded during the measurement and the test frequencies were generally very low, about 1 cycle/sec., or greater than 30 kc./sec. Some damping measurements have been made on loaded specimens, but these have been either at a single low frequency⁸ or in the ultrasonic range.⁹

The present paper includes an interpretation of the material resonances and related effects on the basis of dislocation behavior. The conclusion is that the resonances are due to self-excited oscillations which arise from nonlinear characteristics of dislocation motion. Although the interpretation can be supported by a number of experiments and theories, particulars of the nonlinear behavior are lacking. This precludes the presentation of any theory by which the resonances could be predicted.

Previous Experiments

The initial experiments of Fitzgerald were made with the apparatus developed by him to measure the complex compliance of materials at closely spaced frequency intervals in the range of 50 to 5000 cycles/sec. Inherent in his design is the necessity to prestrain the sample axially between relatively rigid surfaces. The compliance is measured by subjecting the sample to an oscillatory shear, as shown in Figure 1a. The magnitude of the oscillatory stress is very small compared to the stress resulting from the initial prestrain.

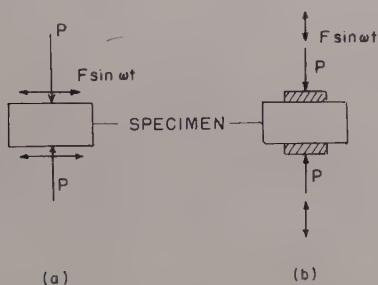
An essential feature of Fitzgerald's tests is that the sample dimensions are very small compared to the wavelength of the oscillatory shearing stress. The sample is therefore uniformly stressed at any instant and inertial effects due to waves in the specimen would be expected to be absent. From another viewpoint, the lowest natural frequency of the sample is much greater than the frequency of the oscillatory stress.

Fitzgerald's observations of the resonance phenomenon are summarized in his recent paper.¹⁰ The important results of his tests are summarized as follows:

1. Resonance dispersions were observed at frequencies much below the lowest natural frequency of the samples. In particular a

strong resonance at about 2850 cycles/sec. was common to many different materials, e.g., lead, indium, aluminum, crystalline quartz, and sodium chloride, and was independent of sample dimensions. The frequency and magnitude of the resonance were somewhat dependent on the initial stress and changed with time. On the other hand, resonances were not observed in polymers in the amorphous state.

I. FITZGERALD'S TESTS



II. RESONANCE TESTS

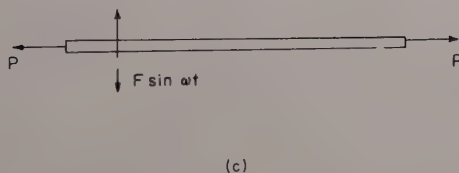


Fig. 1. Loading conditions for observation of anomalous resonances.

2. Negative damping values were obtained over a narrow frequency interval in the vicinity of a large resonance (e.g., Fig. 2). The negative damping value decayed with time but could be reestablished by increasing the axial stress. An unusual energy transfer appears to take place in which the initial strain energy of compression is converted into oscillatory energy. A nonlinear model that exhibits a similar energy transfer is the common mechanical clock.

3. The measurements of the elastic modulus obtained with the FitzGerald apparatus were low compared to the values obtained in the

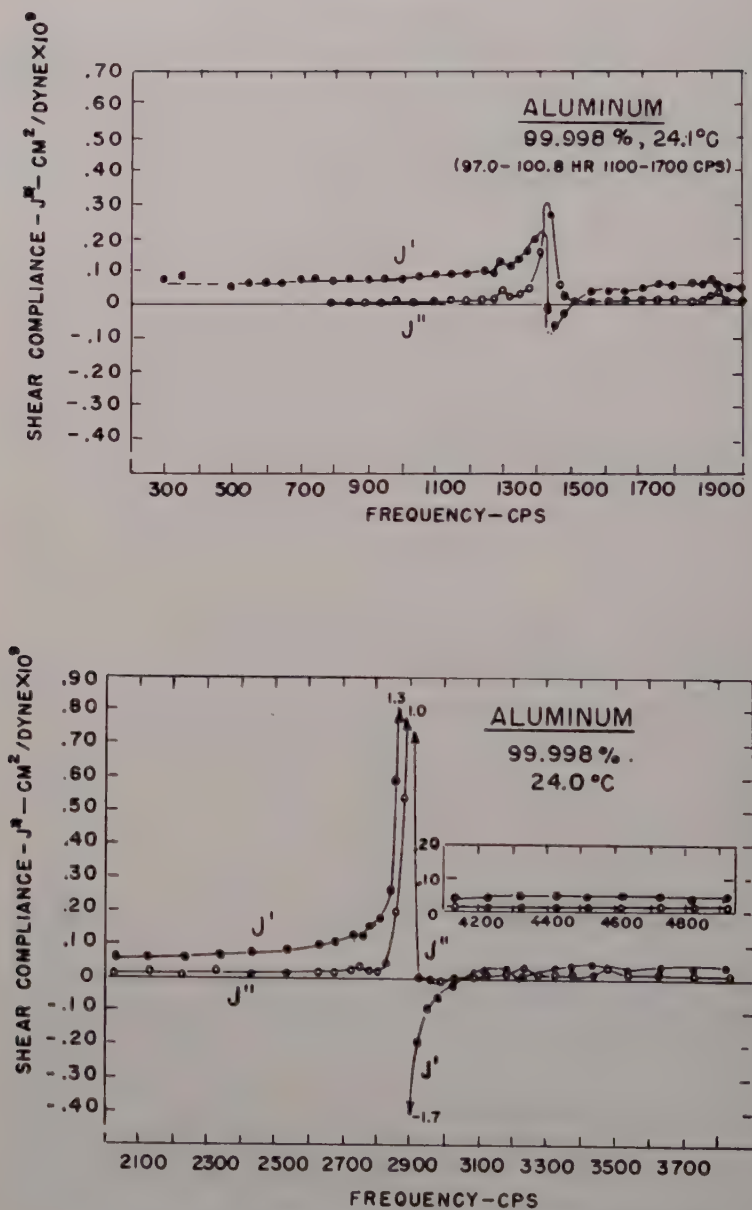


Fig. 2. Resonance dispersion obtained by Fitzgerald for aluminum.¹

usual static or dynamic tests. The difference was most pronounced in the tests on metals—the value for aluminum at about 100 cycles/sec. was only $1/20$ that usually obtained.

Another test arrangement due to Fitzgerald is shown in Figure 1b. The sample, which is again small compared to the wavelength of the oscillatory stress, is sandwiched between two barium titanate crystals and compressed. An alternating voltage is supplied to one crystal which thereby subjects the sample to a small oscillatory axial stress. The other crystal acts as the receiver and its voltage output is a measure of the rigidity of the sample. The interesting result of this test is that if the initial compression is sufficiently large, rapid changes in the compliance occur at the resonant frequencies of the other test. Measurements have not yet been made on the minimum initial stress necessary for the occurrence of the jumps, but they have been observed at stresses well below the yield value.

The author's previous tests⁶ differed basically from Fitzgerald's in that they were based upon the resonance technique, i.e., the wavelength of the oscillatory stresses were of the order of or less than the specimen length (Fig. 1c). Resonances in addition to the usual natural frequencies were observed when the specimens were subjected to axial stress or contained residual stress. In the latter event, a single additional resonance at about 2800 cycles/sec. was observed on some aluminum specimens.

The discussion of ref. 6 indicates how extraneous resonances can arise in an oscillating system if the rigidity of the system varies harmonically with time. The governing equation is then of the Mathieu type, e.g.,

$$M\ddot{x} + (K + \Delta K \sin \omega_k t)x = 0 \quad (1)$$

for which particular combinations of parameters result in unstable motion.

The rigidity of a laterally oscillating beam depends upon the axial stress which, if given a sinusoidal time variation, would lead to a Mathieu equation. This problem is treated in detail in ref. 11. There is little doubt that some of the extra resonances of wire-pulled specimens reported in ref. 6 were of this type and were due to variations of the axial stress caused by motion of the beam ends. Reference 6 suggests that a possible source of some of Fitzgerald's resonances is the applicability of equations of the Mathieu type obtained

from nonlinear continuum considerations. However, from preliminary computations it appears that the specimen dimensions and test frequencies fall far outside the range in which such equations would predict unstable motion. In addition, it appears that the resonances of interest are not dimensionally dependent and hence cannot be predicted by an overall continuum approach. These resonances appear to be of the self-sustained type as will be discussed in a subsequent section. It is noted, however, that the Mathieu equation can be a special case of linear representation of a nonlinear system that exhibits self-sustained oscillations.

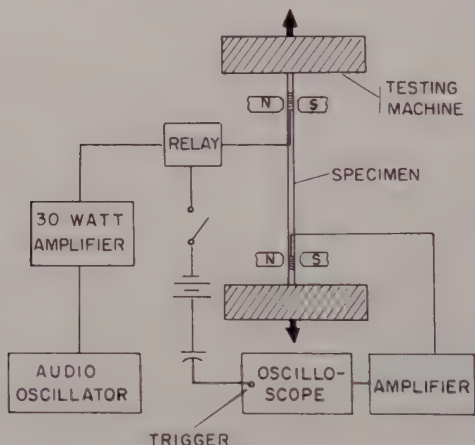


Fig. 3. Experimental arrangement for resonance tests.

Design of New Resonance Tests

The new tests were devised to eliminate resonances that resulted from changes in the applied axial tension caused by motion of the specimen ends. The obvious modification was to clamp the specimen ends to prohibit lateral displacement. Since the specimen was relatively long and thin, the applied loading was a tension to avoid buckling. The load was applied by a very large standard mechanical testing machine which had a capacity more than one hundred times the load applied to the specimen.

The experimental arrangement is shown in Figure 3. The forced lateral oscillation and resulting pickup were obtained by the coil and

magnet technique. The coils were located near the nodal points of the fundamental mode to maximize the input and the response pickup for most of the modes. Damping values were measured by cutting the driving current and recording the amplitude decay on the oscilloscope. This procedure has been used previously in measuring the modulus and damping of lead¹² and of aluminum in the audio range. Only in the case of some cold-worked aluminum specimens were extra resonances observed. In the latter case those resonances were eliminated upon annealing the specimen. In the present tests the testing machine and grips were massive compared to the specimen and were unlikely causes of additional resonances. The specimens were commercial aluminum (2S) rods of $1/2$ in. diameter and about $2\frac{1}{2}$ ft. long. In order to obtain clamped end conditions it was necessary to apply some initial stress to the specimen in attaching the end supports. It was not possible, therefore, to test the clamped specimen without any axial load. The specimen was tested, however, as a completely free beam before and after the measurements in the testing machine were performed.

The amplitude of the maximum oscillatory bending stress was low (about 1 p.s.i.) compared to the axial stress. This value was obtained by strain gages mounted on one of the specimens. The low vibration amplitude created difficulties in the damping measurements, and reasonably accurate values could only be obtained for some of the resonances. The maximum error in those cases is estimated to be less than 25%. The coils contribute to the damping, but measurements made on unloaded annealed aluminum rods using the coil and magnet technique agreed well with other published data. Those tests, moreover, did not reveal any additional resonances. The resonant frequencies could be accurately detected (to within a couple per cent) in the present tests. Although the experimental arrangement provided results that were sufficient for the main purpose of the present paper, various improvements in the detailed techniques could be made. These would increase the accuracy of all the measurements and permit damping values to be obtained at all resonant frequencies.

Experimental Results

The resonant frequencies and associated damping values (logarithmic decrement) of a 2S aluminum specimen are listed in Table I.

TABLE I
Natural Frequencies and Damping Values of Clamped, Stressed 2S Aluminum Rod^a

Holding load	510 p.s.i.	1530 p.s.i.	3060 p.s.i.	3570 p.s.i.	4080 p.s.i.	Free (after testing)
111	114	120	129	131	134	116
295	297 (34) ^b	305	318	321	325 (35)	327 (20)
545	545	555	570	575	579	630
860	860	865	890 (54)	890 (45)	900 (40)	1000
1160	1155	1160	1190	1200	1210 (68)	
1430	1430	1420	1470	1470	1480 (150)	1475 (33)
1950	1920	1950	1970	1900	1930	2070 (13)
2220	2200	2220	2220	2250	2280	
2750	2770 (78)	2780 (130)	2780 (125)	2800 (135)	2800 (135)	2800 (14)
3550	3550	3550	3580	3570 (44)	3580 (67)	3600 (15)

^a Rod dimensions: 27.5 in. long, $\frac{1}{2}$ in. diameter.

^b Numbers in parentheses are damping values (logarithmic decrement) times 10^3 .

The specimen was tested twice under load (the first time up to 3000 p.s.i. axial stress), and tested as a free beam between and after the loading runs. The second run was carried to a tensile stress of 5500 p.s.i. but the response beyond the 4000 p.s.i. level became too low for reliable measurements. The values obtained in the two runs were for the same applied stress, reproducible to within the experimental accuracy. Resonant frequency values were taken on two other specimens and were essentially the same with the exception that for one slightly longer specimen, resonances occurred at both 2750 and 2850 cycles/sec. when the specimen was initially loaded. This double resonance peak merged to a single peak at high values of the applied load as a probable consequence of the increase in damping.

After final testing under load, the specimen ends were cut off so that the free length was equal to the length between the end clamps. The values obtained for the free specimen are listed in the last column

of Table I. Classical theory shows that clamped and free-ended beams of similar dimensions would have identical frequencies. The free beam results are therefore a guide to the natural frequencies expected for the clamped specimen. The difference in the measured frequencies at the lower modes for the two end conditions appeared to be due to the mass of the coils which would have a different effect for the different conditions. The coil masses also introduce a discrepancy between the natural frequencies of the free beam and the classical values. Appropriate corrections could be made for the coil masses in experiments designed to determine the elastic modulus at various frequencies.

Although all the resonances were readily detected, there were appreciable differences in the amplitude of the responses for the same input. These differences were due, in part, to the location of the coils and probably also to the nature of the resonances. The response about 2220 cycles/sec. was very low at low loads and always too low for reliable damping measurements. The amplitude of the resonance at about 1450 cycles/sec. was also low at low loads but increased appreciably with increasing load. The response at about 2780 cycles/sec. was much stronger than all others in the kilocycle range. As expected from classical theory, the resonant frequencies increased with increasing tensile load.

The most convincing feature in the test results of unusual material behavior is the variation of damping with frequency. The logarithmic decrement of annealed unloaded 2S aluminum is about 8×10^{-3} and is not very frequency dependent in the audio range. A general increase in damping for unloaded but cold-worked materials has been observed by many investigators. The present test specimen was loaded slightly beyond the elastic limit (about 5000 p.s.i.) so the larger damping values in the final free beam test are not unexpected. The results in Table I show that at a particular frequency the damping increased rapidly with applied load and subsequently stabilized or decreased with increasing load. Similar behavior has been observed in the ultrasonic range with 2S aluminum.¹³ The very large increase in damping at 1480 and 2800 cycles/sec. is, however, a new and important result. The three fold difference in damping between the 2800 and 3570 cycles/sec. resonances at an axial stress of 3570 p.s.i. was particularly striking and cannot be attributed to experimental error. Fitzgerald's results for pure aluminum, Figure 2.

show large resonance dispersions at 1430 and 2890 cycles/sec. Very large damping (J''/J') occurs in the general vicinity of the resonances although the damping may become negative in a narrow frequency interval. The strong resonance observed in the present tests would appear to be a reinforcement of the natural frequency response by a material resonance. When these did not merge, as in one of the present tests and in earlier tests with specimens with residual stresses, double resonance peaks were observed.

It is difficult to identify the other resonances—in particular, the source of the resonance at 1450 cycles/sec. is somewhat uncertain although this resonance is also characterized by very large damping and agrees with a Fitzgerald resonance, Figure 2. It may be an intrinsic material response or a combination of a natural frequency and a material effect. The response amplitude at 1450 cycles/sec. differed from that at 2800 cycles/sec. in that it was appreciably smaller than those at the adjacent resonances. Although these test results are capable of refinement they do show that intrinsic material effects are present that influence the macroscopic behavior of the specimens.

Interpretation of Experimental Results

The cumulative results of the various experiments supply very strong evidence that the resonances and related effects are a consequence of intrinsic material properties. Although they depend upon the method of testing insofar as they are observed when a small oscillatory stress is superimposed upon a large static stress, they do not follow from overall mechanical considerations. The results indicate that aspects of dislocation behavior are responsible for the resonances and the following discussion is based upon such an interpretation.

Much of the development of dislocation theory has been directed toward an understanding of plastic flow. Whereas the mechanism of plastic flow is dependent upon a great variety of physical properties, the resonance effect is remarkable in the universality of its occurrence in crystalline solids and the common occurrence of the strong resonance at about 2850 cycles/sec. for many materials. In addition, the occurrence of the resonances in quartz, which appears incapable of ordinary plastic flow, points to a dislocation mechanism that must precede plastic flow.

A general interpretation of the test results is that a large number of

potentially mobile dislocations exist in the material due to the initial static stress. The static stress tends to free dislocations from weak pinning points and to create sources by which new dislocations can develop. The stressed material would then offer less resistance to a small additional stress than would be predicted by the elastic modulus. The elementary motion of mobile dislocations can be expected to be nonlinear, i.e., the motion itself gives rise to forces which affect the motion. If the cumulative effect of these additional forces tends to increase the motion, then a self-sustained oscillation can occur. The presence and motion characteristics of mobile dislocations is regarded

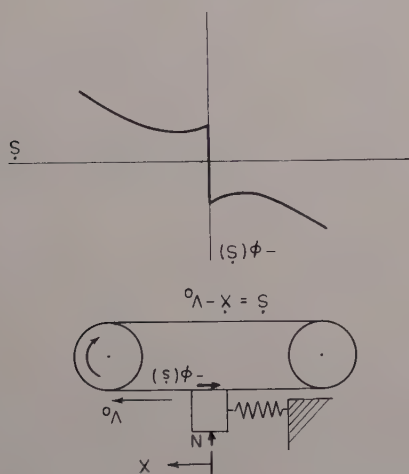


Fig. 4. Mechanical system capable of self-sustained oscillations.

as the source of the low modulus observed by Fitzgerald and the cause of the resonances.

A mechanical model that illustrates self-sustained oscillation is shown in Figure 4 and is due to the characteristics of dry friction. The damping in systems exhibiting self-sustained oscillations is essentially negative for small velocities. In the dry friction model the effective negative damping result from the reduction in friction force at small slipping velocities. It can be shown, e.g., p. 125 of ref. 14, that the system of Figure 4 can experience self-sustained oscillations for particular combinations of normal force, spring constant, and belt velocity. Although such systems are inherently

nonlinear, they can often be represented by linear equations, e.g., the classical approach to flutter problems.

In order for the oscillations of a self-excited system to be maintained, an energy source must be available. This would be the motion of the belt in the friction example and the steady flow of air in the flutter problem. In the present case the energy source is the strain energy of deformation which facilitates dislocation breakaway and/or creates sources for new dislocations. The motion of the dislocations is irreversible and results in a static hysteresis-type energy loss.

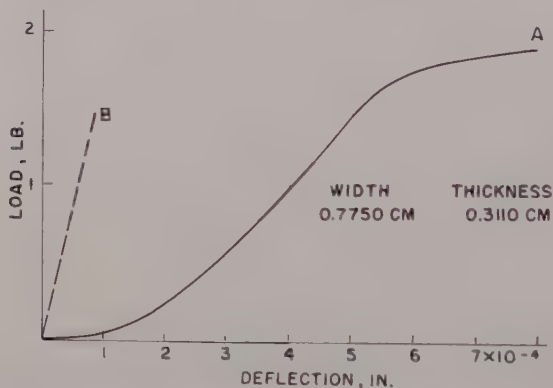


Fig. 5. Initial portion of load-deflection curve for NaCl single-crystal specimen. (A) Experimental curve. (B) Calculated Hooke's law line.¹⁵

The self-excited oscillations have a feed back which is manifested by a decrease in the static strain energy. The essentially negative damping character of the resonances shows up in the negative values of J'' measured by Fitzgerald at frequencies just above the damping peak at resonance (Fig. 2).

An important characteristic of a self-excited system is that the frequency of the oscillations may be far different from the natural frequency of the system in the absence of the energy source. The flutter frequency, for example, is usually appreciably different from the natural frequency of the lifting surfaces based only upon structural considerations. Another example is the system governed by the equation

$$M\ddot{x} + F(\dot{x}) + x = 0$$

where

$$F(\dot{x}) = -\alpha\dot{x} + (\beta/3)\dot{x}^3$$

The damping is negative at low velocities and becomes positive at high velocities. The frequency of the self-sustained oscillation is shown (e.g., pp. 138-140 of ref. 14) to depend only on α —the initial slope of the nonlinear damping term.

A number of experimental observations are available that tend to support the preceding interpretation. Simple static tests on cleaved NaCl crystals reveal an initial inelastic region (or "foot"), Figure 5, which is attributed to the presence of mobile dislocations introduced by the cleavage.¹⁵ The initial slope of the stress strain curve is appreciably lower than the usual elastic modulus. Unfortunately, there appear to be few experiments on the instantaneous response of a loaded specimen to a small increase in load. Some studies on micro-creep or microstrain following deformation indicate that the response of a stressed specimen to small load changes is anelastic, but insufficient measurements on this aspect are available. Tests on the effect of incremental changes on the creep of lead are reported in ref. 16. The results show that the response of a loaded lead wire to a small load increase is much greater than that corresponding to the usual elastic modulus.

Various experiments on the role of dislocations in damping are relevant to the present discussion. The damping measurements of ref. 17 show that dislocation breakaway in pure aluminum occurs at relatively low strains (of the order of 0.01% or less). The presence of impurities, as in 2S aluminum, tends to inhibit breakaway. The increase in ultrasonic attenuation at low strains is attributed to increased loop length due to dislocation breakaway. At higher strains, but below yield, dislocation generation sources start to operate, and the continued increase in ultrasonic attenuation with increasing strain is due to the resulting larger dislocation density. The frequency independent damping measured at low frequencies is strain dependent for sufficiently large strains and has been shown to be related to dislocation breakaway. These results are cited as evidence that relative mobile dislocation motion is possible in the presence of an initial static stress.

A dislocation theory that discusses irreversible dislocation motion at stresses below macroscopic yield is Mott's theory of fine slip.¹⁸

An important point in the theory is that the dislocation motion associated with fine slip can occur at stresses well below yield and in materials that do not demonstrate coarse slip bands or plastic flow (e.g., quartz). The mechanism of fine slip is a discontinuous movement of a dislocation line past repeated obstacles, i.e., successive breakaway. The dislocation moves forward in a series of little jerks and the result on the movement is equivalent to a frictional force. There is therefore a direct analogy between the mechanism of fine slip and the friction model shown in Figure 4. The dislocations in the fine slip mechanism are considered to arise from nondynamic operation of Frank-Read sources. Hence both dislocation breakaway and source operation are inherent in the theory.

As an example of fine slip, Mott discusses the movement of an edge dislocation through an array of screw dislocations. It is noted that, as in dry friction, the force necessary to cause the dislocation line to break away from an obstacle is greater than that necessary to maintain the motion between obstacles. The theory of fine slip is used to account for logarithmic creep, the hysteresis loop of single crystals under reversed stress, and the Bauehinger effect in single crystals. The theory, however, does not give the detailed force velocity characteristics of the dislocation between obstacles which would be essential in order to predict the occurrence of self-sustained oscillations. It is noted, however, that the mean velocity of motion is primarily a function of quantities that are constant for many materials—the interatomic spacing and an atomic frequency.

It should be emphasized that Fitzgerald's modulus is not the dynamic modulus measured in a resonance or wave propagation test. In such tests the usual elastic modulus is obtained for small dynamic strains even though the specimen may be initially stressed well beyond the yield point. For example, the natural frequency at about 100 cycles/sec. in the present test was unaffected by the axial stress except for the slight increase predicted by continuum theory. The wave propagation tests of Sternglass and Stuart¹⁹ showed that small stress increments travel at the elastic velocity in yielded material—in contradiction to the rate independent plastic wave theory. Hillier and Kolsky²⁰ show that for various high polymers under load an enormous difference exists between the dynamic modulus obtained by wave propagation and the slope of the static stress-strain curves.

A distinction must, therefore, be made between Fitzgerald's

modulus and the usual elastic modulus. Fitzgerald's modulus does approach the elastic value for increasing frequency.

From the viewpoint of continuum mechanics the problem is the derivation of stress strain laws that would describe the experimental results. Since the experiments involved only small oscillations from an initial stress state, it would be consistent to look for linear laws to represent the stress-strain relations of the superimposed strains. The experimental measurements were found to be independent of the amplitude of the oscillatory stress over the range tested. Fitzgerald showed in his papers that the compliance in the vicinity of a resonance can be represented by a stress strain law of the form

$$\tau = K_0\epsilon + K_1\dot{\epsilon} + K_2\ddot{\epsilon} \quad (2)$$

Similar equations could be made to be applicable over the complete frequency range if the K 's were appropriately chosen functions of frequency.

It can be shown that the following specialized form of eq. (2) would describe a large number of general test results:

$$\tau = k_0\epsilon + \frac{\mu k_2}{\omega^2[\mu + (1 - \omega^2/\omega_r^2)]} \ddot{\epsilon} \quad (3)$$

This equation represents a linear rate dependent material which has a single material resonance at $\omega = \omega_r$. The model representation of eq. (3) would be simply an elastic element, k_0 , in series with a spring mass system. The constant μ , with reference to the model, would represent the ratio of k_0 to the spring constant, k_2 , of the spring mass component. The value of μ would be expected to be less than unity for an actual material. Although eq. (3) could be made more realistic by including damping terms, $K_1(\omega)$, by making k_0 a function of ω , and by incorporating more material resonances, it is interesting to examine the consequences of adding only the single term to the standard elastic law.

If the material specified by eq. (3) is subjected to an oscillatory stress $\tau = \tau_0 e^{i\omega t}$ under conditions for which the material inertia can be ignored (e.g., Fitzgerald's tests), then the steady state response is

$$\epsilon = (\tau_0/k_0)e^{i\omega t} \left\{ \frac{\mu + [1 - (\omega^2/\omega_r^2)]}{[1 - (\omega^2/\omega_r^2)]} \right\} \quad (4)$$

For very high frequencies ($\omega \rightarrow \infty$), the effective modulus is the ordinary elastic value, k_0 , whereas for low frequencies ($\omega \rightarrow 0$), it is reduced to $k_0[1/(1 + \mu)]$. Since μ would not be expected to be greater than unity, this does not account for the large reduction in modulus at low frequencies observed by Fitzgerald ($1/20$ in aluminum). A larger reduction in modulus can be achieved by further generalization of eq. (3) such as by introducing a number of material resonances, by including viscous damping terms, and by considering k_0 to be frequency dependent.

From eq. (4) material resonance occurs when $\omega \rightarrow \omega_r$ and, since damping is neglected, the strain approaches infinity. The complementary solution of eq. (3) does not appear to have physical meaning since the free oscillations of the material must involve the inertial mass. Under Fitzgerald's test conditions any free oscillation would rapidly decay due to damping and only the steady state oscillation would be observed.

In analyzing resonance and wave propagation tests for the material specified by eq. (3), the mass of the material must be considered. The case of longitudinal waves in a rod has been treated, but the general results would apply as well for the lateral vibration case. Longitudinal waves in a rod of viscoelastic material are dispersive and their main properties can be determined from the dependence of frequency on the wave number. A related problem on the effect of "hidden" resonances on wave propagation is treated in ref. 21.

The equation for longitudinal waves in a rod is

$$\tau_{,x} = \rho \bar{u}_{,tt} \quad (5)$$

where \bar{u} is the displacement along the longitudinal, x , axis, ρ is the mass density, and a comma indicates differentiation. Upon setting

$$\bar{u} = u(x)e^{i\omega t} \quad (6)$$

and utilizing the strain displacement relation $\epsilon = u_{,x}$ and the stress strain relation, eq. (3), the equation of motion becomes

$$\frac{k_0}{\bar{u}} \left\{ \frac{[1 - (\omega^2/\omega_r^2)]}{[\mu + [1 - (\omega^2/\omega_r^2)]]} \right\} u_{,xx} + \omega^2 u = 0 \quad (7)$$

The solution of eq. (7) is of the form

$$u = e^{i\lambda x}$$

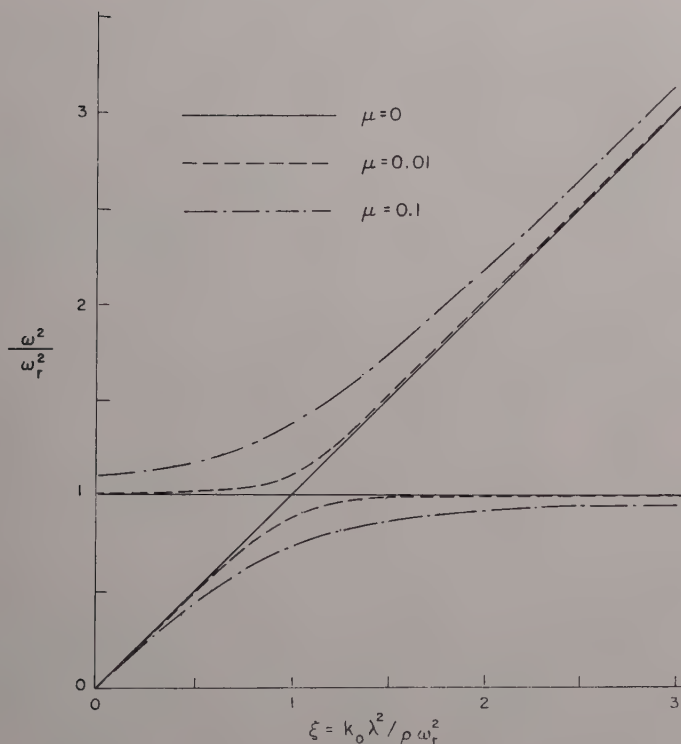


Fig. 6. Characteristic curves for longitudinal waves in a medium that exhibits a resonance dispersion.

where λ is the wave number. Equation (7) reduces to

$$(\omega^2/\omega_r^2)^2 - (1 + \xi + \mu)(\omega^2/\omega_r^2) + \xi = 0 \quad (8)$$

where

$$\xi = k_0 \lambda^2 / \rho \omega_r^2 \quad (9)$$

The dependence of ω^2/ω_r^2 on ξ for different values of μ is shown graphically in Figure 6. For each value of μ , eq. (8) has two branches which are hyperbolic curves. For the case of $\mu = 0$ they reduce to the straight lines

$$\omega^2/\omega_r^2 = 1, \quad \omega^2/\omega_r^2 = \xi$$

The latter is the result of classical theory

$$\omega^2 = (k_0/\rho)\lambda^2 \quad (10)$$

The important result from Figure 6 is that, for small μ , the frequency equation over most of the frequency range is the classical value, eq. (10). This result is approached as the limit value at both ends of the frequency range.

If a natural frequency occurs in the immediate vicinity of the material resonance, then the response would be similar to that of a coupled two degree of freedom system. For a mode corresponding to $\xi = 1$, the apparent natural frequencies obtained from eq. (8) are

$$\omega^2/\omega_r^2 = [1 + (\mu/2)] \pm [\mu + (\mu^2/4)]^{1/2} \quad (11)$$

The same equations [(8) and (11)] are obtained for lateral vibrations, but the wave number parameter ξ' is then equal to

$$\xi' = k_0 R^2 \lambda^4 / \rho \omega_r^2 \quad (12)$$

For this case the space-wise variation of the dependent variable w is taken as

$$w = e^{\lambda z}$$

and R is the radius of gyration of the cross section. From eq. (11), a lateral oscillation mode in the vicinity of $\xi' = 1$ would show up as a double response peak in the resonance tests. The separation between the peaks can be used to determine μ , or alternatively, the mass component in the model representation of the stress strain law. The latter calculation was performed in ref. 6 for the double response peak observed in tests on an aluminum rod which contained residual stress. The computed value was of the same order of magnitude as that obtained by Fitzgerald in analyzing his test results in terms of the same model parameters.

The addition of the single term proportional to $\ddot{\epsilon}$ in the elastic stress-strain relation therefore predicts the following experimental results:

(1) Fitzgerald's Tests: (a) The modulus at high frequencies has the standard elastic value while that at low frequencies is reduced. (b) A resonance occurs at the material resonance frequency ω_r .

(2) Resonance Tests: (a) At frequencies removed from the material resonance frequencies the response is that expected from classical elastic theory. (This assumes that the physical properties corresponding to μ would be small.) (b) At frequencies in the neighborhood of a material resonance an additional resonance peak would occur.

Note Added in Proof: Recent experiments by the author tend to cast doubt on Fitzgerald's low modulus values as an inherent physical property of the material. A number of aluminum alloy specimens (3S-0, 3S-H14, 5052-0) were stressed into the inelastic range (to about 2% strain). At increments of loading they were subjected to small oscillatory strains whose wavelength was much greater than the specimen length in conformity with Fitzgerald's conditions. This was achieved by the specimen serving as the spring in a spring mass resonance system. The natural frequency of the system was designed to be about 200 cycles/sec. Specimens were pulled in tension in both a rigid testing machine and in a massive dead load device and in each case were subjected to small torsional, bending, and extensional oscillations. In all instances, including under creep of plastic flow, the natural frequencies of the system corresponded to the normal elastic modulus of the material (to within the experimental accuracy—about 2%). In addition, no special resonances were observed in the 2500–3000 cycles/sec. range.

From these tests it would appear that Fitzgerald's compliance values are due to coupling of an unusual material property with an elastic testing machine. (By its manner of operation the Fitzgerald apparatus is necessarily an elastic machine. In the crystal tests the crystals themselves are elastic.) The unusual material property is believed to be a negative slope in the stress-strain rate relation similar to the dry friction characteristic. Such behavior has, in fact, been observed for metals and other materials [e.g., Manjoine, *Trans. ASME*, **66**, A211 (1944)] and has been proposed as the cause of the stress oscillations that accompany yielding. Some of the consequences of this behavior, when coupled to a spring mass system, e.g., the testing machine, are discussed in the paper with reference to the model shown in Figure 4. In particular, the system can result in self-excited oscillations which appear as very sharp resonances. The response of such a system to an oscillatory force can differ appreciably from the predictions of linear theory over a wide frequency range and is a problem in nonlinear vibration theory (van der Pol problem).

The argument in the paper was based on the supposition that a mechanism analogous to the friction model, Figure 4, was operative in the material itself. In the light of the new tests, it would appear that the material behavior is less complex and that a material characteristic such as a negative slope in the stress-strain rate relation coupled with an elastic testing machine can lead to most, if not all, of the experimental results. (It is noted that the negative slope property is an important part of the fine slip theory discussed in the paper.) In the case of the bar resonance tests, the resonating bar itself may take the role of the testing machine, i.e., the spring-mass components in the model. The double resonance peaks and the experimental results described in this paper would then result from a coupling of the normal resonance with the negative slope property. The particular unusual aspect of the phenomenon is the apparent frequency dependence of the material property that is responsible for the experimental results obtained with the Fitzgerald apparatus and in the resonance tests.

References

1. Fitzgerald, E. R., *Phys. Rev.*, **108**, 690 (1957).
2. Fitzgerald, E. R., *J. Chem. Phys.*, **27**, 1180 (1957).

3. Fitzgerald, E. R., *J. Appl. Phys.*, **29**, 1142 (1958).
4. Fitzgerald, E. R., *Phys. Rev.*, **112**, 765 (1958).
5. Fitzgerald, E. R., *Phys. Rev.*, **112**, 1063 (1958).
6. Bodner, S. R., *Trans. Soc. Rheology*, **4**, 141 (1960).
7. Tomboulia, R., Annual Meeting, Acoustical Society of America, Brown Univ., June 1960.
8. Maringer, R. E., *J. Appl. Phys.*, **24**, 1525 (1953).
9. Hikata, A., R. Truell, A. Granato, B. Chick, and K. Lücke, *J. Appl. Phys.*, **27**, 396 (1956).
10. Fitzgerald, E. R., *J. Acoust., Soc. Am.*, **32**, 1270 (1960).
11. Lubkin, S., and J. J. Stoker, *Quart. Appl. Math.*, **1**, 215 (1953).
12. Bodner, S. R., and H. Kolsky, "Stress Wave Propagation in Lead," in *Proc. 3rd U.S. Natl. Congr. Appl. Mech.*, June 1958.
13. Hikata, A., and R. Truell, *J. Appl. Phys.*, **28**, 522 (1957).
14. Stoker, J. J., *Nonlinear Vibrations*, Interscience, New York, 1950.
15. Stearns, C. A., A. E. Pack, and R. A. Lad, *J. Appl. Phys.*, **31**, 231 (1960).
16. Onat, E. T., and T. T. Wang, "The Effect of Incremental Loading on Creep Behavior of Metals," Brown University Report Nonr-562(20)-20, (1960).
17. Truell, R., and R. Boyer, *Phys. Rev.*, **110**, 1206 (1958).
18. Mott, N. F., *Phil. Mag.*, **44**, 7th Series, 742 (1953).
19. Sternglass, E. J., and D. A. Stuart, *J. Appl. Mech.*, **20**, 427 (1953).
20. Hillier, K. W., and H. Kolsky, *Proc. Phys. Soc. London*, **B62**, 111 (1949).
21. Tolstoy, J., "Resonances due to Hidden Degrees of Freedom in Stratified Elastic Media" in *Non-Homogeneity in Elasticity and Plasticity*, Pergamon, London, 1959.

Synopsis

Recent experimental work on the measurement of the compliance of initially stressed materials has supplied strong evidence that at least some of the additional resonances (i.e., those not predicted by classical theory, and specifically, those observed by E. R. Fitzgerald), are due to an intrinsic material property. The resonances are viewed as self-excited oscillations caused by nonlinear characteristics of the motion of dislocations in the materials.

The Distribution of Pressures in the Roll Application of Newtonian Fluids

RAYMOND R. MYERS and RAY D. HOFFMAN,* *Lehigh
University, Bethlehem, Pennsylvania*

The flow behavior of thin liquid films during passage through a roll nip is an important determinant of their lubricating qualities in the nip and of the characteristics of the film which emerges. The dynamic aspects were considered as early as 1886,¹ but their exploitation was not possible until Gaskell² provided the basic equation for the pressure variations experienced by a Newtonian fluid inside a roll nip. This equation was subjected to experimental verification by Bergen and Scott³ and extended to shear-sensitive liquids by Gatcombe⁴ and others.⁵

Despite these advances, the general equation which emerged contained too many terms to become a vehicle for general communication; nevertheless, it is applicable to the situation encountered in film splitting, and therefore was accorded an analytical study of its physical meaning and limitations. It was known at the outset that Gaskell's equation applies only in that region of the nip in which the shear is laminar; consequently, the analysis was preceded by a breakdown of the nip into its component regions.

Regions in a Roll Nip

In the steady flow of liquid through a pair of rotating rolls (or through a pair of mating gear teeth), it is possible to recognize three consecutive regions. The upstream region contains a bank of fluid, rejected by the nip and in turbulent motion. The central region covers the entire area of liquid contact downstream from a hypothetical plane of no shear which marks the beginning of truly laminar

* Sun Chemical Corp. Fellow.

flow through the nip. The downstream region is characterized by flow of liquid under tension, generally with a serrated or filamentous free boundary, and begins at a second plane of no shear whose location is symmetrically placed with respect to the upstream plane.⁶

Theoretical deductions by Blokhuis⁷ and experimental work of Miller and Myers⁶ have resulted in the finding that at or above a critical $U\eta$ (velocity-viscosity) product the filamentation region is

TABLE I
Characteristics of Nip Regions

Region	Characterized by
Bank	Widely fluctuating shear rates Turbulent flow Rejection of material
Shear	Laminar flow Rising, then subsiding shear rates High compression, then slight tension (Region of application of Gaskell's equation)
Cavitation	Cavities dispersed in liquid Extremely low shear rate Radial flow from cavity centers (This region disappears in 1st regime flow)
Filamentation	Cavities coalesce Localized high shear in filaments Decaying tension Filaments in air Flow normal to rolls (Region of application of Stefan's equation)

preceded by a region of cavitation. In this study a disc-cone assembly (Discone) was used in place of rolls in order that the interior of the nip could be viewed photographically.

The shear and filamentation regions have been fairly adequately characterized by Gaskell and Stefan,⁸ respectively, for the case of rolls moving at the same peripheral velocity. The cavitation region has been studied only in a kinematic sense.⁶

Table I lists the characteristics of the four regions existing in a nip above the critical $U\eta$ product.

Pressure Profile in the Shear Region

Considerable interest centers around the shape of the pressure profile through the nip. As x , the distance from nip center, increases from $-x_2$ to x_1 (Fig. 1) the pressure drops monotonically from a maximum at $-x_1$ to a minimum at x_1 . This drop in pressure is responsible for the flow of material through the nip (relative to the rolls), whether the process is one of milling, printing, roll coating, calendering, or even lubricating a pair of gears, and regardless of whether the peripheral velocities of the roll surfaces are identical.

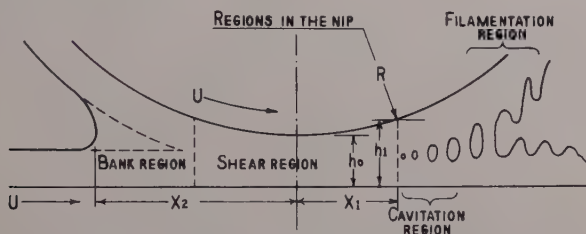


Fig. 1. Model of the roll system. Two wetted surfaces, each traveling with velocity U meet at distance x_2 from the nip center. Vertical dotted lines denote nominal points of initial and final contact, where shear is zero. Minimum clearance h_0 , nominal film thickness h_1 , and cone radius R are shown.

The pressure profile suggested by Gaskell was adopted in this work in an attempt to clear up some of the discrepancies that existed among the various assumed pressure profiles.^{7,9} Special attention was given to the limits imposed by the onset of cavitation on the tension in the liquid because of the experimental findings of Miller and Myers⁶ that cavitation invariably accompanies the splitting thin liquid films between rolls under conditions of practical interest.

Theoretical Analysis of the Pressure Equation

Gaskell's equation, adapted to the geometry of Figure 1 is:

$$p = \frac{3U\eta\sqrt{2Rh_0}}{2h_0^2} \left\{ \sin\theta \cos\theta [(4 - 3h_1/h_0) - \right. \\ \left. \text{Coeff} \qquad \qquad \qquad \text{Grad} \right. \\ \left. 2(h_1/h_0) \cos^2\theta] + (4 - 3h_1/h_0)\theta \right\} + C \quad (1) \\ \text{Bias}$$

where θ is a dimensionless form of the distance from the nip center. It is *not* an angle, but is best identified² in terms of the distance x by the equation

$$\tan^2 \theta = x^2/2Rh_0 = (h/h_0) - 1 \quad (2)$$

Note that θ is determined by a ratio of x to the product of two geometric parameters of the system. It is a similitude or scaling factor used to permit the geometry of Figure 1 to apply to any size roll.

The quantity h_1 represents a particular value of the clearance at a distance x_1 from the nip center where the pressure profile attains a minimum or maximum. The distance x_2 represents the point of initial contact of the two liquid layers. The ratio h_1/h_0 is a parameter of the system, and varies between 1 and $1/3$ for any situation.

Table II gives typical operational values which allow eq. (1) to be evaluated from conditions to be found on the Discone.⁶

TABLE II
Typical Discone Operating Conditions

$\eta = 150$ poises	$h_0 = 30 \times 10^{-4}$ cm. (center clearance)
$U = 8$ cm./sec. (rim velocity)	$x_1 = 3.5 \times 10^{-2}$ cm.
$R = 2.5$ cm. (roll radius)	$\sqrt{2Rh_0} = 0.12$ cm.
$\frac{h_1}{h_0} = (x_1^2/2Rh_0) + 1 = [(0.035)^2/(0.12)^2] + 1 = 1.085$	
$\theta_1 = \arctan[x_1/(2Rh_0)^{1/2}] = \arctan 0.29 = 0.28$	

Equation (1) with these values substituted becomes

$$p = 2.4 \times 10^7 \{ \sin \theta \cos \theta (0.74 - 2.17 \cos^2 \theta) + 0.74\theta \} + C \quad (3)$$

where 2.4×10^7 is an amplitude term in dynes/cm.² established by the material and geometrical constants of Table II; it amounts to about 24 atm., and is called the *coefficient* in subsequent paragraphs. C is a constant which can be adjusted to bring the magnitude of the minimum pressure to the experimentally determined cohesive strength of the liquid. The major task is to identify the two θ terms inside the bracket. They are called *characteristic terms*.

Figure 2 is a plot of the two characteristic terms of eq. (3) as a function of x , the distance from the center of the nip. Here, x rather than $\tan \theta$ is plotted as the abscissa because this plot is applied to a specific case where R and h_0 are known and x has a physical

meaning more readily understandable than θ (although either is perfectly legitimate here).

The graph shows clearly the opposed roles of the two characteristic terms of the equation. The first term behind the bracket is responsible for the *pressure gradient through the nip*, which establishes the amount of shear imparted to the film. It is this term which reflects the rate of shear through the nip.

The contribution of the second bracketed term to the pressure profile is in opposition to the first; it establishes the *pressure head* imparted by the pumping action of the Discone. The contribution from 0.74θ has less influence in creating shear than does the first

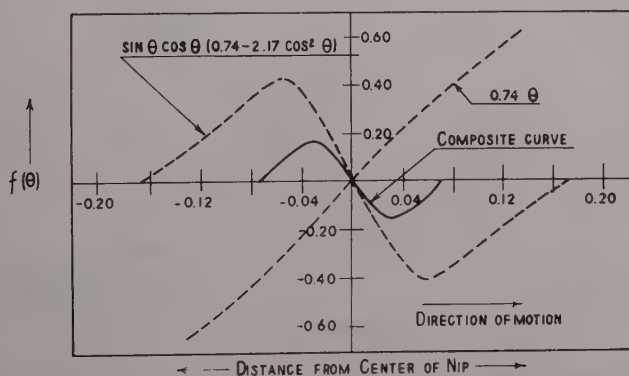


Fig. 2. The two characteristic terms of the nip pressure profile. The two bracketed terms of eq. (3) are shown for the case $h_1/h_0 = 1.085$. The coefficient and bias constant are not included.

term, and it has no cavitation possibilities in the three nip regions under consideration. This term provides an overall pressure increase, or pumping action.

In Figure 3, the effect of the *wedge parameter*, h_1/h_0 , on the composite curve is examined. The parameter h_1/h_0 is the ratio of the film thickness of the material on both surfaces to the minimum clearance. When the ratio is unity, the film just passes between the rolls at the center and no discernible pressure is created, because the wedge of liquid has no taper. As h_1/h_0 exceeds unity, two effects are noted. First, the point of maximum pressure moves upstream (with the bank) as indicated by the curved dotted line in Figure 3; second, the

maximum pressure increases greatly in magnitude. These two effects peak asymptotically at $x = \pm 0.07$. This value of x coincides with the approach of h_1/h_0 to the value, $4/3$.

The pressure cannot exceed the limit imposed by a wedge parameter of 1.33 (or $4/3$). A "maximum effective film thickness" is attained which cannot be exceeded even by complete immersion of the rolls (except for a small hydrostatic effect). In the operating conditions of Table II, there is a maximum pressure of roughly 64 atm. at a maximum effective film thickness of 40μ .

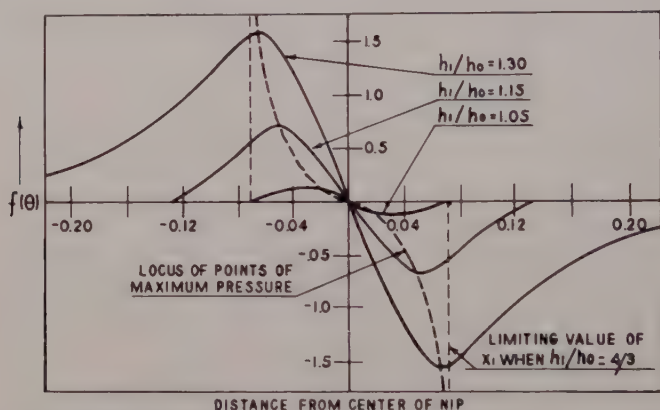


Fig. 3. Effect of film thickness nip clearance ratio on pressure profile. Composite curve from Fig. 2 is shown for three h_1/h_0 ratios. Peak pressure increases and moves outward asymptotically as ratio increases to $4/3$.

The adjustable constant C imposes a *bias* on the pressure. Inclusion of this term is necessary because the equation must fit a determined value of the minimum pressure at x_1 . The pressure at this point cannot *a priori* be selected from the Gaskell treatment because it reflects a cohesive property of the liquid, while the theory considers only viscous properties.

Application of Pressure Equation to Film Application

Figure 4 represents the pressure profile which characterizes flow through a nip under several reasonable conditions. The profile gives a microscopic picture of the situation existing at any point inside the nip, which was the main objective of the Discone program

from its inception. The problem now is to relate this profile to observations made during the application of a Newtonian fluid to a planar substrate.

Figure 4 differs from Figure 3 in that a limiting tension of 1.5×10^6 dynes/cm.² was assumed at the point of cavitation on the downstream side of the nip, although recent work indicates that this is too modest an estimate.¹⁰ This assumption imposed positive bias values of 1.5, 5.0, and 16 million dynes/cm.² on the pressure at the center of the nip for the three assumed values of the wedge parameter h_1/h_0 .

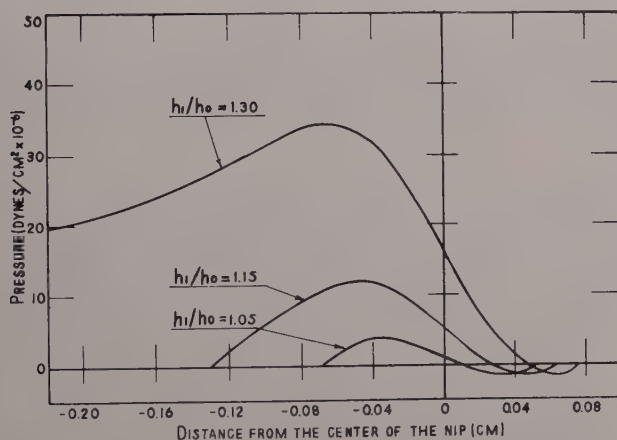


Fig. 4. Actual pressure profile of Newtonian liquid in disc-cone nip. Introduction of coefficient and bias constant produces asymmetrical profile in which finite pressure exists at nip center. Maxima and minima remain highly sensitive to wedge parameter.

In addition, the ordinate of Figure 4 represents true pressure, having been calculated by multiplying the bracketed values of eq. (1) by the coefficient.

In order to find the total force on the roll, it is necessary to integrate eq. (3), the relation depicted in Figure 4. The process of integration gives the area under the pressure profile over the entire contact length as represented from x_2 (the beginning of the bank) through the first plane of no shear to x_1 (second plane of no shear) where cavitation begins. For high values of h_1/h_0 , it may be necessary to approximate the increase in pressure in the bank by assuming that P

increases as $1/x^3$ (ref. 11) up to some arbitrary point in the bank (say $1/10$ th of the roll radius).

Therefore, using the relation between P and x_1 expressed in terms of $\tan \theta$ in eq. (3):

$$F/l = \int_{x_2}^{x_1} p \, dx = \frac{3U\eta R}{h_0} \left[-\frac{h_1}{h_0} \sin^2 \theta + \left(4 - \frac{3h_1}{h_0} \right) \theta \tan \theta \right] + \sqrt{2Rh_0} \left[C \tan \theta \right]_{\theta_2}^{\theta_1} \quad (4)$$

where F/l is the force per unit roll width.

Table III shows some values calculated from the curves of Figure 4.

The integrated value agrees satisfactorily with the force applied to the Discone in the case studied¹² as shown in Table III.

TABLE III
Dependence of Roll Force on Wedge Parameter

h_1/h_0	Force/unit length (dynes/cm.)	
	Calculated	Measured
1.30	6.2×10^6	
1.15	1.11×10^6	1.1×10^6
1.05	0.12×10^6	

In the experiments conducted in this laboratory, the force per unit length of cone was held constant during given experiment. Velocity was the main independent variable; however, due to spreading of the material on the plate, the clearance decreased during the run. Fortunately, the decrease in h_0 occurred at an easily measurable rate.

If the force on the liquid is maintained at a constant value, then during any run the wedge parameter may be changed either by a change in h_0 or by a change in velocity. The question may now be asked as to how h_1/h_0 may be measured from the photographs of Miller and Myers.⁶ Direct measurement of h_0 could not be performed with the necessary precision. From the photographs and the associated data, the film thickness h_1 and the full width of the contact area may be determined. What is not known are the bank width, denoted as d , the value of x_1 , and the roll clearance h_0 .

Equation (2) may be rewritten as

$$x_1 = 2R(h_1 - h_0)^{1/2} \quad (5)$$

and therefore, if x_1 is known, h_0 is known. Also it is evident that the contact width may be written as

$$\text{contact width} = 2x_1 + d = x_1 + x_2 \quad (6)$$

if one assumes that the minimum pressure occurs at the point where the cavities originate. This assumption cannot introduce a large error in the distance parameters.

A third equation is needed in order to evaluate three unknown quantities; and to obtain this equation, a rather arbitrary relation is written between θ_1 and θ_2 :

$$\tan^2 \theta_1 = (1 - e^{-\tan^2 \theta_2}) \tan^2 \theta_{11} \quad (7)$$

where θ_{11} is the value of θ_1 when $h_1/h_0 = 4/3$, and is equal to $1/\sqrt{3}$. This equation is based upon the observed change in θ_2 as θ_1 is changed as a function of h_1/h_0 , and is a reasonable empirical expression of the relation between the bank dimension and the location of the plane of no shear.

If eq. (7) is rewritten as

$$\tan^2 \theta_2 = \ln \left[\frac{1}{1 - \frac{\tan^2 \theta_1}{\tan^2 \theta_{11}}} \right] = \frac{x_2^2}{2Rh_0} \quad (8)$$

and this and eq. (5) are substituted into eq. (6), the relation,

$$\text{contact width} = \sqrt{2Rh_0} [\tan \theta_2 + \sqrt{(h_1/h_0) - 1}] \quad (9)$$

is obtained. This expression may be used to obtain the value of the wedge parameter from experimental contact widths. The experimental values of the wedge parameter (h_1/h_0) must be obtained by an iteration process; that is, one assumes a constant value of h_1/h_0 for a range of velocities; and from the known values of contact width and film thickness calculates contact width/ $\sqrt{2Rh_0}$. Then, using Figure 5, values of h_1/h_0 are determined. The process is repeated until a self-consistent set of values of contact width/ $\sqrt{2Rh_0}$ and the wedge parameter is obtained. Such a set is shown in Table IV.

TABLE IV
Relation between Contact Width and Wedge Parameter

Velocity, r.p.s.	contact width/ $\sqrt{2Rh_0}$	h_1/h_0
0.47	1.45	1.21
0.66	1.38	1.20
0.82	1.25	1.17
1.01	1.22	1.17
1.20	1.18	1.16

In general, the experimental values of the wedge parameter vary in a consistent manner, decreasing with an increase in speed as would be expected if the roll pressure is maintained at a constant value, and generally varying more in Table IV, especially at the lower speeds. Here, the wedge parameter definitely approaches its limiting value of 1.33.

Since both h_1 and h_1/h_0 are known, the minimum clearance in the

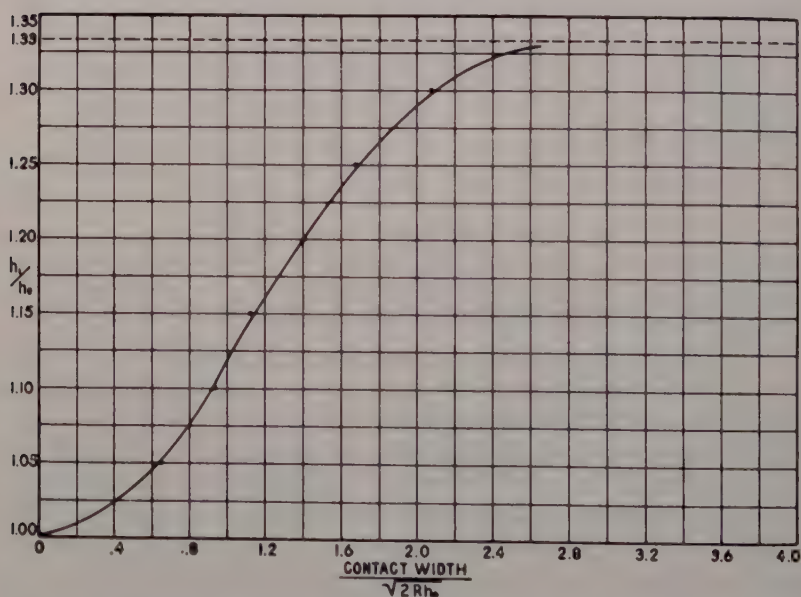


Fig. 5. Relationship between the wedge parameter and the contact width. An empirical relation involving the width of the bank and shear regions is used to relate the wedge parameter to the contact width.

nip can be calculated from three measurable values: film thickness, contact width, and rim velocity.

Conclusions

The pressure variations experienced by a Newtonian liquid passing between two rotating surfaces have been analyzed in terms of four components:

(1) An amplitude term which appears as a coefficient in the general equation. This coefficient contains the well-known velocity-viscosity product which governs the development of tack between two separating surfaces.

(2) A characteristic term which superimposes a wide fluctuation in pressure as the nip center is crossed. This term expresses the pressure gradient which is responsible for the flow of liquid relative to the roll surfaces. This flow is characterized by a parabolic velocity profile.

(3) A second characteristic term which describes a pumping action across the nip and accounts for the ability of a pair of mating surfaces to discharge fluid at a higher pressure than at the nip entrance.

(4) A bias constant which reflects the inability of liquid films to withstand great tensions. Asymmetry of the pressure profile results from this constant.

In addition, an important operational parameter is described which reveals the limits imposed on the wedge of fluid entering the nip. The pressure profile is highly sensitive to this parameter, which varies from 1.0 to 1.333, but a limiting maximum pressure is established for a given nip clearance. The wedge parameter may be determined from experimental data. Although it varies over a narrow range under normal operating conditions for thin liquid films, an accurate determination of its value is necessary in order to calculate the roll clearance.

The authors are indebted to the Sun Chemical Company for the fellowship which made this work possible, and are pleased to acknowledge the continued interest of the National Printing Ink Research Institute in this work.

References

1. Reynolds, O., *Trans. Roy. Soc. London*, **177**, 157 (1886).
2. Gaskell, R. E., *Trans. ASME*, **72**, 334 (1950).

3. Bergen, J. T., and G. W. Scott, Jr., *J. Appl. Mech.*, **18**, 101 (1951).
4. Gatecombe, E. K., *Trans. ASME*, **67**, 177 (1945).
5. Paslay, P. R., *J. Appl. Mech.*, **24**, 602 (1957).
6. Miller, J. C., and R. R. Myers, *Trans. Soc. Rheology*, **2**, 77 (1958).
7. Blokhuis, G., *Intern. Bull. Printing and Allied Trades*, **73**, 64 (1956); L. Sjö Dahl, 1st. Annual Meeting Tec. Assoc. of the Lithographic Industry, Chicago, April 15, 1949.
8. Stefan, J., *Sitzber. Akad. Wiss. Wien II*, **69**, 713 (1874).
9. Banks, W. H., and C. C. Mill, *Proc. Roy. Soc. London*, **223A**, 414 (1954).
10. Erb, R. A., and R. S. Hanson, *Trans. Soc. Rheology*, **4**, 91 (1960).
11. Taylor, J. H., Ph.D. Dissertation, Chemical Engineering Department, Lehigh University, 1959.
12. Miller, J. C., Ph.D. Dissertation, Chemistry Department, Lehigh University, 1956.

Synopsis

An analytical treatment is developed for the passage of a finite thickness of liquid through a roll nip. The contact area between a roll applicator and a planar substrate is divided into four consecutive regions: bank, shear, cavitation, and filamentation; pressures are calculated for the shear and cavitation regions in terms of the velocity-viscosity product, the distance of travel, and geometrical parameters. Two experimental factors are introduced: the first is the development of limiting tensions in the film prior to cavitation, and the second is the existence of a finite film thickness between the two surfaces. This paper shows that both of these factors can be accommodated in the general theory and shows the magnitude of their effects on the pressures attained in the nip. The resulting complex function is broken down into a coefficient and two characteristic terms which are plotted separately in order to show their physical significance. An increase in film thickness or a decrease in roll clearance cause the pressure peak to move outward from the nip center, reaching a limiting distance as the ratio of film thickness to roll clearance approaches $4/3$. This natural limit of operation imposes a limit on the thickness of film which can be deposited on a substrate regardless of the size of the bank of material at the nip entrance.

Capillary Rheometry as a Technique for Predicting Processing of Elastomers

C. C. McCABE and N. N. MUELLER, *Elastomer Chemicals Department, E. I. du Pont de Nemours & Company, Inc., Wilmington, Delaware*

Introduction

All rubber manufacturing processes depend very strongly upon the viscoelastic properties of the raw elastomer. Each processing operation performed on the elastomer, such as mastication, mixing, extruding, calendering, or forming of articles, depends upon the viscoelastic properties and at the same time usually changes them. Thus, it appears reasonable that some quantity which is related to viscoelasticity might serve as a criterion for predicting the processing of elastomers.

Several instruments have been developed for measuring specific viscoelastic properties. Some are currently being used for characterization of elastomers and for control of elastomer quality. The common type is one which measures shear stress responses to shear strains at relatively low shear rates. In the normal use of some of these instruments, for example, the Mooney viscometer, one set of conditions is usually selected, and often only single values of the parameters are measured. This procedure does yield some useful information; however, single points measurements are, in general, inadequate for characterizing the viscoelastic properties of any elastomer.

The objectives of this investigation are to show how appropriate viscoelastic information can be obtained and used to predict the processing characteristics of elastomers. Primary consideration is given to the extrusion process. In this operation, the variables of greatest importance are extrusion rate, die swell, and extrudate smoothness.

The Rheometer

The instrument employed in this study is a capillary rheometer which is shown schematically in Figure 1. It consists of an electrically heated cylinder with precise temperature control, a circular orifice which has certain specifications relative to its diameter and length to diameter ratio, and a plunger for extruding the elastomer through the orifice. The plunger is coupled through a compression-

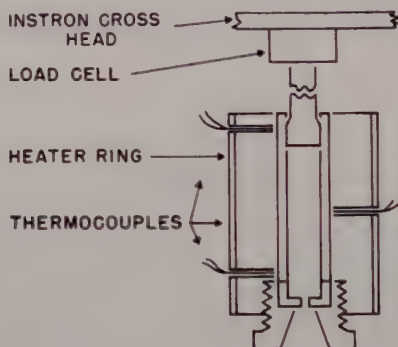


Fig. 1. Capillary rheometer.

type load cell to the crosshead of an Instron tester. Extrusions can be carried out over a wide range of shear rates with shear stress responses recorded continuously. The available practical shear rate range covers seven decades from 5×10^{-2} to $5 \times 10^{+6}$ sec. $^{-1}$.

By use of conventional relationships ($S = \Delta P r / 2l$ and $R = 4Q / \pi r^3$; S = shear stress, dynes/cm. 2 ; ΔP = pressure drop in capillary, dynes/cm. 2 ; r = radius of capillary, cm.; l = length of capillary, cm.; R = shear rate, sec. $^{-1}$; Q = volume rate of flow, cm. 3 /sec.) the data were translated to the more common units of dynes/cm. 2 for shear stress and sec. $^{-1}$ for shear rate.

Strictly speaking, these relationships do not apply to non-Newtonian fluids because the shear rate equation does not take into consideration the shear stress dependence of rate of shear. From a practical point of view, however, there is still real value in using these expressions as approximations for predicting the processing behavior of elastomers.

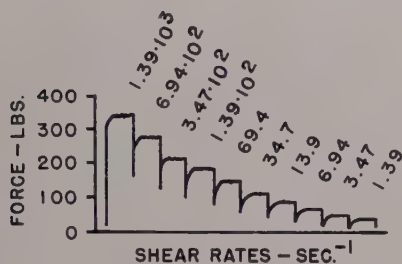


Fig. 2. Recorded rheometer data, Neoprene Type W. $T = 100^{\circ}\text{C}$. $l/2r = 2$
 $r = 0.0381$ cm.

Experimental Data

Figure 2 illustrates the raw data obtained on Neoprene Type W directly from the test unit with the extrusion force recorded continuously at each specific shear rate. It should be noted that shear rate is directly proportional to extrusion rate, and practical extrusions are carried out in the range of 10^2 to 10^3 sec^{-1} . Average shear stresses were determined from the force data. Figure 3 shows these results with log shear stress plotted against log shear rate plot. A change in slope occurs at a shear rate of about 10 sec^{-1} . This phenomenon has been observed in other cases and will be noted in subsequent figures. Similar breaks have been reported in the literature¹ to be correlatable with flow instability in extrusions of high polymers. This condition results in extrudates with irregular surfaces. Even

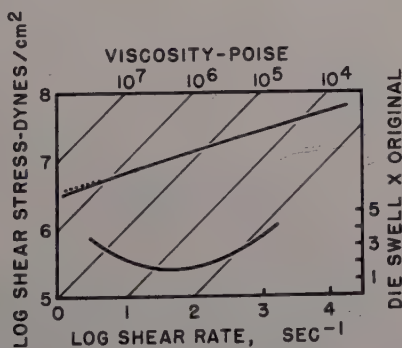


Fig. 3. Flow curves for Neoprene Type W. $T = 100^{\circ}\text{C}$. $l/2r = 2$. $r = 0.0381$ cm.

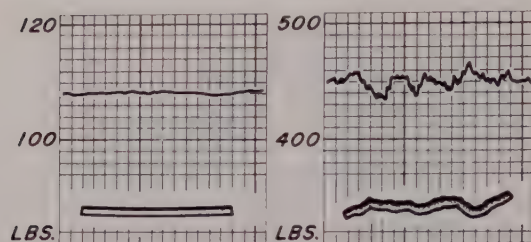


Fig. 4. Pressure fluctuations vs. extrudate smoothness. $T = 100^{\circ}\text{C}$. $l/2r = 2$.
 $r = 0.038$ cm. $R = 3.47 \times 10^2 \text{ sec.}^{-1}$.

though corresponding correlations have not been determined for elastomers, the gradual transition from smooth to rough extrudate surfaces with increasing shear rates gives strong indications that the flow pattern becomes unstable at high shear rates.

The curve shown in the lower half of this figure represents die swell as a function of log shear rate. Values for die swell were obtained by weighing a constant length of the extrudate. The lower die swell at a shear rate of about 10^2 sec.^{-1} is characteristic of some elastomers in the uncompounded form. Since the minimum occurs in the same shear rate range as the transition to very rough extrudates, it is believed that unstable flow contributes to the low die swell values and represents a condition not suitable for practical extrusions. In

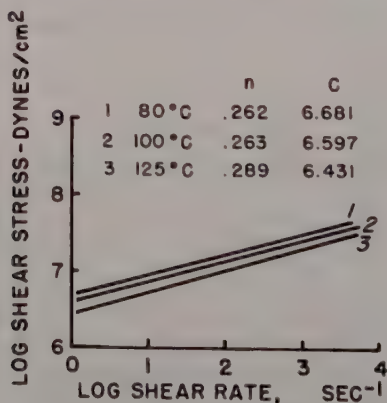


Fig. 5. Effect of temperature on flow curves for Neoprene Type W. $l/2r = 2$.
 $r = 0.0381$ cm.

prototype commercial stocks these minima do not occur, and increased die swell results at higher shear rates.

The third parameter of interest in the extrusion process is surface smoothness, which is normally estimated visually, since a quantitative measurement has not been previously available. A correlation was found to exist between pressure fluctuations recorded by the rheometer and surface smoothness. The smooth extrudate on the left in Figure 4 represents fluctuations of ± 0.5 lb. whereas the very rough extrudate corresponds to fluctuations of more than ± 15 lb. This range of pressure fluctuation is common for measurements on typical elastomers.

The data reported above were collected at a single temperature, 100°C . The temperature effect is easily determined by taking similar measurements at other selected temperatures. Such data give a family of shear stress-shear rate curves with similar general shapes with a tendency toward increased slopes at increased temperature over the temperature range from 50 to 150°C . This effect of Neoprene Type W is shown in Figure 5.

Since the rheometric curve when plotted on a log-log scale can be represented by a straight line, at least over a portion of the shear rate range, it is convenient to represent it by a mathematical expression of the form:

$$\log S = C + \log R^n$$

The two constants C and n depend upon the material being tested and can be used to characterize it. C is actually the log of the shear stress at unity shear rate and n is the slope of the line. Since these constants describe the flow characteristics of the elastomer in the capillary, they should also describe the flow characteristics in an extruder as long as comparisons are made at comparable shear rates.

Processing Comparisons

Interpretations of characteristic flow curves can only be made in an empirical manner at this time. It is obvious that flow rates depend upon the nature of the compound being processed and its viscosity, which is shear stress-shear rate dependent. During the extrusion process, the extruder screw forces the polymer forward with a force dependent upon viscosity, and the stock flows through the die with resistance proportional to viscosity. Likewise, the extrusion

rate is dependent upon any changes in viscosity which result from changes in shear rates during the extrusion process, and therefore the slope of the log shear-stress versus log shear-rate curve may be critical in predicting processing. The results of Eccher² indicate this to be true. In general, commercial extrusion rates are increased as either C or n are reduced. There is a practical lower limit for C since the stock must have sufficient viscosity to be extruded as well as being resistant to collapse after extrusion. This lower limit is estimated to be about 10^6 poises at unit stress.

In an attempt to evaluate the relative merits of C and n in predicting processing performance, two neoprenes of widely different

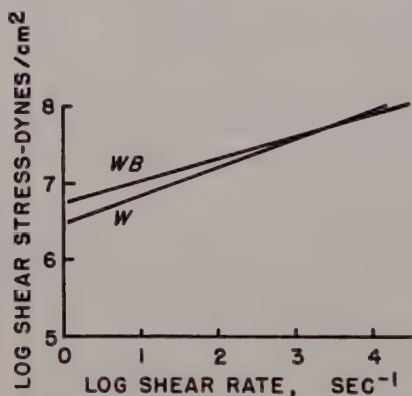


Fig. 6. Flow curves for Neoprene Types W and WB. $T = 125^{\circ}\text{C}$. $l/2r = 1$. $r = 0.0381$ cm.

processing character, Types W and WB were selected for study. The processing behavior of each elastomer has been established in conventional equipment and demonstrates marked differences. Type WB is the faster extruding. Its extrudates are very smooth in appearance and have low die swell, as illustrated in Figure 6. The value of n for Type WB is significantly lower than that of Type W and correlates with its lower die swell. Shear stress values in the practical shear rate range from 10^2 to 10^3 sec.⁻¹ are essentially equivalent for the two elastomers. This fact alone would predict comparable extrusion rates. However, this is not usually observed. There is considerable variation in practical extrusion conditions which tends to obscure the anticipated similarity in flow.

In normal processing procedures an elastomer is subjected to severe mechanical stresses which "break it down" or reduce its viscosity. The degree of "break down" is strongly dependent upon the type of elastomer and processing conditions. The effect of this phenomenon can be seen by a comparison of flow curves for Neoprene Type W with milling times of 0, 2.5, and 5.0 min. as shown in Figure 7. Viscosity at low shear rate, as indicated by C , decreases slightly with increased breakdown. The rate of change of shear stress with increasing shear rate, as indicated by n , is a function of the basic elastomer structure and remains unchanged.

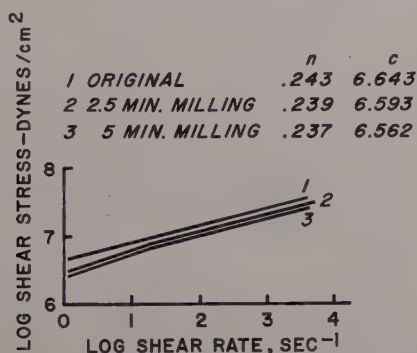


Fig. 7. Effect of milling on flow curves for Neoprene Type W. $T = 100^{\circ}\text{C}$.
 $l/2r = 2$. $r = 0.0381$ cm.

Compounding Effects

The processability of practical elastomer compounds is normally considered to be the sum of the processing characteristics of the base elastomer and any interaction effects between the elastomer and compounding ingredients. The capillary rheometer provides a suitable instrument for studying these interactions.

Determination of interaction effects of various type fillers to elastomer processing was studied using a standard base neoprene stock of the following composition:

Neoprene Type W	100.0 parts
Stearic Acid	0.5
Neozone A	1.0
Magnesium Oxide	2.0

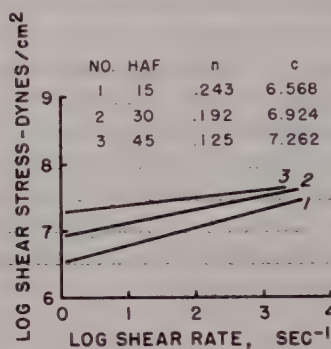


Fig. 8. Flow curves for Neoprene Type W compounds. $T = 100^{\circ}\text{C}$. $l/2r = 2$.
 $r = 0.0381$ cm.

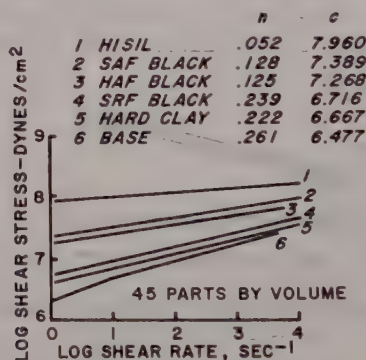


Fig. 9. Flow curves for Neoprene Type W with fillers. $T = 100^{\circ}\text{C}$. $l/2r = 2$.
 $r = 0.0381$ cm.

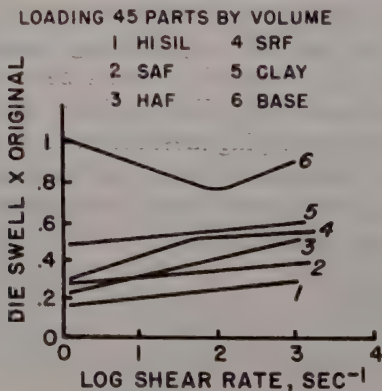


Fig. 10. Die swell Neoprene Type W.

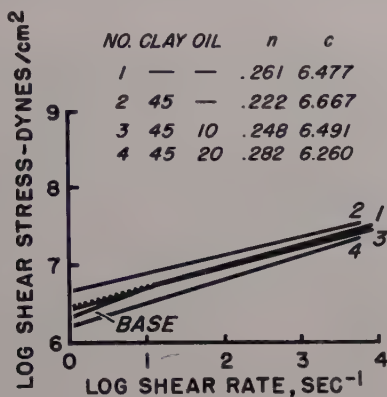


Fig. 11. Flow curves for Neoprene Type W compounds.

Comparisons were then made for various fillers as a function of concentration. The effect of loading with HAF carbon black is shown in Figure 8 for three concentrations with equal milling times of 21 min. With increased concentrations, the value of n decreases while C increases. On the basis of the results just discussed, the well-known fact that addition of carbon black improves the processing of an elastomer would be predicted. Investigation with other type fillers at constant volume loading, as shown in Figure 9, has demonstrated similar effects in each case, differing only in magnitude. The interaction effect which can be characterized specifically by changes

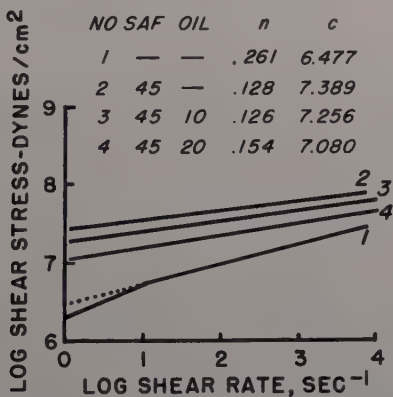


Fig. 12. Flow curves for Neoprene Type W compounds.

in the C 's and n 's is different and is apparently related to particle size of the filler. The order of the curves from 1 to 6 is that of decreasing particle size.

Measurements of die swell indicate the same ordered particle size dependence as shown in Figure 10. A single exception occurs with HAF carbon black at low shear rates.

With this information some limits can be placed on compounded stocks to restrict the shear stress values to practical extrusion experiences. These limits are $\log^{-1} 7.5$ and 6.9 dynes/cm.² in the normal extrusion range of 10^2 to 10^3 sec.⁻¹. Consequently, the level of each type filler that can be tolerated is predictable. The common

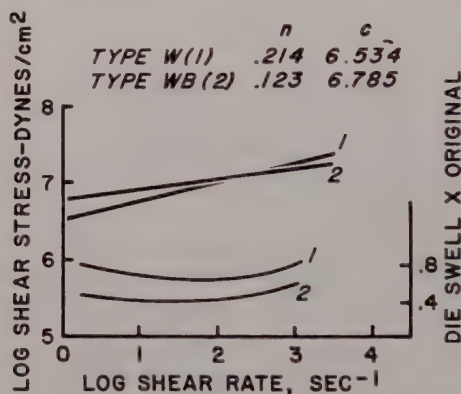


Fig. 13. Flow curves for compounded Neoprene Types W and WB. $T = 100^\circ\text{C}$.
 $l/2r = 2$. $r = 0.0381$ cm.

practice of improving the processability of highly loaded stocks is to add process oil to the compound. Such additions lower the shear stress values with only minor changes in the slopes of the shear stress curves for neoprene stocks containing hard clay, as shown in Figure 11. Similarly the flow curves for compounds containing SAF carbon black in Figure 12 illustrate the improvements which are attributable to the addition of oil. The level of oil that can be used is restricted by the practical lower shear stress limitation. The shear stress values for the clay loaded compound with 20 parts of oil fall below this limit, and it would be predicted to be too soft for satisfactory processing.

Flow curves for some typical compounds of Neoprene Types W and WB are compared in Figure 13. The compounds contain 100

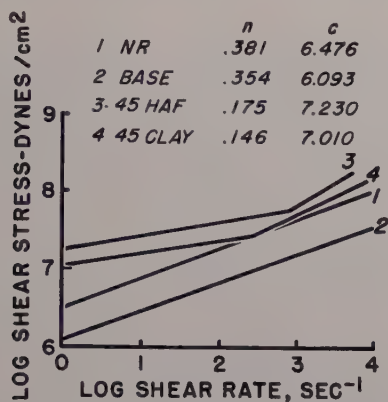


Fig. 14. Flow curves for natural rubber (pale crepe).

parts neoprene, 70 parts hard clay, 10 parts light process oil, and 2 parts magnesium oxide. These flow curves are similar to those of the uncompounded elastomer. However, differences in both die swell and extrudate smoothness are magnified as a result of more stable flow patterns which persist for compounded elastomers.

Since different elastomers may interact with compounding ingredients uniquely, it is necessary to make specific measurements for each elastomer considered. Figure 14 illustrates some results for natural rubber (Curve No. 1) and its compounds. Curve No. 2 is for a com-

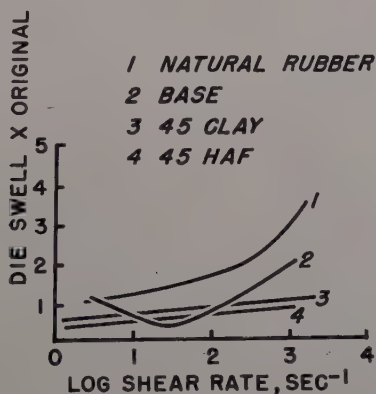


Fig. 15. Die swell natural rubber.

pound (5 parts zinc oxide and 2 parts stearic acid) with milling time of 7 min. The effects of adding 45 parts HAF carbon black and 45 parts clay are shown by Curves No. 3 and 4, respectively, each with a total milling time of 21 min. Die swell curves for these natural rubber stocks in Figure 15 are similar in nature to those of neoprene.

Summary

Any elastomer can be characterized by its flow curves which, in turn, can be defined over specified shear rates by two constants. Similarly, interaction effects between compounding ingredients and the elastomer can be characterized by changes in the flow curves. This information, coupled with die swell and extrudate smoothness values, provides a practical system for predicting processability of elastomers as well as for designing elastomer stocks to conform to prescribed processing conditions.

References

1. Tordella, J. P., *J. Appl. Phys.*, **27**, 454 (1956).
2. Eccher, S., *Ind. Eng. Chem.*, **43**, 479 (1951).

Synopsis

The flow properties of elastomers provide a basis for predicting processing characteristics and are usually determined by measurements which relate a shear stress to some shear rate. Many instruments are available for obtaining such measurements. In this paper the use of a capillary rheometer is described, and data obtained from it are used to predict processability of neoprene. Limited results for other elastomers are also included.

The capillary rheometer to be discussed consists of a constant temperature chamber with a circular orifice described by its diameter and its length to diameter ratio. A piston coupled to a driving mechanism through a force measuring gage is used to extrude polymer through the orifice. Shear stress-shear rate data are collected for various elastomers at selected temperature over a wide range of shear rates. Characteristic curves are then drawn for each elastomer and form the basis for processability comparisons. Interpretation of the data enables one to predict extrusion rates, die swell, and extrudate smoothness.

Similar curves are obtained for each individual elastomer containing increasing amounts of fillers or specific compounding ingredients in a given formulation. The quantitative effect of interaction between compounding ingredient and polymer is established from comparisons of these curves. It is then possible to predict processing characteristics for specific compounds by determining only the characteristics of the base elastomer and applying a suitable correction based on the interaction effects previously determined.

Effect of Die Entry Geometry on Polymer Melt Fracture and Extrudate Distortion

E. B. BAGLEY and H. P. SCHREIBER, *Central Research Laboratory, Canadian Industries Ltd., McMasterville, Quebec, Canada*

1. Introduction

In the extrusion of molten polystyrene through a capillary, Spencer and Dillon showed that there exists, for a given polymer, a critical shear stress, τ_d , and a critical shear rate, G_d , at and above which the extruded filament becomes distorted.¹ Tordella subsequently found the same effect in the extrusion of polyethylene and other polymers,² and, on the basis of a marking technique which permitted examination of the internal structure of the extruded filament and subsequently on the basis of direct observations of flow behavior at the die entry,^{3,4} concluded that melt fracture was occurring and was the basic cause of extrudate distortion. Tordella also noted a 10- to 14-fold increase in the critical shear rate when extrusion took place through a die with a conical included entry angle of 20° rather than a flat entry die (included entry angle 180°). This influence of die entry geometry on extrudate distortion has been confirmed by others.⁵⁻⁸

The apparent dependence on die entry geometry of the point at which extrudate distortion is observed led to the suggestion that the onset of distortion depended not only on the shear stress but also on the rate of change of shear stress.⁶ Doubt was cast on this view because of an observation by Clegg, who noted in a polyethylene filament extruded at high speed through a steeply tapered die that there was evidence of internal flow irregularities even though the filament would be classed as undistorted on the basis of external appearance.⁵ This indicates that melt fracture may be occurring during flow through tapered dies at much lower values of shear rate and shear stress than would be expected on the basis of external filament appearance. Schott and Kaghan,⁸ in considering Clegg's result,

suggested that tapering the die entry would prevent "pulsations and wedging" and hence would leave the extrudate undistorted even though "shear rupture" was occurring.

In this study the internal structure of filaments is examined to determine whether or not the melt fracture point, (τ_d , G_d), is a function of die entry geometry. In addition, some results of a visual study of the flow behavior in the die entry region of tapered dies are presented to illustrate certain characteristics of melt fracture.

2. Experimental Procedure

(a) *Flow Patterns at the Capillary Entry*

The transparent viscometer used in the visual studies reported here has been described previously.⁹ The quartz die used in this work, however, differed from the one previously described in having an included die entry angle of 40° and a capillary length to radius ratio of 20. The die diameter was approximately 0.5 mm. The polymer samples were marked with carbon black as before⁹ and the experiments were carried out at $190 \pm 2^\circ\text{C}$. Sixteen mm. cine films were taken of the flow at 16, 100, and 500 frames/sec.

(b) *Determination of the Internal Filament Structure*

Although the study of the visual patterns at the die entry does, in principle, give all the information needed to show the effect of entry geometry on the melt fracture point, it was found that the quartz dies were not of the required precision necessary for a quantitative study. However, both Tordella and Clegg report that the presence of flow irregularities can be readily detected from the character and position of flow marker lines in the extruded filament. Flow markers of the type used in the visual studies described above⁹ are particularly well adapted to this examination of the internal structure of the filament. If the flow is regular so that the extrudate is undistorted, the flow marker lines will appear as unbroken parallel black lines within the filament. Any flow irregularities will be reflected as irregularities in the black marker lines within the filament.

To obtain filaments for examination, molds of polyethylene $\frac{5}{8}$ in. in diameter were prepared for insertion into the barrel of a previously described, pressure driven viscometer.¹⁰ Black marker filaments were inserted in this molded sample as for visual study of the flow patterns

within the viscometer.⁹ The mold was then inserted in the viscometer, melted, and extruded at various applied pressures through the dies.

Four dies were used in this study. These were made of Inconel of capillary diameter 0.0489 cm. and capillary length 0.447 cm. ($L/R = 18.3$). These dies were of various conical approach angles, the total included die entry angles being 20, 40, 60, and 180° (the last being a flat entry die). The included entry angle was determined by the use of a suitable insert. The die radius was found using plug gages.

Experiments were carried out as follows. A sample was first extruded through the flat entry die, and the critical pressure, P_d , at which extrudate distortion occurred was noted. A series of filaments was obtained at a series of pressures, P_i , above and below P_d with particular attention being given to the region near P_d . Samples of filament extruded through the dies of conical entry angle at the same pressure values, P_i , were then obtained, and a direct visual comparison made of the internal structure of the corresponding filaments. Output rates at the various applied pressures were determined in all cases.

Actually, of course, we should compare results at the same shear stresses, τ , rather than at the same pressures because the pressure required to give a certain output rate will depend to a certain extent on the die entry geometry. The results indicate, however, that the effect of the die entry geometry on pressure losses can be neglected for the purposes of this work.

The polymers reported on here are labelled Polyethylene C, D, and E. All are commercial resins made by the high pressure process by three different manufacturers. Polyethylene C is the same sample referred to in the paper by Bagley and Birks⁹ where the same code symbol was used. The densities of the three resins are 0.92 g., cc., and the resins have melt indices of 2.0.

3. Experimental Results

(a) *Flow Patterns at the Die Entry*

The basic behavior which is observed during flow into dies of conical entry angle is illustrated in Figures 1, 2, and 3. The polymer used for these figures was the previously studied Polyethylene C.⁹ Extrusion took place under an applied pressure of 1000 p.s.i. The figures are all enlargements of the cine film frames taken at 400 frames/sec.



Fig. 1. Melt fracture of Polyethylene C on extrusion at 1000 p.s.i. and 190°C.



Fig. 2 (left) and Fig. 3 (right). These two pictures, taken at 400 frames/sec. during the extrusion of Polyethylene C at 1000 p.s.i. and 190°C., show a typical oscillatory motion across the die entry. The two frames were taken at $1/40$ of a second apart.

Figure 1 shows no dead space, i.e., no polymer is trapped in the die entry region immediately adjacent to the capillary inlet. In previous work using a flat entry die, Polyethylene C showed an extremely large dead space.⁹ Figure 1 shows that melt fracture has nonetheless occurred, as evidence by the broken central flow line which has snapped-back from the die entry. This central line is, for the moment, stationary, and the bending inwards of the flow lines adjacent to this central line indicates a surge of material into the capillary from the annular region about the central, stationary flow line. Consideration of this single frame, however, does not properly illustrate the way in which flow in tapered dies differs from flow in flat entry dies. Observation of the cinefilm itself shows that the frequency of fracture in tapered dies is much higher than in the flat entry case, which is, of course, the reason for the use of high-speed photography techniques in studying flow into tapered entry capillaries. This is also the reason Clegg was unable to see any distortions of the flow patterns when studying flow in dies of 24° included entry angle—the oscillations were simply too rapid.

A second way in which flow into tapered dies differs from flow into flat entry dies is that the magnitude of elastic snap-back on melt fracture in the tapered dies is much less than that found with the flat die. The recovery shown upon melt fracture in Figure 1 is about one die diameter and is the maximum we have observed on dies of this taper. In contrast, the snap-back observed quite routinely during steady flow of this same material into flat entry capillaries would be three or four die diameters, as shown in Figures 5 and 9 of Reference 9.

In addition to the melt fracture process, oscillations are observed at the die entry. This is illustrated by Figures 2 and 3 which are cinefilm frames of Polyethylene C flowing into a die of 20° included entry angle and L/R value of 18 at 1000 p.s.i. applied pressure. Figure 3 is the frame taken $1/40$ of a second after the frame shown in Figure 2. It is readily seen on comparing these photographs that the central flow line has oscillated across the capillary entrance. Comparing the tip of the central flow line in Figures 2 and 3 also shows that laminar flow is occurring within the capillary, at least to the accuracy allowed by the experimental technique. Thus the tip of the central flow line in Figure 2 is about one die diameter within the capillary, while in Figure 3 the tip has moved down to a position about five die diameters from the capillary entrance while the radial position of the

point has remained essentially unchanged. These pictures confirm directly the previous conclusion, drawn from more indirect evidence, that melt fracture occurs outside the capillary and that laminar, regular flow occurs within the capillary even well above the melt fracture point.

At this point it is instructive to consider the effect of die entry geometry on the character of the extruded filaments. This is shown in Figures 4 and 5. In Figure 4 are shown filaments of polyethylene E (melt index 2) obtained at various pressures and shear rates from a flat entry die of $L/R = 18.3$ and $L = 0.447$ cm. Figure 5 shows filaments of the same polymer obtained on extrusion through a die of

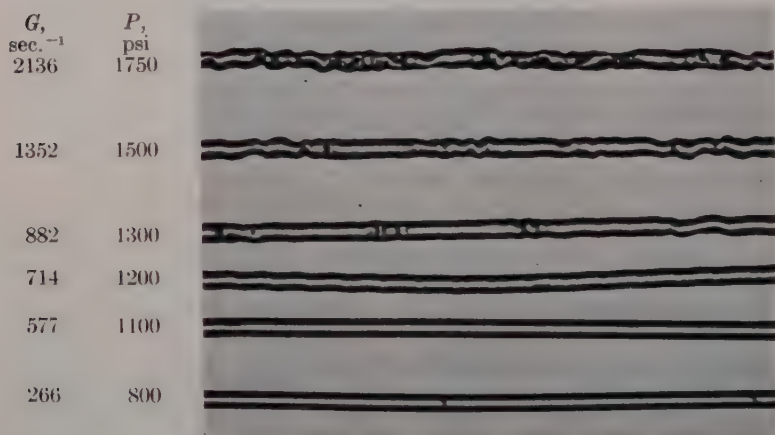


Fig. 4. Filaments of Polyethylene E extruded from a flat entry die at 190°C.

the same land dimensions but included die entry angle of 60°. The point at which extrudate distortion is first noted by superficial visual examination is about 1300 p.s.i. for the flat entry die and about 1700 p.s.i. for the 60° included entry angle die. There has been an apparent increase of some 400 p.s.i. in pressure required for filament distortion. We have many similar examples of such behavior.

In the example given in Figures 4 and 5, the pressure at which extrudate distortion becomes observable is fairly clearly defined, both on the tapered entry (60° included angle) and flat entry dies. For tapered dies this is not generally true, particularly if the included angle is smaller than 60°. The determination of a critical distortion

pressure using tapered dies from the external filament appearance seems to be impossible. Efforts to surmount this difficulty by direct observation through transparent dies proved unsatisfactory for a number of reasons. First, the oscillations and fractures on the tapered dies occurred so rapidly that a very tedious high-speed photographic technique was required. Further, as can be seen in Figures 1, 2, and 3, the capillaries with tapered die entry were not accurately made. We have been able to obtain much better dies in metal. In spite of these objections, preliminary studies of behavior of polyethylene in transparent tapered dies did show that melt fracture was oc-

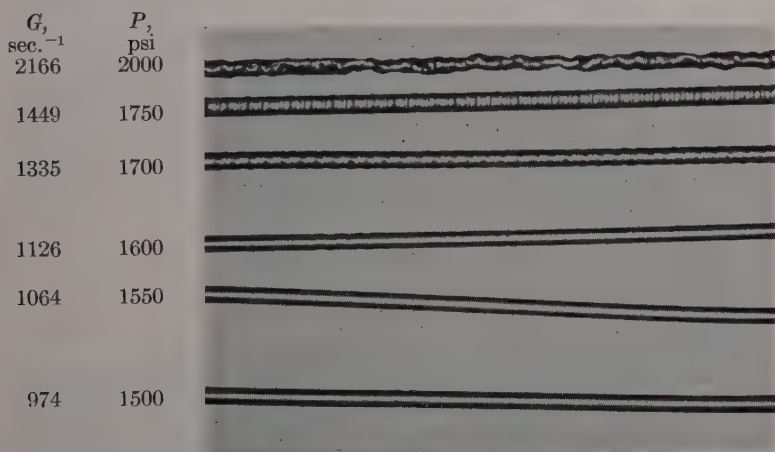


Fig. 5. Filaments of Polyethylene E extruded from a die of included entry angle 60° .

curing at stresses much below those at which obvious external filament distortion was observed, and, to a first approximation, at about the same stress as that which caused melt fracture in flat entry dies.

(b) Flow Patterns Observed in Extruded Filaments

The basic patterns seen internally in filaments of Polyethylene C, a low density resin of melt index 2, extruded through a flat entry die at 190°C. , are shown in Figure 6. The distortion pressure at which melt fracture occurs, as judged by external filament appearance, had previously been determined to be 1050 p.s.i. In Figure 6 there is evidence of fracture at 950 p.s.i., but the first catastrophic fracture is at

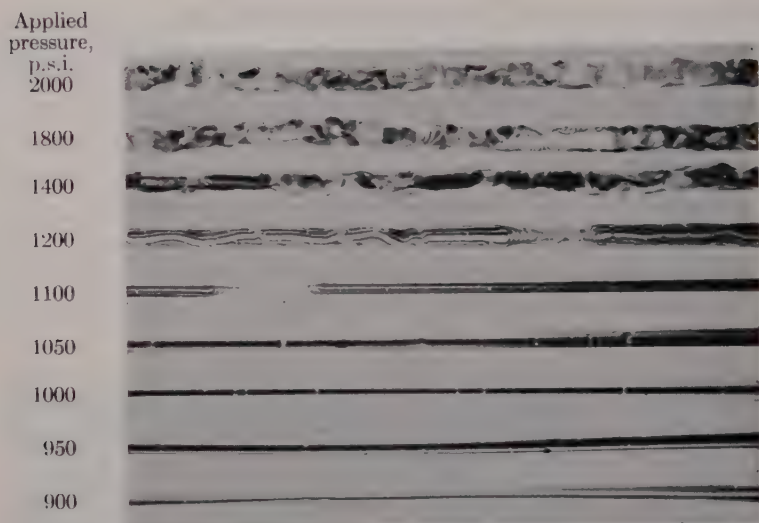


Fig. 6. Polyethylene C, extruded through a flat entry die of $L/R = 18.3$ at 190°C .

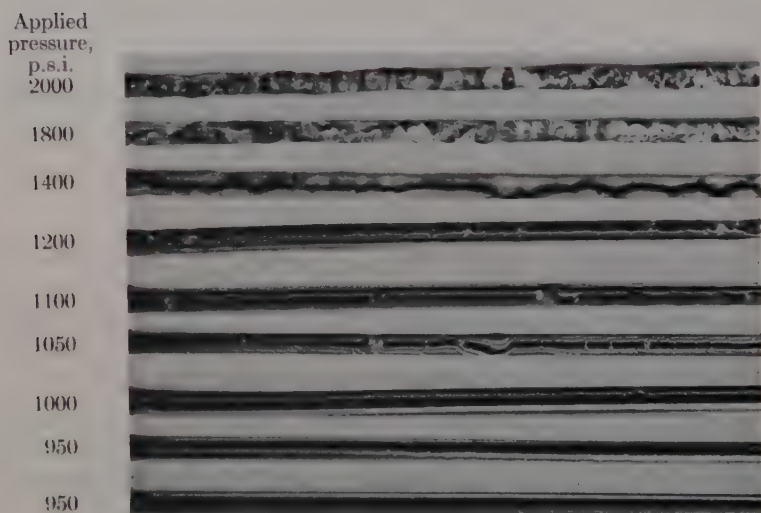


Fig. 7. Polyethylene C, extruded through a die of 60° included entry angle and an L/R of 18.3, at 190°C .

1100 p.s.i. At this pressure a large quantity of unmarked dead space material has been included in the extrudate. At 1200 p.s.i. fracture is frequent and, in addition, it is clear that oscillatory motion has occurred. Above 1400 p.s.i. all semblance of regularity has disappeared.

Figure 7 shows filaments of Polyethylene C extruded through a die of tapered entry angle 60° at the same pressures as in Figure 6. Evidence of melt fracture exists at 950 p.s.i. At 1050 p.s.i. melt fracture is frequent and the occurrence of oscillatory motion is clearly

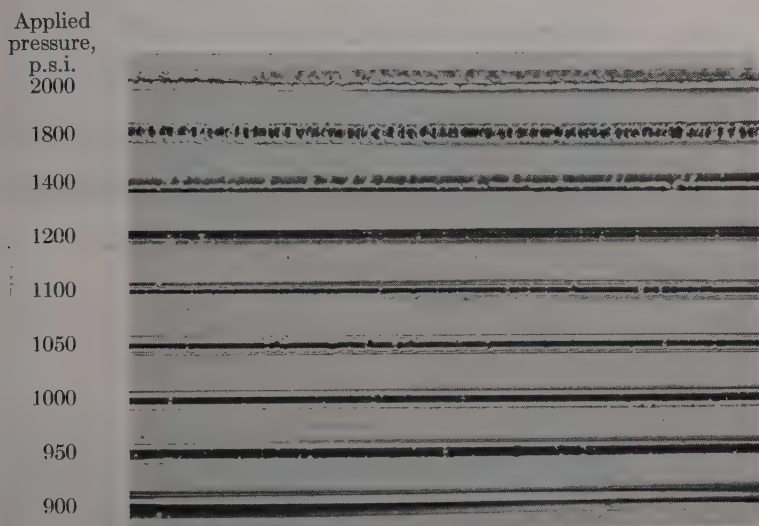


Fig. 8. Polyethylene C, extruded through a die of 40° included entry angle and an $L/R = 18.3$, at 190°C .

visible. No evidence of catastrophic fracture is seen until 1800 p.s.i. is reached, and even here the internal evidence of fracture is less pronounced than in the case of the flat entry die.

Figure 8 shows filaments of Polyethylene C extruded through a die of included entry angle 40° . Evidence of fracture first appears at 950 p.s.i., but melt fracture becomes really pronounced only at 1050 p.s.i. At higher pressures the fractures occur very frequently and with considerably more regularity than they did in the case of the 60° and 180° included entry angle dies.

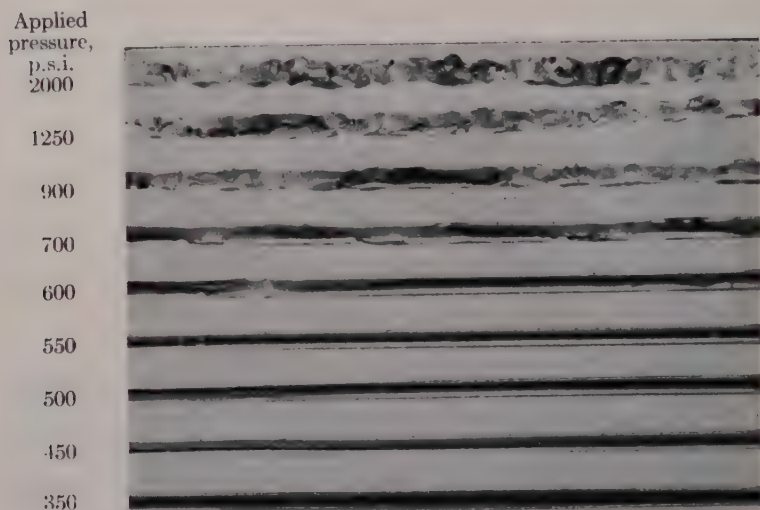


Fig. 9. Polyethylene D, extruded through a flat entry die of $L/R = 18.3$ at 190°C .

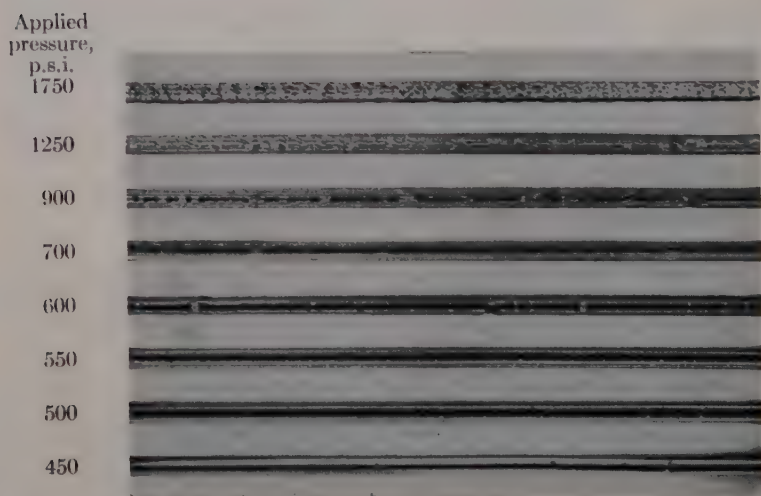


Fig. 10. Polyethylene D, extruded through a die of land length to radius ratio of 18.3 and included entry angle of 40° , at 190°C .

Figures 9 and 10 show the same effects for Polyethylene D, a low density resin of melt index 2. The dies have, respectively, included entry angles of 180 and 40°. The flat entry die shows evidence of melt fracture at 450 p.s.i., but catastrophic fracture resulting in large infusion of dead space material into the filament occurs only at 600 p.s.i. In the case of the 40° included entry angle die (Fig. 10), fracture is again first observed at 450 p.s.i., but at 550 p.s.i. evidence of oscillations sets in, in addition to fracture. At the highest pressure, fracture and oscillations are occurring rapidly and in a fairly uniform manner. The oscillations are of high frequency and do not necessarily result in fracture. They are regarded as incipient fractures.

4. Discussion

In discussing these results it must be recognized that the carbon black particles are introducing a factor into the system which could affect the results. Experiments have been done in which better dispersions, smaller particles, and lower concentrations of carbon black were used with basically the same results as those illustrated in Figures 6 to 10. It is considered that the carbon black serves as a visual aid and is not the cause of the flow irregularities it demonstrates.

The following conclusions are drawn from these carbon black tracer studies. When a polymer melt is extruded through a flat entry capillary, extrudate distortion due to polymer melt fracture is observed above a critical shearing stress. This critical shearing stress does not appear to vary with die entry angle. Rather, as the included angle decreases, the amount of strain inhomogeneity which is introduced into the filament per fracture is decreased and the frequency of fractures increases. These effects combine to reduce the severity of gross visual extrudate distortion and indicate an apparent rise in the critical stress for gross extrudate distortion. These results can be readily understood on the following basis, a more general concept of which is given in a separate publication.¹¹

To consider behavior using the flat entry die first, it is clear that when the highly oriented melt at the die entry fractures and snaps back its place is, perforce, taken by relatively unoriented material from the "dead-space." This introduces a strain inhomogeneity into the filament which is reflected in a swelling or recovery inhomogeneity on emerging from the capillary—i.e., the extrudate becomes distorted because of non-uniform swelling. A flow oscillation which may be

regarded as an incipient fracture can also introduce a strain or orientation inhomogeneity but, of course, on a much smaller scale so that the resultant extrudate distortion is less serious. It is possible that if the die were made long enough all portions of the melt would attain steady state configurations and the resultant extrudate would emerge undistorted. This would imply that the average viscosity should vary with capillary length, but studies of end effects have not shown this expected behavior though such studies on much longer dies could show this effect.

Increased pressure and output rates on the flat entry dies result in more frequent fracture making the extruded filament more and more elastically inhomogeneous and hence resulting in a more and more distorted extrudate. Ultimately, however, this should result in an extrudate in which the elastically different portions are so well dispersed and the inhomogeneities are so fine grained as to lead, for swelling purposes, to an effectively homogeneous and therefore visually smooth extrudate.

In the case of tapered dies, melt fracture occurs at the same shear stress as with flat entry dies. The situation with tapered dies differs from that with flat entry dies in two respects. First, the reservoir of relatively unoriented material is reduced or eliminated. This means that the elastic heterogeneity which can be put into the filament when melt fracture occurs is reduced and hence the degree of distortion possible when the filament swells is reduced.¹¹

A second related point concerns the melt fracture lifetime. When fracture occurs the highly oriented melt which had been ready to flow through the die retracts and hovers expectantly some distance above the die.⁹ Other surrounding material, either from the dead space or remote from the flow funnel, surges in to take the place of this retracted material. This surge continues until the surrounding material, in its turn, suddenly retracts and re-establishes the original flow sequence. The length of time it takes to re-establish this original sequence is the melt fracture lifetime and it decreases as the die entry angle decreases. Thus the heterogeneity introduced per fracture diminishes with decreasing included entry angle with a consequent reduction in filament distortion.

It is also observed with tapered dies that oscillations are much more frequent than in the case of the flat entry dies. These oscillations appear to be stress relieving mechanisms and can perhaps be

regarded as incipient fractures. Their effects in terms of filament distortion is minor.

References

1. Spencer, R. S., and R. E. Dillon, *J. Colloid Sci.*, **4**, 241 (1949).
2. Tordella, J. P., *J. Appl. Phys.*, **27**, 454 (1956).
3. Tordella, J. P., *Trans. Soc. Rheology*, **1**, 203 (1957).
4. Tordella, J. P., *Rheologica Acta*, **1**, 216 (1958).
5. Clegg, P. L., "Elastic Effects in the Extrusion of Polythene," in *Rheology of Elastomers*, Pergamon, London, New York, 1958, p. 174.
6. Bagley, E. B., *Ind. Eng. Chem.*, **51**, 714 (1959).
7. Schulken, R. M., Jr., and R. E. Boy, Jr., *SPE Journal*, **16**, 423 (1960).
8. Schott, H., and W. S. Kaghan, *Ind. Eng. Chem.*, **51**, 844 (1959).
9. Bagley, E. B., and A. M. Birks, *J. Appl. Phys.*, **31**, 556 (1960).
10. Bagley, E. B., *J. Appl. Phys.*, **28**, 624 (1957).
11. Schreiber, H. P., E. B. Bagley, and A. M. Birks, *J. Appl. Polymer Sci.*, **4**, 362 (1960).

Synopsis

When a polymer melt is extruded through a flat entry capillary (180° included angle), extrudate distortion is observed above a critical shearing stress. This is due to polymer melt fracture, and as a result the extruded filament is composed of portions of relatively highly oriented and unoriented melt. Extrudate distortion results when this heterogeneous mixture relaxes on emerging from the die.

With steeply tapered dies much higher values of shearing stress and shear rate can be achieved without apparent filament distortion. This is not due to any dependence of the critical shearing stress for melt fracture on inlet angle. Rather, as the included entry angle decreases, the strain inhomogeneity introduced into the filament per fracture is decreased. At the same time the frequency of fractures increases, making the heterogeneities smaller and more evenly distributed. In tapered dies oscillations also occur, which appear to be incipient fractures. These cause some strain inhomogeneity, but their effect in terms of extrudate distortion is minor.

The Separation of Elastic and Viscous Effects in Polymer Flow

E. B. BAGLEY, *Central Research Laboratory, Canadian Industries Ltd.,
McMasterville, Quebec, Canada*

1. Introduction

Studies of a viscoelastic liquid by capillary viscometry can yield information not only on the viscous but also on the elastic characteristics of the liquid.^{1,2} This communication shows that this separation of viscous and elastic effects in polymer melts can lead to certain interesting and useful conclusions, both in the explanation of certain phenomenological observations and in the determination of polymer structure. The basic problems to be considered concern the calculation of true viscosities and some observations of the phenomenon of extrudate distortion, which is generally observed in polymer extrusion under appropriate conditions.³⁻⁶ From the solution to this last problem comes a new and very simple approach to the determination of polymer molecular weight. Finally, certain elastic effects in polymer solutions and melts are compared.

2. Theory

(a) *End Corrections*

When a polymer melt is forced to flow from a reservoir through a capillary of radius R and length L , the maximum shear stress at the capillary wall is usually computed from the equation

$$\tau_w(\text{dynes/cm.}^2) = PR/2L \quad (1)$$

where P is the pressure applied to the reservoir in dynes/cm.². This equation, however, makes no allowance for pressure losses that arise in the reservoir itself. For Newtonian liquids these pressure losses outside the capillary are taken into account by assuming that an end

correction, e , exists such that the true shear stress at the capillary wall can be computed from

$$\tau_{tw} = PR/2(L + eR) \quad (2)$$

Thus the true shear stress is computed from an effective capillary length given by $(L + eR)$. This method of finding true shear stresses has been shown experimentally to be valid for certain polymeric melts.⁷

In the case of a Newtonian liquid the end correction, e , represents the viscous losses encountered by the liquid as a result of velocity gradients near the capillary entrance. These are termed Couette losses and are generally represented by the letter n . Philippoff and Gaskins¹ showed, however, that in the general cases of viscoelastic liquids, such as polymer melts, the pressure losses in the reservoir arise from two factors. There are Couette losses, as in the case of Newtonian liquids but, in addition, elastic energy is stored in the melt as it is sheared. The Philippoff and Gaskins relationship for the total end correction in this general case is

$$e = n + (S_R/2) \quad (3)$$

where S_R is the recoverable shear strain.

(b) Separation of the Elastic and Viscous Components of the Total End Correction

The determination of recoverable shear strains, S_R , in polymer flow is of considerable theoretical and practical significance. The usual approach to the experimental determination of S_R has been by means of rotational viscometers but this method has many experimental difficulties. However, if Hooke's law in shear is obeyed, S_R values can be obtained from capillary experiments. Hooke's law in shear is given by

$$\tau = \mu S_R \quad (4)$$

where μ is the shear modulus. Equations (3) and (4) can be combined to give the following expression²

$$e = (1/2\mu)\tau + n \quad (5)$$

Plots of e versus τ_{tw} have been found to be linear for some polyethylenes at shear stresses below that corresponding to melt frac-

ture.² From these linear plots the shear modulus, μ , the Couette correction, n , and the recoverable shear strain, S_R , at any stress can be readily found.

(c) Calculation of Viscosity

In capillary viscometry, the most readily calculable viscosity, which will be termed here the apparent viscoelastic viscosity, is given by

$$\eta_a = \tau_{tw} / \dot{\gamma}_{Nw} \quad (6)$$

Here τ_{tw} is the shear stress at the wall of the capillary [defined by eq. (2)] while $\dot{\gamma}_{Nw}$ is the corresponding shear rate at the wall of the capillary calculated, assuming that the fluid is Newtonian, from the following equation:

$$\dot{\gamma}_{Nw} = 4Q / \pi R^3 \quad (7)$$

In this equation Q is the output rate from the capillary in cc./sec. and R is the capillary radius in cm.

Although the apparent viscoelastic viscosity as defined by eq. (6) is frequently used it is, of course, not correct for non-Newtonian fluids because the shear rate given by eq. (7) is not correct for these fluids. Rabinowitsch⁸ has shown that a true shear rate can be computed by taking into account the degree of non-Newtonianism of the melt. This is given by

$$\dot{\gamma}_{tw} = \dot{\gamma}_{Nw} [3/4 + b/4] \quad (8)$$

where

$$b = d \log \dot{\gamma}_{Nw} / d \log \tau_{tw} \quad (9)$$

Using this true shear rate a true viscoelastic viscosity can be found from

$$\eta_{ta} = \tau_{tw} / \dot{\gamma}_{tw} \quad (10)$$

Another complication which arises in computing viscosities for elastic liquids is that as the amount of recoverable shear becomes appreciable the main directions of the stress and strain velocity ellipsoids no longer coincide.^{9,10} As Jobling and Roberts point out¹¹ "...it is necessary to compensate for this angular deviation and to calculate an idealized viscosity coefficient, η_{max} , which would be obtained if the whole of the stress were effective in overcoming viscous resist-

ance . . ." This maximum viscosity will be termed here a true inelastic viscosity and designated by η_{tm} from the equation

$$\eta_{tm} = \eta_{ta} \sqrt{1 + (S_R^2/4)} \quad (11)$$

3. Experimental Results and Discussions

(a) End Correction Studies of Polyethylene

End corrections were determined as described previously⁷ for two polyethylenes, B and C. Polyethylene B was a high density resin of melt index¹² 0.7 which has also been described in a photographic study of polyethylene flow patterns,¹³ and is the same linear resin for which discontinuous flow curves were first reported.⁵ Polyethylene C was a commercial low density resin of melt index 2. The results of this end correction study are shown in Tables I and II.

TABLE I
Viscoelastic Parameters for Polyethylene C at 190°C.

$\dot{\gamma}_{Nw}$ sec. ⁻¹	τ_{tw} $\times 10^{-5}$ dynes/cm. ²	b	$\dot{\gamma}_{tw}$ sec. ⁻¹	$S_R =$ $2(e - n)$ $n = 1.75$	η_a $\times 10^{-4}$, poise	η_{ta} $\times 10^{-4}$, poise	η_{tm} $\times 10^{-4}$, poise
10	1.85	1.40	11.00	2.22	1.85	1.68	2.51
20	2.77	1.88	24.4	3.16	1.39	1.14	2.13
30	3.43	2.01	37.5	4.00	1.14	0.915	2.02
50	4.45	2.12	64.0	5.16	0.890	0.695	1.92
70	5.21	2.16	90.3	6.18	0.745	0.577	1.87
90	5.85	2.22	117.5	6.96	0.650	0.498	1.80
100	6.17	2.29	132.5	7.24	0.617	0.466	1.75
200	8.46	2.30	265.0	9.82	0.423	0.319	1.57
300	10.03	2.34	400.5	11.60	0.334	0.250	1.47
500	12.38	2.39	674.0	14.30	0.248	0.184	1.33
700	14.33	3.00	1050	14.40	0.205	0.136	0.989
900	15.34	3.00	1350	14.98	0.170	0.114	0.862
1000	15.97	3.00	1500	14.92	0.160	0.106	0.798
1250	17.26	3.00	1875	14.86	0.138	0.0921	0.691
1500	18.44	3.00	2250	14.66	0.123	0.0820	0.607
1750	19.32	3.00	2625	14.50	0.110	0.0736	0.549
2000	20.48	3.00	3000	14.36	0.103	0.0683	0.495
3000	23.30	3.00	4500	14.78	0.0777	0.0518	0.386
4000	25.61	3.00	6000	14.84	0.0640	0.0427	0.320
5000	28.01	3.00	7500	14.30	0.0560	0.0373	0.269
6000	29.40	3.00	9000	14.60	0.0490	0.0327	0.244
7000	30.97	3.00	10500	14.80	0.0442	0.0295	0.221

TABLE II
Viscoelastic Parameters for Linear Polyethylene B at 190°C.

$\dot{\gamma}_{Nw},$ sec. ⁻¹	τ_{tw} $\times 10^{-5}$ dynes/cm. ²	b	$\dot{\gamma}_{tw},$ sec. ⁻¹	$S_R =$ $2(e - n)$ $n = 1.95$	η_a $\times 10^{-4},$ poise	η_{ia} $\times 10^{-4},$ poise	η_{tm} $\times 10^{-4},$ poise
8	2.87	1.77	9.52	0.90	3.59	3.01	3.31
10	3.25	1.86	12.3	0.88	3.25	2.44	2.66
20	4.59	2.10	25.6	1.12	2.30	1.79	2.04
30	5.54	2.22	39.3	1.46	1.85	1.41	1.75
40	6.29	2.26	52.8	1.78	1.57	1.19	1.59
60	7.52	2.43	81.6	2.20	1.25	0.922	1.37
80	8.53	2.38	108	2.40	1.07	0.790	1.23
100	9.42	2.49	137	2.58	0.942	0.688	1.12
150	11.10	2.53	207	3.18	0.740	0.536	1.01
200	12.43	2.61	280	3.64	0.622	0.444	0.924
300	14.63	2.74	432	4.10	0.488	0.339	0.773
450	17.20	2.87	662	4.58	0.382	0.260	0.650
600	19.12	2.92	888	5.12	0.319	0.215	0.591
800	21.09	2.93	1180	5.78	0.264	0.179	0.548
1000	22.74	3.06	1520	6.44	0.227	0.150	0.506

The end correction versus true shear stress at the wall plots for these two polyethylenes have been shown to be linear.² Figure 1 shows the resultant linear plots of recoverable shear strain versus true shear stress for these two polymers. The shear moduli calculated from the slope of these plots are 8.6×10^4 and 3.6×10^5 dynes/cm.² for the low and high density resins, respectively. These values differ slightly from the previously reported values for these two materials.² This is because the original values of the end correction used in reference 2 were obtained by visual extrapolation of the standard pressure—(L/R) plots to the $P = 0$ axis, while the new values, given in Tables I and II and in Figure 1, were obtained by a least squares fit of the data.

Wall's equation for the shear modulus, μ , from the kinetic theory of rubberlike elasticity is given by^{14,15}

$$\mu = RT\rho/M \quad (12)$$

where M is the polymer molecular weight, R is the gas constant, T is the absolute temperature, and ρ is the polymer melt density. For the linear resin, Polyethylene B, the shear modulus value of 3.6×10^5 dynes/cm.² and a melt density of 0.759 at 190°C. leads to a molec-

ular weight of 81,000 from eq. (12). The weight-average molecular weight from intrinsic viscosity measurements is 90,000.² This agreement is good enough, considering the errors involved in end correction studies, to argue that the molecular weight which should be used in Wall's expression for the shear modulus [eq. (12)] is a weight-average molecular weight.

For Polyethylene C a molecular weight of 340,000 is calculated from eq. (12) using the observed shear modulus value of 8.6×10^4

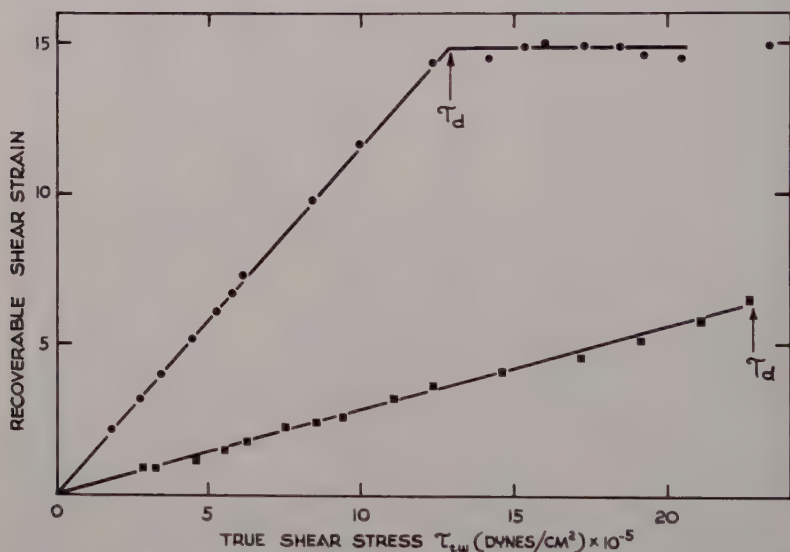


Fig. 1. Recoverable shear strain versus true shear stress plots for Polyethylene B (squares) and Polyethylene C (circles). Polyethylene B is a high density, linear resin while Polyethylene C is a low density branched material.

dynes/cm.². However, this is probably not a true weight-average molecular weight figure because of long chain branching in this material.

Above τ_d , the critical shear stress above which extrudate distortion occurs, the flow curve of Polyethylene B is discontinuous and values of e and hence S_R are not obtainable.^{2,5} The recoverable shear plot of Figure 1 is therefore not given for this resin above the critical shearing stress for melt fracture. This occurs at a recoverable shear value of 6.4. Another experiment on the same material permitted a re-

coverable shear value of 6.9 to be reached before melt fracture occurred, although the shear modulus value was the same as in the initial experiment.

For the branched Polyethylene C of Figure 1 the end correction becomes essentially constant above τ_d .² Thus, assuming the Couette part of the total end correction remains constant at 1.75 above τ_d , it can be concluded that the recoverable shear above τ_d is also constant, as shown in Figure 1 and tabulated in Table I. It is interesting to note here that extrudate distortion or melt fracture occurs at a considerably higher value of recoverable shear in the low density,

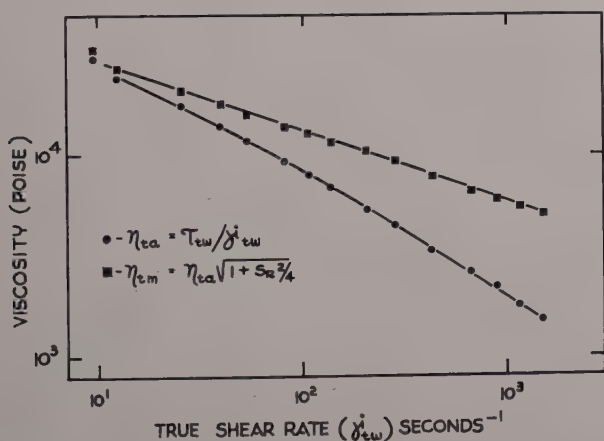


Fig. 2. Comparison of the viscoelastic and inelastic viscosities, as defined by eqs. (10) and (11), for Polyethylene B.

branched Polyethylene C than in the high density linear polyethylene. This point will be referred to subsequently.

It is of interest now to consider the various viscosities which can be calculated for Polyethylenes B and C. If these materials were ideal Newtonian fluids, b [eq. (9)] would be unity, but Tables I and II show that b increases, over the stress range being considered, from a value somewhat higher than unity to maximum values of about three. Values of the true shear rate, $\dot{\gamma}_{tw}$, calculated from eq. (10) are therefore markedly different from the shear rates calculated assuming Newtonian behavior [eq. (6)]. This effect is reflected in the apparent and true viscoelastic viscosities, η_a and η_{ta} .

The effect of including the Rabinowitsch correction is to make the two polymeric materials appear somewhat more non-Newtonian. The true, inelastic viscosity, calculated using the recoverable shear strain correction [eq. (11)], is markedly less shear dependent (i.e., less non-Newtonian) than either of the viscoelastic viscosities. This is readily seen in Figures 2 and 3. In Figure 2, η_{ta} and η_{tm} are plotted against true shear rate at the capillary wall for the high density Polyethylene B. Over the shear rate range shown the inclusion of the recoverable shear term has materially reduced the degree of non-Newtonianism exhibited by this material. In the low shear rate re-

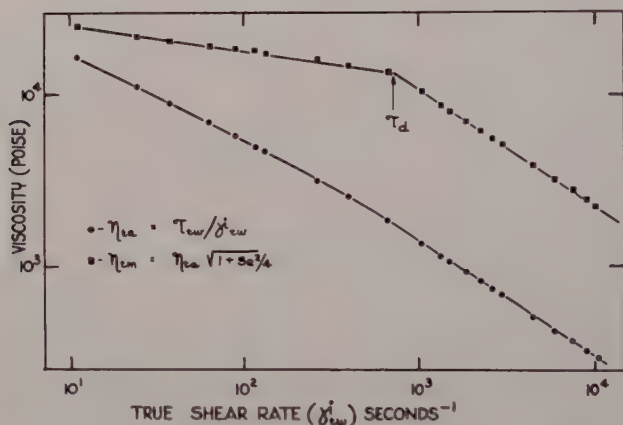


Fig. 3. Comparison of the viscoelastic and inelastic viscosities, as defined by eqs. (10) and (11), for Polyethylene C. The point at which extrudate distortion occurs is marked by an arrow.

gion, of course, the two curves converge, as they must because the recoverable shear must go to zero as the shear rate becomes small.

The same situation is shown in Figure 3 for the low density Polyethylene C. Here portions of the curve both above and below the critical stress at which melt fracture occurs, τ_d , have been included. The situation above τ_d is not particularly illuminating since we have interpreted the end correction results to show that the recoverable shear strain is constant in this region so that above τ_d the curves for the viscoelastic and inelastic viscosities must be parallel. Below τ_d the inelastic viscosity is far less shear rate dependent than the vis-

coelastic viscosity. Once again a large part of the non-Newtonianism has been directly attributable to the elastic nature of the melt.

In Figure 3, as in Figure 2, the two curves for the viscoelastic and inelastic viscosities approach each other as the shear rate decreases. The ultimate Newtonian viscosity for Polyethylene C at 190°C. was found to be 5.8×10^4 poise.*

Similar calculations of what has been termed here an inelastic viscosity have been given by Jobling and Roberts^{11,16} and by Philippoff.¹⁰ In some cases only a small part of the shear dependence of viscosity could be accounted for by this melt elasticity correction. In two cases, however, a large part of the shear dependence disappears on the application of this correction. One case is the polyethylenes reported here; the other is the 7% aluminum laurate in petrol peptized with ethoxyethyl alcohol.¹⁶ The residual shear dependence of the inelastic viscosities is still to be explained.

(b) Onset of Melt Fracture in Various Polymer Systems

It is not often in polymer physics that experimental data is notable for its simplicity. Such is the case, however, in the original observations of Spencer and Dillon on the nature of extrudate distortion.³ They found that for polystyrene the product of weight-average molecular weight, M_w , and the critical shearing stress at which extrudate distortion occurred, τ_d , was a constant. Spencer and Dillon³ and Spencer¹⁷ recognized that the phenomenon of extrudate distortion was an elastic effect and that the constancy of $\tau_d M_w$ was probably a reflection of Hooke's law in shear. Unfortunately, they did not have recoverable shear values to check these opinions but this work on polyethylene seems to amply confirm their views. It is interesting now to consider the data of Spencer and Dillon to compute the recoverable shear range in which they were working.

Hooke's law in shear is given by

$$\tau M = RT\rho S_R \quad (13)$$

where Wall's expression for the shear modulus has been used [eq. (12)]. This equation must be true at the distortion or melt fracture point so that

$$\tau_d M = RT\rho S_{Rd} \quad (14)$$

* The methods used to obtain this Newtonian viscosity will be discussed in a future publication by Bagley, Schreiber, and West.

It is not certain what molecular weight average should be used in eqs. (13) and (14). Spencer and Dillon noted that experimentally $\tau_d M_w$ is constant. This suggests that M_w should be used in eqs. (13) and (14), as in the case of polyethylene and that the constancy of $\tau_d M_w$ should be interpreted as showing that the amount of recoverable shear which polystyrene can undergo before melt fracture occurs is constant, independent of molecular weight, R and T being constant and ρ independent of M_w . Spencer and Dillon also found $\tau_d M_w$ independent of temperature over the range 175 to 225°C. Using the density data of Williams,¹⁸ recoverable shear values at the melt fracture point can now be calculated for polystyrene as a function of temperature. These are shown in Table III, where two points can be noted. First, the amount of recoverable shear (or alternately molecular distortion) required to induce melt fracture in polystyrene decreases slightly with temperature. Second, the value of recoverable shear at fracture for polystyrene is not greatly different than that observed for polyethylene at the same temperature, which, as remarked before, is in the range 6.4 to 6.9.

TABLE III
Calculation of Recoverable Shear Values at the Melt Fracture Point for Polystyrene at Various Temperatures, after Spencer and Dillon³

t , °C.	ρ , g./cc.	$RT\rho \times 10^{-10}$	S_{Rd}
175	0.9911	3.69	7.67
200	0.9775	3.84	7.37
225	0.9653	4.00	7.08

Similar data for the polymethyl methacrylate system have very kindly been made available by Dr. E. R. Howells.¹⁹ At 190°C., over the molecular weight range 20,000 to 120,000, Howells found $\tau_d M$ to be constant. In his work the molecular weight, M , was computed from intrinsic viscosity data of Baxendale, Bywater, and Evans²⁰ and was apparently essentially a weight-average molecular weight, as in the case of polystyrene and polyethylene. On a limited number of Howells' samples, end correction values were 4.0 ± 0.5 at the melt fracture point, essentially independent of molecular weight. In these cases the absolute value of the constant $\tau_d M_w$ was found to be 2.7×10^{11} , which leads to a recoverable shear value at fracture of 7.2, as-

suming a melt density of 0.98 at 190°C. This value of recoverable shear at fracture is essentially identical to that found for polystyrene and polyethylene at fracture.

For linear polymers the simple relationship

$$\tau_d M_w = (RT\rho)S_{Rd} \quad (14a)$$

seems well established. Thus a simple approach to determination of molecular weight is to measure τ_d and S_{Rd} and calculate M_w from eq. (14a). An alternate procedure is to recall that S_{Rd} is a constant for a given polymer species, independent of molecular weight, at the melt fracture point, so that

$$\tau_d M_w = D \quad (14b)$$

Having determined D by calibration on a single member of a polymer species, subsequent molecular weight determinations are done by simply measuring τ_d . A third method which should provide an approximate molecular weight of reasonable reliability is to assume that melt fracture always occurs at 7 units of recoverable shear. Then a molecular weight can be found directly from eq. (14a) if τ_d is known. This method is probably fairly reasonable if measurements are confined to polymer molecules at around 200°C. The recoverable shear at fracture does appear to be temperature dependent, however, and perhaps large discrepancies between recoverable shear at fracture for various polymers would be noted in studies carried out over a wider range of conditions, though D itself [eq. (14b)] appears independent of T .

(c) Comparison of Polymer Melt and Polymer Solution Behavior

It is instructive at this stage to compare our results on recoverable shear strains of polymer melts as a function of shearing stress with the results obtained by Philippoff and Gaskins on polymer solutions.¹ There seems to be a very striking analogy between the polymer melt and polymer solution behavior. In the case of melts of linear polymers we have found that Hooke's law in shear is obeyed up to about seven units of recoverable shear strain. Attempts to increase this recoverable shear value result in polymer melt fracture rather than further elastic deformation. For polyisobutylene-decalin solutions in the concentration range 0.25 to 9.0%, Philippoff and Gaskins¹ found Hooke's law in shear to be obeyed up to about 10 or 12 units of

recoverable shear strain, the shearing stress at which this breakdown of Hooke's law occurred increasing with concentration. It would appear that the breakdown of Hooke's law in shear in the case of solutions is occurring at essentially the same value of recoverable shear at which fracture occurs in the melt. In the case of solutions, however, the breakdown of Hooke's law in shear coincides, not with melt fracture, but with a very rapid increase of recoverable shear values with increasing shearing stress. This rapid increase is followed by a sudden levelling off of the curve in the region of 600 units in recoverable shear. Such high values would be expected if the polymer molecules were actually being uncoiled and stretched out in the flowing solution. The ultimate recoverable shear strain level, if it could be accurately determined, would constitute a direct measure of the polymer chain length. It thus seems that there is one qualitative difference in polymer melt and polymer solution behavior. At shear stresses above those necessary to achieve a certain critical recoverable shear strain, polymer melts fracture while in polymer solutions molecular uncoiling occurs.

4. Conclusions

For a low and high density polyethylene resin the applicability of Hooke's law in shear, coupled with a quantitative relationship given by Philippoff and Gaskins relating end corrections and recoverable shear strain in capillary flow, permits the calculation of recoverable shear strains, S_R , in flowing polymer melts over a wide shear stress range. The shear modulus so found was predictable for the linear polyethylene from Wall's version of the kinetic theory of rubberlike elasticity.

In comparing data on other polymer systems it appears that the onset of polymer melt fracture, which results in extrudate distortion in capillary flow, occurs at an essentially constant value of recoverable shear, independent of molecular weight or polymer type provided no long chain branching is present. Polymer solutions have also been shown by Philippoff and Gaskins to obey Hooke's law in shear up to a certain critical recoverable shear strain value, which is approximately the same value as that at which shear fracture occurs in the melt. In the solution case, however, shear fracture does not occur at this critical recoverable shear strain value. The results indicate that the polymer molecules uncoil and stretch out fully in the flow field to an

ultimate recoverable shear value which must be a measure of total chain length.

In computing the apparent viscosity of a flowing system, η_a , the simple ratio of shear stress to shear rate is usually taken. In elastic systems the main directions of stress and strain velocity no longer coincide. In this case a more realistic value of viscosity, termed here the inelastic viscosity, can be computed if recoverable shear data are available. This has been possible for two polyethylenes, and it was found that this inelastic viscosity is far less shear dependent than the apparent viscosity. Thus a large part of the apparent non-Newtonian flow behavior of these polyethylenes is directly attributable to the elastic nature of the melt.

The author wishes to express his thanks to Dr. A. Rudin, Dr. H. P. Schreiber, and Dr. D. C. West for their interest and help in this work and to Canadian Industries Ltd. for permission to publish this paper.

References

1. Philippoff, W., and F. H. Gaskins, *Trans. Soc. Rheology*, **2**, 263 (1958).
2. Bagley, E. B., *J. Appl. Phys.*, **31**, 1126 (1960).
3. Spencer, R. S., and R. E. Dillon, *J. Colloid Sci.*, **4**, 251 (1949).
4. Tordella, J. P., *J. Appl. Phys.*, **27**, 454 (1956).
5. Bagley, E. B., I. M. Cabott, and D. C. West, *J. Appl. Phys.*, **29**, 109 (1958).
6. Tordella, J. P., *Trans. Soc. Rheology*, **1**, 203 (1957).
7. Bagley, E. B., *J. Appl. Phys.*, **28**, 624 (1957).
8. Rabinowitsch, B., *Z. physik. Chem.*, **A145**, 1 (1929).
9. Weissenberg, K., *Arch. Geneve*, **17**, 1 (1935).
10. Philippoff, W., *J. Appl. Phys.*, **27**, 984 (1956).
11. Jobling, A., and J. E. Roberts, *J. Polymer Sci.*, **36**, 433 (1959).
12. Am. Soc. Testing Materials, D-1238-57T.
13. Bagley, E. B., and A. M. Birks, *J. Appl. Phys.*, **31**, 556 (1960).
14. Wall, F. T., *J. Chem. Phys.*, **10**, 485 (1942).
15. Treloar, L. R. G., *Trans. Faraday Soc.*, **39**, 36 (1943).
16. Jobling, A., and J. E. Roberts, in *Rheology*, Vol. 2, F. R. Eirich, ed., Academic Press, New York, 1958.
17. Spencer, R. S., *J. Polymer Sci.*, **5**, 591 (1950).
18. Williams, M. L., *J. Appl. Phys.*, **29**, 1395 (1958).
19. Howells, E. R., I.C.I., Plastics Division, Welwyn Garden City, Private Communication.
20. Baxendale, J. H., S. Bywater, and M. G. Evans, *J. Polymer Sci.*, **1**, 236 (1946).

Synopsis

It is shown for two polyethylene melts that Hooke's law in shear is obeyed. This permits the separation of elastic and viscous effects using a capillary viscom-

eter. From the results it is shown that melt fracture occurs at a constant value of recoverable shear, independent of polymer type or molecular weight providing no long chain branches are present. An analagous situation appears to exist for polymer solutions, except that at the critical recoverable shear value instead of fracture in shear there is a breakdown in Hooke's law in shear and apparent molecular uncoiling occurs. Experimentally determined recoverable shear values were used to calculate an "inelastic" viscosity which shows far less shear stress dependence than the apparent viscosity as usually calculated.

Flow and Shape of Drops in Non-Newtonian Fluids

A. FARAROUÏ* and R. C. KINTNER, *Department of Chemical Engineering, Illinois Institute of Technology, Chicago, Illinois*

In the course of investigations into the properties of dispersed liquid-liquid systems, it was deemed desirable to use solutions of certain organic materials, such as sodium carboxymethyl cellulose (CMC), to increase the viscosity of the field fluids. The shapes of large moving drops in these non-Newtonian liquids differed radically from drops of similar size moving in comparable liquids of constant viscosity. Inquiry was therefore instituted into the phenomena which has been qualitatively reported in recent literature.¹⁻⁷

Previous Work

An inverted tear drop shape was reported by Philippoff¹ for air bubbles rising through non-Newtonian solutions of a time-dependent nature. Still larger air bubbles assume a spherical cap shape with a well-rounded edge.² Philippoff's qualitative explanation of the shape seems plausible. The tear drop shape with trailing filament has been reported for liquid drops by Arnold,³ Savic,⁴ Garner et al.,⁵ Warshay et al.,⁶ and by Mhatre and Kintner.⁷ A recent paper by Harmathy⁸ presents an excellent review and bibliography of the movement of drops and bubbles through Newtonian fluids. Slattery⁹ treated the fall of rigid spheres through power function liquids. Mhatre and Kintner used apparent viscosity to define a Reynolds number for use in a drag curve correlation for the fall of liquid drops through pseudo-plastic liquids.

Theoretical

Any consideration of the flow of a fluid around a submerged object (or the movement of such an object through a fluid of infinite extent)

* Present address: B. F. Goodrich Iran S. A., Tehran, Iran.

must begin with the classical Navier-Stokes equations. For our incompressible systems they may be written;

$$\rho(D\vec{v}/Dt) = -\nabla p - \nabla \cdot \vec{\tau} + \rho \vec{g} \quad (1)$$

For a power function fluid, the value of the shear stress is (assuming ρ constant);

$$\vec{\tau} = \left\{ -K \left[(1/2 \dot{\Delta} : \dot{\Delta})^{1/2} \right]^{n-1} \right\} \dot{\Delta} \quad (2)$$

Substitution of eq. (2) into eq. (1) yields

$$\rho(D\vec{v}/Dt) = -\nabla p + K \nabla \cdot \left[\left\{ \left[(1/2 \dot{\Delta} : \dot{\Delta})^{1/2} \right]^{n-1} \right\} \dot{\Delta} \right] + \rho \vec{g} \quad (3)$$

In order to express the motion of a drop falling through a non-Newtonian fluid, one can apply dimensional analysis as described by Bird et al.¹⁰ Define

$$\vec{v}^* = \vec{v}/V, \quad X_i^* = x_i/L, \quad t^* = tV/L, \\ p^* = p/\rho V^2, \quad \text{and} \quad \nabla^* = L \nabla \quad (4)$$

Then

$$(D\vec{v}/Dt) = (V^2/L)(D\vec{v}^*/Dt^*) \\ \nabla p = (1/L)\rho V^2 \nabla^* p^* \\ \dot{\Delta} = (V/L)\dot{\Delta}^* \\ \dot{\Delta} : \dot{\Delta} = (V^2/L^2)\dot{\Delta}^* : \dot{\Delta}^* \quad (5)$$

Substitution of eqs. (5) into eq. (3) gives

$$\frac{D\vec{v}^*}{Dt^*} = -\nabla^* p^* + \left(\frac{K}{L^n \rho V^{2-n}} \right) \nabla^* \cdot \left[\left\{ \left[(1/2 \dot{\Delta}^* : \dot{\Delta}^*)^{1/2} \right]^{n-1} \right\} \dot{\Delta}^* \right] \\ + \left(\frac{Lg}{V^2} \right) \left(\frac{\vec{g}}{g} \right) \quad (6)$$

or

$$\frac{D\vec{v}^*}{Dt^*} = -\nabla^* p^* + \left(\frac{1}{N_{Ren}} \right) \nabla^* \cdot \left[\left\{ \left[(1/2 \dot{\Delta}^* : \dot{\Delta}^*)^{1/2} \right]^{n-1} \right\} \dot{\Delta}^* \right] \\ + C_D \left[\frac{3}{4} \frac{\rho}{\Delta \rho} \right] \left(\frac{\vec{g}}{g} \right) \quad (7)$$

in which

$$N_{Re_n} = L^n \rho V^{2-n} / K$$

and

$$C_D = \frac{4}{3} \frac{dg}{V^2} \frac{\Delta \rho}{\rho}$$

For a specific system ρ and $\Delta \rho$ are constant and eq. (7) leads to

$$C_D = \Phi(N_{Re_n}, n) \quad (8)$$

For the motion of a sphere in an infinite medium, the drag coefficient should be considered as a friction factor. By analogy with flow in a pipe, the average shear stress at the surface of the sphere may be defined as proportional to the kinetic energy of the moving sphere. This average shear stress, which is based on the surface area of the sphere at terminal velocity, is

$$\bar{\tau}_s = F_D / \pi d^2 = F_B / \pi d^2 = [(\pi d^3 / 6) \Delta \rho g] / \pi d^2 \quad (9)$$

Therefore:

$$\bar{\tau}_s = \frac{1}{6} d \Delta \rho g \quad (10)$$

An average shear rate must now be evaluated which, when used with the above shear stress, will satisfy the characteristics of Newtonian as well as non-Newtonian fluids of the power function type;

$$\bar{\tau}_s = K \left(\frac{du}{dr} \right)_s^m = K \left(\frac{du}{dr} \right)_s^{n-1} \left(\frac{du}{dr} \right)_s = \mu_a \left(\frac{du}{dr} \right)_s \quad (11)$$

in which μ_a is termed an apparent viscosity of the non-Newtonian fluid. For such a non-Newtonian, when Re_n is small enough, one can substitute the value of μ_a from eq. (11) into Stokes' equation to obtain

$$F_D = 3\pi d \mu_a U \quad (12)$$

Equating the right-hand members of eqs. (9) and (11) and substitution of F_D from eq. (12) results in

$$\mu_a \left(\frac{du}{dr} \right)_s = \frac{F_D}{\pi d^2} = \frac{3\pi d}{\pi d^2} \mu_a U \quad (13)$$

or

$$\left(\frac{du}{dr}\right)_s = 3U/d$$

Finally, from eqs. (10), (11) and (13)

$$\bar{\tau}_s = 1/6 d \Delta \rho g = K \left(\frac{3U}{d}\right)^n \quad (14)$$

which is analogous to the equation by Metzner and Reed¹¹ for flow through a cylindrical tube.

With the defined shear stress and shear rate of eq. (14), the drag coefficient may now be seen as a function of the Reynolds number in eq. (8), thus

$$\begin{aligned} C_D &= \frac{1}{3} \left(\frac{\Delta \rho}{\rho}\right) \left(\frac{gd}{U^2}\right) = \frac{1}{6} \left(\frac{d \Delta \rho g}{\rho U^2/8}\right) = \frac{\bar{\tau}_s}{\rho U^2/8} \\ &= \frac{K(du/dr)^n}{\rho U^2/8} = \frac{K(3U/d)^n}{\rho U^2/8} \\ &= \frac{24[K(3)^{n-1}]}{\rho U^{2-n} d^n} \end{aligned} \quad (15)$$

or

$$C_D = 24K_1/d^n U^{2-n} \rho = 24/Re_n$$

where

$$Re_n = d^n U^{2-n} \rho / K_1 \quad \text{and} \quad K_1 = (3)^{n-1} K \quad (16)$$

Experimental

If eq. (15) is to be used as a basis for the prediction of terminal velocities of drops in non-Newtonian liquids, it must be checked by experimental data on known systems. The limited range data of Mhatre and Kintner⁷ were used and supplemented with new data for larger drops.

Terminal velocity was determined by timing the fall of a drop of measured volume over a distance of 60 cm. To avoid end effects, the drop was allowed to fall 40 cm. before the 0.01 sec. electric stopwatch was started and the lower end of the timing section was 20 cm. above the bottom of the test tank. Drops were delivered into the tank by pouring them from small beakers held below the liquid surface.

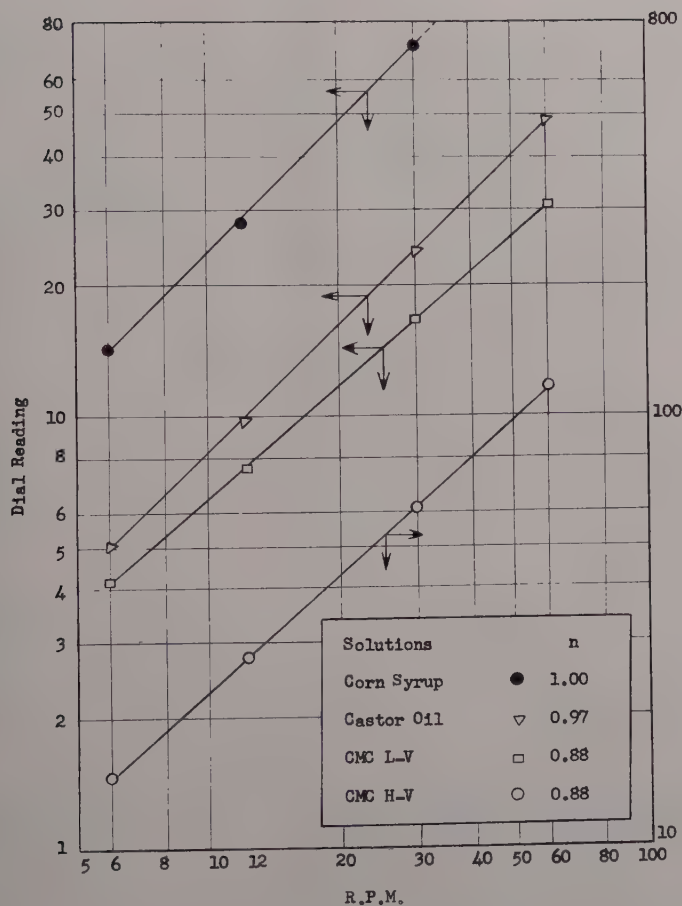


Fig. 1. Brookfield viscometer data.

The drops were composed of nitrobenzene and tetrachloroethane, mixed in such proportions as to provide a $\Delta\rho$ of 0.20 g./cm.³. Substances added to distilled water to produce solutions of elevated viscosity were carboxymethyl cellulose (CMC) (Hercules Powder Co.), corn syrup (Corn Products Refining Co.) and glycerol (Armour and Company). Castor oil, U.S.P., was obtained from a laboratory supply company.

Physical properties of importance were densities, viscosities, and

interfacial tensions. They were checked daily to note possible changes. Densities were determined with a calibrated specific gravity bottle and interfacial tensions by a ring tensiometer. A Brookfield rotational viscometer was used to establish the shear stress vs. shear rate relationship, Figure 1, as described by Metzner and Otto.¹² The bob used was a cylinder of 0.25 in. diameter and 2.375 in. length, made especially for this work. Values of K and n in the power function equation were established from a logarithmic plot of dial reading vs. rpm. These constants are recorded in Table I.*

TABLE I
Fluid Characteristics of Field Fluid

Field fluid	n	K	T
Lytron 890 No. 1	0.562	6.77	29.55
Lytron 890 No. 2	0.554	8.31	29.45
CMC solution No. 1	0.879	3.01	28.50
CMC solution No. 2	0.855	5.11	21.50
CMC solution No. 3	0.806	6.13	29.00
CMC 7-MSP	0.880	13.55	31.80
Castor oil	0.965	7.30	27.50
Corn syrup solution No. 1	1.000	2.80	23.80
Corn syrup solution No. 2	1.000	3.61	24.25
Corn syrup solution No. 3	1.000	4.63	25.10
Corn syrup viscous	1.000	13.50	24.30

Drop shapes were photographed with a 4×5 Speed Graphic with f -4.7 lens. An electronic flash unit with a 200 w.-sec. tube permitted use of very slow Kodak Contrast Ortho film. The stop used was f -11 to f -16. Motion pictures of the falling drops were taken on 16 mm. Tri-X Reversal film with a Kodak K-100 or a Fastax WF3 camera.

From the dimensionless groups in eq. (7), there should be a unique curve representing the relationship between N_{Re_n} and C_D . Such a relationship was also established between Re_n and C_D by using the shear stress defined by eq. (14). Values of C_D and Re_n were experimentally determined for the systems of Table I and are plotted in Figure 2. For values of Re_n less than about 0.1 the experimental points fall above the line $C_D = 24/Re_n$, while for values of Re_n higher

* Detailed tables of data are contained in the M.S. thesis of A. Fararoui, "Flow and Shape of Drops in non-Newtonian Fluids," 1960, available on inter-library loan from Illinois Institute of Technology, Chicago 16, Illinois.

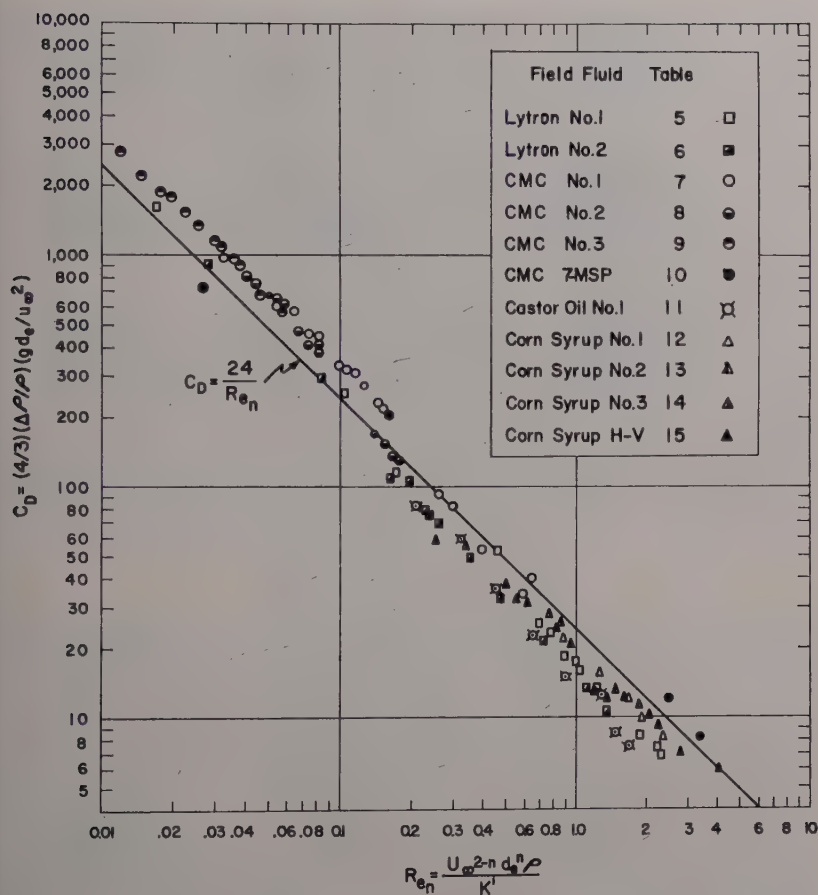


Fig. 2. Correlation of drag coefficient with the defined Reynolds number.

than about 0.2, they were located under the line. This transition region coincides with the change in drop shape. Drops in non-Newtonian fluids changed to the ovate shape, presenting a smaller projected frontal area in fall. Drops in the Newtonian corn syrup showed a change to the mushroom shape at an $Re = 2$ region. For such drops, the flow to the rear presents a modified regime. The line $C_D = 24/Re_n$ is based on a rigid spherical shape. The utility of the Reynolds number in eq. (16) depends (as shown by Metzner and Reed for flow in pipes) on the constancy of K_1 and n at the surface of the

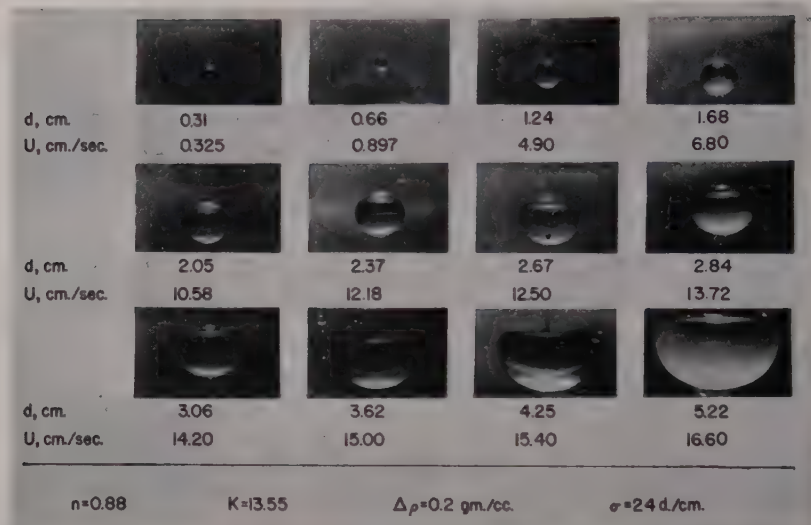


Fig. 3. Nitrobenzene drops falling through carboxymethyl cellulose (CMC).

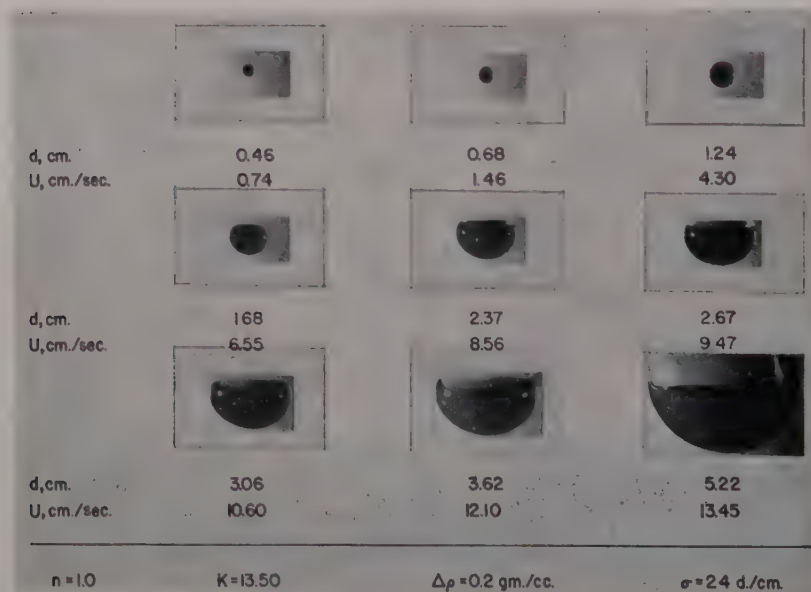


Fig. 4. Nitrobenzene + tetrachloroethane mixture drops falling through corn syrup.

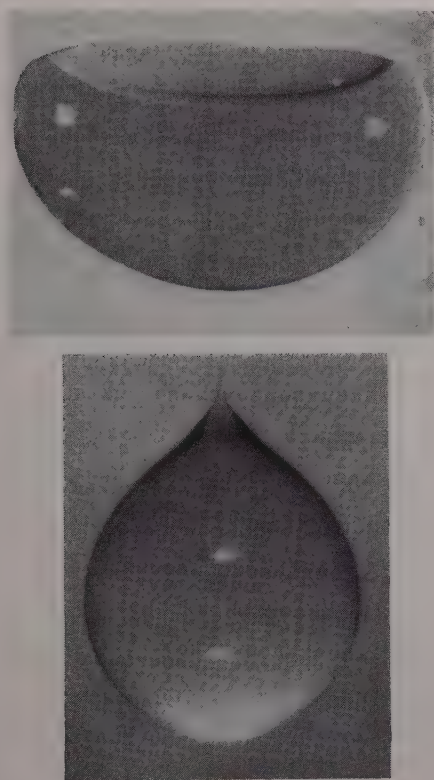


Fig. 5. Comparison of drop shapes in Newtonian and non-Newtonian fields. Top: Drop of nitrobenzene + tetrachloroethane in corn syrup; $d_e = 3.06$ cm.; $U_\infty = 1.52$ cm./sec. Bottom: Drop of water in castor oil; $d_e = 2.12$ cm.; $U_\infty = 1.52$ cm./sec.

drop. At the present time, there is not enough available data to permit an assessment to be made of the assumption which has been made regarding the average shear stress at the surface of the drop.

Figures 3-5 show the complete series of drop shapes in both Newtonian and non-Newtonian liquids. Drop sizes range from 0.31 to 5.22 cm. equivalent spherical diameter. This range is much wider than that of Mhatre and Kintner.⁷ For a drop moving in a Newtonian liquid such as corn syrup, the distortion progresses from spherical to spheroidal to oblate ellipsoidal as drop size is increased. Further increase in drop size results in a flattened rear surface of the

drop and this rear surface finally folds in as a depression in the very largest drop sizes. Garner et al.⁵ reported such a shape for drops of chloroform falling in glycerine. They concluded that the distortion of drops in the Stokes Law region depends on the relative changes in the outside hydrodynamic pressure and the inside pressure due to circulation. Depending upon the physical properties of the field fluid and liquid drop, a different series of shape changes was observed for drops falling through non-Newtonian liquids. At a drop size such that the surface forces are overcome by viscous drag,⁴ the shape changes from spherical to ovate with increasing drop size. Further increase in drop size will result in a tear-drop shape with trailing filament. Since the hydrodynamic suction is high, a tail is formed before internal circulation is fully developed. Finally, for very large drops, the ratio of vertical to horizontal diameters will decrease and the rear surface begins to fold inward. This depression at the rear stagnation point of very large drops (about 5 cm. equivalent diameter) has not been previously reported. Further study should be made of the effects of surface layer rigidity, circulation, and balance between interfacial tension and the surface shear⁴ for the various drop shapes.

The values of K_1 and n used in eq. (15) should be checked experimentally over a wide range of $(3U/d)$ or $(\Delta\rho dg/6g_c)$ to evaluate their constancy. For some fluids they are not constant, and care must be taken to insure that the range of integration is small. The particular value of K_1 and n used should be valid for the actual value of $(3U/d)$ or $(\Delta\rho dg/6g_c)$.

Summary

The fall of liquid drops through non-Newtonian field liquids can be characterized by means of a drag coefficient as a function of a generalized Reynolds number as defined by eq. (15) and illustrated by Figure 2.

The average shear stress as expressed by eq. (14) seems valid but needs further experimental confirmation. This is in progress.

The change in shape of drops (with increasing drop size) from spherical to ovate, back to spherical, and thence to spherical cap shapes has been reported for drops in non-Newtonian fields. The rear surface of the very large spherical cap shaped drops was folded inward.

Thanks are due to the National Science Foundation for financial support of the work and to Dr. K. M. Bischoff for his review of the mathematics involved.

Nomenclature

Symbol	Definition
C_D	Drag coefficient, eq. (15)
d	Diameter of sphere; equivalent spherical diameter of drop
du/dr	Shear rate; $(du/dr)_s$ is shear rate at the surface of a sphere
F	Force; F_B is buoyancy force; F_D is drag force
g	Gravitational acceleration
K	Fluid consistency index, eq. (11)
K_1	$K(3)^{n-1}$
L	A characteristic length
n	Flow behavior index, eq. (11)
p	Pressure
N_{Re}	Generalized Reynolds number, eq. (7)
Re_n	Generalized Reynolds number, eq. (16)
t	Time
T	Temperature
u	Local velocity; U is terminal velocity
V	A characteristic velocity; \vec{V} is vectorial velocity
σ	Interfacial tension
∇	Del; operator; defined as $\left(i \frac{\partial}{\partial x} + j \frac{\partial}{\partial y} + k \frac{\partial}{\partial z} \right)$
Δ_{ij}	$= \left(\frac{\partial v_i}{\partial x_j} + \frac{\partial v_j}{\partial x_i} \right)$
$\Delta : \Delta$	$= \Sigma_i \Sigma_j \Delta_{ij} \Delta_{ji}$
$D\vec{v}/Dt$	$= (\partial \vec{v} / \partial t) + (\vec{V} \cdot \nabla) \vec{V}$
μ	Viscosity; μ_a is apparent viscosity, eq. (11)
τ	Shear stress; $\bar{\tau}_s$ is average shear stress over the surface of a sphere
ρ	Field fluid density
$\Delta \rho$	Density difference between drop and field fluids
Φ	A function

References

1. Philippoff, W., *Rubber Chem. and Technol.*, **10**, 76 (1937).
2. Azim, S., M.S. Thesis, Illinois Institute of Technology, 1957.
3. Arnold, H. D., *Phil. Mag.*, **22**, 755 (1911).
4. Savic, P., Rept. Natl. Res. Council of Canada, July, 1953.
5. Garner, F. H., K. D. Mathur, and V. G. Jenson, *Nature*, **180**, 331 (1957).
6. Warshay, M., E. Bogusz, M. Johnson, and R. C. Kintner, *Can. J. Chem. Eng.*, **37**, 29 (1959).

7. Mhatre, M. V., and R. C. Kintner, *Ind. Eng. Chem.*, **51**, 865 (1959).
8. Harmathy, T. Z., *A.I.Ch.E. Journal*, **6**, 281 (1960).
9. Slattery, J. C., Ph.D. Thesis, Univ. of Wisconsin, 1959.
10. Bird, R. B., W. E. Stewart, and E. N. Lightfoot, *Notes on Transport Phenomena*, Wiley, New York, 1958.
11. Metzner, A. B., and J. C. Reed, *A.I.Ch.E. Journal*, **1**, 434 (1955).
12. Metzner, A. B., and R. E. Otto, *A.I.Ch.E. Journal*, **3**, 4 (1958).

Synopsis

A relationship, analogous to that for flow in a cylindrical conduit, expressing an average shear stress at the surface of a moving drop in terms of its shear rate is developed. A drag coefficient for the drop moving in slow motion and a Reynolds number permitted the correlation of terminal velocity data for drops of 0.3 cm. to 5.0 cm. equivalent spherical diameter. Field fluids were castor oil and solutions of corn syrup, carboxy methyl cellulose, and Lytron 890 with fluid consistencies of the order of 300 to 1500 centipoises. As drop size was increased, the drop shape changed from spherical to ovate, back to spherical and thence to an inverted spherical cap with a depression on the rear surface. The tear drop shape with trailing filament was observed only in non-Newtonian fluids.

Abstracts

Molecular Weight-Temperature-Concentration Relationships for the Viscosity of Polyvinyl Acetate and Its Solutions in Diethyl Phthalate and in Cetyl Alcohol

H. NAKAYASU and T. G. FOX,
Mellon Institute, Pittsburgh, Pennsylvania

Previous measurements of the viscosity of linear polyvinyl acetate fractions in a thermodynamically good solvent, diethyl phthalate, have been extended to lower molecular weights; measurements have been made as well in a thermodynamically border line solvent, cetyl alcohol, at the temperature (123°C.) and above. These cover the range in molecular weight from 8×10^3 to 1.3×10^6 , in temperature from 160 to 35°C., and in concentration from 0.1 to 1.0 volume fraction of polymer. The observed viscosities, ranging from 2×10^{-2} to over 2×10^6 poises are represented by simple empirical equations and interpreted in the light of current molecular concepts of flow.

Dynamic Mechanical Properties and Creep of Poly-2-ethyl Butyl Methacrylate

THEODORE P. YIN and JOHN D. FERRY,
University of Wisconsin, Madison, Wisconsin

The real (J') and imaginary (J'') components of the complex compliance have been measured between 0.05 and 3600 cycles/sec.

in the temperature range from 20 to 151°C. for a fractional poly-2-ethyl butyl methacrylate with molecular weight 2.20×10^6 . The creep compliance, $J(t)$, and creep recovery were measured from 101 to 151°C. The glass transition temperature was determined to be 11°C. The method of reduced variables gave superposed curves in the transition zone with shift factors following the WLF form of equation; the WLF parameters were $f_g = 0.021$, $\alpha_f = 1.8 \times 10^{-4}$ deg.⁻¹. In the plateau zone (including the creep) an additional f -reduction for temperature dependence of entanglement was necessary, with $H = 4.4$ kcal. The retardation and relaxation spectra was calculated; the latter is almost identical in shape throughout with that of the n -butyl polymer. The logarithm of the monomeric friction coefficient is -3.69 at 100°C. and 4.79 at T_g . The average degree of polymerization between the entanglement coupling points is calculated to be 83, 115, and 178, respectively, from the plateau in the spectra, from the height of the maximum in J'' , and from the position of the latter on the frequency scale. In general, the viscoelastic behavior of the 2-ethyl butyl polymer resembles that of the n -butyl much more closely than that of the n -hexyl which has the same side chain molecular weight.

[To be published in the *Journal of Colloid Science*]